



Rebecca Mansur de Castro Silva

**Textile reinforced concrete with polymer- and mineral-
impregnated carbon fabrics: from a material
characterization to a structural application**

Tese de Doutorado

Thesis presented to the Programa de Pós-Graduação em Engenharia Civil of PUC-Rio in partial fulfillment of the requirements for the degree of Doutor em Ciência – Engenharia Civil.

Advisor: Prof. Flávio de Andrade Silva

Rio de Janeiro
April 2023



Rebecca Mansur de Castro Silva

**Textile reinforced concrete with polymer- and mineral-
impregnated carbon fabrics: from a material
characterization to a structural application**

Thesis presented to the Programa de Pós-Graduação em Engenharia Civil of PUC-Rio in partial fulfillment of the requirements for the degree of Doutor em Ciência – Engenharia Civil. Approved by the Examination Committee.

Prof. Flávio de Andrade Silva

Advisor

Department of Civil and Environmental Engineering – PUC-Rio

Prof. Daniel Carlos Taissum Cardoso

Department of Civil and Environmental Engineering – PUC-Rio

Prof. Antonio Domingues de Figueiredo

USP

Prof. Dimas Alan Strauss Rambo

USJT

Prof. Fernanda Steffens

UFSC

Rio de Janeiro, April 19th, 2023

All rights reserved.

Rebecca Mansur de Castro Silva

Graduated in Civil Engineering at Universidade Federal Fluminense in 2014 and obtained her M.Sc. Degree in Civil Engineering from the Pontifícia Universidade Católica do Rio de Janeiro in 2018.

Bibliographic data

Silva, Rebecca Mansur de Castro

Textile reinforced concrete with polymer- and mineral-impregnated carbon fabrics: from a material characterization to a structural application / Rebecca Mansur de Castro Silva ; advisor: Flávio de Andrade Silva. – 2023.

258 f. : il. color. ; 30 cm

Tese (doutorado)–Pontifícia Universidade Católica do Rio de Janeiro, Departamento de Engenharia Civil e Ambiental, 2023.

Inclui bibliografia

1. Engenharia Civil e Ambiental - Teses. 2. Concreto têxtil. 3. Tecido de carbono. 4. Fibras de carbono com impregnação mineral. 5. Temperaturas elevadas. 6. Reforço externo. I. Silva, Flávio de Andrade. II. Pontifícia Universidade Católica do Rio de Janeiro. Departamento de Engenharia Civil e Ambiental. III. Título.

CDD: 624

To my parents, Danielle and Miguel,
for initiating my pleasure in studies and knowledge.

Acknowledgements

Many people were essential for me to be able to complete this work, and I would like to express my gratitude to some of them.

To my advisor, Prof. Flávio de Andrade Silva, for trusting in me and my work. Thank you for all the support and suggestions necessary for the completion of this research.

To my mother, Danielle, and my father, Miguel, for all their support and unconditional love for me. No matter in which direction I decide to follow, you always encourage and give me strength. Much of the professional that I am today is because of the example I had from you. Thank you for everything. To my brothers, Leonardo and Antônio Miguel, I am extremely grateful to have you in my life. To my fiancé, my roommate, and my best friend, Bernardo, thank you for all your support. For encouraging me to follow new paths and letting me trail my own steps. Thank you for believing in me more than I do and making me want to be a better person.

To my family and friends, who, in their own way, encouraged and supported me to get here. Thank you for understanding my absence sometimes and for celebrating my achievements with me.

To conduct experimental research, a whole team is needed. Thus, I would like to express my deep gratitude to all the technicians at the LEM-DEC Laboratory: Euclides, Rogério, José Nilson, Jhansen, Marques, and Anderson. Thank you very much for your help and company in the day-to-day work in the lab.

During the Ph.D. period, I had the opportunity to do a sandwich doctorate in Dresden, Germany. I am very grateful to the entire technical staff and research group of the Institute of Construction Materials at TU Dresden, led by Prof. Viktor Mechtcherine, for the support and welcome. The time I spent on this exchange was undoubtedly very enriching for my research but also contributed significantly to my personal and professional development. The friends I made in this process will always be fondly remembered for making me feel at home and easing my homesickness.

The doctoral years are challenging. But within the chaotic routine, some people brought lightness to this madness of studies and research. I want to thank all the friends I made on this journey. I won't mention any names because I don't want to forget anyone. But thank you all for the company and the laughs shared at lunches, afternoon coffee, and barbecue parties.

Among the friends I've made, I would like to give special thanks to Ana, Daiana, Letícia, Raylane, and Tathiana. It's cliché, but you are the greatest gift I got for entering academic life. You are my safe haven in this emotional madness that is post-graduation. You give me strength in the most difficult times, especially in those situations where I think I won't make it. You make me see that I am capable, but that it's ok if I can't, I don't need to be the Wonder Woman all the time. Without you, it would be possible to finish this journey, but I have no questions that the path would be rougher. I am immensely grateful for all your support. Thank you for existing in my life. I know that I can count on your friendship forever.

I would also like to thank the Professors and member of this thesis committee for their availability and careful reading of this study.

This study was financed in part by the Coordenação de Aperfeiçoamento de Pessoal de Nível Superior – Brasil (CAPES) – Finance Code 001, and also by CNPq.

Abstract

Mansur de Castro Silva, Rebecca; de Andrade Silva, Flávio (Advisor). **Textile reinforced concrete with polymer- and mineral-impregnated carbon fabrics: from a material characterization to a structural application.** Rio de Janeiro, 2023. 258 p. Tese de Doutorado – Departamento de Engenharia Civil e Ambiental, Pontifícia Universidade Católica do Rio de Janeiro.

Steel Reinforced Concrete (RC) structures may need strengthening during their service life. Textile Reinforced Concrete (TRC) presents elevated mechanical behavior and low self-weight, presenting as a suitable alternative for strengthening RC elements. Polymeric-coated carbon fabrics present high mechanical properties but low thermal resistance. Mineral impregnations can increase the bond of carbon yarns towards cementitious matrices even at elevated temperatures. This work aims to assess the mechanical behavior of Mineral-Impregnated Carbon Fibers (MCF) fabrics TRCs. For this, MCF yarns with a cement-based (C) and a geopolymer (GP) suspension were produced. Both MCF yarns yielded high tensile strength and modulus of elasticity. The bond of the MCF yarns towards a cementitious matrix was evaluated through pull-out tests at different elevated temperature levels and compared to a yarn of a currently commercially epoxy-coated (EP) carbon fabric. The C-MCF yarn presented higher bond strength towards the matrix than the GP-MCF. At elevated temperatures, the bond between the EP yarn and the matrix became considerably weaker, while the MCF yarns could maintain a sufficient bond up to 300°C. The mechanical behavior of TRCs with MCF and EP carbon fabrics was characterized through direct tensile tests at room temperature and after being submitted to a thermal regime. The TRC with MCF fabrics presented strain-hardening behavior with a multiple-cracking pattern. The heating up to 300 °C did not significantly affect the mechanical performance of the TRC with C-MCF fabric. A structural application analysis of these composites was also performed. For this, RC beams were externally strengthened with MCF- and EP-carbon fabrics TRCs. All TRC strengthening was able to increase the RC beam load capacity. Furthermore, the TRC-strengthened beams presented a multiple-cracking pattern

with very fine cracks. In general, the outcome of this study demonstrated that MCF fabrics can be used as an alternative reinforcement in textile reinforced concretes, mainly in situations in which elevated temperatures are expected. With adequate substrate preparation, the MCF-TRC system can also be successfully implemented as a strengthening material for RC beams.

Keywords

Textile reinforced concrete (TRC); Carbon fabric; Mineral-Impregnated Carbon Fibers (MCF); Elevated temperatures; RC external strengthening

Resumo

Mansur de Castro Silva, Rebecca; de Andrade Silva, Flávio (Advisor). **Concreto têxtil reforçado com tecido de carbono com impregnações polimérica e mineral: da caracterização do material até uma aplicação estrutural**. Rio de Janeiro, 2023. 258 p. Tese de Doutorado – Departamento de Engenharia Civil e Ambiental, Pontifícia Universidade Católica do Rio de Janeiro.

Estruturas de concreto armado (CA) podem precisar serem reforçadas durante a sua vida útil. Concretos têxteis apresentam elevadas propriedades mecânicas e baixo peso próprio, o que faz com esse material seja uma alternativa adequada para o reforço de elementos de CA. Tecidos de carbono impregnados com material polimérico possuem elevadas propriedades mecânicas, porém baixa resistência térmica. Impregnações minerais são capazes de melhorar a aderência de cordões de carbono com matrizes cimentícias, mesmo em temperaturas elevadas. Este trabalho tem como objetivo avaliar o comportamento mecânico de concretos têxteis reforçados com tecidos de fibras de carbono com impregnações minerais (MCF). Assim, cordões MCF foram produzidos com uma suspensão cimentícia (C) e de geopolímero (GP). Os dois cordões MCF apresentaram elevada resistência à tração e módulo de elasticidade. A aderência destes cordões com uma matriz cimentícia foi avaliada através de ensaios de arrancamento executados em diferentes níveis de temperatura. Os resultados foram comparados com os de um cordão retirado de um tecido de carbono impregnado com resina epóxi (EP) comercialmente disponível. O cordão C-MCF apresentou maior aderência com a matriz cimentícia do que o cordão GP-MCF. Em temperaturas elevadas, houve uma considerável perda da aderência do cordão EP com a matriz, enquanto o cordão C-MCF foi capaz de manter um bom nível de aderência. O comportamento mecânico de concretos têxteis reforçados com tecidos de carbono MCF e EP foi avaliado por meio de ensaios de tração direta em temperatura ambiente e após os corpos de prova serem submetidos a um regime térmico. O concreto têxtil com os tecidos MCF apresentaram comportamento strain-hardening com múltipla fissuração. O aquecimento até 300 °C não afetou de forma significativa o desempenho mecânico

dos concretos têxteis com tecido C-MCF. A análise desses compósitos como aplicação estrutural também foi investigada. Para isso, vigas de CA foram reforçadas com concretos têxteis com tecidos MCF e EP. Todos os sistemas de reforço aumentaram a capacidade de carga das vigas de CA. Além disso, as vigas reforçadas com concreto têxtil apresentam um padrão refinado de múltipla fissuração. De forma geral, esse estudo demonstrou que tecidos MCF podem ser utilizados como uma alternativa de reforço em concretos têxteis, principalmente em situações nas quais temperaturas elevadas são esperadas. Além disso, como o método de preparo do substrato adequado, o concreto têxtil reforçado com tecidos MCF pode ser implementado satisfatoriamente como reforço externo em vigas de CA.

Palavras – chave

Concreto têxtil; Tecido de carbono; Fibras de carbono com impregnação mineral (MCF); Temperaturas elevadas; Reforço externo

Table of contents

Acknowledgements	5
Abstract	7
Resumo	9
Table of contents	11
List of figures	14
List of tables	22
1 Introduction	25
1.1. Motivation	25
1.2. Objectives	27
1.3. Thesis organization	27
1.4. References	28
2 Literature review	31
2.1. Textile reinforced concrete	31
2.2. Mechanical performance	33
2.2.1. Bond Behavior	33
2.2.2. Tension and flexural mechanical behavior	39
2.2.3. Effect of temperature on the TRC mechanical behavior	41
2.2.4. Effect of load rate on the TRC mechanical behavior	44
2.3. Structural applications	46
2.3.1. New load-bearing elements	47
2.3.2. Strengthening of existing structures	50
2.4. References	54

3 Bond behavior of polymer- and mineral-impregnated carbon fiber yarns towards concrete matrices at elevated temperature levels and different strain rates	69
3.1. Introduction	69
3.2. Experimental Program	73
3.2.1. Carbon yarns	73
3.2.2. Fine-grained concrete matrix	75
3.2.3. Impregnation process	76
3.2.4. Uniaxial Tension Tests on Carbon Yarn	78
3.2.5. Pull-out Tests on Yarns	80
3.2.6. Morphological Analyze	84
3.3. Results and discussion	84
3.3.1. Fine-grained concrete matrix	84
3.3.2. Uniaxial Tension Tests on Yarns	85
3.3.3. Carbon Yarn Pull-out Behavior	92
3.4. Conclusions	117
3.5. References	119
4 Mechanical behavior of textile reinforced concrete with newly developed mineral-impregnated carbon fabrics submitted to uniaxial tensile loads and exposed to elevated temperatures	129
4.1. Introduction	130
4.2. Experimental Program	134
4.2.1. Materials	134
4.2.2. Composite manufacturing	140
4.2.3. Direct tensile tests	143
4.2.4. Morphological characterization	145
4.3. Results and discussion	146
4.3.1. Fine-grained concrete matrix	146
4.3.2. Tensile mechanical behavior – MCF fabrics	148
4.3.3. Tensile mechanical behavior – TRC	152
4.3.4. Morphological characterization of the TRC	179
4.4. Conclusions	181
4.5. References	183

5 Strengthening of RC beams using textile reinforced concrete (TRC) with polymer- and mineral-impregnated carbon fabrics	193
5.1. Introduction	194
5.2. Experimental Program	199
5.2.1. Materials	199
5.2.2. Strengthening protocol	203
5.2.3. Bending tests	209
5.3. Results and discussion	212
5.3.1. Strengthening protocols	212
5.3.2. Strengthening efficiency	224
5.3.3. Analytical model	238
5.4. Conclusions	244
5.5. References	246
6 Conclusions and suggestions for future works	254
6.1. Conclusions	254
6.2. Suggestions for future works	257

List of figures

Figure 2.1 – Different connection methods of the yarns: (a) woven fabrics, (b) knitted fabrics, (c) braided fabrics, and (d) bonded fabrics (adapted from [2]).	32
Figure 2.2 – Geometry of a multifilament yarn (a) plain and (b) epoxy-coated (adapted from [1]).	34
Figure 2.3 – Telescopic failure (adapted from [26]).	34
Figure 2.4 – (a) Pull-out test setup with single yarn [31]. (b) Variation of pull-out test with single yarn [32]. (c) Two-sided pull-out test setup [1].	38
Figure 2.5 – Typical stress vs. strain curve of Textile Reinforced Concretes (TRC) obtained from direct tensile tests.	39
Figure 2.6 – Application of the TRC strengthening in the Maracanã Stadium, Brazil, performed by the S&P Clever Brasil company [153].	53
Figure 3.1 – Impregnation system: a) Overall view with the wheel; b) Yarn alignment guides and kiss-coater; c) Impregnation bath; d) Deflection rollers; e) ready MCF yarns.	77
Figure 3.2 – Setup for the yarn uniaxial tension tests.	79
Figure 3.3 – Specimen for the yarn uniaxial tension tests. a) Manufacturing; b) Geometry and dimensions.	80
Figure 3.4 – Procedure for the pull-out specimens manufacturing. a) Plastic mold; b) Yarn positioned in the center of the mold; c) Specimens after casting with the steel holder already positioned; d) Pull-out specimens after demolding.	81
Figure 3.5 – Setup for the pull-out tests at (a) room temperature and (b) elevated temperatures.	82
Figure 3.6 – Heating regime for the pull-out specimens.	83
Figure 3.7 – Schematic average interfacial shear stress vs. slip curve obtained from pull-out tests.	84

Figure 3.8 – Compressive strengths of the fine-grained concrete matrix at different temperatures.	85
Figure 3.9 – Tensile vs. strain curves obtained for all specimens of the (a) C-MCF yarns, and (b) GP-MCF yarns. (c) Representative tensile stress vs. strain curves for the carbon yarns. *Curve constructed using the data from the supplier.	86
Figure 3.10 – Representative tensile stress vs. strain curves obtained with the displacement recorded by the video-extensometer and the actuator displacement for the C-MCF and GP-MCF yarns.	88
Figure 3.11 – Failure modes of the (a) C-MCF and (b) GP-MCF yarns at different strain rates.	89
Figure 3.12 – Tensile vs. strain curves obtained for all specimens of the C-MCF yarns at (a) 0.02 s^{-1} and (b) 0.2 s^{-1} , and GP-MCF yarns at (c) 0.02 s^{-1} and (d) 0.2 s^{-1} .	90
Figure 3.13 – Representative tensile stress vs. strain curves obtained from the yarn tension tests at different strain rates for the (a) C-MCF and (b) GP-MCF.	91
Figure 3.14 – Average interfacial shear stress vs. slip curves obtained in the pull-out tests for the (a) C-MCF, (b) GP-MCF (with washing process), and (c) EP yarns.	94
Figure 3.15 – Representative average interfacial shear stress vs. slip curves obtained in the pull-out tests for the C-MCF, GP-MCF (with washing process), and EP yarns.	94
Figure 3.16 – Images from the matrix-yarn interface region from the (a) C-MCF, (b) GP-MCF, and (c) EP yarns after the pull-out tests at room temperature (RT), $150 \text{ }^{\circ}\text{C}$, $200 \text{ }^{\circ}\text{C}$, and $300 \text{ }^{\circ}\text{C}$.	95
Figure 3.17 – Images from the pull-out channels for the (a) C-MCF, (b) GP-MCF, and (c) EP yarns after the pull-out tests at room temperature (RT), $150 \text{ }^{\circ}\text{C}$, $200 \text{ }^{\circ}\text{C}$, and $300 \text{ }^{\circ}\text{C}$.	96
Figure 3.18 - μCT images of pull-out test specimens: (a,b) C-MCF; (c,d) GP-MCF with washing process; (e,f) EP; and (g,h) GP-MCF without washing process.	97

- Figure 3.19 – Representative average interfacial shear stress vs. slip curves obtained in the pull-out tests for the GP-MCF without and with the washing process (H₂O). 100
- Figure 3.20 – Average interfacial shear stress vs. slip obtained in the pull-out tests for the C-MCF yarn at (a) 150 °C, (b) 200 °C, and (c) 300 °C. (d) Representative average interfacial shear stress vs. slip obtained in the pull-out tests for the C-MCF yarn at different temperatures. 104
- Figure 3.21 – Average interfacial shear stress vs. slip obtained in the pull-out tests for the GP-MCF yarn at (a) 150 °C, (b) 200 °C, and (c) 300 °C. (d) Representative average interfacial shear stress vs. slip obtained in the pull-out tests for the GP-MCF yarn at different temperatures. 105
- Figure 3.22 – Average interfacial shear stress vs. slip obtained in the pull-out tests for the EP yarn at (a) 150 °C, and (b) 200 °C. (d) Representative average interfacial shear stress vs. slip obtained in the pull-out tests for the EP yarn at different temperatures. 106
- Figure 3.23 – Diameter variation obtained for the C-MCF, GP-MCF, and EP yarns after heating at 150 °C, 200 °C, and 300 °C. 110
- Figure 3.24 – Comparative representation of the Temperature Modification Factor k_d for T_{max} , W_1 and W_{total} for the C-MCF, GP-MCF and EP yarns. 111
- Figure 3.25 – Average interfacial shear stress vs. slip obtained in the pull-out tests for the C-MCF yarn at (a) 0.01 s⁻¹, (b) 0.1 s⁻¹, and (c) 1 s⁻¹. (d) Representative average interfacial shear stress vs. slip obtained in the pull-out tests for the C-MCF yarn at different strain rates. 112
- Figure 3.26 – Average interfacial shear stress vs. slip obtained in the pull-out tests for the GP-MCF yarn at (a) 0.01 s⁻¹, (b) 0.1 s⁻¹, and (c) 1 s⁻¹. (d) Representative average interfacial shear stress vs. slip obtained in the pull-out tests for the GP-MCF yarn at different strain rates. 113
- Figure 3.27 – Average interfacial shear stress vs. slip obtained in the pull-out tests for the EP carbon yarn at (a) 0.01 s⁻¹, (b) 0.1 s⁻¹, and (c) 1 s⁻¹. (d) Representative average interfacial shear stress vs. slip

obtained in the pull-out tests for the EP carbon yarn at different strain rates.	114
Figure 3.28 – Comparative representation of the (a) Maximum average interfacial shear stress and (b) Total work at different strain rates for the C-MCF, GP-MCF and EP yarns.	117
Figure 4.1 – Wooden mold for the fabrication of the MCF fabrics.	138
Figure 4.2 – Procedure for the manufacture of the MCF fabrics (a) Impregnation system; (b) Placement of the transversal yarns; (c) Placement of the longitudinal yarns.	138
Figure 4.3 – (a) C-MCF (b) EP, and (c) GP-MCF carbon fabrics.	139
Figure 4.4 – MCF fabric specimen.	140
Figure 4.5 – Hand lay-up technique for the TRC manufacturing. (a) placement of a thin layer of the fine-grained concrete matrix over the bottom plate to reduce the thickness in the gage length, (b) positioning of the fabric, (c) and (d) placement of the final matrix layer, the top plate, and finishing procedure.	142
Figure 4.6 – Detail of the MCF fabrics knot regions with the transversal and longitudinal yarns overlaying.	143
Figure 4.7 – Setup for the direct tensile tests in the (a) MCF fabric specimens, and (b) TRC specimens.	144
Figure 4.8 – Thermal regime for the TRC specimens.	145
Figure 4.9 – Residual compressive strength of the fine-grained concrete matrix at room temperature (~20 °C) and after being submitted to thermal regimes with target temperatures of 150 °C, 200 °C, and 300 °C.	146
Figure 4.10 – Tensile stress vs. strain curves obtained from the direct tension tests for the (a) C-MCF and (b) GP-MCF fabrics. (c) Representative tensile stress vs. strain curves obtained from the direct tension tests for the C-MCF and GP-MCF fabrics and yarns.	148
Figure 4.11 – Representative tensile stress vs. strain curves obtained from the direct tension tests comparing the strain obtained with the displacement recorded by LVDTs and the actuator displacement for the C-MCF and GP-MCF fabrics.	151

Figure 4.12 – Tensile stress vs. actuator displacement curves obtained from the direct tension tests for the (a) C-MCF and (b) GP-MCF fabrics specimens, and (c) representative curves.	152
Figure 4.13 – Tensile stress vs. strain curves obtained from the direct tension tests for the TRC with the (a) C-MCF, (b) GP-MCF, and (c) EP fabrics.	153
Figure 4.14 – Representative tensile stress vs. strain curves obtained from the direct tension tests for the TRC with the C-MCF, GP-MCF, and EP fabrics.	154
Figure 4.15 – TRC with the EP fabric after the direct tensile test.	157
Figure 4.16 – Crack pattern just before failure for the TRC with (a) C-MCF, (b) GP-MCF, and (c) EP fabrics.	158
Figure 4.17 – Crack pattern of the TRC with the C-MCF and GP-MCF fabric at the strain of 0.2% and 0.7%.	159
Figure 4.18 – Crack pattern observed in the TRC specimens with the C-MCF fabrics immediately post-heating regime and at various strain levels.	164
Figure 4.19 – Crack pattern observed in the TRC specimens with the C-MCF fabrics immediately post-heating regime and at various strain levels.	167
Figure 4.20 – Residual tensile stress vs. strain curves obtained from the direct tension tests after the thermal regime up to (a) 150 °C, (b) 200 °C, and 300 °C for the TRC with the C-MCF fabric specimens. (d) Representative residual tensile stress vs. strain curves.	169
Figure 4.21 – Residual tensile stress stress vs. strain curves obtained from the direct tension tests after the thermal regime up to (a) 150 °C, (b) 200 °C, and 300 °C for the TRC with the GP-MCF fabric specimens. (d) Representative residual tensile stress vs. strain curves.	170
Figure 4.22 – Residual tensile stress stress vs. strain curves obtained from the direct tension tests after the thermal regime up to (a) 150 °C, (b) 200 °C, and 300 °C for the TRC with the EP carbon fabric specimens. (d) Representative residual tensile stress vs. strain curves.	171

Figure 4.23 – TRC with C-MCF fabrics after the direct tensile tests after temperature exposure of a) 150 °C, b) 200 °C, and c) 300 °C.	174
Figure 4.24 – TRC with GP-MCF fabrics after the direct tensile tests after temperature exposure of a) 150 °C, b) 200 °C, and c) 300 °C.	177
Figure 4.25 – TRC with EP carbon fabrics after the direct tensile tests after temperature exposure of a) 150 °C, b) 200 °C, and c) 300 °C.	178
Figure 4.26 – μ CT images showing the TRC specimens with (a) EP carbon, (b) C-MCF, and (c) GP-MCF fabrics after temperature exposure of 20 °C and 300 °C.	181
Figure 5.1 – Schematic beam details and dimensions (dimensions in mm).	203
Figure 5.2 – Summary of the adopted strengthening protocols.	204
Figure 5.3 – Strengthening protocols: (a) Pattern Roughing (PR); (b) Total Roughening - I (TR-I); (c) Total Roughening - II (TR-II); (d) Retarder Paper HEBAU “Green” (PHG); (e) Retarder Release Agent Ortolan SR (RAO).	206
Figure 5.4 – Textile reinforcements with the overlap for the external TRC strengthening. (a) C-MCF; (b) GP-MCF; (c) EP carbon fabric.	208
Figure 5.5 – Strengthening procedure with TRC composites. (a) Substrate moistening with the adopted strengthening protocol already executed and assembly of the strengthening mold; (b) Placement of the first fine-grained concrete matrix layer; (c) Positioned of the carbon textile reinforcement; (d) Placement of the second and last fine-grained concrete matrix layer and finishing operations.	209
Figure 5.6 – (a) Overview and (b) scheme of the experimental setup of the beams four-point bending tests.	211
Figure 5.7 – Detail of the strain gage placed on the textile reinforcements.	212
Figure 5.8 – Load vs. actuator displacement of the beams from (a) Batch 1 – PR-EP, PR-C, and PR-G; (b) Batch 2 – TR-I-EP, PHG-EP, and RAO-EP; (c) Batch 3 – TR-II-C and TR-II-G; and (d) Batch 4 – PHG-C and PHG-G.	213

- Figure 5.9 – Failure modes of the (a) REF; (b) PR-EP; (c) PR-C; (d) PR-G; (e) TR-I-EP; (f) PHG-EP; (g) RAO-EP; (h) TR-II-C; (i) TR-II-G; (j) PHG-C; (k) PHG-G beams. 217
- Figure 5.10 – Crack pattern at the actuator displacement (δ_{MTS}) of 2 mm, 3 mm, and 5 mm obtained from the DIC analysis for the (a) REF; (b) PR-EP; (c) PR-C; (d) PR-G; (e) TR-I-EP; (f) PHG-EP; (g) RAO-EP; (h) TR-II-C; (i) TR-II-G; (j) PHG-C; (k) PHG-G beams. 221
- Figure 5.11 – Load vs. deflection at midspan of the reference beam and the RC beams strengthened with the TRC with the C-MCF, GP-MCF, and EP carbon fabric at the a) 1st loading stage (pre-loading); and (b) 2nd loading stage. 225
- Figure 5.12 – Moment vs. curvature of the reference beam and the RC beams strengthened with the TRC with the C-MCF, GP-MCF, and EP carbon at the a) 1st loading stage (pre-loading); and (b) 2nd loading stage. 228
- Figure 5.13 – (a) Moment vs. textile curvature curve of the RC beams strengthened with the TRC with the C-MCF, GP-MCF, and EP carbon; and (b) zoom in the early stages. 230
- Figure 5.14 – Moment vs. textile curvature curve of the TR-I-EP, PHG-EP, and RAO-EP beams. 231
- Figure 5.15 – Cracking pattern of the (a) REF; (b) TR-I-EP; (c) PHG-C; and (d) PHG-G beams at the maximum load (equivalent to the SLS-DEF) and after unloading in the pre-loading stage. 232
- Figure 5.16 – Cracking pattern at different deflection levels in the second loading for the (a) REF; (b) TR-I-EP; (c) PHG-C; and (d) PHG-G beams. 236
- Figure 5.17 – Internal strain and stress distribution for the RC beams. 238
- Figure 5.18 – Constitutive laws assumed in the model for the (a) concrete in compression (adapted from [69]); (b) concrete in tension (adapted from Hinton and Owen apud [78]); (c) steel reinforcement in tension (adapted from [68]); (d) TRC strengthening layer. 239
- Figure 5.19 – Flow of steps to obtain the moment-curvature vectors of the reference beam. 241

Figure 5.20 – Moment vs. curvature curves. (a) Analytical for the reference and TRC strengthened beams; (b) zoom of the initial section of the curves in a; (c) Experimental and analytical curves for the reference beam; (d) Experimental and analytical curves for the TR-I-EP beam; (e) Experimental and analytical curves for the PHG-C beam; (f) Experimental and analytical curves for the PHG-G beam. 242

List of tables

Table 3.1 – Properties of the SIGRAFIL® C T50-4.4/255 – E100	74
Table 3.2 – Cement suspension composition	74
Table 3.3 – Geopolymer suspension composition	75
Table 3.4 – Technical data of the Solidian GRID Q85/85-CCE-21	75
Table 3.5 – Fine-grained concrete composition.	76
Table 3.6 – Average results and standard deviation (given in parenthesis) obtained from the yarn tension tests at different strain rates	87
Table 3.7 – Results obtained from the pull-out tests at different temperatures (average values, standard deviations are given in parenthesis).	102
Table 3.8 – Results obtained from the pull-out tests at different strain rates (average values, standard deviations are given in parenthesis).	115
Table 4.1 – Fine-grained concrete matrix composition and mechanical properties.	134
Table 4.2 – Technical data of the continuous carbon fiber tow (according to the supplier).	135
Table 4.3 – Technical data of the commercial carbon fabric (according to the supplier).	135
Table 4.4 – Cement-based suspension composition	136
Table 4.5 – Geopolymer suspension composition	136
Table 4.6 – TRC specimens for direct tensile tests	143
Table 4.7 – Average results and standard deviation of the MCF fabrics obtained from the direct tensile tests	149
Table 4.8 – Average results and standard deviation from the direct tensile tests on TRC	154
Table 4.9 – Average results and standard deviation obtained from the cracking analysis of the TRC specimens at the ultimate load in the direct tensile tests.	158

Table 4.10 – Average results and standard deviation obtained from the cracking analysis of the TRC specimens post-heating regime and post-testing at the ultimate load in the direct tensile tests.	161
Table 4.11 – Average results and standard deviation from the direct tensile tests on TRC after exposure to elevated temperatures	172
Table 5.1 – Technical data of the continuous carbon fiber tow according to the supplier.	200
Table 5.2 – Mineral suspensions compositions	200
Table 5.3 – Mechanical properties of the MCF fabrics according to [47].	200
Table 5.4 – Technical data of the commercial carbon fabric according to the supplier.	201
Table 5.5 – Fine-grained concrete matrix composition	201
Table 5.6 – Concrete composition and mechanical properties	202
Table 5.7 – Summary of the adopted strengthening protocols	204
Table 5.8 – Main results obtained for the reference and strengthened RC beams.	217
Table 5.9 – Main results obtained from the four-point bending tests for the reference and TRC-strengthened beams.	226
Table 5.10 – Number of cracks, mean spacing between cracks, and mean crack width at different deflection levels in both loading stages.	237
Table 5.11 – Limit parameters for the tri-linear tensile vs. strain analytical curve for the TRC.	240

*“Pra quem não sabia contar gotas
‘Cê aprendeu a nadar
O mar te cobriu sereno
Planeta marte
Sem ponto, sem vírgula, sem meia, descalça
Descascou o medo pra caber coragem
Sem calma, sem nada, sem ar.”*

Liniker

1 Introduction

1.1. Motivation

Concrete is one of the most used construction materials, mainly due to their ease of production, low cost, and ability to be molded in various shapes [1]. Steel Reinforced Concrete (RC) structures can suffer damages or even have their design purposes altered along their service life. From a sustainability point of view, it is more interesting to repair and strengthen these structures than demolishing and rebuilding. Over the years, different techniques and materials have been used with this intent. Textile Reinforced Concrete (TRC) is a fine-grained concrete reinforced with one or multiple layers of fabrics, which present elevated mechanical properties aligned with a high load-bearing capacity [2]. Due to the non-corrosive characteristic of the reinforcement textiles, the TRC can be fabricated with only a small thickness of the concrete cover, thus allowing the production of very thin elements with a low self-weight. Additionally, cementitious matrices present excellent thermal resistance [1], which is crucial to the structural safety in fire situations. The combination of these properties makes this material a suitable alternative for strengthening and repair of RC elements.

The mechanical characteristics of the TRC depend on the properties of the cementitious matrix and the textile reinforcement and also the interaction between these two phases. The amount and arrangement of the fibrous materials used in the textiles are parameters that significantly affect the mechanical capacity of the composite. The Young's modulus of the fibers must be higher than that of the cementitious matrix, and both high fiber tenacity and breaking elongation are required to obtain an effective reinforcement [2]. Since the cementitious matrix is alkaline [1], the fibers have to withstand this environment without losing their properties, guaranteeing the durability of the composite element. Alkali-resistant glass, carbon, and aramid fibers can be noted as examples of fibers that meet the requirements and can be used to produce textiles reinforcements [3].

Carbon fibers show elevated mechanical and durability properties [4–6] compared to other fibers materials. Moreover, due to modern fabrication technology, it is possible to economically produce carbon fabrics with reproducible and predictable properties. For those reasons, the use of carbon textiles as reinforcement in cementitious matrices is becoming extremely attractive. However, due to the hydrophobic property of the carbon fibers and the multifilament characteristic of the yarns, carbon fabrics present a low bond towards cementitious matrices, negatively affecting the TRC performance since this adhesion issues prevent the achievement of their ultimate strength capacity [7–10]. There are methods [7,11–14] that can be used to improve this fiber-matrix interaction and, consequently, enhance the mechanical response of the TRC, such as the polymeric impregnation [7,9,11,12,15], for example.

Still, this method might not be suitable for all applications, including fire situations. Due to the low thickness of the TRC, the textile reinforcement rapidly achieves highly degradable elevated temperatures. These polymers are commonly low thermal resistant [16,17], which makes the use of the TRC unfeasible in situations in which elevated temperatures may be involved. Recently, studies [7,8,13,14,18] have shown the viability of using mineral impregnations to increase the bond of carbon yarns toward the fine-grained concrete matrix. These studies have also shown a potentially increased thermal resistance of this impregnation without jeopardizing the TRC capacity.

Recently, at TU Dresden, Germany, a methodology to produce Mineral-Impregnated Carbon Fiber (MCF) yarns was developed [14,19,20]. This material achieved elevated mechanical properties, and due to its characteristics, it has the potential of, eventually, replacing carbon fabrics with polymeric coatings in situations that require thermal resistance. For this to happen, it is necessary to fully characterize the material, not only regarding its individual properties but also as a reinforcement of cementitious matrices. Thus, it is important to evaluate the bond of the MCF yarns towards cementitious matrices and the mechanical behavior of a TRC with MCF fabrics. Furthermore, the viability of such composites in structural applications must also be assessed so that, in a long-term perspective, this material could be used in practical applications.

1.2. Objectives

The main objective of this work is to assess the potential of a Mineral-Impregnated Carbon Fiber (MCF) fabric as a replacement for polymer-coated carbon fabrics in situations facing elevated temperatures. For this, two mineral impregnations were evaluated: a cement-based suspension and a geopolymer one investigated to overcome the disadvantage of the long curing period of cementitious materials. To accomplish the main objective, secondary goals were drawn as follows:

- Characterization of the MCF yarns in tension;
- Investigation of the bond of the MCF yarns towards a fine-grained concrete matrix at different elevated temperatures and strain rates;
- Characterization of a TRC with the MCF fabrics through direct tensile tests at room temperature and after submitting the specimens to a thermal regime;
- Analysis of the TRC with MCF fabrics in a structural application as strengthening in RC beams.

To analyze the effectiveness of the new MCF material, a currently commercially epoxy-coated (EP) carbon fabric was used as a comparison.

1.3. Thesis organization

The thesis is composed of this introduction, a literature review, followed by three chapters structured as individual full papers, conclusions and future work suggestions, as follows:

- **Chapter 1:** The introduction presents the motivation, objectives, and the structure of the study.
- **Chapter 2:** The literature review presents an overview of the Textile Reinforced Concrete (TRC) and its mechanical performance. The TRC use in structural applications is also assessed.
- **Chapter 3:** Bond behavior of polymer- and mineral-impregnated carbon fiber yarns towards concrete matrices at elevated temperature levels and different strain rates. Part of the results of this chapter have been

published in *Cement and Concrete Composites* (<https://doi.org/10.1016/j.cemconcomp.2022.104685>) [21].

- **Chapter 4:** Mechanical behavior of textile reinforced concrete with newly developed mineral-impregnated carbon fabrics submitted to uniaxial tensile loads and exposed to elevated temperatures.
- **Chapter 5:** Strengthening of RC beams using textile reinforced concrete (TRC) with polymer- and mineral-impregnated carbon fabrics.
- **Chapter 6:** The conclusion with the most relevant results of the previous chapters, followed by future works and suggestions.

It is important to mention that part of the experimental program, mainly Chapters 3 and 4, developed in this thesis was carried out at the Institute of Construction Materials, at the Technische Universität Dresden, Germany, under the supervision of Prof. Viktor Mechtcherine. This collaboration was part of the program Probral (project 8887.144079/2017-00), and the exchange period lasted 13 months between July 2019 and August 2020.

1.4. References

- [1] MEHTA, P. K.; MONTEIRO, P. J. M. **Concrete: Microstructure, properties and materials**. [s.l.] McGraw-Hill, 2006.
- [2] BRAMESHUBER, W. **Report 36: textile reinforced concrete-state-of-the-art report of RILEM TC 201-TRC**. [s.l.] Rilem publications, 2006.
- [3] PELED, A.; BENTUR, A.; MOBASHER, B. **Textile Reinforced Concrete**. [s.l.] CRC Press Taylor & Francis Group, 2017.
- [4] CHAND, S. Review - carbon fibers for composites. **Journal of Materials Science**, v. 35, n. 6, p. 1303–1313, 2000.
- [5] SAUDER, C.; LAMON, J.; PAILLER, R. The tensile behavior of carbon fibers at high temperatures up to 2400 °C. **Carbon**, v. 42, n. 4, p. 715–725, 2004.
- [6] ARBOLEDA, D.; BABAEIDARABAD, S.; NANNI, A. **Durability of fabric reinforced cementitious matrix (FRCM) composites**. 7th. International Conference of FRP Composites in Civil Engineering, International Institute for FRP in Construction. **Anais...International Institute for FRP in Construction**, 2014
- [7] DVORKIN, D.; PELED, A. Effect of reinforcement with carbon fabrics

impregnated with nanoparticles on the tensile behavior of cement-based composites. **Cement and Concrete Research**, v. 85, p. 28–38, 2016.

[8] NADIV, R. et al. Micro- and nanoparticle mineral coating for enhanced properties of carbon multifilament yarn cement-based composites. **Composites Part B: Engineering**, v. 111, p. 179–189, 2017.

[9] RAUPACH, M.; ORLOWSKY, J.; BÜTTNER, T. **Epoxy-impregnated textiles in concrete – Load bearing capacity and durability**. (J. Hegger, W. Bramehuber, N. Will, Eds.) ICTRC'2006 - 1st International RILEM Conference on Textile Reinforced Concrete. **Anais...Aachen: RILEM Publications SARL**, 2006

[10] PELED, A.; ZAGURI, E.; MAROM, G. Bonding characteristics of multifilament polymer yarns and cement matrices. **Composites Part A: Applied Science and Manufacturing**, v. 39, n. 6, p. 930–939, 2008.

[11] XU, S. et al. Bond Characteristics of Carbon, Alkali Resistant Glass, and Aramid Textiles in Mortar. **Journal of Materials in Civil Engineering**, v. 16, n. 4, p. 356–364, 2004.

[12] DONNINI, J.; CORINALDESI, V.; NANNI, A. Mechanical properties of FRCM using carbon fabrics with different coating treatments. **Composites Part B: Engineering**, v. 88, p. 220–228, 2016.

[13] PELED, A. et al. **Modifying carbon roving-cement matrix bond by inorganic coating**. High Performance Fiber Reinforced Cement Composites (HPFRCC7). **Anais...Struttgart, Germany: RILEM**, 2015

[14] SCHNEIDER, K. et al. Mineral-impregnated carbon fibre reinforcement for high temperature resistance of thin-walled concrete structures. **Cement and Concrete Composites**, v. 97, n. December 2018, p. 68–77, 2019.

[15] KRÜGER, M.; REINHARDT, H.-W.; FICHTLSCHERER, M. Bond behaviour of textile reinforcement in reinforced and prestressed concrete. **Otto-Graf-Journal**, v. 12, p. 33–50, 2001.

[16] BISBY, L. A.; GREEN, M. F.; KODUR, V. K. R. Response to fire of concrete structures that incorporate FRP. **Progress in Structural Engineering and Materials**, v. 7, n. 3, p. 136–149, 2005.

[17] SUMIDA, A.; MUTSUYOSHI, H. Mechanical properties of newly developed heat-resistant FRP bars. **Journal of Advanced Concrete Technology**, v. 6, n. 1, p. 157–170, 2008.

[18] LU, M. et al. Improved interfacial strength of SiO₂ coated carbon fiber in

cement matrix. **Cement and Concrete Composites**, v. 91, n. April, p. 21–28, 2018.

[19] MECHTCHERINE, V. et al. Mineral-impregnated carbon fiber composites as novel reinforcement for concrete construction: Material and automation perspectives. **Automation in Construction**, v. 110, n. September 2019, p. 103002, 2020.

[20] LIEBSCHER, M. et al. Influence of roller configuration on the fiber-matrix distribution and mechanical properties of continuously produced mineral-impregnated carbon-fibers (MCF). **Fibers**, v. 10, n. 5, p. 42, 2022.

[21] SILVA, R. M. DE C. et al. Bond behavior of polymer- and mineral-impregnated carbon fiber yarns towards concrete matrices at elevated temperature levels. **Cement concrete composite**, v. 133, p. 104685, 2022.

2 Literature review

2.1. Textile reinforced concrete

Textile Reinforced Concrete (TRC) is a cementitious matrix composite with one or multiple layers of fabrics made with several types of fibers. These composites present elevated mechanical and durability properties, thus being suitable for different load-bearing applications.

The cementitious matrix consists of a fine-grained concrete. The maximum aggregate size is in the order of 2 mm [1], which makes the matrix technically a mortar, so that a full penetration between the fabric mesh is achieved. Before the matrix cracking, both matrix and textile reinforcement work together, so it is interesting that the cementitious matrix presents adequate mechanical properties [2]. The addition of short fibers to the fine-grained concrete matrix can improve the pseudo-ductile behavior and refine the multiple-cracking pattern of TRC composites [3–6]. Depending on the type of fabric used, the cementitious matrix also has to fulfill some durability requirements. In the case of glass and natural fabrics, for example, some adjustments regarding the alkalinity of the cement-based matrix must be performed since such fibers can considerably deteriorate with a chemical attack by alkalis [7–11].

Regarding the reinforcement, yarns are made of several single filaments. The fineness of the yarn, expressed in tex (yarn linear mass density), depends on the number of filaments, the average filament diameter, and the fiber density [1]. The multifilament yarns assembled compose the fabric structure. The connection method of the yarns impacts the fabric geometry, properties, and handling [2]. Figure 2.1 presents different fabric structures base on the method of yarns connection. Woven fabrics are produced by interlacing two sets of yarn perpendicular to each other, crossing one over and the other under alternately (Figure 2.1.a). Knitted fabrics present interloped yarns with are pulled by spaced needles forming loops (stitches), see Figure 2.1.b. Braided fabrics are manufactured by intertwining sets of continuous yarns together (Figure 2.1.c). Bonded fabrics are

composed of two perpendicular sets of yarns glued at their junctions (Figure 2.1.d). This type of fabric exhibits strong connections, which allows a wide range of meshes, and the yarns are stretched in both directions. The fabric structure considerably influences the mechanical performance of the TRC [2]. Woven fabrics can improve the bond towards cementitious matrix due to their crimped structure that provides mechanical anchorage [12,13]. Complex yarn geometries, such as short weft knit fabrics, improve the TRC mechanical performance [14]. In the case of warp-knitted fabrics, increasing loop size enhances the composite performance [15]. Depending on the structure of the fabric, the transversal yarns can improve the bond of the textile towards the matrix, as in the case of woven fabrics, or hinder this bond, as in weft insertion knitted fabrics [14,16].

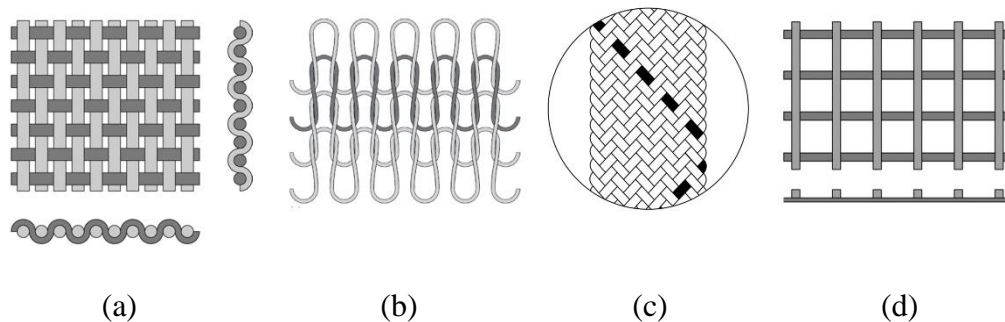


Figure 2.1 – Different connection methods of the yarns: (a) woven fabrics, (b) knitted fabrics, (c) braided fabrics, and (d) bonded fabrics (adapted from [2]).

Several types of fibers can be used to produce the fabrics. The mechanical properties of textile reinforced concrete are directly influenced by the mechanical properties of the fibers. Carbon fibers present elevated tensile strength and modulus of elasticity, with values ranging from 2500 MPa to 6000 MPa and 230 GPa to 600 GPa, respectively [2], depending on its precursor and fabrication process [17]. Moreover, carbon fibers exhibit excellent durability properties, with high resistance to acid, alkaline, and organic solvents [2,18,19]. For those reasons, they appear as an interesting alternative to be used as reinforcement in cementitious matrices. The main disadvantage of carbon fabrics is their hydrophobic characteristic, which prejudices the bond towards the hydrophilic cementitious matrix [19]. However, this can be managed by the use of special coatings, as will be discussed in Section 2.2.

2.2. Mechanical performance

The mechanical behavior principle of the TRC is the same as the fiber reinforced concretes (FRC). With the subsequent increase of the load, the tensile strength of the matrix is reached, leading to the formation of a crack in the matrix. After the first matrix crack, the load is transferred and supported by the textile reinforcement [1,20]. The quality of this transfer is mainly related to the bond properties between the fine-grained concrete matrix and the textile reinforcement. Therefore, the overall mechanical performance of a TRC is dependent on the properties of the cementitious matrix, the fabric, and the interaction between these two phases.

2.2.1. Bond Behavior

The load-bearing capacity of composite materials is influenced not only by the properties of the materials used but mostly by the bond between the reinforcement and the matrix. Textile reinforcements do not present a homogeneous cross-section, and thus their bond behavior towards cementitious matrices is affected by different mechanisms.

The yarns that compose the fabrics are made of several filaments that can be distinct into inner (or core) and outer (or sleeve) filaments [1], as shown in Figure 2.2.a. The cementitious matrix cannot penetrate the yarn due to an incompatibility between the cement particles sizes (usually in the range of 10 to 75 μm [21]) and the filament diameters (generally smaller than 9-15 μm , 13 μm , and 10 μm for AR-glass, basalt, and carbon [20,22], respectively). The outer filaments are directly anchored in the cementitious matrix and present a good bond performance. On the other hand, the inner filaments are relatively free inside the yarn, and the bond is guaranteed through friction between the filaments. Since the yarn is not fully anchored in the cementitious matrix, when the composite is loaded, the stress distribution in the yarn is not uniform, and the outer filaments fail first, increasing the first crack load. The failure of the inner filaments is characterized by a telescopic type of pull-out, in which the core filaments slip against the sleeve ones, as can be seen in Figure 2.3 [1,20,23,24]. A low sleeve-to-core ratio leads to low composites'

mechanical performance. An enhancement in this ratio promotes an improvement in the load transfer between the cracked matrix and the textile reinforcement, leading to a better mechanical performance of the composite [1,25,26]. Additionally, carbon fibers are naturally hydrophobic, which may further contribute to hindering the bond towards the hydrophilic cementitious matrix and, consequently, the composite performance [27].

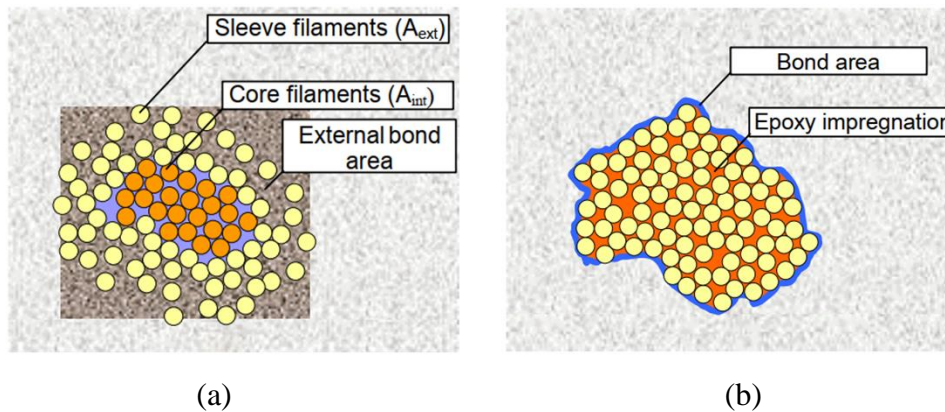


Figure 2.2 – Geometry of a multifilament yarn (a) plain and (b) epoxy-coated (adapted from [1]).

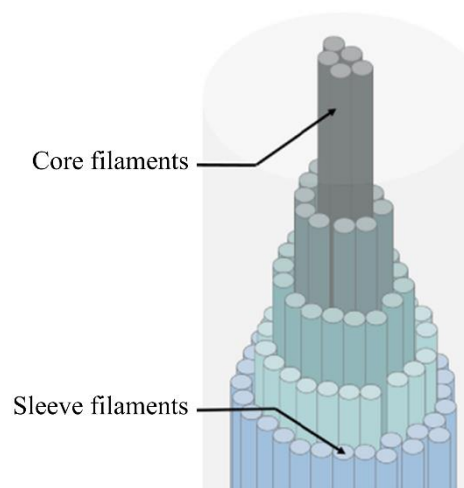


Figure 2.3 – Telescopic failure (adapted from [26]).

The use of polymeric impregnations is a well-established method to improve the bond of multifilament yarns toward matrices. Thermosetting or thermoplastic polymers fill the spaces between the filaments, and the yarn can be considered a rigid unit [25]. The slippage of the inner filaments is eradicated, and all filaments

are stressed uniformly, which enhances the composites' ultimate capacity [1]. Previous studies [23,26,28–30] have demonstrated an improvement in the mechanical performance of TRCs with polymer-impregnated carbon fabrics compared to TRCs with untreated carbon fabrics. The efficiency of the polymer impregnation is directly related to the nature of the resin. Epoxy resins are more effective than styrene-butadiene resins in improving the mechanical properties of carbon-TRCs, most probably due to their higher modulus of elasticity and shear modulus [30–33]. Nevertheless, in some tests, marked delamination associated with large spacing between cracks was observed in the composites reinforced with polymer-impregnated carbon fabrics [26]. This behavior can be associated with weak chemical compatibility between the hydrophobic polymer-impregnated fabric and the hydrophilic cementitious matrix [25]. The addition of a sand layer over the fresh polymer increases the friction and interlock mechanism, reducing the delamination [28,31,34].

Despite the significant advantages of using polymeric impregnations, these materials present low thermal resistance, which becomes an obstacle to their use. Carbon fibers can maintain good properties up to approximately 400 °C in an oxygen environment [17,35–37]. The tensile strength at 400 °C is approximately 80% of the value at room temperature [36]. However, polymer-coated carbon fibers are extremely affected due to the glass transition temperature (T_g) of the polymer materials, generally in the range of 50 – 180 °C [38,39], and the subsequent decomposition temperature of the polymer at temperatures between 300 °C and 400 °C.

Recently, mineral impregnations have been used to improve the bond between carbon fabrics and cementitious matrices. To bind all filaments and make the yarn work as a single unit, the particles must present an adequate size to penetrate the spaces of the multifilament yarns. Peled et al. [25], Dvorkin and Peled [26], and Nadiv et al. [27] showed that a micro-sized silica fume was able to provide an enhancement in the bond between the carbon yarn and the cementitious matrix, while a nano-silica considerably reduced the bond strength, due to an extensive agglomeration caused by the extraordinary fineness, in the range of 9 nm. In contrast, Lu et al. [40] observed an enhancement in the interfacial strength of nano-silica-modified carbon fibers towards a cementitious matrix. Schneider et al. [32] also demonstrated that finer particles can easier penetrate the carbon yarns, leading

to better bond levels towards cementitious matrices. However, the dispersion of these finer particles is not elementary. Special and intensive mixing techniques have to be applied to avoid agglomeration of the mineral particles, which could compromise the mechanical behavior of the composite. Furthermore, the amorphous silica content can produce a pozzolanic reaction with the calcium hydroxide (CH) of the cementitious matrix, enhancing the interaction between the reinforcement and the matrix [26,27]. For the proper infiltration of the mineral impregnation within the yarns, the fabrics cannot present a great amount of polymeric sizing, which is normally used in their fabrication. Nevertheless, Schneider et al. [41] showed that plasma treatment can be efficient in improving the interaction of an epoxy-sized carbon yarn coated with a mineral-based coating and, subsequently, the bond between these yarns and the concrete matrix. The plasma treatment may cause the surface of the carbon yarns, initially chemically inert, to have a higher polar portion, thereby increasing their affinity with the mineral coating and the cementitious matrix. The mineral coating adhered to the fiber surface increases its bond with the matrix due to friction and interlock mechanisms. Furthermore, these mineral impregnations present elevated thermal resistance. Schneider et al. [32,42] demonstrated that a micro-cement and micro-silica-based impregnation was able to enhance the bond behavior towards a cementitious matrix even at temperatures up to 500 °C. Moreover, this treatment with cement-based suspension has the potential for being implemented in automated processes [43,44]. However, the cement-based suspension exhibits a limited processing window due to its fast increased viscosity caused by the evolution of the hydration process.

The use of geopolymer binders is an interesting alternative to ensure the stable rheological properties necessary for the continuous production of mineral-impregnated carbon fibers. Geopolymer is a ceramic material produced through the combination of an alkali source with an aluminosilicate material, usually metakaolin and fly ash [45,46]. This class of material exhibit mechanical properties comparable to cement-based concretes [47–51] and excellent thermal stability over wide temperature ranges [47,52,53]. Moreover, when submitted to thermal curing (at approximately 100 °C), geopolymers are able to reach high strengths at very early ages [45,54,55]. Additionally, geopolymers seem to present a good bond with carbon fibers [56,57].

- Pull-out tests

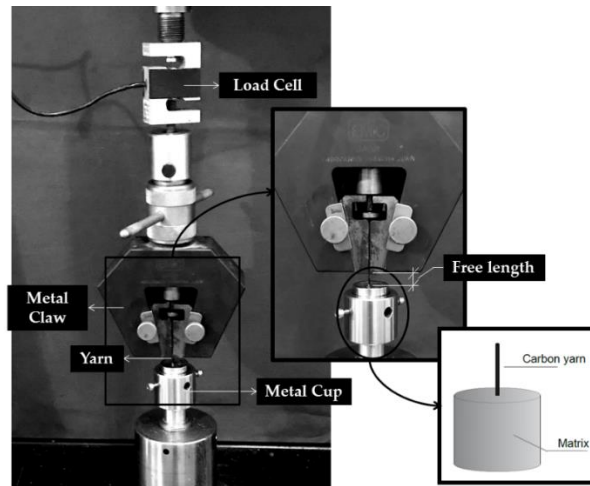
To investigate the bond behavior, usually, pull-out tests are performed. Different test configurations for yarns and textiles have been reported in the literature [1,31,32,34,58–60]. Up to the elaboration of this literature review, there is no standard establishing the parameters and configurations for pull-out tests, and, therefore, it is not adequate to perform a comparison between the results obtained with different setups.

One pull-out configuration is developed from tests in single-filament fibers [46,61,62] and consists basically of pulling out a yarn from a matrix specimen that is attached and confined into the machine [1,31,59,60]. Figure 2.4.a shows a setup from a pull-out test with carbon yarns. A variation of this method is presented in Figure 2.4.b, in which the yarn is embedded in two matrix blocks connected by a free length of this same yarn [32]. One of the blocks is pulled out by the machine promoting the pull-out of the embedded yarn in the opposite block. The pull-out results can be analyzed through the average interfacial shear stress that, although do not present a clear physical meaning since this approximation assumes a uniform interfacial shear stress distribution along the whole embedded length, still offers a good possibility to comparatively assess the quality of the bond. The average interfacial shear stress (τ) can be obtained through Equation 2.1.

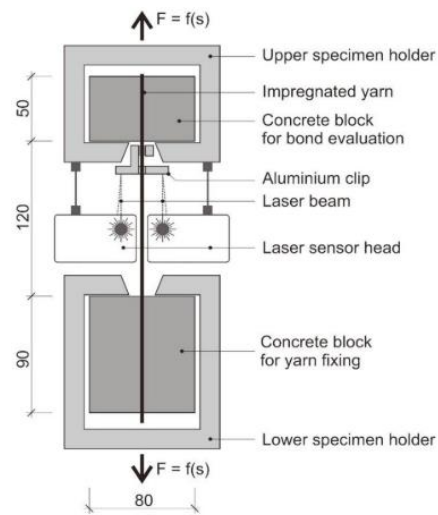
$$\tau = \frac{P}{2\pi r l_e} \quad (2.1)$$

where P is the pull-out load obtained from the test, l_e is the embedded length, and $2\pi r$ is the perimeter of the yarn cross-section.

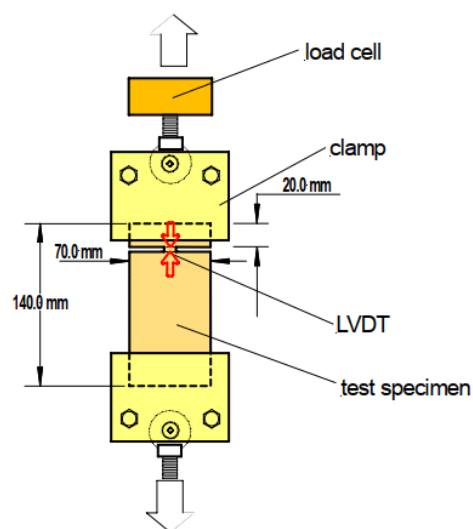
Another method to measure the bond-stress slip relation between the reinforcement and the matrix is through two-sided embedment pull-out tests [1,34,58,63]. In this type of test, TRC plates are manufactured, and a notch is made so that only one yarn is left intact in the middle of the specimen. Figure 2.4.c presents a schematic of this test setup. Only the yarn that remained intact will be pulled out from the matrix. This test configuration allows the measurement of the real material behavior as it occurs in a crack.



(a)



(b)



(c)

Figure 2.4 – (a) Pull-out test setup with single yarn [31]. (b) Variation of pull-out test with single yarn [32]. (c) Two-sided pull-out test setup [1].

2.2.2. Tension and flexural mechanical behavior

Textile Reinforced Concretes submitted to tensile or flexural loading present strain/deflection-hardening behavior with a multiple-cracking pattern [1]. The stress *vs.* strain curve usually is divided into three stages [1]. Figure 2.5 presents a typical stress *vs.* strain curve of TRCs obtained from direct tensile tests. Stage I corresponds to a linear-elastic region where both matrix and reinforcement behave linearly. This stage ends with the formation of the matrix's first crack. This point is known as the bending over point (BOP). With the subsequent increase of the strain more cracks are formed, characterizing Stage II. After the multiple cracking, the load-carrying capacity of the TRC does not reduce due to the ability of the fabric to provide ways to transfer the stresses through the cracks. Thus, in Stage III there is no formation of new cracks, and the widening of the existing cracks leads to a stretching of the fabric and posterior failure of the composite.

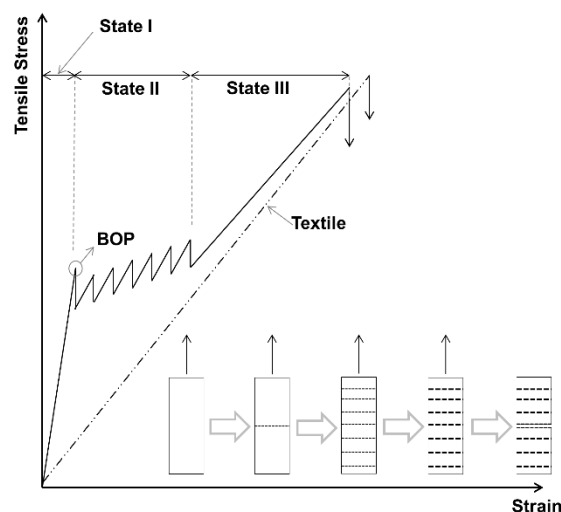


Figure 2.5 – Typical stress *vs.* strain curve of Textile Reinforced Concretes (TRC) obtained from direct tensile tests.

The load capacity and mechanical behavior of textile reinforced concretes under static and quasi-static loading conditions are influenced by the cementitious matrix and textile reinforcement properties and also by the interaction between these two phases [1]. The fiber material, the roving thickness, the reinforcement ratio and orientation, the fabric structure, and the coating material of the textile significantly affect the mechanical response of the composite.

The strength and modulus of elasticity of the textile reinforcements are related to the multiple-cracking behavior and load capacity of the TRC. Carbon fibers

present higher strength and higher ductility compared to other fibers generally used for textile reinforcement manufacturing [20,64]. Thus, their use as reinforcement in TRC would imply composites with elevated mechanical properties. Textile reinforced concrete with carbon fabrics presents higher tensile strength and modulus of elasticity than TRC with AR-glass [1,65] and basalt fabrics [65]. However, it is important to emphasize that the full textile capacity can only be achieved by guaranteeing a proper interaction between the fabric and the matrix. If the textile reinforcement does not develop an adequate bond towards the cementitious matrix, the stress transfer between the two materials is impaired, which can lead to premature failure of the composite, as discussed in Section 2.2.1. Silva and Silva [31] demonstrated that TRCs with carbon fabrics can present considerably distinguished ultimate mechanical capacity depending on the coating material of the fabric. Teixeira and Silva [66] and Souza et al. [67] developed a curauá-TRC that reached higher tensile strength than an SBR-coated-carbon-TRC [31], even the curauá fiber presenting tensile strength and modulus of elasticity about 2.2 and 8 times less, respectively, than the carbon fabric.

The TRC is a composite material, and, therefore, its mechanical capacity is influenced by the reinforcement ratio, which is the ratio of the textile reinforcement amount to the matrix amount. According to the rule of mixture, the upper limit composite properties are the weighted average of the properties of its components [20]. Thus, an increase in the reinforcement ratio leads to an increase in the load capacity of the composite [1,59]. Furthermore, the presence of two or more layers can also enhance the stress-hardening behavior due to a possible retarded cracking in the portion of the matrix between the fabric layers [31]. Previous studies demonstrate the effect of the enhancement in the number of textile layers in the mechanical response of TRC with AR-glass [68,69], basalt [22,70–72], carbon [31,73], sisal [74,75], jute [76], and curauá [67] fabrics. Nonetheless, Hegger et al. [77] observed a decrease in the tensile strength of an AR-glass-TRC with the enhancement in the textile layer, which was attributed to a reduction in the bond performance due to the influence of one fabric layer on the others. According to Colombo et al. [69] and Caggegi et al. [78], when two fabric layers are in direct contact without a matrix layer in between, there is the sliding of one fabric against the other, considerably affecting the bond of the textile reinforcement towards the cementitious matrix and, consequently, decreasing the composite response. The

hand lay-up technique used to manufacture the TRC can ensure a proper interface between the matrix and the textile reinforcement, guaranteeing that the fabrics will be in direct contact with the surrounding matrix.

The influence of the roving thickness and the coating applied to the fabric in the mechanical response of the TRC is related to the bond developed between the textile reinforcement and the cementitious matrix, discussed in Section 2.2.1. The multifilament nature of the yarns leads to two categories of filaments, the outer ones, directly anchored to the matrix, and the inner filaments, which are free to slip against each other. The proportion of inner and outer filaments directly influences the mechanical capacity of the composite [1]. The use of coating/impregnation materials is a well-established technique to increase the ratio between inner and outer filaments and, consequently, enhance the bond and the mechanical performance of TRCs [1].

2.2.3. Effect of temperature on the TRC mechanical behavior

In the design of buildings, human safety must be considered in case of a fire situation. The structural elements have to be able to retain a sufficient load-bearing capacity for a considerable period, allowing rescue operation. Concrete, further than retaining sufficient strength during fires, has the advantage of being incombustible and does not emit toxic fumes [21]. Many factors control the mechanical behavior of concrete at very high temperatures, such as its composition and permeability. Fine-grained concrete presents low pore volume, high cementitious materials content, and small aggregate size, thus microcracking is expected to be reduced. However, its microstructure changes with increasing temperatures. At approximately 100 °C, there is a loss of the physical and chemically bonded water. If the permeability of the concrete is such that does not allow water evaporation, vapor pressure will increase inside the element. When the vapor pressure reaches the tensile strength of the concrete, spalling will occur [21].

One of the major advantages of the TRC is the possibility of manufacturing thin structures due to the non-corrosive characteristic of the textile reinforcements that dismiss the need for large concrete covers. Thus, the TRC elements are prone to quick heating when exposed to fire, and due to the low thickness, the textile reinforcements must withstand very high temperatures, and its fire behavior is

crucial to the fire load-bearing capacity of the composite [1]. Carbon fibers present superior thermal resistance when compared to glass and aramid fibers [1], mainly due to their manufacturing process, which involves high temperatures for carbonization and graphitization processes [64]. However, as mentioned in Section 2.2.1, to improve the bond of these fibers towards the cementitious matrix and, consequently, the composite performance, the carbon fabrics usually present a polymeric impregnation. The most common polymers used present low thermal resistance, which significantly affects the coated-carbon-TRC behavior at elevated temperatures.

To evaluate and understand the behavior of TRC in a fire situation, mechanical tests are usually performed at different temperature levels. This type of approach, also referred to as in-situ, has the primary goal of characterizing the material response during a fire, and it is not trivial to be conducted. To understand the material's residual capacity, the specimens are submitted to a heating up to different target temperatures and a subsequent cooling regime before being tested.

2.2.3.1. In-situ mechanical behavior at elevated temperatures

To evaluate the mechanical response of TRC at elevated temperatures, direct tensile and bending tests are performed at those temperatures. Basically, two configurations are possible: steady-state and transient tests [79]. In the first, the specimen is submitted to the target temperature, and after an established exposure time, the load is applied. In the second configuration, the specimen is subjected to a pre-established load, and only then the temperature is varied.

Carbon-TRCs submitted to direct tensile loading were able to maintain their mechanical capacity in temperatures up to 120 °C [80], with a slight reduction of 11% in the tensile strength being observed at 120 °C [80]. As mentioned in Section 2.2.1, to improve the bond of carbon fabrics towards the cementitious matrix and, consequently, the composite performance, these textiles usually present a polymeric impregnation. The most common polymers used present low thermal resistance, which significantly affects the coated-carbon-TRC behavior at elevated temperatures. After the decomposition temperature of the polymeric coating is reached, the behavior of a coated-carbon-TRC is the same as the plain-carbon-TRC [1,63]. Donnini et al. [80] observed a reduction of 70% in the tensile strength of a

TRC with an epoxy resin and sand-coated carbon fabric submitted to 80 °C. Pull-out tests performed at this temperature level demonstrated a significant reduction in the bond between the coated fabric-matrix interface [80]. An SBR coating reduced the burning length capacity, i.e., the period of time that the specimens were able to withstand the stresses at the test temperatures, of a carbon-TRC I-shaped specimen submitted to 4-point bending test exposed to a fire condition [1].

The tensile stress level at which a TRC is subjected influences its mechanical response when exposed to high temperatures. Ehlig et al. [81] showed that above 65% of the composite tensile strength load level, local spalling occurs shortly before the failure, which took place between 400 °C and 600 °C, depending on the heating rate.

2.2.3.2. Residual mechanical behavior after exposure to elevated temperatures

Exposure to high temperatures affects the residual tensile strength of plain carbon yarns. According to [37], after an exposure of 30 minutes at 300 °C, no effect on the average tensile strength could be detected. Enhancing the exposition temperature to 500 °C, a 42% reduction in the carbon yarn tensile strength was observed. The residual tensile strength of carbon yarns is reduced to nearly zero after being exposed to 700 °C and 1000 °C [37].

A carbon-TRC can maintain its residual flexural behavior to temperatures up to 600 °C [82]. The addition of an epoxy coating, although considerably enhancing the mechanical behavior at room temperature, led to a total loss of load capacity at 400 °C [82]. As previously mentioned, polymeric coatings can considerably affect the mechanical behavior of the composites at high temperatures due to the low thermal resistance of the polymers. Besides the target temperature, the exposure time can also influence the mechanical response of coated-fabrics-TRCs. Xu et al. [83] showed that a TRC with an epoxy-coated carbon/AR-glass fabric can maintain its structural integrity and bending load-bearing capacity after a pre-heating up to 120 °C for 30 minutes. However, an increase in the pre-heating time to 90 minutes caused a slight decrease in the bending load-bearing capacity, which was attributed to the beginning of the epoxy resin degradation. On the other hand, Rambo et al. [22] showed that an increase in the exposure time from 1 to 3, and 6 hours did not

significantly influence the stress-strain relation of a polymer-coated basalt-TRC heated to 200 °C. A pre-heating up at 200 °C for 60 or 90 minutes greatly reduced the bending load-bearing capacity of a TRC with carbon fabric [82] and carbon/AR-glass fabric [83], both coated with epoxy resin, due to the degradation of the polymeric coating. At 400 °C, occurs the polymers' coating thermal decomposition, resulting in a nearly complete loss of the crack-bridging ability of the yarn [63]. Rambo et al. [22] observed an increase in the residual tensile strength of a styrene-acrylic latex coated-basalt-TRC after heating up to 150 °C, which was associated with an enhancement of the matrix-polymer interlock mechanism promoted by the heating followed by the cooling of the thermoplastic polymer. A subsequent increase in the target temperature led to a decrease in the tensile response, due to the coating's thermal decomposition and matrix dehydration, until the complete TRC failure at temperatures ranging from 600 °C to 1000 °C.

2.2.4. Effect of load rate on the TRC mechanical behavior

During their lifetime, structures may be subject to dynamic loadings from earthquakes, wind gusts, wind-driven objects, fast-moving traffic, machine vibrations, blast explosions, and projectiles. In these cases, the structure element is subjected to very high strain rates due to a large amount of energy that is transmitted to it in a very short period of time [84]. TRC exhibits high energy absorption capacity under static or quasi-static conditions. For this reason, its use in applications subject to dynamic loading seems to be quite promising.

Mechanical characteristics of materials subjected to high strain rates can be different from those obtained under static or quasi-static loading (low strain rates). In a quasi-static situation, the element is in a static balance, and the sum of the forces acting on it is approximately equal to zero. There is a sequence of equilibrium states. In dynamic situations, the loading rate applied is very high, and therefore only a part of the element is stressed. The stress and its associated deformation have to pass through the material at a specific speed. Dynamic deformation occurs through the propagation of waves [85].

Several experimental techniques exist to investigate high strain rate properties: split Hopkinson pressure bar (SHPB), falling weight devices, Charpy, Izod, fly-wheel facilities, hydraulic machines, and others [86–88]. Nonetheless,

there is a lack of a general agreement of standards and methodologies to study the behavior of materials subjected to dynamic conditions because of problems that appear at high rate loading due to inertial effect, non-uniform loading, and difficulties in measuring a reliable mechanical characteristic of the materials [87]. Therefore, the dynamic properties of a material can be extremely dependent on the loading rate, testing method, and sample geometry.

In order to properly design a composite system subjected to dynamic conditions, the strain rate sensitivity of the material has to be measured, and the modes of failure and energy absorption well characterized. The mechanical properties of cement-based composites are highly dependent on the loading rate due to the rate-dependent nature of the material [86].

Under direct tensile loadings, TRC with AR-glass [87,89–91], carbon [87], polyethylene (PE) [87], polypropylene (PP) [91], and sisal [92] fabrics exhibited a strain-hardening behavior with multiple-cracking even at dynamic conditions. Zhu et al. [87] observed the same pattern between the properties of the textile reinforcement and the composite at high strain rates and quasi-static conditions. Compared to quasi-static tests, the TRC with AR-glass [86,90] and sisal fabrics [92] achieved higher tensile strength at higher strain rates. However, Silva et al. [89] noted that, when shifting from the quasi-static to the dynamic situation, there is a drop in the tensile strength of AR-glass-TRCs, which was attributed to a possible strain rate effect on the glass fibers and stress concentrations in regions close to the lower grips during high-speed tensile tests. The TRC with PE fabric showed a similar level of tensile strength at quasi-static and high speed [87]. For carbon-TRCs, Gong et al. [6] observed a pronounced increase in the tensile strength of carbon-TRCs at dynamic loadings, while Zhu et al. [87] observed a decrease in this property. Similar to quasi-static situations [5,93], the addition of short fibers promotes a finer crack pattern due to the capacity of the short fibers in bridging the micro-cracks and enhancing load transfer [6,90]. However, different from static results, the short fibers were not able to contribute to an increase in an AR-glass-TRC tensile strength at all high strain rates [90]. Gong et al. [6], on the other hand, observed an increase in the tensile strength of a carbon-TRC with the addition of PBO and PE short fibers. However, it is important to emphasize that the plain carbon-TRC was not able to achieve a strain-hardening behavior due to the fabric's lack of anchorage length imposed by the test configuration [94].

The evaluation of dynamic properties has also been reported through impact tests [84,86,95,96]. Compared to Fiber Reinforced Concrete (FRC), the TRC exhibited higher performance under dynamic conditions [95]. The direction of the impact considerably influences the response of the TRC. A TRC submitted to an impact loading parallel to the textile reinforcement presents a ductile behavior with relatively low stiffness, while a TRC under an impact loading perpendicular to its textile reinforcement exhibits relatively brittle behavior and higher stiffness [84,95]. Furthermore, the perpendicular impact results in significantly higher load-carrying capacity, and the failure mode of the composite is characterized by a not complete fracture [84]. For specimens submitted to parallel impact, the damage process was initiated by the formation and distribution of flexural cracks, and the failure mode is characterized by matrix cracking and delamination [84,86]. Compared to quasi-static test, sisal-TRC submitted to impact loads presented no significant variation in the ultimate strength, but an increase in the dissipated energy was observed [86]. The same pattern was observed for an AR-glass-TRC with a low reinforcement ratio, while for high reinforcement ratio, an enhancement in the ultimate flexural stress was noted with the increase of the strain rate [97]. For basalt-TRC, the maximum impact force and energy absorption increase with increasing impact velocity [96].

2.3. Structural applications

Focusing on sustainability, the use of new materials and technologies that saves natural resources is rapidly increasing. Textile reinforced concrete (TRC) is a new composite material consisting of a cementitious matrix and non-corrosive fabrics. The fabrics are not subjected to corrosion damage, which allows for very thin concrete covers. The thinner required concrete cover reduces the required amount of cement, reducing CO₂ emissions.

The elevated load-bearing capacity, excellent mechanical behavior, and reduced low weight possible make the TRC an outstanding material for the production of thin elements. Several studies already show the potential of the TRC in thin structures [98–106], such as slabs, self-supporting sandwich panels, shell structures, and as external strengthening of existing structures [107–114].

Nevertheless, to enhance the use of this material in a large scale is necessary to establish a design guide for TRC structures.

2.3.1. New load-bearing elements

Several regions of the world face hard winters, with negative temperatures and snow. It is a common practice in these places to use salt to accelerate the de-icing of streets, roads, and parking garages. This leads to high chemical concentrations over time and considerable damage to concrete structures due to the corrosion of the steel reinforcement [21]. To avoid or reduce those damages, it is necessary to apply an expensive protection system, such as special coatings, or use special concrete mixtures to compose the structures. When using textile reinforced concrete instead of steel reinforced concrete, those expensive protection systems are no longer necessary since the textile reinforcements are non-corrosive. Furthermore, as the concrete cover around the reinforcement is not needed for the durability of the structure, and only to transfer the external loads to the reinforcement, the amount of concrete used can be reduced [98].

Schumann et al. [98] showed the potential of carbon-TRC parking slabs. The thickness of the TRC slab was 50% lower than a steel reinforced concrete slab. A new design anchorage was developed to overcome the increased anchorage length required by the textile reinforcement due to its superior ultimate load. An analytical model based on the bending model for steel reinforced concrete was effective to determine the mechanical capacity of the TRC slab.

May et al. [99] developed and investigated a new lightweight precast ceiling slab made of carbon-TRC based on a flat pressure arch. Compared with a standard RC slab with a full cross-section and the same span, the new ceiling system was able to reduce the self-weight by 50%. The experimental results obtained for the deflection of the slab due to creep and shrinkage for 6 months were considerably smaller than the predicted value obtained through the Eurocode 2 [115]. Additionally, the failure load was 12 times higher than the predicted service load.

The slenderness of shell structures is achieved by the activation of membrane action to carry external loads. Until the late 1960s, shell structures were commonly used. However, these structures were mainly plane and straight, with a large cross-section and a high amount of reinforcement [106]. Due to the flexibility of the

reinforcement and elevated mechanical properties, TRC can be used to produce complex geometry elements. The bearing capacity can be improved, especially by the formation of two-dimensional building components. The easy forming of the textiles enables a simple realization of curved surfaces, such as shell elements [101,106].

One-way shells, such as cylindrical shells, are commonly used to roof structures. They are often supported continuously over their edges, and the outer loadings are transmitted to the supports by membrane action. The roof can consist of one large cylindrical shell cast onsite. With this method, large spans can be achieved, and no supporting structure is necessary. However, the formwork setup of curved elements is complex, time-consuming, and has elevated costs. To avoid these disadvantages, the roof structure can be composed of several small shells or segments of shells that can be pre-cast. Though, in these cases, usually, it is necessary a supporting structure consisting of girders and/or columns, which limits the flexibility of the building [106]. According to Hegger et al. [101], in the case of barrel shell roofs, the shell effect of thin concrete elements can be very effective. With low TRC thickness, the structure is extremely lightweight, and the shell is rigid in both longitudinal and lateral directions. The utilization of shotcrete facilitates the production of such structures, besides allowing the concrete and reinforcement placement in alternating layers.

Domes, cooling towers of power plants, and doubly curved roof structures are examples of shells with multi-axial load transfer. While the first two structures are supported relatively in a continuum way over the free edges, the last one is often supported locally only at some edges or at columns [106]. Usually, these shell structures are cast on-site, which results in the time-consuming and cost-intensive building of formwork and reinforcement positioning. Hegger et al. [106] demonstrated the applicability of a TRC shell structure with two layers of carbon fabric. The building concept developed consisted of doubly curved, triangular shell elements with a maximum edge length of approximately 5 m and a structural thickness of 40 mm. The concrete was pumped into an enclosing formwork to achieve double-sided exposed concrete quality. The load-bearing-TRC shells can be mounted and disassembled as often as required. Scholzen et al. [116,117] described the structural design and the construction method of a pavilion with a roof structure made of carbon-TRC shell. The load-bearing structure is composed of four

shells, each one supported by a steel reinforced concrete column at the center. The TRC shells were produced as precast parts, and they were connected to each other and to the column through prestressed bolts.

The high ductility of TRC shell structures is obtained through the material strain-hardening behavior and the stress redistribution over large zones of the shell. Sharei et al. [105] performed a finite element simulation and a large-scale test of a TRC vault shell serving as a roof structure over a bicycle stand to validate a modeling approach for the design of shell elements. The test setup aimed to obtain the structural behavior with a high degree of stress redistribution and damage propagation through the shell. Therefore, local failure of a cross-section due to high local bending and local shear failure near the supports was avoided. Slight differences between the test results and the simulation were observed. These differences were caused by imperfections in the shell geometry, which induced nonsymmetric deformation. Further studies on the sensitivity of TRC shell structures' structural behavior concerning geometric imperfections caused during casting are necessary.

Precast concrete sandwich panels are used worldwide to provide an insulated outer shell to buildings, thus reducing heating and cooling costs for the structure [118]. Usually, structural sandwich elements consist of a structural load-bearing layer, a heat insulation layer, and an outer-facing layer. Mostly this last layer does not have a structural function. Nevertheless, when it is made of concrete, it is necessary a steel reinforcement to support constraint forces caused by deformations induced by temperature and shrinkage. Therefore, it is crucial a minimum concrete cover to protect the bars from corrosion, and the sandwich element has an elevated thickness and, consequently, self-weight. TRC seems to be an interesting alternative to the outer-facing layer, also acting as the load-bearing one. In this case, it is possible to reduce the overall thickness of the element by about 5 to 6 cm [101]. The use of TRC as inside and outer facings combined with sustainable, heat-insulating rigid polyurethane (PU) foam allows the construction of lightweight sandwich structures with large spans. Hegger et al. [101] produced sandwich elements with PU rigid foams as the core layer and TRC-facings with spans of 1.90 m and 4.90 m and verified a satisfactory load-bearing behavior under bending. The sandwich elements technology can also be applied to design modular buildings consisting of load-bearing and demountable sandwich elements for walls and

roofing [101]. Hegger et al. [119] demonstrated the successful application of an AR-glass-TRC cladding panel as an exterior façade in a pilot project, at the Institute for Structural Concrete, at the Technical University of Aachen, Germany.

2.3.2. Strengthening of existing structures

Structural elements are prone to suffer damage during their service life, implying repair procedures. In some cases, it is necessary to strengthen a structure due to changes in its loading condition. Nowadays, there are several repair and strengthening methods, from more traditional techniques, such as cross-section enlargement [120–123] and external prestressing with tendons [124–127], to more recent fiber-based composite systems [128–134].

Fiber-Reinforced Polymers (FRPs) are composites of a polymeric matrix reinforced with different types of fibers, such as aramid, carbon, and glass [135]. Due to the polymer nature of the matrix, this strengthening system does not present great resistance in case of fire situations. Most polymeric materials present low thermal resistance, with their decomposition at low-temperature levels [136,137]. Additionally, the FRP exhibits an incompatibility with concrete substrates, which can lead to long-term durability issues [135,138]. In this scenario, the Textile Reinforced Concrete has gained attention. The organic cementitious matrix presents elevated temperature resistance [21]. Moreover, the textile reinforcements used in the TRC are non-corrosive [2], which reduces the required concrete cover, allowing the manufacturing of thin elements with reduced self-weight. The TRC characteristic, i.e., low weight and high mechanical and durability properties, make it an outstanding material to be used for the strengthening and repair of RC structures, with the extra advantage of presenting good compatibility to concrete substrates.

Previous studies have shown that the TRC can be successfully used for flexural and shear strengthening, enhancing the bending [66,107–109,139–145] and shear capacity [107,110,146,147] of RC elements; column confinement [111,112,148,149]; and seismic upgrading [112].

Brückner et al. [107], Larbi et al. [144], and Verbruggen et al. [143] demonstrated the enhancement of the load-bearing capacity of RC beams strengthened with a glass TRC. Furthermore, the TRC-strengthening was able to

better control the cracking behavior, increasing the serviceability of the RC element. Ambrisi and Focacci [108] showed that carbon- and PBO-TRCs were able to increase the maximum load of RC concrete beams. The rupture of the strengthened beams was associated with the loss of strengthening action of the TRC layer due to the fibers debonding. Ombres [109] and Babaeidarabad et al. [142] also demonstrated the ability of a PBO-TRC to increase the bending load performance of RC beams. The failure mode was directly related to the amount of textile reinforcement; higher PBO layers led to beam premature failure due to debonding of the TRC-strengthening system. Gopinath et al. [145] demonstrated that a basalt-TRC strengthening was able to increase the energy absorption and ductility of RC beams under monotonic and low-cycle fatigue loading. Teixeira and Silva [66] observed an increase in the maximum load of RC beams strengthened with a curauá-TRC-like composite submitted to bending tests. Hadad et al. [139] showed an increase in the ultimate capacity of RC beams strengthened with a carbon-TRC.

The effectiveness of glass, carbon, and basalt-TRC in enhancing the shear loading capacity of RC beams was demonstrated by Brückner et al. [107], Azam and Soudki [146], and Al-Salloum et al. [110]. Teixeira et al. [147] achieved a stiffness enhancement of an RC beam with a U-wrapped curauá-TRC-like strengthening. According to Al-Salloum et al. [110], the effect of the textile orientation and the matrix mechanical properties increases with the increase in the number of textile layers. For rectangular beams, the ultimate load of the TRC-strengthened beam is not considerably affected by a fully wrapped, U-shaped, or bonded-sided anchorage system [107,146], which is attributed to enough anchorage length to fully transfer all tensile forces from the textile reinforcement to the concrete within the compression zone of the beams [107]. On the other hand, T-shaped beams require a mechanical anchoring system to guarantee adequate tensile forces transfer [107].

Peled [111], Ortlepp et al. [148], and Triantafillou et al. [149] observed an enhancement in the ultimate load of concrete cylinders strengthened with a TRC reinforced with carbon, glass, Kevlar, PP, and PE fabrics due to hoop effect provided by strengthening system [111]. Bournas et al. [112] demonstrated that carbon and glass-TRC jackets are able to increase the cyclic deformation capacity and energy dissipation of RC columns with poor detailing by delaying the steel bars buckling and preventing splitting bond failures at columns with inadequate overlap

lengths. The enhancement in the compression properties of the confined concrete is associated with the textile reinforcements properties [111]. The number of textile reinforcement layers also influences the ultimate load capacity [148,149]. For confinement strengthenings, the fabric stiffness can considerably difficult the application of the TRC to the concrete substrate. The use of low-modulus fabrics, such as PP and PE textiles, can facilitate this procedure [111].

Nowadays, it is possible to find in the technical literature examples of the use of TRC as a strengthening system of existing structures all over the world [138,150–152]. In Italy, the flexural and shear capacity of the RC beams of the Stadium San Siro was increased with a carbon-TRC [150]. Also in Italy, the vaults of a concrete bridge were strengthened with a PBO-TRC aiming to change the failure mechanism of the structure and increase its safety [138]. Butler et al. [151] reported the strengthening of a roof shell that presented large deformations with a carbon-TRC in Germany. In Russia, an RC bridge pier was strengthened with a PBO-TRC after a repair with epoxy resin failed [138]. A PBO-TRC was chosen to increase the circumferential flexural strength of a tunnel lining in Greece [138]. A carbon-TRC was used for strengthening a concrete roof that presented insufficient load-carrying capacity and, due to monument conservation, could not withstand a new structure system [151]. In Brazil, some of the columns of the Maracanã Stadium were strengthened with a carbon-TRC to support the additional loads from a new roof structure [150,153,154]. The carbon-TRC was also used to reinforce part of the old stadium tiers. The strengthening was performed by S&P Clever Brasil and Figure 2.6 shows the TRC application. A carbon-TRC was also used to strengthen a motorway bridge, in Germany, aiming to increase its lifespan [152]. Another bridge in Germany, considered a historic monument, was also strengthened with a carbon-TRC due to corrosion damages in the structure [152].

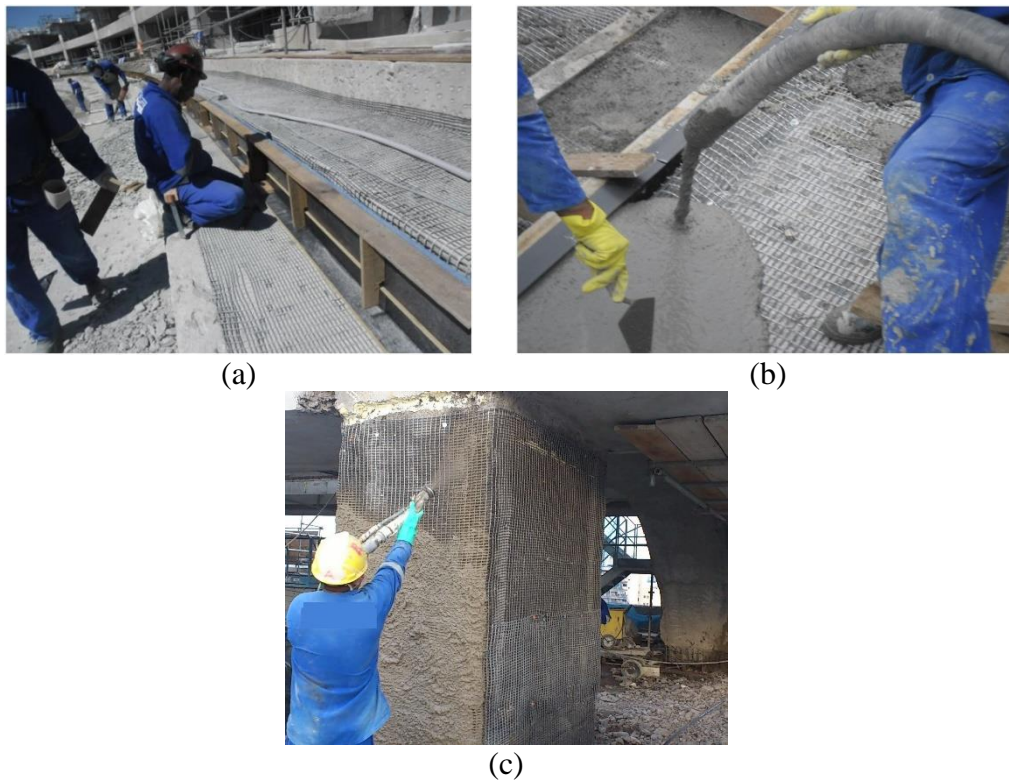


Figure 2.6 – Application of the TRC strengthening in the Maracanã Stadium, Brazil, performed by the S&P Clever Brasil company [153].

One concern regarding the use of TRCs as strengthening is related to the adhesion between the TRC and the concrete substrate of the RC element. The bond models developed for FRP and steel plate strengthening systems, basically based on adhesive bond laws with the assumption of slip in the adhesive joint, are not valid for the TRC strengthening [155]. According to Ortlepp et al. [156], there are three characteristic failure modes in a TRC-strengthened RC element: i) failure of the TRC layer characterized by the delamination in the textile layer; ii) failure in the substrate/TRC-strengthening interface; iii) failure in the RC element. The first and third modes depend mainly on the individual mechanical capacity of the TRC and RC elements. The second mode is related to the bond between the old and new concretes and can be avoided with an adequate pre-treatment of the RC surface. The sandblasting of the concrete substrate, followed by the casting of the TRC directly to the RC element, improves the bond by creating a strong interlocking between the old concrete and the TRC-strengthening layer [155]. Additionally, the multiple-cracking behavior of the TRC leads to discontinuities of the strain behavior in the bond area with the RC substrate [155]. Usually, single- and double-lap shear tests are performed to analyze the bond behavior between the TRC-strengthening layer

and the concrete substrate. Most studies are carried out taking into account a pre-treatment of the concrete substrate, either with sandblasting [157–160] or water jetting [161]. Results obtained without any substrate pre-treatment can also be found, although in lesser frequency [159,162]. Several factors can influence the bond capacity of TRC-strengthening systems towards concrete substrates, such as the TRC properties, which are directly related to the bond between the textile reinforcement and the fine-grained concrete matrix [161,162]. The effect of the number of textile reinforcement layers in the bond behavior depends on the failure mode of the strengthened beams [161]. For elements presenting a failure in the textile-matrix interface, the increase in the number of textile layers leads to an increase in the bond behavior due to a lower shear stress per unit area of the textile for a particular load [161]. On the other hand, when the failure occurs in the interface of the strengthening and the concrete substrate, the addition of textile layers leads to an enhancement in the strengthening thickness and, thus, to a lower bond capacity [161,163]. According to D’Antino et al. [159], the substrate preparation has a limited role in the bond between the TRC strengthening and the concrete element. However, pre-existing cracks in the TRC matrix, due to shrinkage, for example, can negatively affect the bond behavior and lead to premature failure of the strengthened element due to detachment of the TRC layer. The bond length also impacts the bond behavior, with higher bond lengths leading to higher bond capacity [157,161,162]. For bond lengths higher than an effective bond length, this enhancement can be attributed to an increase in the interlocking mechanism [160–162]. Differently from what is observed in FRP systems, the width of the TRC strengthening does not considerably affect the bond behavior between the strengthening layer and the concrete substrate, which is attributed to the independent behavior of the longitudinal yarns of the textile reinforcement [157,158].

2.4. References

- [1] BRAMESHUBER, W. **Report 36: textile reinforced concrete-state-of-the-art report of RILEM TC 201-TRC**. [s.l.] Rilem publications, 2006.
- [2] PELED, A.; BENTUR, A.; MOBASHER, B. **Textile Reinforced Concrete**. [s.l.] CRC Press Taylor & Francis Group, 2017.

- [3] BUTLER, M.; HEMPEL, R.; SCHIEKEL, M. **The Influence of short glass fibres on the working capacity of textile reinforced concrete.** (J. Hegger, W. Bramehuber, N. Will, Eds.)Textile reinforced concrete: Proc. of the 1st International RILEM Symposium. **Anais...RILEM**, 2006
- [4] HINZEN, M.; BRAMESHUBER, W. **Influence of short fibres on strength, ductility and crack development of textile reinforced concrete.** Proceedings of the Fifth International RILEM Workshop on High Performance Fiber Reinforced Cement Composites (HPFRCC5). **Anais...RILEM Proceedings PRO**, 2007
- [5] BARHUM, R.; MECHTCHERINE, V. Effect of short, dispersed glass and carbon fibres on the behaviour of textile-reinforced concrete under tensile loading. **Engineering Fracture Mechanics**, v. 92, p. 56–71, 2012.
- [6] GONG, T. et al. The impact-tensile behavior of cementitious composites reinforced with carbon textile and short polymer fibers. **Applied Sciences**, v. 9, p. 4048, 2019.
- [7] MAJUMDAR, A. J.; WEST, J. M.; LARNER, L. J. Properties of glass fibres in cement environment. **Journal of Materials Science**, v. 12, p. 927–936, 1977.
- [8] BUTLER, M.; MECHTCHERINE, V.; HEMPEL, S. Experimental investigations on the durability of fibre-matrix interfaces in textile-reinforced concrete. **Cement and Concrete Composites**, v. 31, n. 4, p. 221–231, 2009.
- [9] TOLÊDO ROMILDO D., F. D. et al. Development of vegetable fibre-mortar composites of improved durability. **Cement and Concrete Composites**, v. 25, n. 2, p. 185–196, 2003.
- [10] WEI, J.; MEYER, C. Degradation mechanisms of natural fiber in the matrix of cement composites. **Cement and Concrete Research**, v. 73, p. 1–16, 2015.
- [11] SOUZA, L. O. DE; SOUZA, L. M. S.; SILVA, F. DE A. **Study of Cracking Pattern and Its Evolution on Natural Textile Reinforced Concrete By Image Analysis.** 4th Brazilian Conference on Composite Materials. **Anais...2018**
- [12] PELED, A.; BENTUR, A.; YANKELEVSKY, D. Woven fabric reinforcement of cement matrix. **Advanced Cement Based Materials**, v. 1, n. 5, p. 216–223, 1994.
- [13] PELED, A.; BENTUR, A. Reinforcement of cementitious matrices by warp knitted fabrics. **Materials and Structures**, v. 31, n. 8, p. 543–550, 1998.
- [14] PELED, A.; BENTUR, A. Geometrical characteristics and efficiency of textile fabrics for reinforcing cement composites. **Cement and Concrete Research**, v. 30,

n. 5, p. 781–790, 2000.

[15] PELED, A. et al. Influences of textile characteristics on the tensile properties of warp knitted cement based composites. **Cement and Concrete Composites**, v. 30, n. 3, p. 174–183, 2008.

[16] BENTUR, A.; PELED, A. **Cementitious composites reinforced with textile fabrics**. Workshop on High Performance Fiber Reinforced Cement Composites (HPFRCC 3). **Anais...RILEM Publications**, 1999Disponível em: <http://apps.isiknowledge.com/full_record.do?product=UA&search_mode=GeneralSearch&qid=3&SID=T1pkhhwuy1CgynLww4t&page=1&doc=1>

[17] CHAND, S. Review - carbon fibers for composites. **Journal of Materials Science**, v. 35, n. 6, p. 1303–1313, 2000.

[18] DIVISION, M. D. Review Carbon fibre-reinforced cement. **Symposium A Quarterly Journal In Modern Foreign Literatures**, v. 12, 1977.

[19] MORGAN, P. **Carbon Fibers and their Composites**. [s.l.] CRC Press, 2005.

[20] BENTUR, A.; MINDESS, S. **Fiber Reinforced Cementitious Composites**. [s.l.] CRC Press, 2006.

[21] MEHTA, P. K.; MONTEIRO, P. J. M. **Concrete: Microstructure, properties and materials**. [s.l.] McGraw-Hill, 2006.

[22] RAMBO, D. A. S.; SILVA, F. DE A.; TOLEDO FILHO, R. D. Effect of elevated temperatures on the mechanical behavior of basalt textile reinforced refractory concrete. **Materials and Design**, v. 65, p. 24–33, 2015.

[23] RAUPACH, M.; ORLOWSKY, J.; BÜTTNER, T. **Epoxy-impregnated textiles in concrete – Load bearing capacity and durability**. (J. Hegger, W. Bramehuber, N. Will, Eds.)ICTRC'2006 - 1st International RILEM Conference on Textile Reinforced Concrete. **Anais...Aachen: RILEM Publications SARL**, 2006

[24] PELED, A.; ZAGURI, E.; MAROM, G. Bonding characteristics of multifilament polymer yarns and cement matrices. **Composites Part A: Applied Science and Manufacturing**, v. 39, n. 6, p. 930–939, 2008.

[25] PELED, A. et al. **Modifying carbon roving-cement matrix bond by inorganic coating**. High Performance Fiber Reinforced Cement Composites (HPFRCC7). **Anais...Struttgart, Germany: RILEM**, 2015

[26] DVORKIN, D.; PELED, A. Effect of reinforcement with carbon fabrics impregnated with nanoparticles on the tensile behavior of cement-based composites. **Cement and Concrete Research**, v. 85, p. 28–38, 2016.

- [27] NADIV, R. et al. Micro- and nanoparticle mineral coating for enhanced properties of carbon multifilament yarn cement-based composites. **Composites Part B: Engineering**, v. 111, p. 179–189, 2017.
- [28] DONNINI, J.; CORINALDESI, V.; NANNI, A. Mechanical properties of FRCM using carbon fabrics with different coating treatments. **Composites Part B: Engineering**, v. 88, p. 220–228, 2016.
- [29] XU, S. et al. Bond Characteristics of Carbon, Alkali Resistant Glass, and Aramid Textiles in Mortar. **Journal of Materials in Civil Engineering**, v. 16, n. 4, p. 356–364, 2004.
- [30] KRÜGER, M.; REINHARDT, H.-W.; FICHTLSCHERER, M. Bond behaviour of textile reinforcement in reinforced and prestressed concrete. **Otto-Graf-Journal**, v. 12, p. 33–50, 2001.
- [31] SILVA, R. M. DE C.; SILVA, F. DE A. Carbon textile reinforced concrete: materials and structural analysis. **Materials and Structures/Materiaux et Constructions**, v. 53, n. 1, 2020.
- [32] SCHNEIDER, K. et al. Mineral-impregnated carbon fibre reinforcement for high temperature resistance of thin-walled concrete structures. **Cement and Concrete Composites**, v. 97, n. December 2018, p. 68–77, 2019.
- [33] RAMPINI, M. C. et al. Mechanical Behaviour of TRC Composites: Experimental and Analytical Approaches. **Applied Sciences**, v. 9, n. 7, p. 1492, 2019.
- [34] XU, S.; LI, H. Bond properties and experimental methods of textile reinforced concrete. **Journal Wuhan University of Technology, Materials Science Edition**, v. 22, n. 3, p. 529–532, 2007.
- [35] PAPAKONSTANTINO, C. G.; BALAGURU, P.; LYON, R. E. Comparative study of high temperature composites. **Composites Part B:Engineering**, v. 32, n. 8, p. 637–649, 2001.
- [36] YOUNES, A. et al. Mechanical behaviour of carbon and glass filament yarns under high temperatures for composite applications. **Journal of the Textile Institute**, v. 104, n. 3, p. 251–259, 2013.
- [37] MICHELS, J. et al. Structural Strengthening of Concrete with Fiber Reinforced Cementitious Matrix (FRCM) at Ambient and Elevated Temperature — Recent Investigations in Switzerland. **Advances in Structural Engineering**, v. 17, n. 12, p. 1785–1799, 2014.

- [38] BISBY, L. A.; GREEN, M. F.; KODUR, V. K. R. Response to fire of concrete structures that incorporate FRP. **Progress in Structural Engineering and Materials**, v. 7, n. 3, p. 136–149, 2005.
- [39] SUMIDA, A.; MUTSUYOSHI, H. Mechanical properties of newly developed heat-resistant FRP bars. **Journal of Advanced Concrete Technology**, v. 6, n. 1, p. 157–170, 2008.
- [40] LU, M. et al. Improved interfacial strength of SiO₂ coated carbon fiber in cement matrix. **Cement and Concrete Composites**, v. 91, n. April, p. 21–28, 2018.
- [41] SCHNEIDER, K. et al. Mineral-based coating of plasma-treated carbon fibre rovings for carbon concrete composites with enhanced mechanical performance. **Materials**, v. 10, n. 4, 2017.
- [42] SCHNEIDER, K. et al. Verbundverhalten mineralisch gebundener und polymergebundener Bewehrungsstrukturen aus Carbonfasern bei Temperaturen bis 500 °C. **Beton- und Stahlbetonbau**, v. 113, n. 12, p. 886–894, 2018.
- [43] MECHTCHERINE, V. et al. Extrusion-based additive manufacturing with carbon reinforced concrete: Concept and feasibility study. **Materials**, v. 13, n. 11, 2020.
- [44] MECHTCHERINE, V. et al. Mineral-impregnated carbon fiber composites as novel reinforcement for concrete construction: Material and automation perspectives. **Automation in Construction**, v. 110, n. September 2019, p. 103002, 2020.
- [45] DUXSON, P. et al. Geopolymer technology: The current state of the art. **Journal of Materials Science**, v. 42, n. 9, p. 2917–2933, 2007.
- [46] TRINDADE, A. C. C.; BORGES, P. H. R.; SILVA, F. DE A. Evaluation of Fiber–Matrix Bond in the Mechanical Behavior of Geopolymer Composites Reinforced with Natural Fibers. **Advances in Civil Engineering Materials**, v. 8, n. 3, p. 20180136, 2019.
- [47] TRINDADE, A. C. C. et al. On The Mechanical Behavior of Metakaolin Based Geopolymers Under Elevated Temperatures. **Materials Research**, v. 20, n. suppl 2, p. 265–272, 2017.
- [48] CHINDAPRASIRT, P. et al. High-Strength Geopolymer Using Fine High-Calcium Fly Ash. **Journal of Materials in Civil Engineering**, v. 23, n. 3, p. 264–270, 2011.
- [49] GÖRHAN, G.; ASLANER, R.; ŞINIK, O. The effect of curing on the

properties of metakaolin and fly ash-based geopolymer paste. **Composites Part B: Engineering**, v. 97, p. 329–335, 2016.

[50] SINGH, N. B.; MIDDENDORF, B. Geopolymers as an alternative to Portland cement: An overview. **Construction and Building Materials**, v. 237, p. 117455, 2020.

[51] TRINDADE, A. C. C. et al. Influence of elevated temperatures on the mechanical behavior of jute-textile-reinforced geopolymers. **Journal of Ceramic Science and Technology**, v. 8, n. 3, p. 389–398, 2017.

[52] DUXSON, P.; LUKEY, G. C.; DEVENTER, J. S. J. VAN. Thermal evolution of metakaolin geopolymers: Part 1 - Physical evolution. **Journal of Non-Crystalline Solids**, v. 352, n. 52–54, p. 5541–5555, 2006.

[53] DUXSON, P.; LUKEY, G. C.; DEVENTER, J. S. J. VAN. Physical evolution of Na-geopolymer derived from metakaolin up to 1000 °c. **Journal of Materials Science**, v. 42, n. 9, p. 3044–3054, 2007.

[54] DOAN, T. et al. New Generation of Geopolymer Composite for Fire-Resistance. In: TESINOVA, P. (Ed.). . **Advances in Composite Materials - Analysis of Natural and Man-Made Materials**. [s.l.] InTech, 2011. p. 73–92.

[55] ZHAO, J. et al. Development and testing of fast curing, mineral-impregnated carbon fiber (MCF) reinforcements based on metakaolin-made geopolymers. **Cement and Concrete Composites**, v. 116, n. September 2020, 2021.

[56] LYON, R. E. et al. Fire-resistant aluminosilicate composites. **Fire and Materials**, v. 21, n. 2, p. 67–73, 1997.

[57] TRAN, D. H. et al. Effect of Curing Temperature on Flexural Properties of Silica-Based Geopolymer-Carbon Reinforced Composite. **Manufacturing Engineering**, v. 37, n. 2, p. 492–497, 2009.

[58] LORENZ, E.; ORTLEPP, R. Bond behavior of textile reinforcements - Development of a pull-out test and modeling of the respective bond versus slip relation. **RILEM Bookseries**, v. 2, p. 479–486, 2012.

[59] SILVA, R. M. DE C.; SILVA, F. DE A. **Mechanical and Bond Behavior of Carbon Textile Reinforced Concretes Under Tensile Loading**. 4th Brazilian Conference on Composite Materials. **Anais...Rio de Janeiro: 2018**

[60] GOLIATH, K. B.; CARDOSO, D. C. T.; SILVA, F. DE A. Flexural behavior of carbon-textile-reinforced concrete I-section beams. **Composite Structures**, v. 260, p. 113540, 2021.

- [61] CASTOLDI, R. DE S.; SOUZA, L. M. S. DE; ANDRADE SILVA, F. DE. Comparative study on the mechanical behavior and durability of polypropylene and sisal fiber reinforced concretes. **Construction and Building Materials**, v. 211, p. 617–628, 2019.
- [62] ALENCAR MONTEIRO, V. M. DE; LIMA, L. R.; ANDRADE SILVA, F. DE. On the mechanical behavior of polypropylene, steel and hybrid fiber reinforced self-consolidating concrete. **Construction and Building Materials**, v. 188, p. 280–291, 2018.
- [63] SILVA, F. DE A. et al. Effects of elevated temperatures on the interface properties of carbon textile-reinforced concrete. **Cement and Concrete Composites**, v. 48, p. 26–34, 2014.
- [64] MOBASHER, B. **Mechanics of Fiber and Textile Reinforced Cement Composites**. [s.l.] CRC Press, 2012.
- [65] WILLIAMS PORTAL, N. et al. Sustainable Potential of Textile-Reinforced Concrete. **Journal of Materials in Civil Engineering**, v. 27, n. 7, p. 04014207, 2015.
- [66] TEIXEIRA, F. P.; ANDRADE SILVA, F. DE. On the use of natural curauá reinforced cement based composites for structural applications. **Cement and Concrete Composites**, v. 114, n. July, 2020.
- [67] SOUZA, L. O. DE; SOUZA, L. M. S. DE; SILVA, F. DE A. Mechanics of natural curauá textile-reinforced concrete. **Magazine of Concrete Research**, v. 73, n. 3, p. 135–146, 2021.
- [68] COLOMBO, I. et al. Tensile behavior of textile: Influence of multilayer reinforcement. **RILEM Bookseries**, v. 2, n. January, p. 463–470, 2012.
- [69] COLOMBO, I. G. et al. Textile Reinforced Concrete: Experimental investigation on design parameters. **Materials and Structures/Materiaux et Constructions**, v. 46, n. 11, p. 1933–1951, 2013.
- [70] DU, Y. et al. Experimental study on basalt textile reinforced concrete under uniaxial tensile loading. **Construction and Building Materials**, v. 138, p. 88–100, 2017.
- [71] DU, Y. et al. Flexural behavior of basalt textile-reinforced concrete. **Construction and Building Materials**, v. 183, p. 7–21, 2018.
- [72] LARRINAGA, P. et al. Experimental and numerical modeling of basalt textile reinforced mortar behavior under uniaxial tensile stress. **Materials and Design**, v.

55, p. 66–74, 2014.

[73] ZHOU, F. et al. Uniaxial tensile behavior of carbon textile reinforced mortar. **Materials**, v. 12, n. 3, p. 1–19, 2019.

[74] SILVA, F. DE A. et al. **Effect of reinforcement ratio on the mechanical response of compression molded sisal fiber textile reinforced concrete**. High Performance Fiber Reinforced Cement Composites (HPFRCC5). **Anais...2007**

[75] CEVALLOS, O. A.; OLIVITO, R. S. Effects of fabric parameters on the tensile behaviour of sustainable cementitious composites. **Composites: Part B**, v. 69, p. 256–266, 2015.

[76] FIDELIS, M. E. A.; ANDRADE SILVA, F. DE; TOLEDO FILHO, R. D. The Influence of Fiber Treatment on the Mechanical Behavior of Jute Textile Reinforced Concrete. **Key Engineering Materials**, v. 600, n. September, p. 469–474, 2014.

[77] HEGGER, J. et al. Load-bearing behaviour and simulation of textile reinforced concrete. **Materials and Structures**, v. 39, n. 8, p. 765–776, 2006.

[78] CAGGEGI, C. et al. Tensile behaviour of a basalt TRM strengthening system: Influence of mortar and reinforcing textile ratios. **Composites Part B: Engineering**, v. 130, p. 90–102, 2017.

[79] DIEDERICHS, U.; JUMPPANEN, U.-M.; PENTTALA, V. **Behavior of high strength concrete at high temperatures**Helsinki University of Technology, **Department of Structural Engineering, Report 92**. [s.l: s.n.].

[80] DONNINI, J. et al. Fabric-reinforced cementitious matrix behavior at high-temperature: Experimental and numerical results. **Composites Part B: Engineering**, v. 108, p. 108–121, 2017.

[81] EHLIG, D. et al. **High Temperature Tests on Textile Reinforced Concrete (TRC) Strain Specimens**. (W. Brameshuber, Ed.)International RILEM Conference on Material Science – MATSCI. **Anais...Aachen: Rilem publications**, 2010

[82] XU, S.; SHEN, L.; WANG, J. The high-temperature resistance performance of TRC thin-plates with different cementitious materials: Experimental study. **Construction and Building Materials**, v. 115, p. 506–519, 2016.

[83] XU, S. et al. High temperature mechanical performance and micro interfacial adhesive failure of textile reinforced concrete thin-plate. **Journal of Zhejiang University SCIENCE A**, v. 15, n. 1, p. 31–38, 2014.

- [84] ZHU, D.; GENCOGLU, M.; MOBASHER, B. Low velocity flexural impact behavior of AR glass fabric reinforced cement composites. **Cement and Concrete Composites**, v. 31, n. 6, p. 379–387, 2009.
- [85] MEYERS, M. A. **Dynamic Behavior of Materials**. [s.l.] John Wiley & Sons, Inc., 1994.
- [86] SILVA, F. DE A. et al. Impact behavior of sisal fiber cement composites under flexural load. **ACI Materials Journal**, v. 108, n. 2, p. 168–177, 2011.
- [87] ZHU, D.; PELED, A.; MOBASHER, B. Dynamic tensile testing of fabric-cement composites. **Construction and Building Materials**, v. 25, n. 1, p. 385–395, 2011.
- [88] ZHU, D.; MOBASHER, B.; RAJAN, S. D. Dynamic Tensile Testing of Kevlar 49 Fabrics. **Journal of Materials in Civil Engineering**, v. 23, n. 3, p. 230–239, 2011.
- [89] SILVA, F. DE A. et al. Strain rate effect on the tensile behaviour of textile-reinforced concrete under static and dynamic loading. **Materials Science and Engineering A**, v. 528, n. 3, p. 1727–1734, 2011.
- [90] YAO, Y. et al. Tension stiffening in textile-reinforced concrete under high speed tensile loads. **Cement and Concrete Composites**, v. 64, p. 49–61, 2015.
- [91] YAO, Y. et al. Distributed cracking mechanisms in textile-reinforced concrete under high speed tensile tests. **Materials and Structures/Materiaux et Constructions**, v. 49, n. 7, p. 2781–2798, 2016.
- [92] SILVA, F. DE A. et al. High speed tensile behavior of sisal fiber cement composites. **Materials Science and Engineering A**, v. 527, n. 3, p. 544–552, 2010.
- [93] BARHUM, R.; MECHTCHERINE, V. Influence of short dispersed and short integral glass fibres on the mechanical behaviour of textile-reinforced concrete. **Materials and Structures**, v. 46, n. 4, p. 557–572, 2013.
- [94] HERAVI, A. A. et al. Mechanical characterization of textile reinforced cementitious composites under impact tensile loading using the split Hopkinson tension bar. **Cement and Concrete Composites**, v. 114, n. August, p. 103769, 2020.
- [95] BUTNARIU, E.; PELED, A.; MOBASHER, B. **Impact Behavior of Fabric-Cement Based Composites**. Brittle Matrix Composites 8. **Anais...**Woodhead Publishing Limited, 2006Disponível em: <<http://dx.doi.org/10.1533/9780857093080.293>>

- [96] LIU, S. et al. Impact response of basalt textile reinforced concrete subjected to different velocities and temperatures. **Construction and Building Materials**, v. 175, n. May, p. 381–391, 2018.
- [97] LI, A. et al. Dynamic flexural behavior of AR-glass textile reinforced concrete under low-velocity impact loading. **Journal of Sustainable Cement-Based Materials**, v. 12, n. 1, p. 49–67, 2023.
- [98] SCHUMANN, A. et al. Parking slabs made of carbon reinforced concrete. **Structural Concrete**, v. 19, n. 3, p. 647–655, 2018.
- [99] MAY, S. et al. Lightweight ceiling system made of carbon reinforced concrete. **Structural Concrete**, n. October 2017, p. 1–11, 2018.
- [100] MAY, S. et al. Precast Slab Structures Made of Carbon Reinforced Concrete. **Structures**, p. #pagerange#, 2018.
- [101] HEGGER, J.; ZELL, M.; HORSTMANN, M. Textile Reinforced Concrete—Realization in applications. **Symposium of Tailor Made Concrete Structures**, p. 357–362, 2008.
- [102] COLOMBO, I. G.; COLOMBO, M.; PRISCO, M. DI. Bending behaviour of Textile Reinforced Concrete sandwich beams. **Construction and Building Materials**, v. 95, p. 675–685, 2015.
- [103] ANH NGUYEN, V.; JESSE, F.; CURBACH, M. Experiments to establish the loadbearing behaviour of lightweight sandwich beams using textile-reinforced and expanded polystyrene concrete. **Structural Concrete**, v. 17, n. 5, p. 760–767, 2016.
- [104] JUNES, A.; SILARBI, A. An experimental and theoretical study of sandwich panels with TRC facings: Use of metallic connectors and TRC stiffeners. **Engineering Structures**, v. 113, p. 174–185, 2016.
- [105] SHAREI, E. et al. Structural behavior of a lightweight, textile-reinforced concrete barrel vault shell. **Composite Structures**, v. 171, p. 505–514, 2017.
- [106] HEGGER, J. et al. Innovative design concepts: Application of textile reinforced concrete to shell structures. **Structural Concrete**, v. 19, n. 3, p. 637–646, 2018.
- [107] BRÜCKNER, A.; ORTLEPP, R.; CURBACH, M. Textile reinforced concrete for strengthening in bending and shear. **Materials and Structures**, v. 39, n. 8, p. 741–748, 2006.
- [108] AMBRISI, A. D.; FOCACCI, F. Flexural strengthening of RC beams with

cement-based composites. **Journal of Composites for Construction**, v. 15, n. 5, p. 707–720, 2011.

[109] OMBRES, L. Flexural analysis of reinforced concrete beams strengthened with a cement based high strength composite material. **Composite Structures**, v. 94, n. 1, p. 143–155, 2011.

[110] AL-SALLOUM, Y. A. et al. Experimental and Numerical Study for the Shear Strengthening of Reinforced Concrete Beams Using Textile-Reinforced Mortar. **Journal of Composites for Construction**, v. 16, n. 1, p. 74–90, 2012.

[111] PELED, A. Confinement of Damaged and Nondamaged Structural Concrete with FRP and TRC Sleeves. **Journal of Composites for Construction**, v. 11, n. November, p. 514–522, 2007.

[112] BOURNAS, D. A. et al. Textile-Reinforced Mortar versus FRP Jacketing in Seismic Retrofitting of RC Columns with Continuous or Lap-Spliced Deformed Bars. **Journal of Composites for Construction**, v. 13, n. 5, p. 360–371, 2009.

[113] BABAEIDARABAD, S.; CASO, F. DE; NANNI, A. Out-of-Plane Behavior of URM Walls Strengthened with Fabric-Reinforced Cementitious Matrix Composite. **Journal of Composites for Construction**, v. 18, n. 4, p. 04013057, 2013.

[114] BABAEIDARABAD, S.; CASO, F. DE; NANNI, A. URM Walls Strengthened with Fabric-Reinforced Cementitious Matrix Composite Subjected to Diagonal Compression. **Journal of Composites for Construction**, v. 18, n. 2, p. 04013045, 2013.

[115] EUROPEAN STANDARD EN. **EN 1992 - Eurocode 2: Design of concrete structures - Part 1-1: General rules and rules for buildings**, 2004.

[116] SCHOLZEN, A.; CHUDOBA, R.; HEGGER, J. Thin-walled shell structures made of textile-reinforced concrete: Part I: Structural design and construction. **Structural Concrete**, v. 16, n. 1, p. 106–114, 2015.

[117] SCHOLZEN, A.; CHUDOBA, R.; HEGGER, J. Thin-walled shell structures made of textile-reinforced concrete: Part II: Experimental characterization, ultimate limit state assessment and numerical simulation. **Structural Concrete**, v. 16, n. 1, p. 115–124, 2015.

[118] SALMON, D. C. et al. Full scale testing of precast concrete sandwich panels. **ACI Structural Journal**, v. 94, p. 239–247, 1997.

[119] HEGGER, J. et al. Exterior Cladding Panels as an Application of Textile

Reinforced Concrete. **SP-224. Farmington Hills (MI, USA): American Concrete Institute**, p. 55–70, 2004.

[120] DIAB, Y. G. Strengthening of RC beams by using sprayed concrete: Experimental approach. **Engineering Structures**, v. 20, n. 7, p. 631–643, 1998.

[121] TSONOS, A. D. G. Performance enhancement of R/C building columns and beam-column joints through shotcrete jacketing. **Engineering Structures**, v. 32, n. 3, p. 726–740, 2010.

[122] DEMIR, A.; TEKIN, M. Strengthening of reinforced concrete (RC) beams with prefabricated reinforced concrete (RC) plates. **Scientific Research and Essays**, v. 6, n. 21, p. 4577–4586, 2011.

[123] GANESH, P.; MURTHY, A. R. Repair, retrofitting and rehabilitation techniques for strengthening of reinforced concrete beams - A review. **Advances in Concrete Construction**, v. 8, n. 2, p. 101–117, 2019.

[124] HARAJLI, M. H. Strengthening of Concrete Beams by External Prestressing. **PCI Journal**, v. 38, n. 6, p. 76–88, 1993.

[125] TAN, K. H.; TJANDRA, R. A. Strengthening of RC Continuous Beams by External Prestressing. **Journal of Structural Engineering**, v. 133, n. 2, p. 195–204, 2007.

[126] ZOU, J. et al. Experimental study on flexural behavior of concrete T-beams strengthened with externally prestressed tendons. **Mathematical Biosciences and Engineering**, v. 16, n. 6, p. 6962–6974, 2019.

[127] SEREÇA, S.; FAUSTMANN, D. H. Flexural strengthening of reinforced concrete beams using external tendons. **Engineering Structures**, v. 252, n. November 2021, 2022.

[128] TRIANTAFILLOU, T. C.; PLEVRIS, N. Strengthening of RC beams with epoxy-bonded fibre-composite materials. **Materials and Structures**, v. 25, n. 4, p. 201–211, 1992.

[129] CHAJES, M. J. et al. Flexural strengthening of concrete beams using externally bonded composite materials. **Construction and Building Materials**, v. 8, n. 3, p. 191–201, 1994.

[130] ARDUINI, M.; NANNI, A. Behavior of precracked RC beams strengthened with carbon FRP sheets. **Journal of Composites for Construction**, v. 1, n. 2, p. 63–70, 1997.

[131] NANNI, A. Carbon FRP Strengthening: New Technology Becomes

Mainstream. **Concrete International**, v. 19, n. 6, p. 1–23, 1997.

[132] KHALIFA, A.; NANNI, A. Rehabilitation of rectangular simply supported RC beams with shear deficiencies using CFRP composites. **Construction and Building Materials**, v. 16, n. 3, p. 135–146, 2002.

[133] ESHWAR, N.; IBELL, T. J.; NANNI, A. Effectiveness of CFRP strengthening on curved soffit RC beams. **Advances in Structural Engineering**, v. 8, n. 1, p. 55–68, 2005.

[134] BAGGIO, D.; SOUDKI, K.; NOËL, M. Strengthening of shear critical RC beams with various FRP systems. **Construction and Building Materials**, v. 66, p. 634–644, 2014.

[135] AMERICAN CONCRETE INSTITUTE (ACI). **ACI 440.2R-17: Guide for the Design and Construction of Externally Bonded FRP Systems for Strengthening Concrete Structures**, 2017.

[136] BISBY, L. Fire Resistance of Textile Fiber Composites Used in Civil Engineering. In: TRIANTAFILLOU, T. C. (Ed.). . **Textile Fibre Composites in Civil Engineering**. [s.l.] Woodhead Publishing, 2016. p. 169–185.

[137] RAOOF, S. M.; BOURNAS, D. A. TRM versus FRP in flexural strengthening of RC beams: Behaviour at high temperatures. **Construction and Building Materials**, v. 154, p. 424–437, 2017.

[138] NANNI, A. A New Tool for Concrete and Masonry Repair. **Concrete International**, n. april, p. 43–49, 2012.

[139] SCHLADITZ, F. et al. Bending load capacity of reinforced concrete slabs strengthened with textile reinforced concrete. **Engineering Structures**, v. 40, p. 317–326, 2012.

[140] LORETO, G. et al. Performance of RC Slab-Type Elements Strengthened with Fabric-Reinforced Cementitious-Matrix Composites. **Journal of Composites for Construction**, v. 18, n. 3, p. A4013003, 2013.

[141] BABAEIDARABAD, S.; LORETO, G.; NANNI, A. Flexural strengthening of RC beams with an externally bonded fabric-reinforced cementitious matrix. **Journal of Composites for Construction**, v. 18, n. 5, p. 04014009-1- 04014009–12, 2014.

[142] VERBRUGGEN, S. et al. Bending of beams externally reinforced with TRC and CFRP monitored by DIC and AE. **Composite Structures**, v. 112, n. 1, p. 113–121, 2014.

- [143] SI LARBI, A.; CONTAMINE, R.; HAMELIN, P. TRC and hybrid solutions for repairing and/or strengthening reinforced concrete beams. **Engineering Structures**, v. 45, p. 12–20, 2012.
- [144] GOPINATH, S. et al. Behaviour of reinforced concrete beams strengthened with basalt textile reinforced concrete. **Journal of Industrial Textiles**, v. 44, n. 6, p. 924–933, 2015.
- [145] AKBARI HADAD, H.; ERICKSON, B.; NANNI, A. Flexural analysis and design of FRCM-strengthened RC beams. **Construction and Building Materials**, v. 244, p. 118371, 2020.
- [146] AZAM, R.; SOUDKI, K. FRCM strengthening of shear-critical RC beams. **Journal of Composites for Construction**, v. 18, n. 5, p. 04014012, 2014.
- [147] TEIXEIRA, F. P.; CARDOSO, D. C. T.; ANDRADE SILVA, F. DE. On the shear behavior of natural curauá fabric reinforced cement-based composite systems. **Engineering Structures**, v. 246, n. August, 2021.
- [148] ORTLEPP, R.; ORTLEPP, S.; CURBACH, M. **Experimental Investigations About Construction**. (J. Hegger, W. Brameshuber, N. Will, Eds.)1st International Conference Textile Reinforced Concrete (ICTRC). **Anais...Aachen: RILEM Publications SARL**, 2006
- [149] TRIANTAFILLOU, T. C.; PAPANICOLAOU, C. G.; ZISSIMOPOULOS, P. Concrete Confinement with Textile-Reinforced Mortar Jackets Concrete Confinement with Textile-Reinforced Mortar Jackets. **ACI Structural Journal**, v. 103, n. January-February, p. 28–37, 2006.
- [150] TRIANTAFILLOU, T. C. **Textile Fibre Composites in Civil Engineering**. [s.l.] Woodhead Publishing, 2016.
- [151] BUTLER, M.; LIEBOLDT, M.; MECHTCHERINE, V. Application of Textile-Reinforced Concrete (TRC) for structural strengthening and in prefabrication. **Advances in Cement-Based Materials**, p. 127–136, 2010.
- [152] WAGNER, J. et al. Strengthening of Reinforced Concrete Structures with Carbon Reinforced Concrete—Possibilities and Challenges. **CivilEng**, v. 3, n. 2, p. 400–426, 2022.
- [153] S&P CLEVER BRASIL. **SP-Reinforcement**. Disponível em: <<https://www.sp-reinforcement.com.br/service/armo-mesh/>>. Acesso em: 25 feb. 2023.
- [154] **Reforço de vigas e pilares - Estádio do Maracanã - Rio de Janeiro, Brasil.**

Disponível em: <<https://www.sp-reinforcement.pt/pt-PT/projectos/reforco-de-vigas-e-pilares-estadio-do-maracana-rio-de-janeiro-brasil>>. Acesso em: 25 feb. 2023.

[155] ORTLEPP, R.; ORTLEPP, S.; CURBACH, M. Stress transfer in the bond joint of subsequently applied textile reinforced concrete strengthening. **6th International RILEM Symposium on Fibre Reinforced Concretes**, n. September, p. 1483–1494, 2004.

[156] ORTLEPP, R.; HAMPEL, U.; CURBACH, M. A new approach for evaluating bond capacity of TRC strengthening. **Cement and Concrete Composites**, v. 28, n. 7, p. 589–597, 2006.

[157] SNEED, L. H. et al. A comparison of the bond behavior of PBO-FRCM composites determined by double-lap and single-lap shear tests. **Cement and Concrete Composites**, v. 64, p. 37–48, 2015.

[158] D'ANTINO, T. et al. Matrix-fiber bond behavior in PBO FRCM composites: A fracture mechanics approach. **Engineering Fracture Mechanics**, v. 117, p. 94–111, 2014.

[159] D'ANTINO, T. et al. Influence of the substrate characteristics on the bond behavior of PBO FRCM-concrete joints. **Construction and Building Materials**, v. 101, p. 838–850, 2015.

[160] SNEED, L. H.; D'ANTINO, T.; CARLONI, C. Investigation of bond behavior of polyparaphenylene benzobisoxazole fiber-reinforced cementitious matrix composite-concrete interface. **ACI Materials Journal**, v. 111, n. 5, p. 569–580, 2014.

[161] YOUNIS, A.; EBEAD, U. Bond characteristics of different FRCM systems. **Construction and Building Materials**, v. 175, p. 610–620, 2018.

[162] D'ANTINO, T. et al. Experimental analysis of the bond behavior of glass, carbon, and steel FRCM composites. **Key Engineering Materials**, v. 624, n. January, p. 371–378, 2015.

[163] OMBRES, L. Analysis of the bond between Fabric Reinforced Cementitious Mortar (FRCM) strengthening systems and concrete. **Composites Part B: Engineering**, v. 69, p. 418–426, 2015.

3 Bond behavior of polymer- and mineral-impregnated carbon fiber yarns towards concrete matrices at elevated temperature levels and different strain rates

The bond of textile reinforcements towards concrete matrices plays an important role in the mechanical performance of Textile Reinforced Concretes, and the textile impregnation material is a crucial factor. In this chapter, the bond between different carbon yarns towards a concrete matrix was evaluated at elevated temperatures. A lab-developed cement-based (C) and geopolymer-based (GP) Mineral-impregnated Carbon Fibers (MCF) and commercially available epoxy resin (EP) coated carbon yarns were assessed. Both MCF yarns yielded high tensile strength and modulus of elasticity, compatible with commercial EP yarns. The C-MCF yarn showed higher bond strength towards the matrix than the GP-MCF yarn, probably due to better chemical compatibility. The EP yarn yielded the strongest bond towards the matrix at room temperature. At elevated temperatures, the bond between the EP yarn and concrete matrix became considerably weaker, while the MCF yarns could maintain a sufficient bond up to 300 °C.

The experimental program of this chapter was conducted at the Institute of Construction Materials at the Technische Universität Dresden, Germany.

Published article: July 16th, 2022 – *Cement and Concrete Composites*

<https://doi.org/10.1016/j.cemconcomp.2022.104685>

3.1. Introduction

Textile reinforced concrete (TRC) is a fine-grained concrete matrix composite reinforced with one or several layers of fabrics [1]. This relatively new class of material is becoming a promising alternative to conventional construction materials due to its excellent mechanical properties aligned with the high potential of building thin-walled elements, which can considerably reduce the material consumption, and consequently the CO₂ emissions generated in their production. The use of textile reinforced concrete has been reported in the literature as a material

for repair and strengthening of steel reinforced concrete structures [2–5] and masonry [4,6–8], and also for the construction of new structural elements, such as bridges and walkways [9–11], facades [12,13], and others [14–19].

In recent years, carbon fiber (CF) reinforcements have been becoming more and more often used in the construction sector due to their superior mechanical and durability properties compared to other fiber reinforcement types [20–22]. The fabrics used as reinforcement consist of several multifilament CF yarns arranged in a bi- or three-dimensional structure. Due to the incongruity between the cement particle sizes (ranging mostly from 10 to 75 μm [23]) and the filament diameters (usually smaller than 10 μm [24]), the matrix cannot well penetrate into the core of the multifilament bundle. Thus, the external filaments, also called sleeve filaments, are in direct contact with the surrounding cementitious matrix, while the internal filaments, or core, are relatively free inside the yarn. Therefore, the sleeve filaments can be potentially well-bonded to the matrix and fail first, usually increasing the first crack level of the loaded composite. In contrast, the failure mechanism of the core filaments underlays a telescopic type of pull-out, in which the core filaments slip against the sleeve ones [1,24–26]. A low sleeve-to-core ratio leads to a low reinforcing ability and a poor mechanical performance of the composite. By increasing this ratio, the load transfer between the matrix and the reinforcement is improved, leading to an increase in the effectiveness of the textile reinforcement, and consequently, the composite mechanical performance [1,27,28]. It is important to note that, in the case of CF fabrics, the hydrophobic characteristic of the fibers may additionally hinder the bond and consequently the composite performance [29] due to their incompatibility with the water-based cementitious matrices.

Over the years, different methods have been used to improve the bond of multifilament yarns towards matrices. Polymeric impregnation materials are the state-of-art technology in the conventional composite industry to produce the so-called “prepregs”. Thereby, thermosetting or thermoplastic polymers gradually fill the spaces between the filaments of the yarns so that the bundle can be considered as a rigid unit [27]. Hence, the evident slippage between individual filaments is eliminated, and all of them are stressed more uniformly, resulting in more filaments taking part in the load-bearing function [1]. Previous studies [25,28,30–32] have shown that the mechanical performance of composites reinforced with polymer coated fabrics is superior to that of composites with untreated fabrics, highly

dependent on the polymer materials and their impregnation quality. According to [30,33], epoxy resins are proven to be more efficient in enhancing the composite mechanical properties than styrene-butadiene-based resins, probably due to their higher modulus of elasticity and shear modulus. However, even with the elevated mechanical performance, observations on the crack pattern of TRC subjected to direct tensile loadings still showed a large spacing between the cracks, and, in some cases, delamination due to a debonding between the fabric layers and the cementitious matrix [28]. This can be traced back to the weak chemical compatibility between the polymer impregnated fabric (hydrophobic) and the cementitious matrix (hydrophilic) [27]. By adding a sand layer over the fresh polymer, an increase in friction and mechanical interlocking can be created, thus reducing the delamination [32–34].

Despite the advantages of using polymeric coatings, their low thermal resistance still severely limits the use of TRC in the practice of construction. Generally, non-coated CF yarns can maintain good mechanical properties up to approximately 400 °C in an oxygen environment [20,35–37]. However, for polymer-coated carbon yarns, the glass transition temperature (T_g), as well as the decomposition temperature of the respective polymers, need to be considered. Below the T_g polymers possess a relatively high stiffness which decreases suddenly when reaching or exceeding this particular temperature. Subsequently, a decomposition of polymers chains occurs, in an oxygen atmosphere commonly at temperatures ranging between 300 °C and 400 °C.

CF fabrics are non-corrosive materials [20,38]. Thus, in contrast to the steel of conventional reinforced concrete, which requires large concrete coverings [39], TRC elements are generally thin. However, in the case of fire, the reinforcements of thin-walled construction elements become more rapidly subjected to elevated temperatures. Even with CF having high melting point [20], the low thermal resistance of the polymeric coating leads to a drastic reduction in the mechanical performance of the TRC when exposed to elevated temperatures. Ehlig et al. [40] showed significant changes in the strain capacity of the TRC under constant tensile loading and escalating temperatures after the decomposition of the polymeric coating. Silva et al. [41] showed that the benefits of the polymeric coating on the bond performance between the CF yarn and the cementitious matrix are only valid up to 200 °C. Through bending tests, Xu et al. [42] confirmed this bond loss, which

led to a significant drop in the ultimate bearing capacity of TRC with CF fabrics coated with epoxy resin above 200 °C. Donnini et al. [43] demonstrated that even with the addition of a sand layer on the polymeric coating, still a significant reduction in the tensile strength at elevated temperatures can be observed.

Recently, mineral impregnations have been used as coatings on carbon fabrics to improve their bond with cementitious matrices. Due to the small dimension of the CF multifilaments, the mineral particles must have such small grain sizes that they can penetrate in the spaces between the filaments of the yarn, usually in the order of a few micrometers, thus acting similarly to the polymeric coatings, binding all the filaments and making the yarn work as a unit and increasing its bond with the matrix. Peled et al. [27], Dvorkin and Peled [28], and Nadiv et al. [29] showed that inorganic coatings based on micro-silica are able to improve the bond between a carbon yarn and a cementitious matrix and consequently enhance the mechanical properties of the composites. The amorphous silica can promote a pozzolanic reaction with the calcium hydroxide (CH) from the cementitious binder, improving the bond between the CF yarn and the matrix. Furthermore, these mineral coatings usually present high thermal resistance, which makes them a promising alternative to the commonly applied polymeric coatings. Schneider et al. [44,45] demonstrated that a mineral impregnation coating based on micro-cements and micro-silica was able to enhance the flexural strength of carbon yarns and the bond behavior towards a cementitious matrix, even at temperatures up to 500 °C. Moreover, this new-developed technology presents great potential for being used as reinforcement into 3D concrete printing layers [46]. However, the cement-based suspension can provide merely a limited processing window due to its fast increased viscosity caused by the successive hydration.

To ensure stable rheological properties for continuous production, the use of geopolymer binders is an interesting approach. Furthermore, geopolymers exhibit excellent thermal stability over wide temperature ranges [47–49] and comparable mechanical properties to cement binders [49–53]. Geopolymers are produced through alkali activation of aluminosilicate sources, such as metakaolin or fly ash [54,55]. Different from cement-based binders, geopolymers can be synthesized at slightly elevated temperatures (<100 °C), similar to thermosets, being able to reach high strengths at early ages and saving the necessary time for curing [54,56]. Additionally, geopolymers seem to present a good bond with CF [57,58]. With a

controlled heat curing at 75 °C, a fast setting and rapid early-strength development of metakaolin-based Mineral-Impregnated Carbon Fibers (MCF) yarn have been achieved in the first 8 hours, as demonstrated in a prior study performed by Zhao et al. [59].

During their lifetime, structures may be subject to dynamic loadings from earthquakes, wind gusts, wind-driven objects, fast-moving traffic, machine vibrations, blast explosions, and projectiles. In these cases, the structure element is subjected to very high strain rates due to a large amount of energy that is transmitted to it in a very short period of time [60]. TRC exhibits high energy absorption capacity under static or quasi-static conditions. For this reason, its use in applications subject to dynamic loading seems to be quite promising. Under direct tensile loadings, TRC with AR-glass [61–64], carbon [61], polyethylene (PE) [61], polypropylene (PP) [64], and sisal [65] fabrics exhibited a strain-hardening behavior with multiple-cracking even at dynamic conditions.

This work presents a novel evaluation regarding the bond of a metakaolin-based geopolymer (GP) Mineral-Impregnated Carbon Fibers (MCF) towards a fine-grained concrete matrix. For this, pull-out tests were performed at temperatures up to 300 °C. Additionally, a cement-based (C) MCF and a commercially available carbon yarn with an epoxy resin coating were also assessed, allowing a comparative analysis of the three different reinforcing yarns. The methodology for the manufacture of the MCF yarns is as well addressed in the paper. Moreover, these yarns were characterized through yarn uniaxial tension tests. Three different strain rates were applied in order to evaluate the rate-dependency of the material.

3.2. Experimental Program

3.2.1. Carbon yarns

The CF yarn used for both MCF was a SIGRAFIL® C T50-4.4/255 – E100, from SGL Group, Germany, which provides the high processing ability with the mineral impregnation. It consists of 50,000 (50k) filaments and has a fineness of 3,450 tex. Table 3.1 presents further properties provided by the supplier.

Table 3.1 – Properties of the SIGRAFIL® C T50-4.4/255 – E100

Number of filaments	50k
Fineness of yarn (tex)	3450
Density (g/cm ³)	1.80
Filament diameter (μm)	6.9
Tensile strength (GPa)	4.4
Tensile modulus (GPa)	255
Elongation at break (%)	1.65
Sizing type	Epoxy
Sizing level (%)	1

For the mineral impregnations, a micro-cement-based suspension and a geopolymer suspension were used. The cement suspension was based on previous work by Schneider et al. [45], and its composition is presented in Table 3.2. It consists of commercial micro-cements from Dyckerhoff, Germany. According to the supplier, the Mikrodur R-X is a granulated blast furnace slag-based extra-fine micro-cement with a maximum grain d₉₅ of 6 μm, and the Mikrodur P-U is a Portland cement clinker based ultrafine micro-cement with maximum grain d₉₅ of 9.5 μm. A micro-silica suspension produced by MC-Bauchemie, Germany, with a solid content of 48% to 52% was used. To obtain proper workability for the impregnation process, the superplasticizer Master Rheobuild 30 from BASF, Germany, was added to the mixture.

Table 3.2 – Cement suspension composition

Micro-cement Mikrodur R-X (kg/m ³)	500
Micro-cement Mikrodur P-U (kg/m ³)	500
Micro-silica suspension Centrilit Fume SX (kg/m ³)	500
Water (kg/m ³)	464
Superplasticizer Master Rheobuild 30 (kg/m ³)	45

The geopolymer suspension was produced through the combination of a liquid alkali with an aluminosilicate source. Table 3 gives its composition, following the prescriptions described in [66]. A commercially available potassium-based water glass (WG) Geosil® 14517, from Woellner, Germany, with a SiO₂/K₂O molar ratio of 1.7 was used as alkali activator, which contains a solid content of approximately 45% of potassium silicate. The aluminosilicate source was metakaolin (MK) Metamax® from BASF, Germany, with high reactivity and a low average particle diameter of 1.3 μm [67]. The WG-to-MK ratio is 1.82. To obtain

an adequate flowability for the impregnation process and dispersion, the superplasticizer Sapetin® D27 from Woellner, Germany, with a solid content of approximately 45%, was used in a dosage of 4% by mass of GP, as suggested by [59,68,69].

Table 3.3 – Geopolymer suspension composition

Waterglass Geosil (kg/m ³)	1000
Metakaolin (kg/m ³)	549.33
Superplasticizer Sapetin® D27 (kg/m ³)	61.97
WG/MK ratio	1.82

As a matter of comparison, a commercially available carbon yarn with a polymer-based impregnation (epoxy resin, EP) was also used as a reference. The yarn was extracted from the carbon fabric GRID Q85/85 – CCE – 21 from Solidian. Table 4 presents the technical data provided by the supplier.

Table 3.4 – Technical data of the Solidian GRID Q85/85-CCE-21

Impregnation material	Epoxy resin
Cross-section of the strand (mm ²)	1.81
Tensile strength of the roving (GPa)	2.50

3.2.2. Fine-grained concrete matrix

To evaluate the bond of the carbon yarns with the cementitious matrix, a fine-grained concrete similar to the one used in previous work [33] with a mix proportion of 1 : 1 : 0.3 (sand : cementitious material : water by weight) was used. Table 5 presents its composition. Portland cement CEM II-A/LL 42.5 N from Dyckerhoff GmbH, Germany, defined by the European Standard [70], and sand from Ottendorf, Germany, with a maximum particle diameter of 1 mm were used. Fly ash Steament H4 from STEAG Power Minerals GmbH, Germany, and Silica Fume from Elkem, Germany, were incorporated as mineral admixtures. A superplasticizer, MasterGlenium SKY 593 from BASF Construction Solutions GmbH, Germany, was used to achieve good workability of the fine-grained concrete for casting. Compression and flexural tests based on the European Standard EN 196-1 [71] were performed, and the compressive and flexural strengths at 28 days and room temperature were 67.8 ± 5.3 MPa and 6.81 ± 1.07 MPa, respectively.

Table 3.5 – Fine-grained concrete composition.

Sand (0-1 mm) (kg/m ³)	947
Cement CEM II/A-LL (kg/m ³)	632
Water (kg/m ³)	273.38
Fly ash (kg/m ³)	265
Silica fume (kg/m ³)	50.5
Superplasticizer (kg/m ³)	14.05

Compression tests at elevated temperatures were performed in a quasi in-situ condition as well. The specimens were heated at a rate of 3 °C/min until the desired temperature in a Universal Furnace UF1060 from Memmert GmbH + Co. KG, Germany. The temperature was kept constant for a minimum period of 4.5 hours. The specimens tested at 300 °C were first pre-heated at 200 °C to allow the slow evaporation of the free and physically bound water. After being removed from the hot furnace, the specimens were immediately tested.

3.2.3. Impregnation process

The cement impregnation suspension was produced using a standard kitchen blender. First, the water and the micro-silica were mixed with half of the total amount of superplasticizer. The micro-cements were gradually added to the mixture while constantly stirring to avoid agglomerations and evenly distribute the cement grains. Then, the remaining amount of the superplasticizer was added in parts without stop stirring. To dissolve existing agglomerates and guarantee a full dissolution of the particles, the slurry was finally mixed with a T 50 digital ULTRA-TURRAX® disperser from IKA® for 2 minutes at 7000 rpm.

The same disperser device was used to produce the geopolymer suspension. Firstly, the water glass and the metakaolin were mixed for 3 minutes at 7000 rpm. Then the superplasticizer was added to the mixture, and mixing was performed for another 3 minutes. After that, the suspension was vibrated for 2 minutes to eliminate entrapped air voids.

To be adequate for the impregnation method used in the development of the MCF, the mineral suspensions must present certain flowability [72]. A small funnel with a volume of approximately 150 ml and an opening diameter of 7 mm was used to determine the funnel flow time of both suspensions. The cementitious suspension presented a flow time of 8.35 s, and the geopolymer one of 23.25 s.

An automated, continuous pultrusion process was developed at the Institute for Construction Materials of the Technische Universität Dresden, Germany, for manufacturing MCFs [73]. The impregnation process is controlled by the “TwinCat” software and powered by a hexagonal, motor-driven wheel, as shown in Figure 3.1. The yarns are firstly unwound from the spool, pulled via three yarn guiding levels, a motor-driven kiss-coater, and a suspension bath containing five-roller deflections, and shaped by a plastic nozzle of 4 mm. Following the initial impregnation, the freshly impregnated yarns are continuously placed on the wheel side by side, controlled by an engine-driven linear unit. The hexagonal wheel (see Figure 3.1.a) has a total diameter of 2.40 m, with each edge being 1.20 m long and 0.80 m wide. The pulling velocity of 20 cm/s is chosen to secure high impregnation quality and industrial production efficiency. Three yarn guiding levels ensure the yarn alignment during processing to avoid fiber damages; see Figure 3.1.b. The five-roller configuration used can offer the optimal impregnation quality for the production of MCF; see Figure 3.1.d. Figure 3.1.e presents the impregnated MCF yarns in their final state.

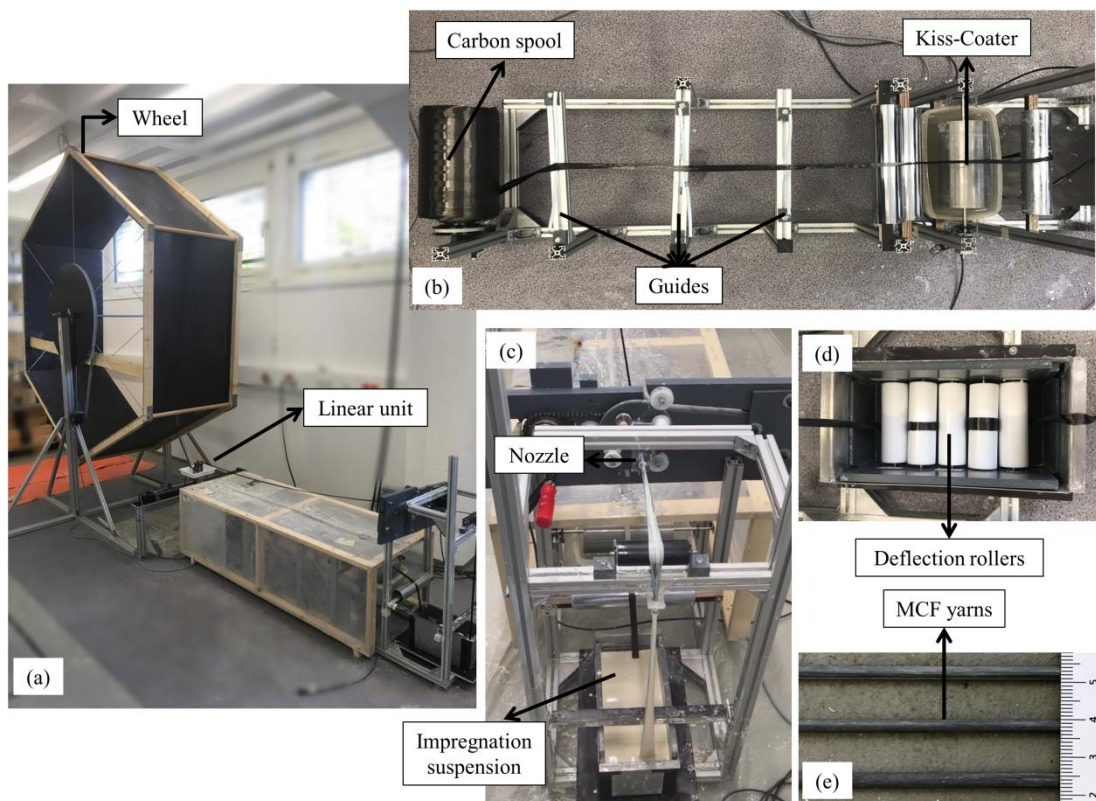


Figure 3.1 – Impregnation system: a) Overall view with the wheel; b) Yarn alignment guides and kiss-coater; c) Impregnation bath; d) Deflection rollers; e) ready MCF yarns.

After the pultrusion, the freshly impregnated C-MCF yarns were firstly stored over a plane surface for 7 days to enable initial hydration reactions. Subsequently, they were immersed in water for further 7 days, followed by the storage under standard climate (55% RH and 20 °C) until the manufacturing of the pull-out specimens, at a yarn age of 28 days, or the execution of the uniaxial tension tests.

The fresh GP-MCF yarns, after being removed from the wheel, were placed in a sealed wooden box and heated at 75 °C for 20 hours, as suggested in [59]. Following the heat curing, the GP-MCF yarns were submitted to a washing process, in which they were immersed in water for 7 days with water replacement every day so that the alkali concentration on the GP-MCF surface and in the pore solution of the geopolymer matrix [74,75] could be reduced. PH indicator strips showed a pH of 10.5 for the unwashed GP-MCF yarns. As a result of the washing process, the pH was reduced to 8. Before the preparation of the pull-out specimens, the yarns were removed from the water and air-dried for 24 hours.

3.2.4. Uniaxial Tension Tests on Carbon Yarn

To assess the tensile properties of these newly developed reinforcement yarns, uniaxial tension tests were conducted at yarn ages of 110 days and 95 days for C-MCF yarns and GP-MCF yarns, respectively, as shown in Figure 3.2. The yarns had a total length of 160 mm and a free length of 100 mm; see Figure 3.3b. Each end of the specimen was anchored by epoxy resin blocks with an anchoring length of 30 mm. For the manufacture of the specimens, a mold with three independent blocks, as shown in Figure 3.3.a, was used. First, the carbon yarn was positioned in the center of the mold, and both Blocks A (see Figure 3.3a) were filled with the liquid epoxy resin. To guarantee a better penetration of the epoxy resin between the filaments and improve the anchorage of the yarn, the yarns were open and spread in the anchorage region. After 24 hours, the time necessary for the resin to harden, the specimens were removed from the molds.

The tests were performed in a servo-hydraulic testing machine Instron model 8501 with a maximum load capacity of 100 kN. The force from the testing machine was introduced to the specimen through specific aluminum grippers; see Figure 3.2. The tests were controlled by the actuator displacement at three different rates: 0.02

mm/s, 2 mm/s, and 20 mm/s, corresponding to strain rates of 0.0002 s^{-1} , 0.02 s^{-1} , and 0.2 s^{-1} , respectively. The strain rate was obtained dividing the rate of the actuator displacement by specimen gauge length. An optical video-extensometer Model 200XR from Rudolph, Germany, was used to measure the displacement of the specimen at a gauge length of 100 mm. Two target marks made from black and white stripes were fixed on the edges of the aluminum device for this purpose. At least 5 specimens for each variable were tested.

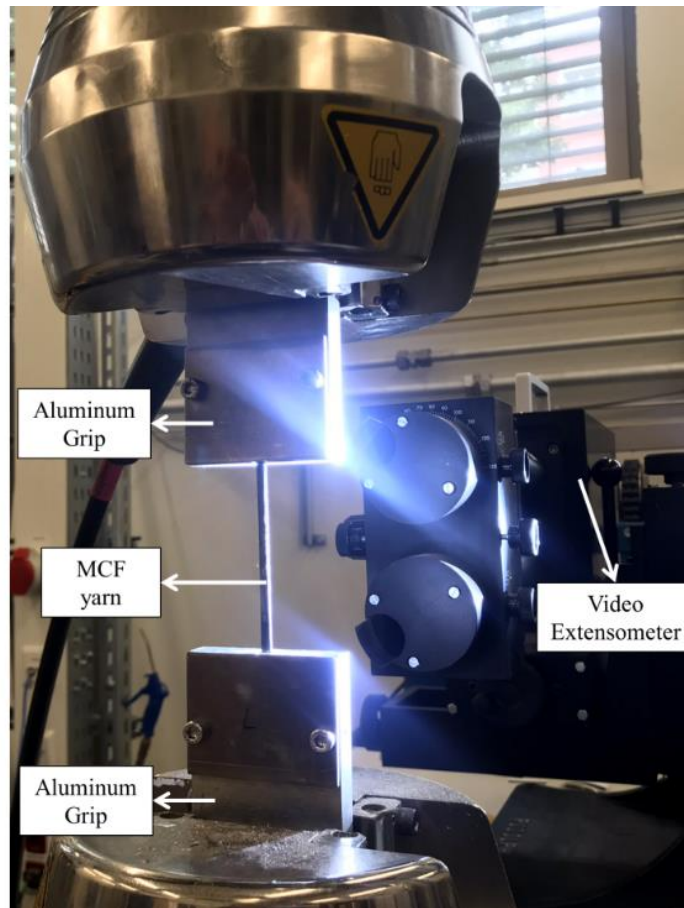


Figure 3.2 – Setup for the yarn uniaxial tension tests.

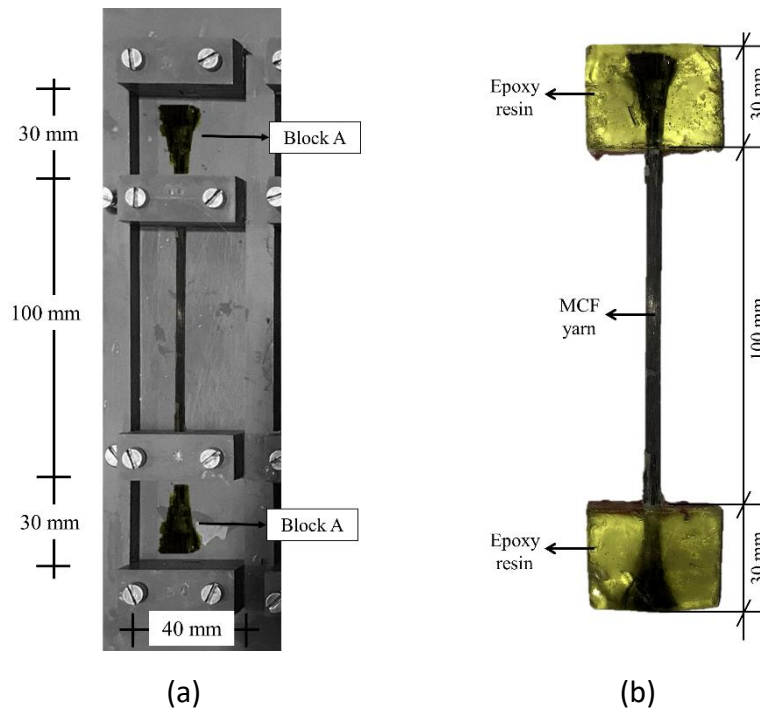


Figure 3.3 – Specimen for the yarn uniaxial tension tests. a) Manufacturing; b) Geometry and dimensions.

3.2.5. Pull-out Tests on Yarns

Yarn pull-out tests were performed to evaluate the bond between the carbon yarns and a fine-grained concrete matrix. The specific testing setup and corresponding specimen geometry were developed at the Institute for Construction Materials of the Technische Universität Dresden, Germany [45]. The pull-out specimens consist of two blocks of the fine-grained concrete matrix connected by the testing carbon yarn, as shown in Figure 3.4 – Procedure for the pull-out specimens manufacturing. a) Plastic mold; b) Yarn positioned in the center of the mold; c) Specimens after casting with the steel holder already positioned; d) Pull-out specimens after demolding.

. The yarn pull-out occurs in the upper block. An embedded length le of 20 mm was selected for both mineral- and polymer-impregnated CF yarns. The lower block has the function of anchoring the yarn and introducing the force into the specimen.

For the pull-out specimens manufacturing, a plastic mold with the dimensions presented in Figure 3.4.a was used. The carbon yarns were first positioned centrally in the molds, with the exact embedded length in the upper block, as presented in Figure 3.4.b, and then both upper and lower blocks were cast with the fine-grained

concrete matrix. Just after casting, while the matrix was still fresh, a steel holder was positioned connecting the upper and lower fine-grained concrete blocks (see Figure 3.4.c) to preserve the carbon yarn during handling and transportation of the specimens. After 24 hours, the specimens were removed from the molds (Figure 3.4.d) and stored in a climatic chamber at 55% relative humidity and 20 °C for 28 days. The steel holder was unscrewed from the specimens just before testing. At least 5 specimens were manufactured for each test variable.

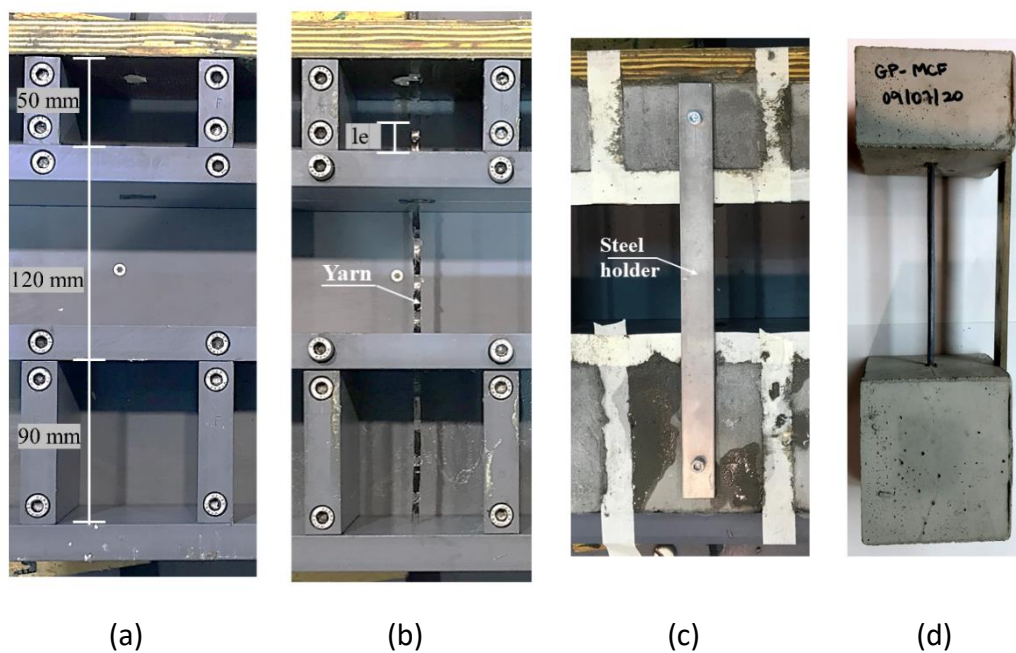


Figure 3.4 – Procedure for the pull-out specimens manufacturing. a) Plastic mold; b) Yarn positioned in the center of the mold; c) Specimens after casting with the steel holder already positioned; d) Pull-out specimens after demolding.

The pull-out tests were carried out in a servo-hydraulic testing machine Instron model 8501 with a maximum load capacity of 100 kN; see Figure 3.5a. The displacement of the machine holder was recorded as the pull-out slip. The tests were controlled by the actuator displacement at 4 different rates: 0.02 mm/s, 0.2 mm/s, 2 mm/s, and 20 mm/s, corresponding to strain rates of 0.001 s^{-1} , 0.01 s^{-1} , 0.1 s^{-1} , and 1 s^{-1} , respectively. The strain rate was obtained dividing the rate of the actuator displacement by the specimen gauge length, i.e., the embedded length.

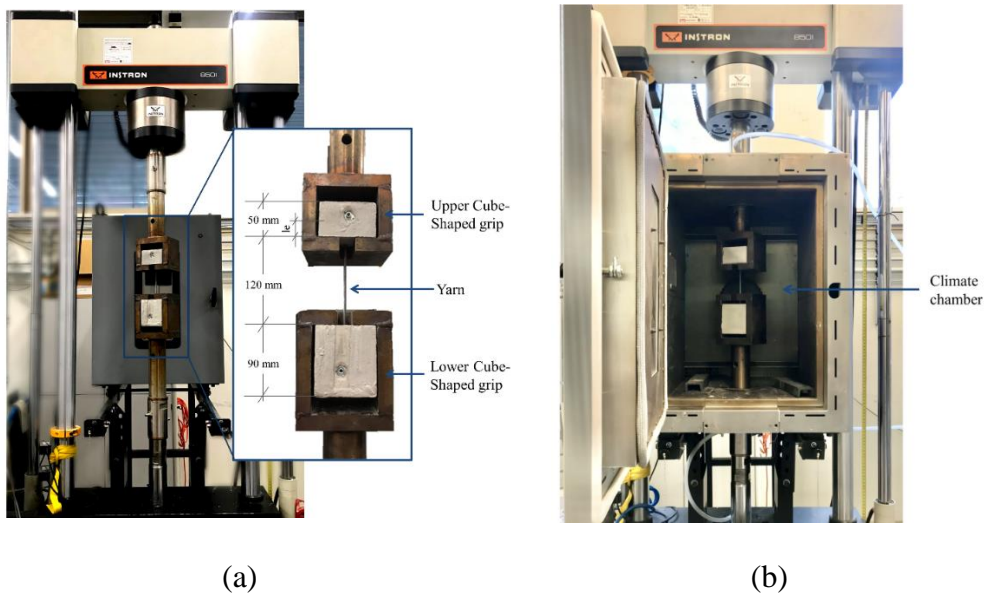


Figure 3.5 – Setup for the pull-out tests at (a) room temperature and (b) elevated temperatures.

For the temperature in-situ tests, a temperature-controlled climate chamber of INSTRON Type 3119-608 was used; see Figure 3.5b. The specimens were tested at 150 °C, 200 °C, and 300 °C. These temperatures were chosen in such way that at least one of the them was above the glass transition point of the polymer-based impregnation, which generally range between 50 °C to 180 °C [76,77].

Before testing, the specimens were preheated in a Universal Furnace UF1060 from Memmert GmbH + Co. KG at a rate of approximately 3 °C/min up to the desired temperature. Based on previous works [44,45], the specimens tested at 150 °C and 200 °C were maintained at the target temperature for approximately 20 hours. The specimens tested at 300 °C were preheated for approximately 16 hours at 200 °C to allow the slow evaporation of the physically and partially chemically bound water. Figure 3.6 shows the heating regime for all target temperatures [45].

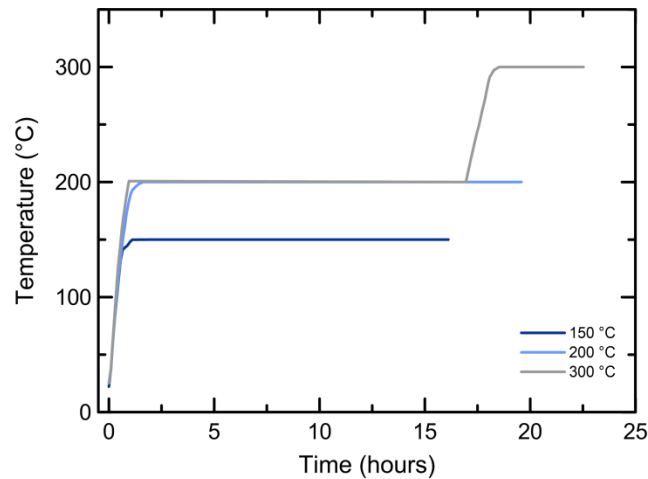


Figure 3.6 – Heating regime for the pull-out specimens.

The pull-out results were analyzed by means of the average interfacial shear stress. While this value has no clear physical meaning since this approximation assumes a uniform interfacial shear stress distribution along the whole embedded length [24], it still offers a good possibility to comparatively assess the quality of the bond. The average interfacial shear stress τ was obtained through the simplified equation below (Eq. 3.1):

$$\tau = \frac{P}{2\pi r l_e} \quad (3.1)$$

where P is the pull-out load, l_e is the embedded length, and $2\pi r$ is the perimeter of the yarn cross-section, obtained with the software ImageJ.

Figure 3.7 presents a schematic average interfacial shear stress vs. slip curve obtained from pull-out tests. Based on it, five parameters were established to characterize the bond behavior between the carbon yarns and the fine-grained concrete matrix. The maximum average interfacial shear stress τ_{max} is the ultimate stress value reached before the beginning of the drop of the average interfacial shear stress vs. slip curve. This parameter was considered as the main one to analyze the quality of the bond. Similar to what was performed in previous work [45], to estimate the crack-bridging effect of the reinforcement in concrete structures, the pull-out stress values were obtained for a slip of 0.5 mm ($\tau_{0,5}$), representing small crack widths and thus contemplating the Serviceability Limit State (SLS), and for a slip of 2 mm (τ_2), representing the large deformations scenario. The specific work to pull-out W_1 , up to a slip of 1.0 mm, and the total work W_{total} , up to a slip of 4.5

mm, were also obtained. Both were calculated as the area under the stress vs. slip curve up to the correspondent slip.

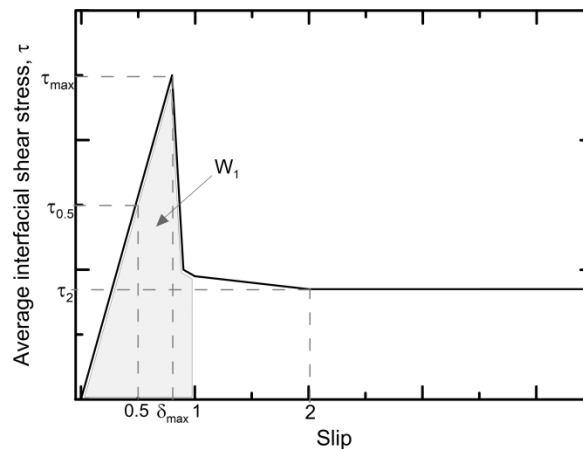


Figure 3.7 – Schematic average interfacial shear stress vs. slip curve obtained from pull-out tests.

3.2.6. Morphological Analyze

A digital microscope model VHX-6000 with a CMOS sensor camera with 18 megapixels from Keyence and μ CT-scans on CT-XPRESS from ProCon X-Ray, Germany, at a voltage of 95 kV and 132 mA was used to analyze the interface and the pull-out channel of the embedded carbon yarns after the pull-out tests.

3.3. Results and discussion

3.3.1. Fine-grained concrete matrix

Figure 3.8 shows the compressive strength of the fine-grained concrete matrix at room temperature ($\sim 20\text{ }^{\circ}\text{C}$), $150\text{ }^{\circ}\text{C}$, $200\text{ }^{\circ}\text{C}$, and $300\text{ }^{\circ}\text{C}$. At $150\text{ }^{\circ}\text{C}$, there is a drop in the compressive strength, while when heating to $200\text{ }^{\circ}\text{C}$ and $300\text{ }^{\circ}\text{C}$, a recovery in strength can be observed. It is important to emphasize that there is only a little difference in the strength values at $200\text{ }^{\circ}\text{C}$ and $300\text{ }^{\circ}\text{C}$. The standard deviation of the results at $300\text{ }^{\circ}\text{C}$ is slightly higher than at $200\text{ }^{\circ}\text{C}$, which is probably due to the higher temperature itself. A similar trend was reported by [78–80], and can be partially explained by the corresponding water loss over increasing temperatures. The degradation of hardened cement pastes starts with the slow loss of the free water at temperatures up to $100\text{ }^{\circ}\text{C}$ [23]. From $100\text{ }^{\circ}\text{C}$ to $200\text{ }^{\circ}\text{C}$, the bound water from the calcium silicate hydrate (C-S-H) starts to be lost [23,78]. The dehydration

of ettringite begins at around 35 °C [81,82], and its decomposition is in the range of 120 °C – 130 °C [83,84]. At temperatures around 100°C to 150°C, Hager and Pimienta [80] and Pimienta et al. [78] stated that the physically bound water is still not fully released due to the high density of High Strength (HS) cement pastes. This creates a vapor pressure inside the specimen, and due to thermodynamic equilibrium, there is a reduction of the surface energy and, consequently, in the compressive strength. The recovery of the compressive strength at temperatures in the range of 250°C is due to the free-water full evaporation [78,80].

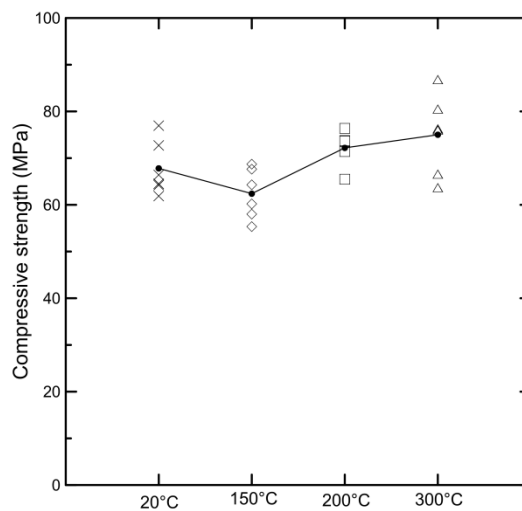


Figure 3.8 – Compressive strengths of the fine-grained concrete matrix at different temperatures.

3.3.2. Uniaxial Tension Tests on Yarns

Figure 3.9 shows the tensile stress vs. strain curves obtained from the tension tests performed on the C-MCF and GP-MCF yarns, for all specimens and the representative ones. In some cases, the data obtained contained considerable noise, so a fitting polynomial curve was obtained to represent the specimen. As a reference, the tensile stress vs. strain curve for the EP yarn was calculated using the data from the supplier. Table 3.6 presents the obtained tensile strength σ_t , modulus of elasticity E , and maximum strain ε_{rup} for the MCF yarns.

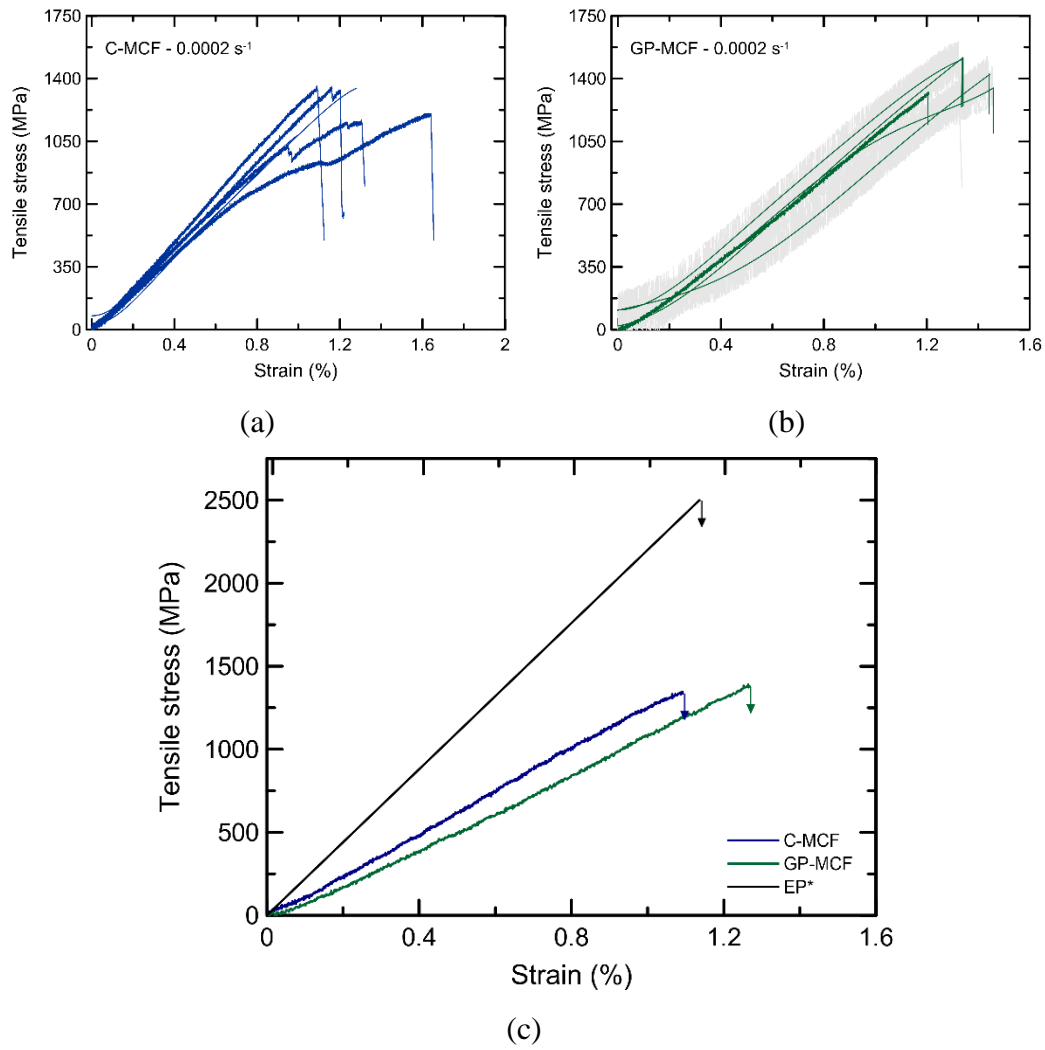


Figure 3.9 – Tensile vs. strain curves obtained for all specimens of the (a) C-MCF yarns, and (b) GP-MCF yarns. (c) Representative tensile stress vs. strain curves for the carbon yarns. *Curve constructed using the data from the supplier.

Table 3.6 – Average results and standard deviation (given in parenthesis) obtained from the yarn tension tests at different strain rates

Strain rate (s ⁻¹)	σ_t (MPa)	E (GPa)	ε_{rup} (%)
C-MCF			
0.0002	1373 (300)	118 (10)	1.30 (0.24)
0.02	1459 (260)	123 (8)	1.33 (0.25)
0.2	1108 (360)	111 (16)	1.07 (0.25)
GP-MCF			
0.0002	1517 (81)	114 (6)	1.36 (0.07)
0.02	1482 (205)	122 (6)	1.26 (0.23)
0.2	1282 (252)	112 (15)	1.33 (0.21)

Both C-MCF and GP-MCF yarns showed similar mechanical behavior. An elastic behavior up to their brittle rupture can be observed, which is in accordance with the expected nature of carbon fibers [85] and impregnation materials. The C-MCF yarns yielded tensile strength of 1373 MPa and modulus of elasticity of 118 GPa. The GP-MCF yarns had tensile strength and modulus of elasticity of 1517 MPa and 114 GPa, respectively.

The tensile strength of the GP-MCF yarn was approximately 11% higher than that of the C-MCF. This could indicate higher efficiency of the geopolymer suspension in filling the spaces between the filaments. As a result, all filaments are more uniformly loaded, leading to an increase in the failure stress [1]. It is important to emphasize that the strength of the hardened suspension and the bond between the inner filaments would also influence the tensile strength of the MCF yarns. More studies should be performed to understand the contribution of each mechanism on the results.

The modulus of elasticity obtained for both MCF yarns was relatively low when compared to the available data in the literature for carbon fibers [24]. This could actually be a characteristic of the MCF yarns, or else an error in the data acquisition, namely in the strain, could have occurred in the tests. An optical video-extensometer was used to obtain the displacements. The target marks used as reference were fixed in the aluminum grippers since it was not possible to fix them

directly to the yarn due to its small diameter. Thus, the displacement obtained from the tests could have been the displacement of the entire system, including the gripping, the specimen holder, and the specimen itself. Figure 3.10 presents the representative tensile stress vs. strain curves comparing the strain obtained with the displacement recorded by the video-extensometer and the actuator displacement. It is possible to observe that both curves are practically coincident, indicating that the video-extensometer did not record the specimen displacement. Thus, the modulus of elasticity obtained does not represent the mechanical property of the MCF yarns and can only be used to qualitatively compare the C- and GP-MCF yarns' behavior.

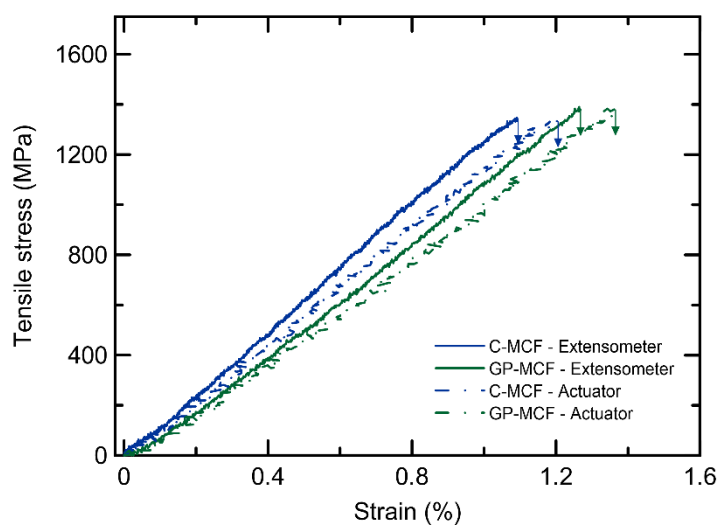


Figure 3.10 – Representative tensile stress vs. strain curves obtained with the displacement recorded by the video-extensometer and the actuator displacement for the C-MCF and GP-MCF yarns.

Figure 3.11 presents the failure modes of the C-MCF and GP-MCF yarns. Both types of yarns did not show total rupture. Instead, they exhibited some fibers' rupture and some delamination, the first being more dominant in the C-MCF yarns and the second in the GP-MCF yarns.

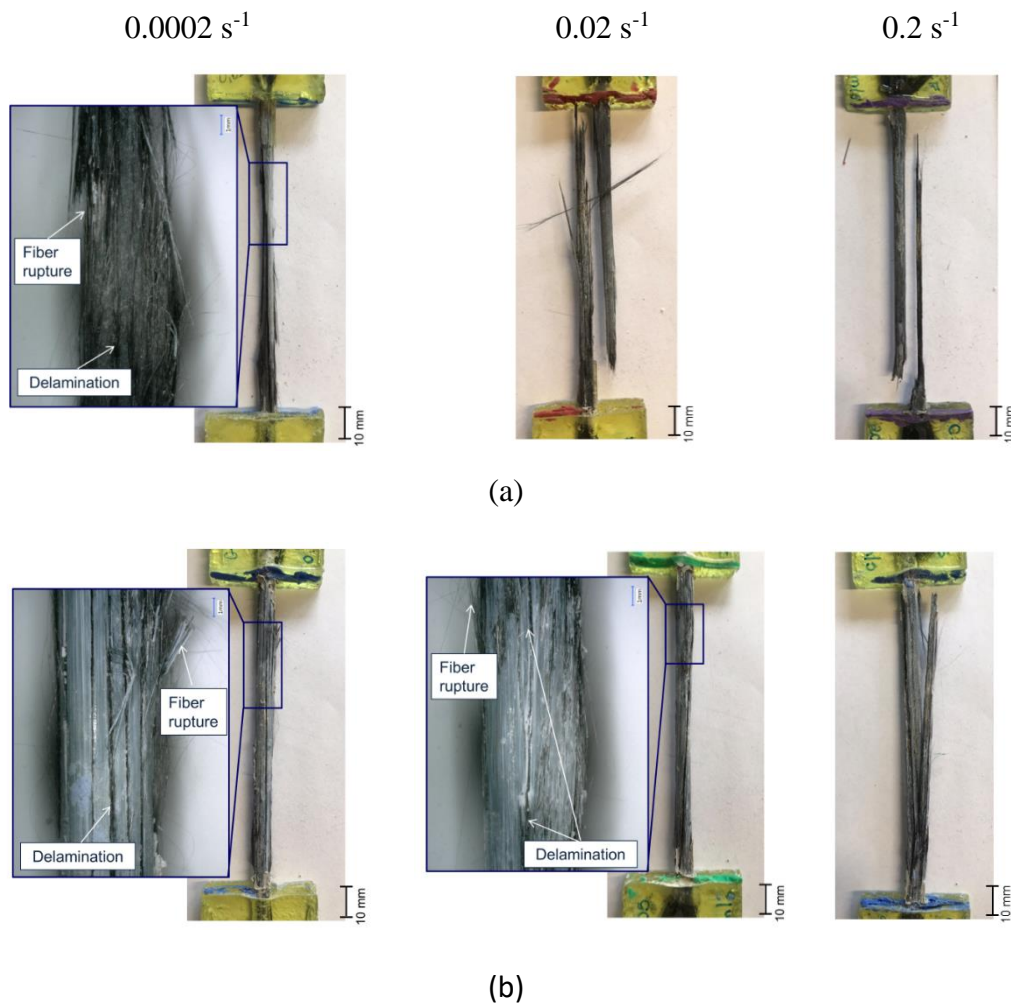


Figure 3.11 – Failure modes of the (a) C-MCF and (b) GP-MCF yarns at different strain rates.

3.3.2.1. Effect of different strain rates

The dependence of the mechanical properties of the MCF yarns with the loading application speed was also evaluated. Figure 3.12 and Figure 3.13 shows the tensile stress vs. strain curves obtained from the tension tests performed on the C-MCF and GP-MCF yarns at different strain rates for all specimens and the representative curves, respectively. Table 3.6 presents the obtained average tensile strength σ_t , modulus of elasticity E , and maximum strain ϵ_{rup} for the MCF yarns.

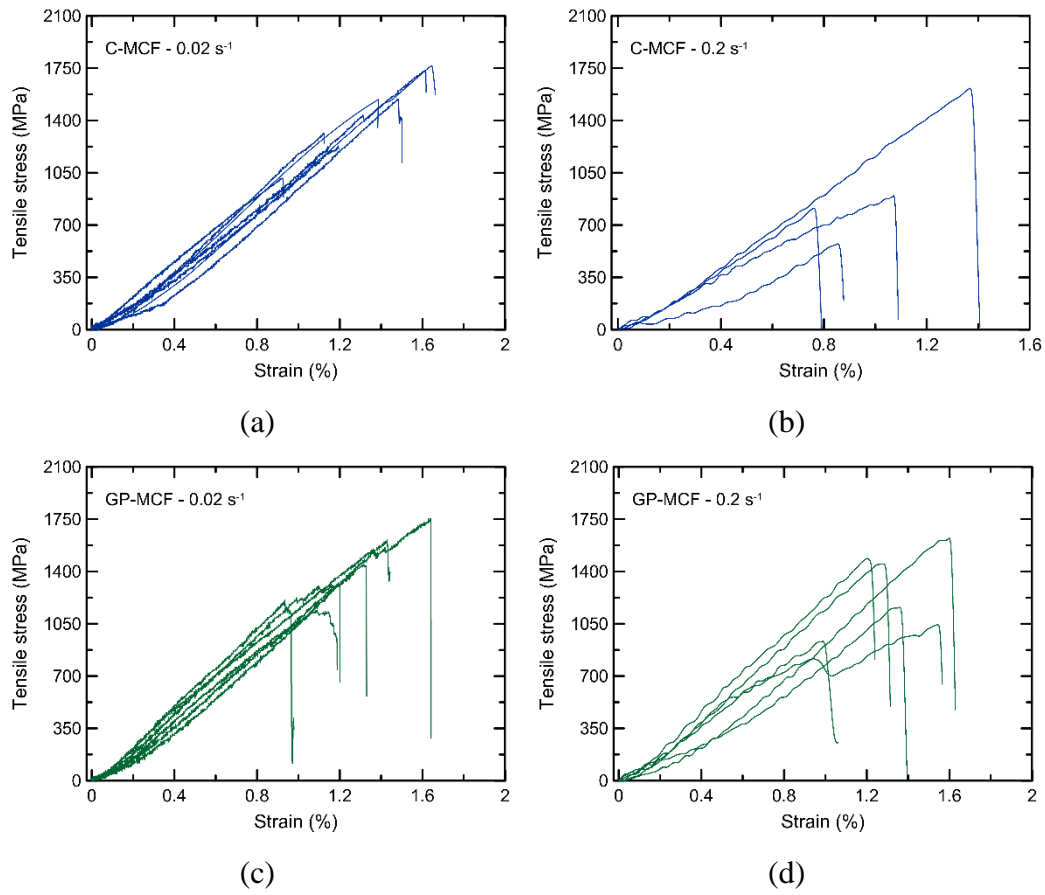
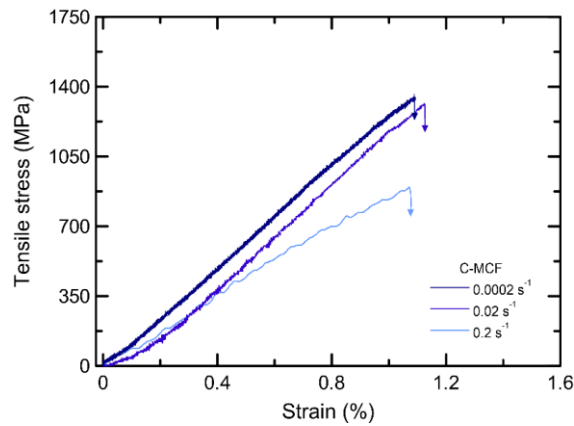
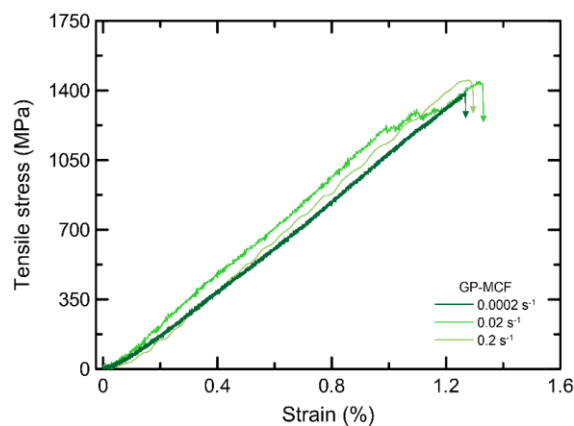


Figure 3.12 – Tensile vs. strain curves obtained for all specimens of the C-MCF yarns at (a) 0.02 s⁻¹ and (b) 0.2 s⁻¹, and GP-MCF yarns at (c) 0.02 s⁻¹ and (d) 0.2 s⁻¹.



(a)



(b)

Figure 3.13 – Representative tensile stress vs. strain curves obtained from the yarn tension tests at different strain rates for the (a) C-MCF and (b) GP-MCF.

Similar to the quasi-static results, both C-MCF and GP-MCF yarns presented a fragile behavior up to their rupture at all strain rates. No significant difference in the average tensile strength and modulus of elasticity of the specimens could be observed with an increase in the test strain rate, indicating that the carbon yarns can still maintain their mechanical properties in this range of strain rates. It is important to emphasize that a considerable variation in the results for the C-MCF yarns at 0.2 s^{-1} was observed. This could be related to problems in the specimen manufacturing, difficulty to perform the tests at this rate (seven specimens were produced for this variation, but only four tests were successful), or sensitivity of this material to elevated strain rates. Further studies must be performed to access the influence of the strain rate on a dynamic regime level on the mechanical behavior of the carbon yarns.

With the increase in the strain rate, the tensile strength of the GP-MCF yarns was still slightly higher than the tensile strength of the C-MCF yarns. This increase was approximately 2% and 16% for the strain rates of 0.002 s^{-1} and 0.2 s^{-1} , respectively. However, this increase was not linear with the increase in the strain rate.

Figure 3.11 shows the failure modes of the C- and GP-MCF, respectively, at different strain rates. Although no significant difference could be observed in the mechanical properties with the increase of the strain rate, a marked change in the failure mode can be noted. As mentioned before, in the lowest strain rate, both C- and GP-MCF yarns presented some fibers rupture and some delamination, the first being more dominant in the C-MCF and the second in the GP-MCF yarns. With an increase in the strain rate, the failure mode of both mineral impregnated carbon yarns changed. At the strain rates of 0.02 s^{-1} and 0.2 s^{-1} , the C-MCF specimens presented a total yarn rupture. On the other hand, the failure mode of the GP-MCF yarn was only modified to a total yarn rupture with an increase in the strain rate to 0.2 s^{-1} . This delay in changing the failure mode could indicate that the GP-MCF yarns are less susceptible to changes in their behavior with increasing loading speed. Trindade et al. [72] demonstrated that, compared to PE-SHCC (strain-hardening cementitious composites with polyethylene fibers), SHGCPE (strain-hardening geopolymer composites with polyethylene fibers) presented better mechanical performance regarding the behavior after the first crack formation and multiple-cracking pattern, showing diminished effects of rate-dependency. Textile reinforcements that do not present a significant strain-rate dependency result in TRCs with a more ductile behavior and higher energy absorption when submitted to impact loadings [86]. Furthermore, when the failure mode of the textile is not governed by the rupture of all filaments at the same time but by the failure of only some filaments within the yarn, the composite with this type of reinforcement may present a pseudo-ductile behavior [61].

3.3.3. Carbon Yarn Pull-out Behavior

Figure 3.14 and Figure 3.15 presents the average interfacial shear stress vs. slip curves for the C-MCF, GP-MCF (with washing process), and EP yarns for all the specimens and the representative ones, respectively, obtained from the pull-out

tests at room temperature. The respective results for the maximum average interfacial shear stress τ_{max} , the slip δ_{max} at τ_{max} , the average interfacial shear stress at 0.5 mm $\tau_{0.5}$, the average interfacial shear stress at 2 mm τ_2 , the specific work to pull-out W_I , and the total work W_{total} are presented in Table 3.7. Figure 3.16 presents the matrix-yarn interface region, and Figure 3.17 the pull-out channel of the different carbon yarns embedded in the fine-grained concrete matrix after the pull-out tests at room temperature obtained through microscopic analysis. The interface region and the pull-out channel were also analyzed through μ CT. Figure 3.18 presents the μ CT images captured in the fiber direction, showing the interface region between the reinforcement and the fine-grained concrete matrix and the specimens' pull-out channel. All samples were prepared by cutting the anchoring parts of the pull-out specimens without damaging them. The components are colored in different shades of gray according to their density. The pronouncedly black or dark gray areas indicate either plain carbon filaments or voids, which have low densities. All specimens presented a failure pattern in the matrix-yarn interface region with a pull-out behavior. From the interface region images, it is possible to observe that the C-MCF and EP yarns were better bonded to the fine-grained concrete matrix than the GP-MCF. However, no fibers attached to the matrix could be observed in the pull-out channel of the EP yarn, as shown in Figure 3.17.

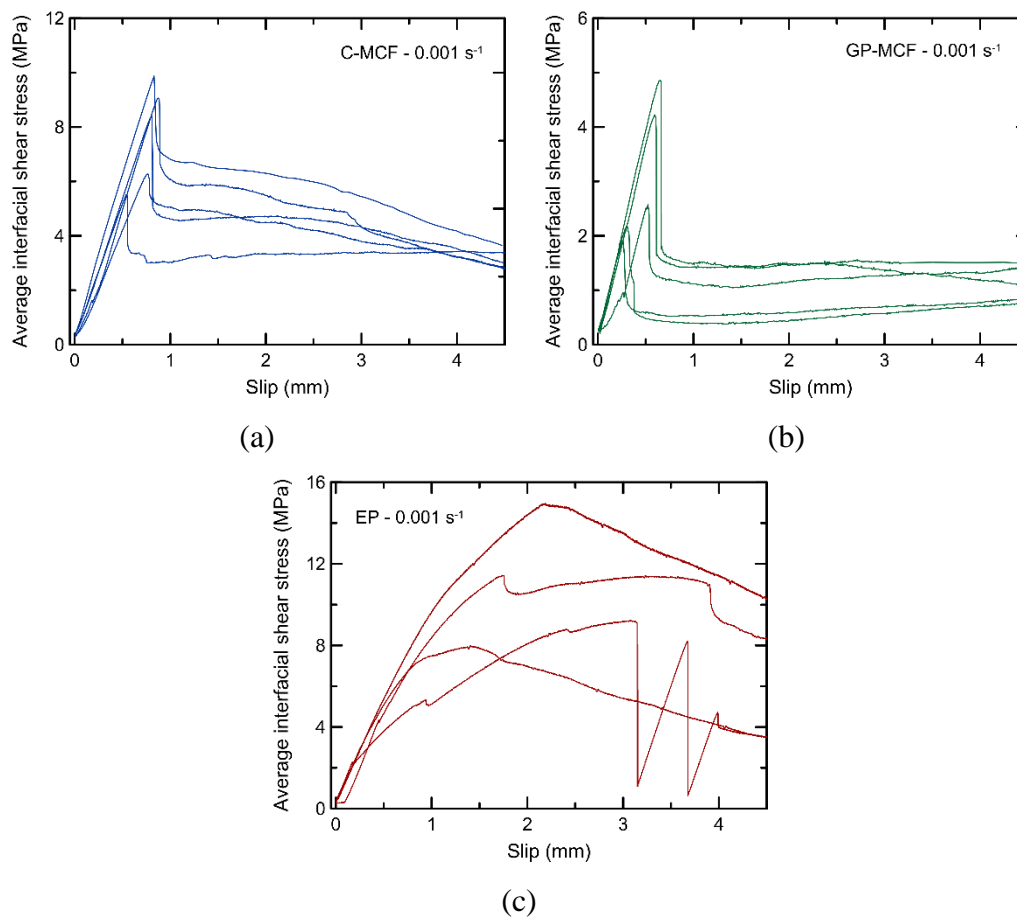


Figure 3.14 – Average interfacial shear stress vs. slip curves obtained in the pull-out tests for the (a) C-MCF, (b) GP-MCF (with washing process), and (c) EP yarns.

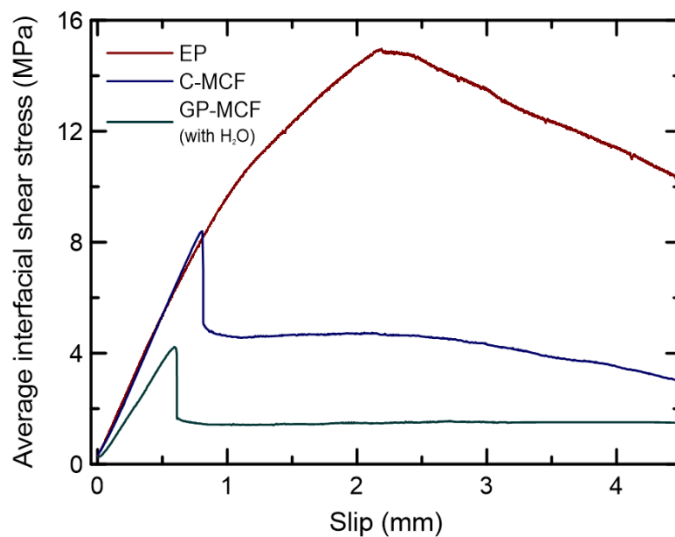


Figure 3.15 – Representative average interfacial shear stress vs. slip curves obtained in the pull-out tests for the C-MCF, GP-MCF (with washing process), and EP yarns.

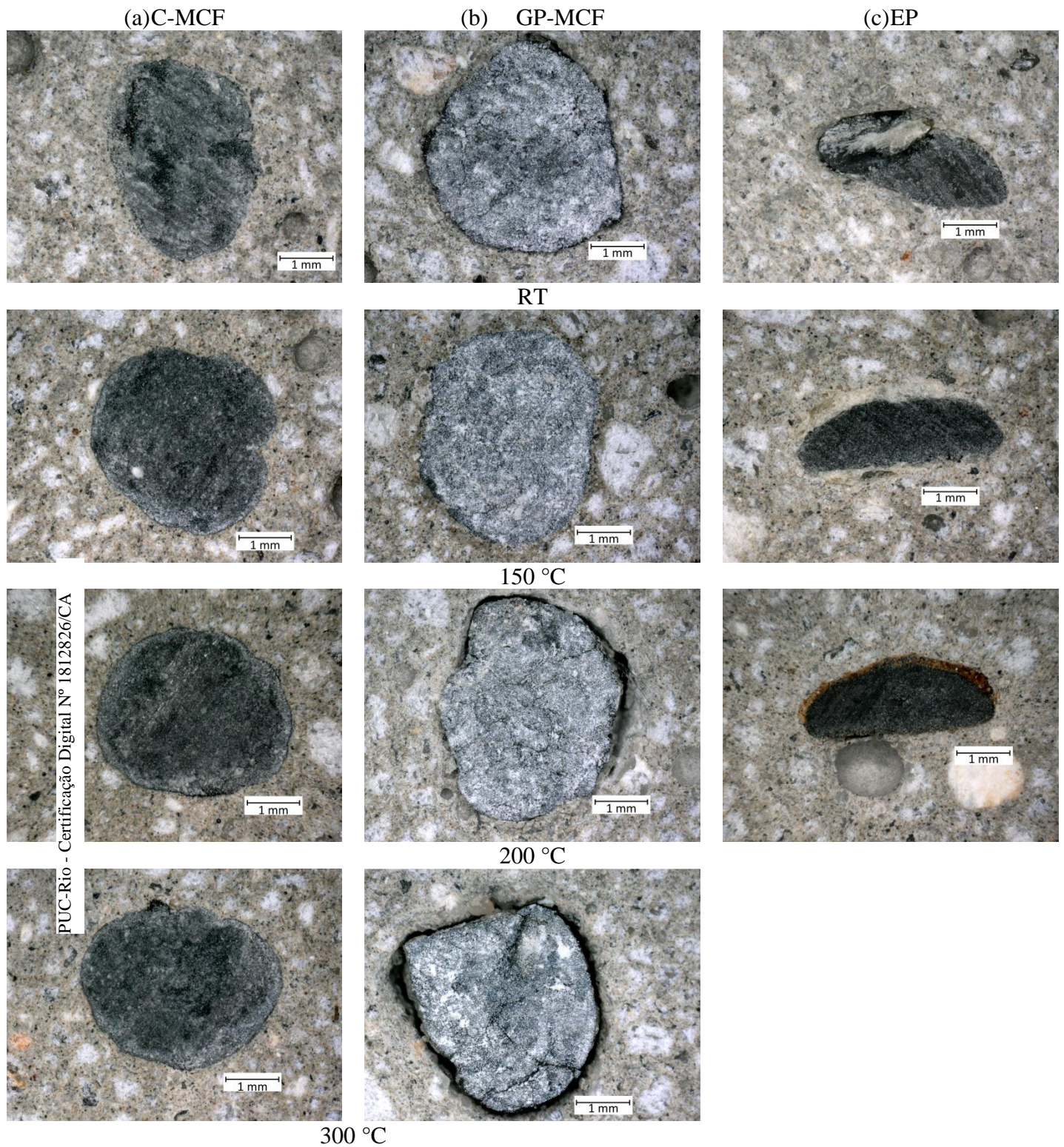


Figure 3.16 – Images from the matrix-yarn interface region from the (a) C-MCF, (b) GP-MCF, and (c) EP yarns after the pull-out tests at room temperature (RT), 150 °C, 200 °C, and 300 °C.

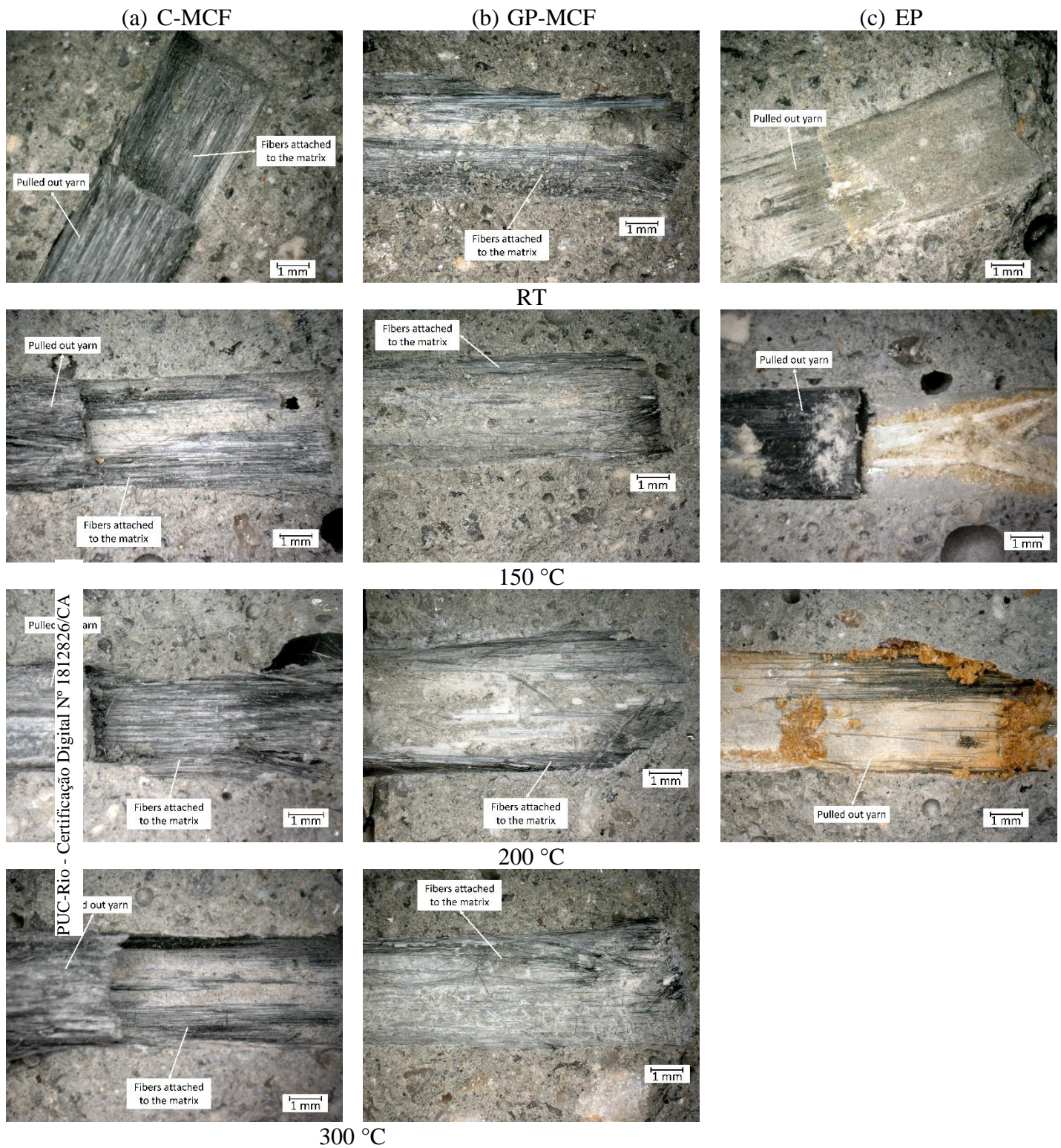


Figure 3.17 – Images from the pull-out channels for the (a) C-MCF, (b) GP-MCF, and (c) EP yarns after the pull-out tests at room temperature (RT), 150 °C, 200 °C, and 300 °C.

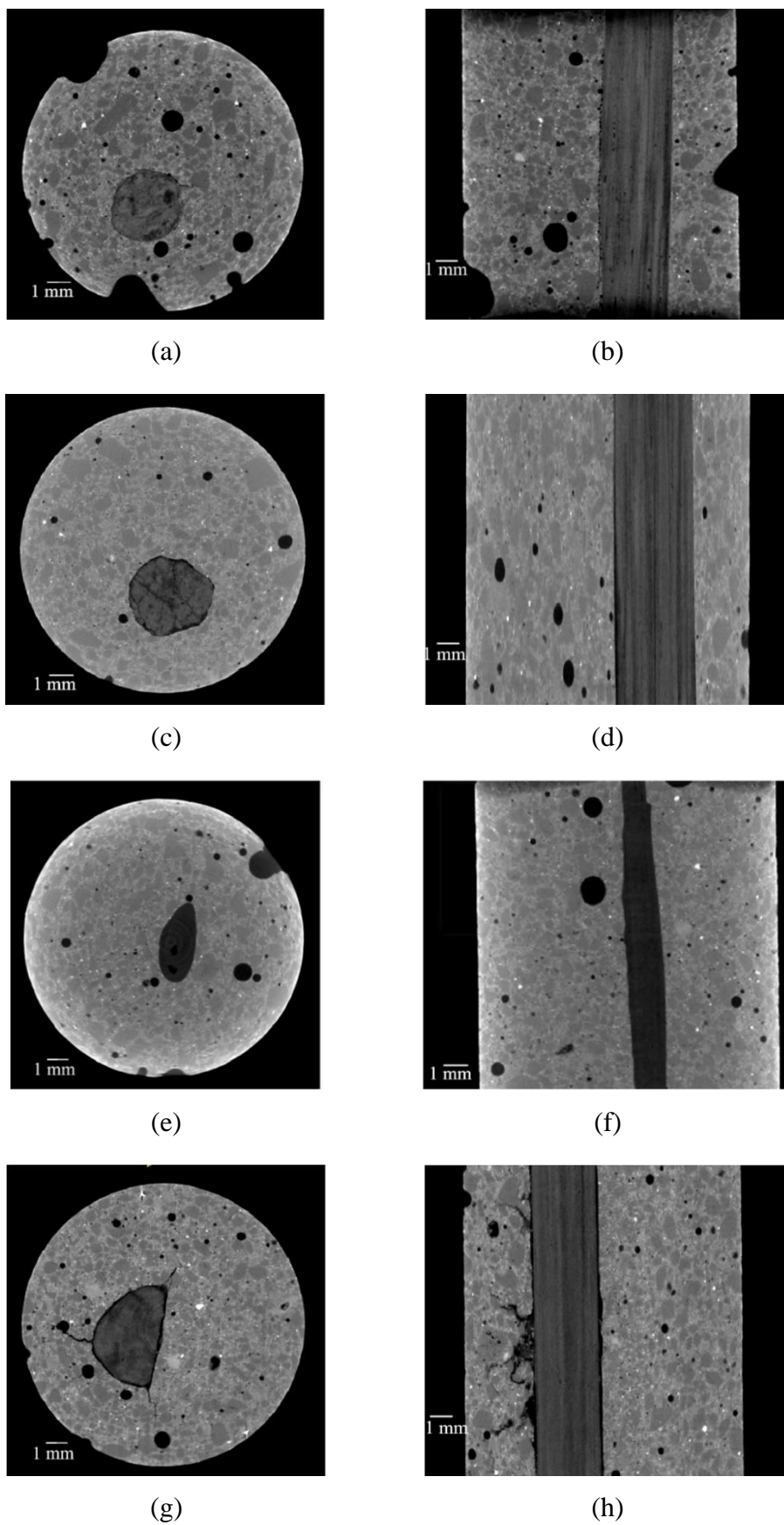


Figure 3.18 - μ CT images of pull-out test specimens: (a,b) C-MCF; (c,d) GP-MCF with washing process; (e,f) EP; and (g,h) GP-MCF without washing process.

All three CF yarns show a linear behavior up to the maximum average interfacial shear stress. After reaching the peak value, the MCF yarns presented an abrupt drop, followed by a plateau in the case of the GP-MCF, or a very soft decay in the case of the C-MCF. This clear difference in the final stage for both MCF yarns may be related to the roughness of the yarns' surface. The GP-MCF possesses a very smooth surface, whereby the C-MCF appears more porous. Latter has pores with higher diameters (up to 10 μm) [45], whereby the GP-MCF yarn is rather dense, having pores' sizes up to 0.1 μm [59]. This may result from a better wetting of the C-MCF by the fine-grained concrete. In contrast, the CF yarn with epoxy impregnation presented a gradual drop in the stress in the pull-out stage.

Considering the interfacial shear strength of the respective samples, the C-MCF and GP-MCF yarns reached maximum average stresses of 7.85 MPa, and 3.15 MPa, respectively. Thus, the C-MCF yarns yielded a stronger bond with the fine-grained concrete matrix in comparison to the GP-MCF, probably due to its higher chemical compatibility to the cementitious matrix. Figure 3.16a,b and Figure 3.18a, c show the matrix-yarn interface region of the C-MCF and GP-MCF yarns after the pull-out tests. At room temperature, the C-MCF yarn is well attached to the matrix, indicating chemical compatibility of the cement suspension and the fine-grained concrete matrix, which may have favored the formation of hydration products in the yarn-matrix interface region. Furthermore, no apparent cracks can be observed in the C-MCF μCT samples (Figure 3.18a,b), confirming their excellent embedment within the fine-grained concrete matrix. The well-embedded yarns are able to build a good mechanical interlocking due to the transverse pressure of the matrix, and in the case of the C-MCF, this is favorable to the formation of the chemical bond of these yarns towards cementitious matrices. Differently, there is a gap between the GP-MCF yarn and the fine-grained concrete matrix. Some incompatibility between the geopolymer and the fine-grained concrete matrix may have occurred, which could prevent the chemical interfacial reaction, characterized by the empty spaces between the yarn and the matrix, leading to a weakness of this region.

Good compatibility has been reported between geopolymer mortars and concrete [87–91]. However, the results obtained in this study points out into another direction. The fine-grained concrete matrix used contains amorphous silica from the silica fume addition, which is used to increase the strength [23,92–94] and

decrease the porosity [95,96] of cementitious materials. The GP-MCF yarn presents an alkaline surface (pH equal to 8). The presence of high alkaline content on the yarn and the mixing water from the fine-grained concrete are potentially a favorable environment for alkali-silica reaction (ASR) to occur in the yarn-matrix interface region [97,98]. ASR is common to occur in concretes with siliceous aggregates [23,97,98]. Under favorable conditions, the silica can react to form a gel, which is expansive and can lead to micro-cracks in the surrounding concrete, thus decreasing its strength [97,98]. The μ CT analysis (see Figure 3.18) showed the formation of micro-cracks in the interface between the GP-MCF yarn and the fine-grained concrete matrix. Additionally, with the dissolution and gelation of the silica, less silica at the yarn-matrix interface could be available to react with the CH formed in the Portland cement hydration forming secondary C-S-H, which further weakens the interface region, and thus could affect the bond between the GP-MCF yarn and the fine-grained concrete matrix. Further analysis needs to be conducted to corroborate this assumption. The reduction in the pH values after washing indicates that the amount of alkali ions on the GP-MCF surface and in the pores of the geopolymer suspension was reduced and leached out, effectively inhibiting these effects. The μ CT analysis showed that, for the GP-MCF without the washing process, continuous extensive cracks are formed around the reinforcement in the matrix microstructure and propagate along the fiber longitudinal direction through the entire sample, almost fully destroying the possible chemical bond with the fine-grained concrete; see Figure 3.18g,h. These cracks are potentially caused by the ASR. Moreover, the loosely compacted interface formed tends to spread out to some extent in the direction perpendicular to the yarn and may offer very limited formfitting with the surface of the MCF. With the washing process, much less and discontinuous cracking was formed in the GP-MCF samples, see Figure 3.18c,d, indicating that the ASR has been significantly inhibited, and a higher amount of silica might be available, which could increase the strength of the matrix in the interface region with the yarn. Trial pull-out tests confirmed that the washing post-treatment indeed improved the bond between the GP-MCF yarn and the fine-grained concrete matrix, as shown in Figure 3.19. Future studies should be conducted to fully understand the bond mechanism of GP-MCF yarns when embedded in fresh fine-grained concrete matrices.

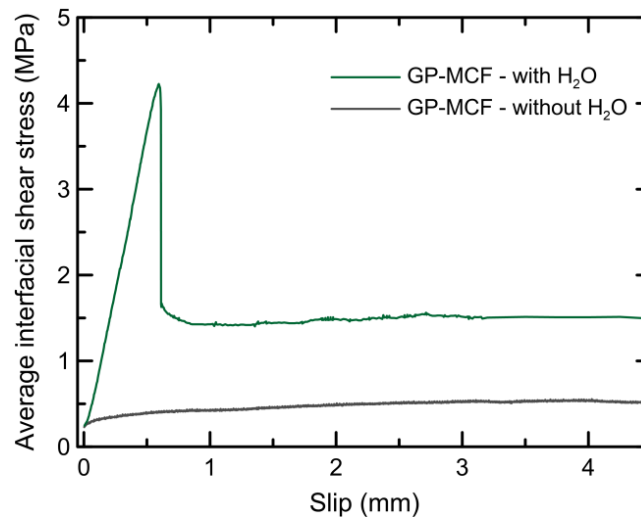


Figure 3.19 – Representative average interfacial shear stress vs. slip curves obtained in the pull-out tests for the GP-MCF without and with the washing process (H₂O).

The EP yarns reached the highest maximum average interfacial shear stress at room temperature, i.e., 14.1 MPa, indicating the best bond with the fine-grained concrete matrix. As previously discussed, for this type of coating, the pull-out curve presents a soft decay after reaching its peak. The images obtained from the pull-out channel after the tests, shown in Figure 3.17, emphasize that the bond mechanisms between the mineral impregnated yarns and the one with the polymeric coating are indeed different. On the images from the mineral impregnated yarns (see Figure 3.17a,b), it can be seen that some fibers remain attached to the matrix after the yarn is pulled out. This could be an indication that the bond between the carbon yarns with mineral impregnation presents a significant portion of a chemical bond. The amount of remaining fibers in the pull-out channel is higher for the C-MCF yarns, which could be related to the chemical compatibility of the cementitious impregnation with the matrix. On the other hand, after the pull-out of the epoxy yarn, no fibers could be observed in the pull-out channel. That could mean that the major bond mechanism of this type of yarn is a mechanical interlock. Nadiv et al. [29] stated that, after pull-out tests, only a small amount of cement products could be observed at the surface of an epoxy coated carbon yarn. Additionally, the EP yarns were prepared out of the textile mesh, and therefore present irregularities along their length due to the removal of the transversal yarns, which could have positively contributed to the mechanical interlocking mechanism. This is corroborated by the presence of a soft drop in the pull-out curve after the maximum

average interfacial shear stress is reached [26]. The lack of fibers in the pull-out channel indicates that only weak chemical bond could be developed and, although the polymer impregnated yarns were well embedded in the fine-grained concrete matrix, as can be observed in Figure 3.16c and Figure 3.18e, a weak yarn-matrix interface is formed. Dvorkin and Peled [28] showed that textile reinforced concretes with CF coated with epoxy resin, although presenting excellent mechanical properties under tensile loading, had a multiple-cracking pattern with large distances between the cracks, indicating a weak interface between the yarns and the fine-grained concrete. Furthermore, as observed in the μ CT images, the microstructure of the EP yarn presents a lower density than the MCF yarns, represented by a darker gray pattern, which could indicate a higher fiber volume fraction.

The EP yarns yielded τ_{max} approximately 80% greater than that of the C-MCF yarns. However, the differences in the values of $\tau_{0.5}$ and W_1 between these two yarns were not so expressive. In fact, the C-MCF presented a $\tau_{0.5}$ value approximately 12.5% higher than that of the EP yarns. Meanwhile, the value of W_1 of the EP yarns was only 16% higher than the one obtained for the C-MCF yarns. These minor differences observed at small deformations could be a positive factor for the C-MCF yarns' use in practical concrete structures since they must be designed to attend the Serviceability Limit State.

Table 3.7 – Results obtained from the pull-out tests at different temperatures (average values, standard deviations are given in parenthesis).

	τ_{\max} (MPa)	δ_{\max} (mm)	$k_d \tau_{\max}$	$\tau_{0.5}$ (MPa)	τ_2 (MPa)	W_1 (MPa·mm)	$k_d W_1$	W_{total} (MPa·mm)	$k_d W_{\text{total}}$
Room Temperature									
C-MCF	7.85 (1.69)	0.77 (0.12)	1	5.19 (0.66)	4.86 (0.99)	4.26 (0.86)	1	19.4 (3.29)	1
GP-MCF	3.15 (1.18)	0.46 (0.16)	1	2.23 (1.47)	1.02 (0.44)	1.37 (0.62)	1	5.07 (1.90)	1
EP	14.1 (4.98)	2.73 (1.07)	1	4.54 (0.69)	11.7 (3.41)	4.94 (1.78)	1	47.3 (21.7)	1
150 °C									
C-MCF	1.78 (0.48)	0.38 (0.32)	0.23	1.21 (0.30)	1.99 (0.60)	1.25 (0.264)	0.29	8.28 (2.42)	0.43
GP-MCF	1.48 (0.50)	0.40 (0.29)	0.471	0.61 (0.14)	0.80 (0.31)	0.70 (0.16)	0.51	3.99 (1.52)	0.85
EP	3.17 (1.08)	2.79 (1.26)	0.23	1.50 (0.41)	2.37 (0.91)	1.41 (0.31)	0.29	10.2 (3.42)	0.22
200 °C									
C-MCF	4.19 (0.48)	0.95 (0.48)	0.53	2.89 (0.78)	3.99 (0.92)	2.11 (0.31)	0.50	14.9 (3.86)	0.77
GP-MCF	1.41 (0.44)	0.37 (0.25)	0.45	0.74 (0.27)	0.88 (0.32)	0.79 (0.20)	0.58	3.80 (1.00)	0.81
EP	0.49 (0.08)	0.71 (1.20)	0.03	0.27 (0.12)	0.34 (0.13)	0.29 (0.13)	0.06	1.47 (0.58)	0.03
300 °C									
C-MCF	3.71 (0.48)	0.48 (0.08)	0.47	2.75 (0.41)	3.54 (0.59)	2.28 (0.17)	0.54	14.9 (2.32)	0.77
GP-MCF	1.32 (0.36)	0.25 (0.05)	0.42	0.11 (0.02)	0	0.28 (0.07)	0.201	0.30 (0.08)	0.06

3.3.3.1. Effect of elevated temperatures

Figure 3.20, Figure 3.21, and Figure 3.22 present the average interfacial shear stress vs. slip curves for the C-MCF, GP-MCF, and EP yarns, respectively, obtained from the pull-out tests at elevated temperatures. The maximum average interfacial shear stress τ_{max} , the deformation δ_{max} at τ_{max} , the interfacial shear stress at 0.5 mm $\tau_{0.5}$, the interfacial shear stress at 2 mm τ_2 , the specific work to pull-out W_I , and the total work W_{total} are presented in Table 3.7. Temperature Modification Factors k_d were also obtained to easily compare the average values of τ_{max} , W_I , and W_{total} at elevated temperatures with the respective values obtained at room temperature. Figure 3.16 presents the matrix-yarn interface region, and Figure 3.17 the pull-out channel of the different carbon yarns embedded in the fine-grained concrete matrix after the pull-out tests at 150 °C, 200 °C, and 300 °C obtained through microscopic analysis. The enhancement of the temperature level degraded the yarn-matrix interface region, mainly for the GP-MCF and EP yarns. In the pull-out channel of the EP yarns, it is also possible to observe the degradation of the epoxy resin, marked by a change in the color of the interface region.

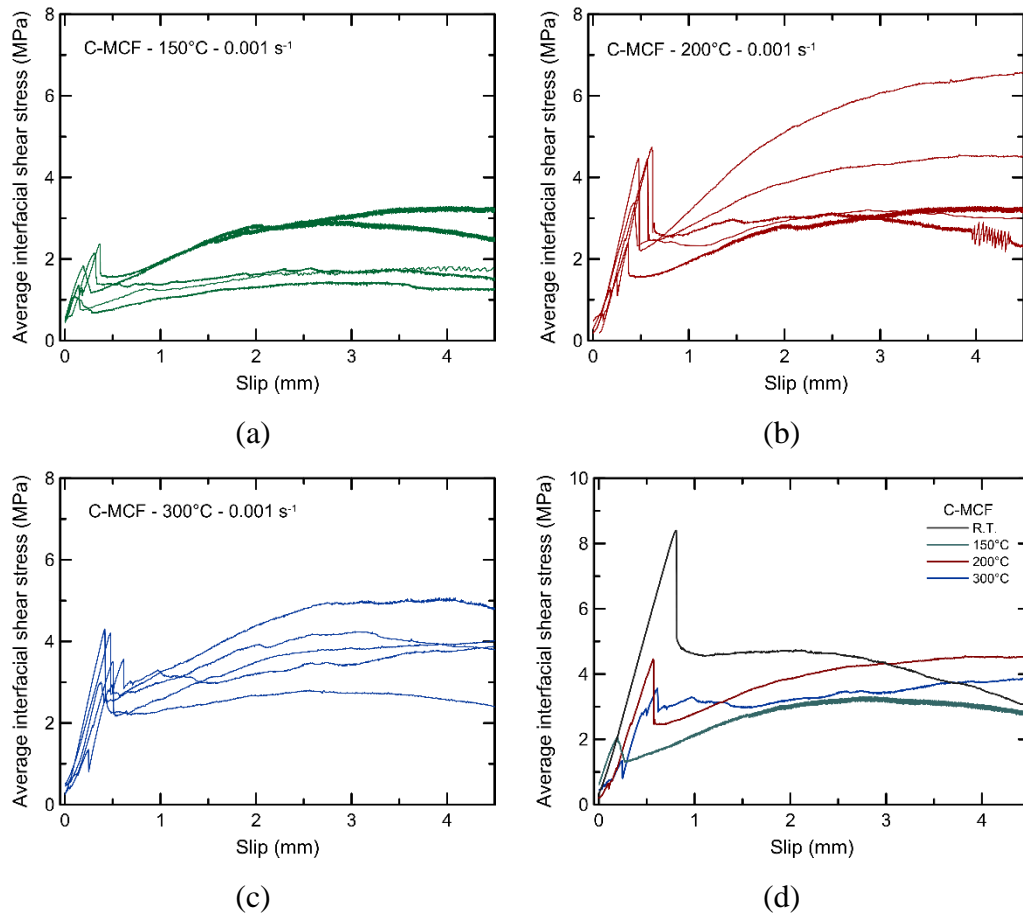


Figure 3.20 – Average interfacial shear stress vs. slip obtained in the pull-out tests for the C-MCF yarn at (a) 150 °C, (b) 200 °C, and (c) 300 °C. (d) Representative average interfacial shear stress vs. slip obtained in the pull-out tests for the C-MCF yarn at different temperatures.

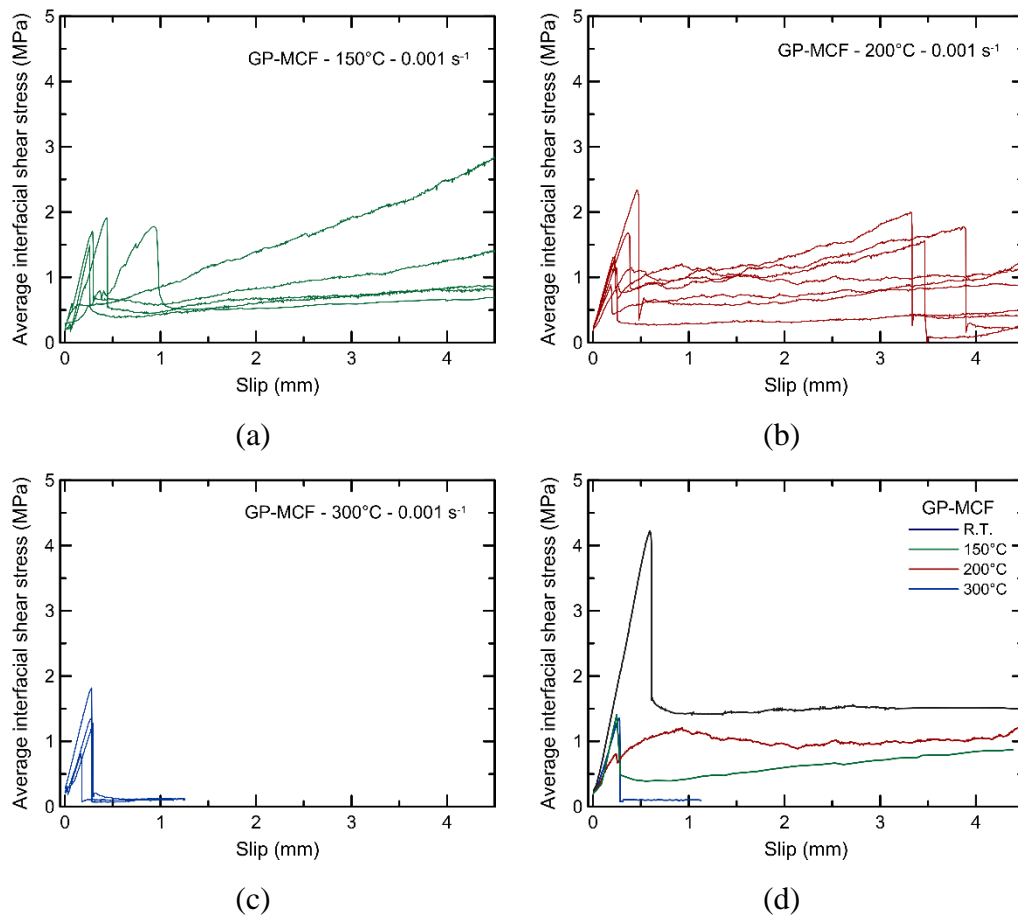


Figure 3.21 – Average interfacial shear stress vs. slip obtained in the pull-out tests for the GP-MCF yarn at (a) 150 °C, (b) 200 °C, and (c) 300 °C. (d) Representative average interfacial shear stress vs. slip obtained in the pull-out tests for the GP-MCF yarn at different temperatures.

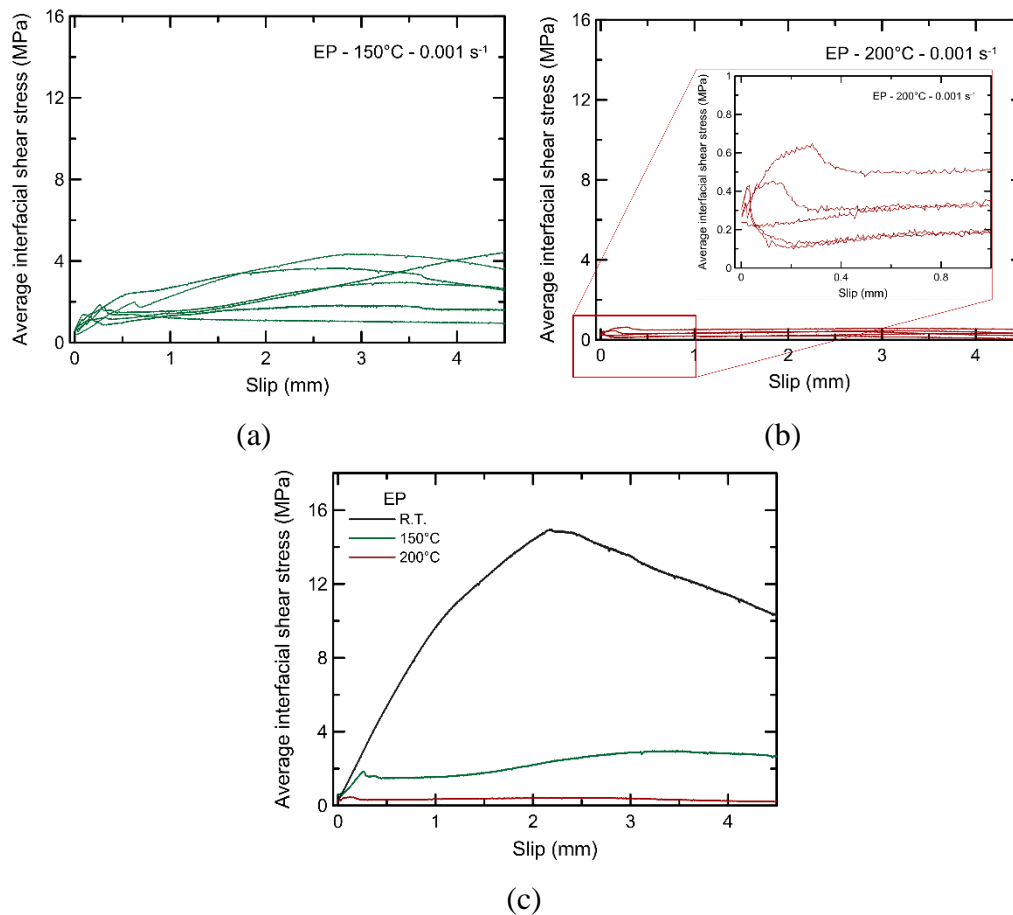


Figure 3.22 – Average interfacial shear stress vs. slip obtained in the pull-out tests for the EP yarn at (a) 150 °C, and (b) 200 °C. (d) Representative average interfacial shear stress vs. slip obtained in the pull-out tests for the EP yarn at different temperatures.

- C-MCF yarns

The temperature increase significantly affected the bond between the C-MCF yarns with the fine-grained concrete matrix, as seen in Figure 3.20. The increase in the test temperature led to a drop in the maximum average interfacial shear stress τ_{max} of these yarns. However, this decrease did not occur linearly to the enhancement in the temperature level. The temperature of 150 °C was the one that most pronouncedly affected the bond between the C-MCF yarn and the fine-grained concrete matrix, with a reduction in the τ_{max} of about 77%. However, at 200 °C and 300 °C, the drop in the τ_{max} was less distinct, approximately 47% and 53%, respectively. The values obtained for $\tau_{0.5}$ and τ_2 followed a similar trend, presenting the highest decrease at 150 °C. While the reduction level observed for the $\tau_{0.5}$ was similar to that of τ_{max} , the drop was less pronounced for the values of τ_2 , approximately 59%, 18%, and 27% for 150 °C, 200 °C, and 300 °C, respectively.

As seen in the pull-out curves, this relatively minor impact of the temperature observed in the τ_2 values is due to a recovery in the interfacial shear stress level after the abrupt drop following the maximum shear stress value. At 150 °C, τ_2 is even greater than τ_{max} , since τ_{max} is greatly affected by the effect of temperature. The recovery of the interfacial shear stress mentioned above may indicate a change in the bonding mechanism of the C-MCF yarns with the matrix. The connection of the yarn with the matrix was broken earlier, i.e., lower interfacial shear stress levels were necessary for this to occur. On the other hand, stronger mechanical interlocking might occur in the pull-out channel due to shrinkage of the concrete as well as thermal expansion of the yarn, thus creating a higher resistance at larger pull-out deformation; see discussion below. The increase in the test temperature also influenced the pull-out work, with the specific work to pull-out W_I being more significantly affected than the total work W_{total} . At 150 °C, 200 °C, and 300 °C a drop of approximately 71%, 50%, and 46% in the W_I values was observed, respectively. This reduction degree is similar to the ones obtained for the τ_{max} , which makes sense, since W_I is directly related to this parameter. Meanwhile, the reduction in the W_{total} values was similar to what was observed for the τ_2 : about 57%, 23%, and 23% for 150 °C, 200 °C, and 300 °C, respectively, which was mostly due to the already mentioned recovery of the interfacial shear stress level after the initial post-peak drop in the pull-out curve.

The lower performance of the bond observed for the C-MCF yarns at 150 °C could be an indication that, at this temperature, the degradation is such that affects the yarn-matrix interface. However, the images from the matrix-yarn interface region (see Figure 3.16.a) and the pull-out channel (see Figure 3.17a) obtained after the pull-out tests show no clear evidence of such interface degradation, neither at 150 °C nor at any other temperature. A similar trend of presenting the lower performance at 150 °C was also observed in the fine-grained concrete matrix compressive strength, which presented the lowest level when heated to 150 °C. The lower strength of the matrix might affect the interface region, leading to a loss of the bond quality. Slama et al. [99] and Simões et al. [100] also observed a decrease in the maximum pull-out load with the reduction of the concrete matrix compressive strength. Moreover, the cement-based impregnation could also have experienced some deterioration, further contributing to the bond loss.

- GP-MCF yarns

For the GP-MCF yarns, the increase in the temperature had a considerable impact on its bond with the fine-grained concrete matrix. This impact was similar at 150 °C and 200 °C. A reduction of approximately 53% and 55% in τ_{max} was observed at 150 °C and 200 °C, respectively. However, although the reduction was similar in quantitative terms, it is possible to observe that the interface region is considerably more degraded at 200 °C than at 150 °C, see Figure 3.16.b. Similar to the C-MCF yarns, the lower strength of the fine-grained concrete matrix at 150 °C might affect the interface region, leading to a loss of the bond quality. At 300 °C, the temperature effect was more substantial. Although the decrease in τ_{max} was at a similar level of the other temperatures, with a 58% reduction compared to the room temperature, just after reaching the τ_{max} , the average interfacial shear stress *vs.* stress curve showed an abrupt drop with no eventual recovery of the stress, indicating the complete pull-out of the yarn. As a result, a decrease of 94% in the total work was observed. Thus, it can be concluded that the GP-MCF yarns are able to maintain some bond properties with the fine-grained concrete matrix at temperatures of 150 °C and 200 °C, but not at 300 °C.

Geopolymers present high thermal resistance, being able to maintain considerably mechanical properties even at elevated temperatures [47–49,101]. However, their thermal behavior in the current application is highly dependent on the mix design a heating regime. The geopolymer suspension used for impregnation contained a relatively high amount of water in its composition to ensure sufficient workability and high impregnation quality, and presents a porous and permeable microstructure [53]. This probably led to excessive thermally induced shrinkage, damaging the interface between the yarns and the fine-grained concrete matrix, and consequently loss of the bond at elevated temperatures. Available results from Thermogravimetric Analysis (TGA) up to 100 °C showed that the degradation of metakaolin-based geopolymers begins with the evaporation of the free water contained in the pores [49,53,59,67]. In this temperature range, the water loss leaves empty spaces within the material, increasing its porosity [67]. Between 100 °C and 250 °C, the loss of the chemically bonded water occurs, resulting in the dehydration of the structures present in the aluminosilicate gel, which is an endothermic process

[49,53,59,67]. This process results in shrinkage of the GP [47,48,57,101]. The extent of shrinkage increases with increasing water content in the GP [48].

From the observation of the matrix-yarn interface region (see Figure 3.16.b) and the pull-out channel (see Figure 3.17.b) after testing, it can be seen that the gap between the GP-MCF yarn and the fine-grained concrete matrix is greater at 200 °C, and even more at 300 °C. This could be due to the decomposition of the geopolymer impregnation that in some way affected the interface region between the yarn and the fine-grained concrete matrix, enhancing the chemical incompatibility of these two materials and thus contributing to the loss of the bond performance at elevated temperatures. Furthermore, the fine-grained concrete is also affected by the increase in temperature, which can contribute to the weakness of the yarn-matrix interface region, thus affecting the bond behavior. The alkali-silica reaction can also become severer at high temperatures, with an increase in the extent of the damage and microstructural cracking due to expansion of the ASR gel [102,103], further degrading the interface between the GP-MCF yarn and the fine-grained concrete matrix.

- EP yarns

The bond of the EP yarns with the fine-grained concrete matrix was considerably affected by the increase in temperature. When heated to 150 °C, the maximum average interfacial shear stress τ_{max} yielded a reduction of approximately 78% and the total absorbed energy W_{total} a reduction of 62%, compared to the room temperature. With heating to 200 °C, no bond between the EP yarns and the fine-grained concrete matrix could be observed. All analyzed parameters were approximately zero, presenting a drop of 94% or more compared to the room temperature. The lower bond performance of the epoxy yarns with the fine-grained concrete matrix can be traced back to the low thermal resistance of the polymer. When reaching the glass transition temperature, the material changes from elastic and brittle to viscous or rubbery behavior [104,105]. Commonly, those critical transitions range between 50 °C to 180 °C [76,77]. Figure 3.16.c and Figure 3.17.c present the yarn-matrix interface region and the pull-out channel of the epoxy yarns after the pull-out tests at different temperatures. At 150 °C, it is possible to notice the beginning of the epoxy resin degradation, marked by a soft change in the color of the interface region. This effect is more evident in the observation of the pull-

out channel under the microscope. At 200 °C, this degradation is even more visible in the pull-out channel image, which shows that filaments were loose within the yarn.

- Yarn shrinkage analysis

After heating, the diameter of the C-MCF, GP-MCF, and EP yarns was measured; Figure 3.23 presents the results. The C-MCF yarns yielded a diameter increase of 2.23%, 3.08%, and 3.37% at 150 °C, 200 °C, and 300 °C, respectively. Such expansion could lead to the increase in mechanical interlocking that enhances the bond of the yarn towards the fine-grained concrete matrix at elevated temperatures. In contrast, the GP-MCF and EP yarns, exhibited a reduction in their diameter when being exposed to different temperatures. The shrinkage suffered may lead to a decrease in the transverse pressure, leaving the yarns looser inside the concrete matrix. Due to the weak chemical bond with the fine-grained concrete at room temperature, this can decrease the bond strength and facilitate the pull-out at high temperatures. For the GP-MCF yarns, the decrease in the diameter was 0.39%, 4.03%, and 4.38% at 150 °C, 200 °C, and 300 °C, respectively. The EP yarns presented a shrinkage of 0.49% and 6.80% at 150 °C, and 200 °C, respectively.

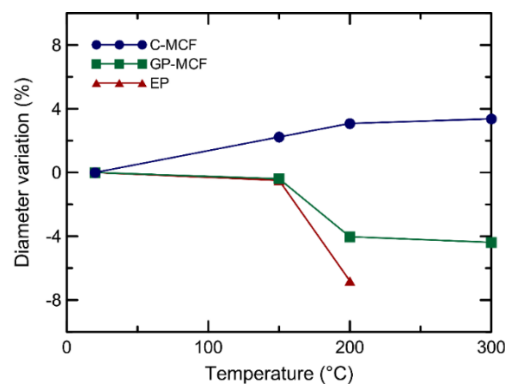


Figure 3.23 – Diameter variation obtained for the C-MCF, GP-MCF, and EP yarns after heating at 150 °C, 200 °C, and 300 °C.

- Temperature Modification Factor (k_d) analysis

Figure 3.24 presents a comparative representation of the Temperature Modification Factor k_d for τ_{max} , W_I , and W_{total} for the yarns under investigation. Through the analysis of parameter k_d , a comparison of the effect of the temperature

in the bond of the different CF yarns with the fine-grained concrete matrix was performed. The EP yarn was the one that had its bond performance with the fine-grained concrete matrix most affected by the increase of the temperatures, as expected due to the low thermal resistance of the polymeric coating. This is evidenced by the lowest values of k_d for τ_{max} , W_1 , and W_{total} obtained at both 150 °C and 200 °C. For the mineral impregnations, at 150 °C, the C-MCF yarns were more affected than the GP-MC. At 200 °C, the C-MCF yarns presented a recovery of their bond with the fine-grained concrete matrix, probably due to the above-mentioned expansion of the yarn cross-section that led to an enhancement in the interlocking mechanism. It is possible to say that, at this temperature level, the bonding of both the C-MCF yarn and GP-MCF yarn towards the fine-grained concrete matrix was similarly affected by the heating. At 300 °C, the impact of the temperature on the bond of the carbon yarn and the fine-grained concrete matrix was less pronounced for the C-MCF specimens. Although the yarns with both mineral impregnations presented similar k_d values for τ_{max} , the bond of the GP-MCF yarns with the fine-grained concrete matrix degraded to a higher extent due to the heating, with significant impact on the pull-out work W_1 and especially W_{total} . At 300 °C, a significant bond of CF yarns with a fine-grained concrete matrix could only be observed for specimens with the C-MCF yarns.

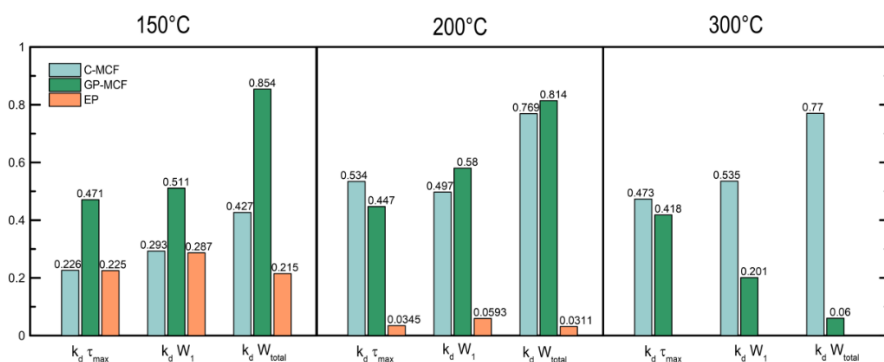


Figure 3.24 – Comparative representation of the Temperature Modification Factor k_d for T_{max} , W_1 and W_{total} for the C-MCF, GP-MCF and EP yarns.

3.3.3.2. Effect of different strain rates

To evaluate the influence of the strain rate on the pull-out behavior of three carbon yarns with different impregnation/coating materials, pull-out tests were performed at four different strain rates.

Figure 3.25, Figure 3.26, and Figure 3.27 present the average interfacial shear stress vs. slip curves for the C-MCF, GP-MCF, and EP yarns, respectively, obtained from the pull-out tests at different strain rates and room temperature. The average results for the maximum average interfacial shear stress τ_{max} , the deformation δ_{max} at τ_{max} , the interfacial shear stress at 0.5 mm $\tau_{0.5}$, the interfacial shear stress at 2 mm τ_2 , the specific work to pull-out W_I , and the total work W_{total} are presented in Table 3.8. The respective standard deviations are shown in parenthesis. A Strain-rate Modification Factor k_s was also obtained to correlate the average values of τ_{max} , W_I , and W_{total} at moderate strain rates with the respective values obtained at the lowest strain rate (0.001 s^{-1}) tested. Figure 3.28 presents a comparative representation of the τ_{max} and W_{total} at different strain rates for the C-MCF, GP-MCF and EP yarns.

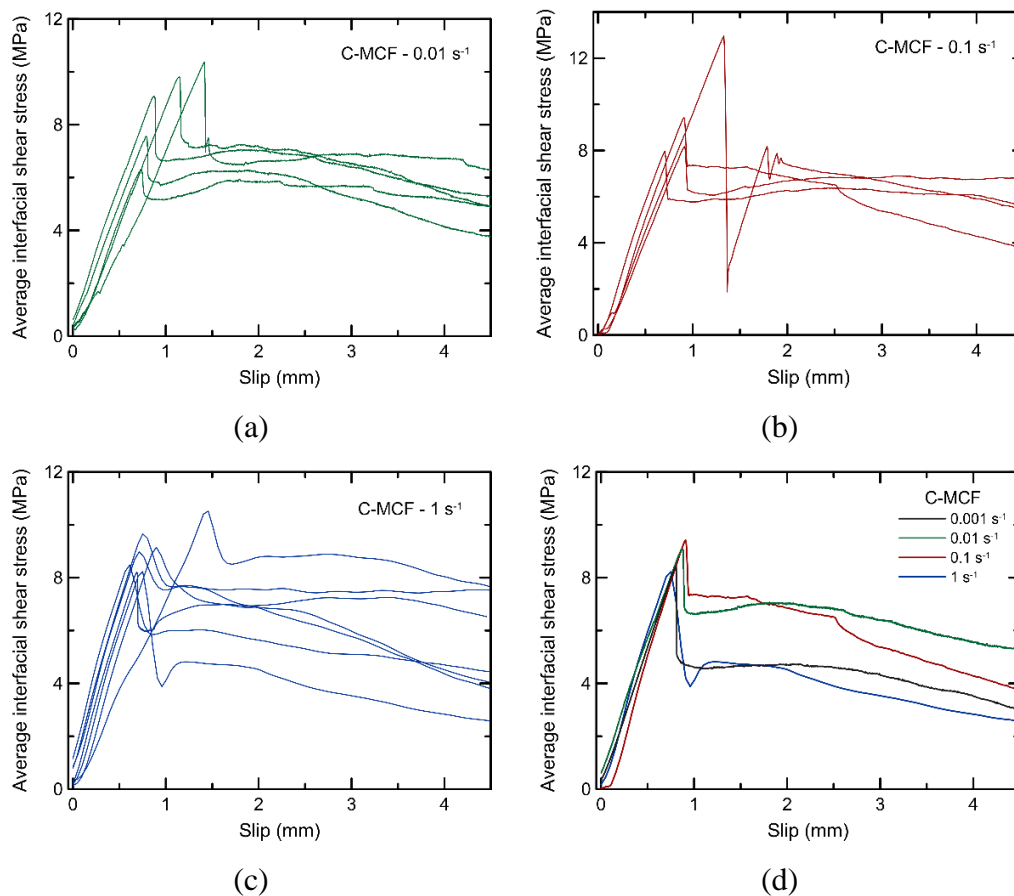


Figure 3.25 – Average interfacial shear stress vs. slip obtained in the pull-out tests for the C-MCF yarn at (a) 0.01 s^{-1} , (b) 0.1 s^{-1} , and (c) 1 s^{-1} . (d) Representative average interfacial shear stress vs. slip obtained in the pull-out tests for the C-MCF yarn at different strain rates.

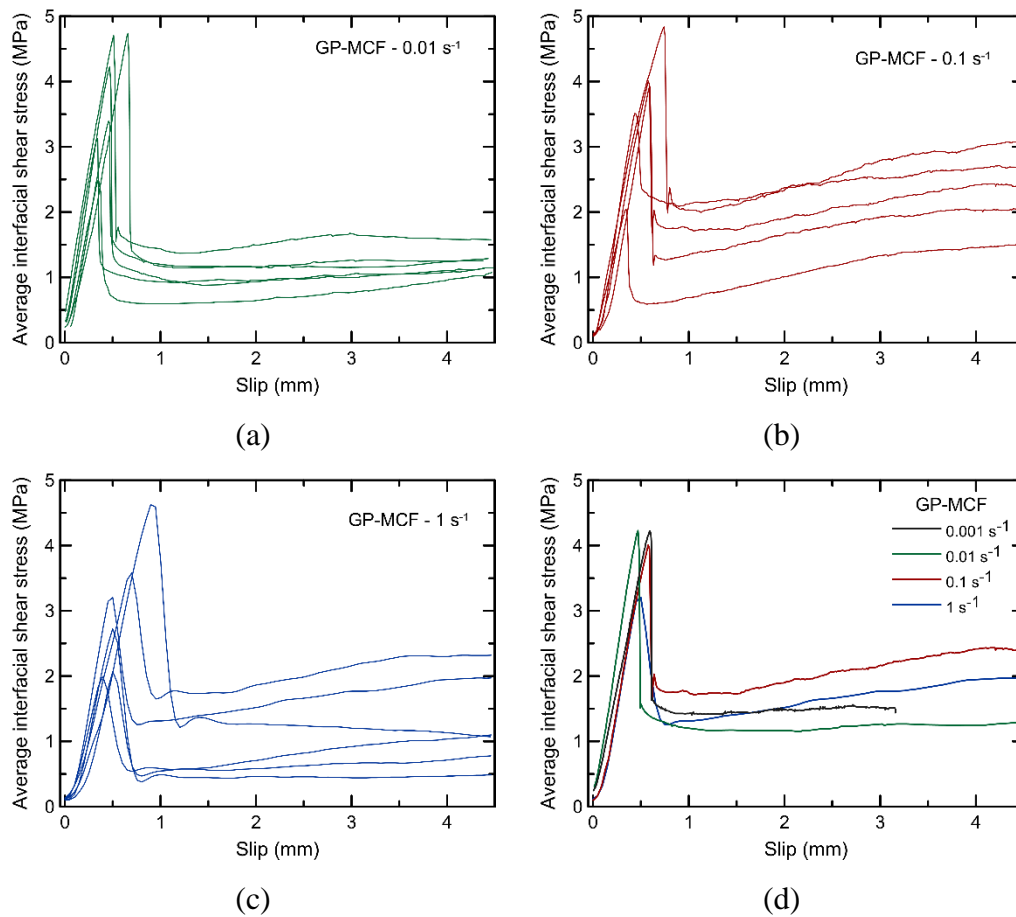


Figure 3.26 – Average interfacial shear stress vs. slip obtained in the pull-out tests for the GP-MCF yarn at (a) 0.01 s^{-1} , (b) 0.1 s^{-1} , and (c) 1 s^{-1} . (d) Representative average interfacial shear stress vs. slip obtained in the pull-out tests for the GP-MCF yarn at different strain rates.

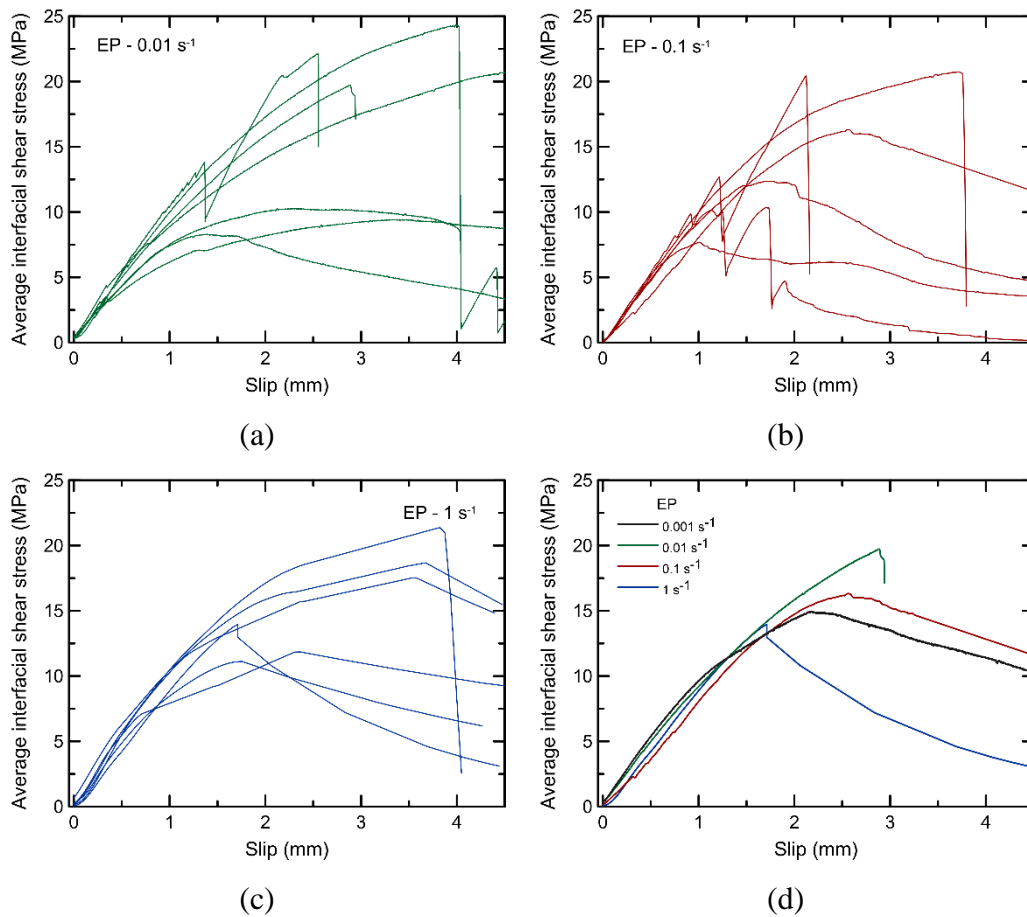


Figure 3.27 – Average interfacial shear stress vs. slip obtained in the pull-out tests for the EP carbon yarn at (a) 0.01 s^{-1} , (b) 0.1 s^{-1} , and (c) 1 s^{-1} . (d) Representative average interfacial shear stress vs. slip obtained in the pull-out tests for the EP carbon yarn at different strain rates.

Table 3.8 – Results obtained from the pull-out tests at different strain rates (average values, standard deviations are given in parenthesis).

	τ_{\max} (MPa)	δ_{\max} (mm)	$k_s \tau_{\max}$	$\tau_{0.5}$ (MPa)	τ_2 (MPa)	W_1 (MPa.mm)	$k_s W_1$	W_{total} (MPa.mm)	$k_s W_{\text{total}}$
0.001 s^{-1}									
C-MCF	7.85 (1.69)	0.765 (0.119)	1	5.19 (0.664)	4.86 (0.990)	4.26 (0.859)	1	19.4 (3.29)	1
GP-MCF	3.15 (1.18)	0.466 (0.157)	1	2.23 (1.47)	1.02 (0.439)	1.37 (0.618)	1	5.07 (1.90)	1
EP	14.1 (4.98)	2.73 (1.07)	1	4.54 (0.693)	11.7 (3.41)	4.94 (1.78)	1	47.3 (21.7)	1
0.01 s^{-1}									
C-MCF	8.62 (1.49)	0.990 (0.255)	1.10	4.49 (0.842)	6.56 (0.498)	4.16 (0.674)	0.977	25.7 (2.19)	1.33
GP-MCF	3.78 (0.836)	0.465 (0.106)	1.20	2.12 (1.41)	1.06 (0.264)	1.52 (0.433)	1.11	5.42 (1.24)	1.16
EP	16.4 (6.31)	3.02 (1.04)	1.17	4.80 (0.593)	13.0 (4.18)	4.66 (0.547)	0.852	40.3 (14.1)	0.852
0.1 s^{-1}									
C-MCF	9.63 (2.00)	0.965 (0.227)	1.23	4.84 (0.639)	6.80 (0.406)	4.39 (0.265)	1.03	26.7 (1.39)	1.38
GP-MCF	4.07 (0.481)	0.588 (0.108)	1.29	3.20 (0.454)	2.06 (0.299)	1.98 (0.358)	1.45	9.80 (1.44)	2.10
EP	14.7 (4.94)	2.15 (0.845)	1.04	4.78 (0.572)	12.0 (5.55)	4.67 (0.440)	0.946	33.3 (14.6)	0.703
1 s^{-1}									
C-MCF	8.01 (1.41)	0.701 (0.156)	1.02	5.92 (1.15)	5.78 (1.41)	5.17 (0.592)	1.22	23.7 (5.73)	1.22
GP-MCF	3.03 (0.910)	0.582 (0.168)	0.963	2.31 (0.598)	1.07 (0.518)	1.34 (0.473)	0.977	5.40 (2.37)	1.16
EP	14.6 (3.01)	2.62 (0.854)	1.04	5.22 (0.846)	13.4 (2.59)	4.65 (0.538)	0.943	47.2 (12.4)	0.997

For the C-MCF yarns, the variation of the strain rate did not lead to a significant change in their pull-out behavior (Figure 3.25). An increase in the maximum average interfacial shear stress τ_{max} could be observed with the enhancement of the strain rate, as shown in Figure 3.28.a. This increase was approximately 10% when the strain rate passed from 0.001 s^{-1} to 0.01 s^{-1} , and 23% from 0.01 s^{-1} to 0.1 s^{-1} . However, when moving to the dynamic regime, there was a decrease in the enhancement pattern, and the increase observed was only approximately 2%. This same variation pattern was observed for the parameter W_{total} (Figure 3.28.b), with higher enhancements within the quasi-static regime and a reduction of this increase when passing to the dynamic regime.

Similar to the C-MCF yarns, the variation in the strain rate does not seem to have affected the bond mechanisms between the GP-MCF yarns and the cementitious matrix. No changes in the shape of the pull-out curves obtained could be observed (Figure 3.26). However, analyzing quantitatively (Figure 3.28), in general, an increase in the strain rate within the quasi-static regime generated an increase in the bond between the GP-MCF yarns and the cementitious matrix. The increase in the τ_{max} was approximately 20% and 29% from 0.001 s^{-1} to 0.01 s^{-1} and 0.1 s^{-1} , respectively. At the strain rate of 0.1 s^{-1} , the GP-MCF yarns presented the highest bond with the cementitious matrix. However, when moving to the dynamic regime, there was an interruption of this pattern. At 1 s^{-1} , the bond of the GP-MCF with the cementitious matrix returned to the level of the one observed at the lowest strain rate.

No general correlation between the enhancement in the strain rate and the bond level between the EP yarns and the cementitious matrix could be traced (Figure 3.28). With the increase of the strain rate from 0.001 s^{-1} to 0.01 s^{-1} , there was an improvement in the yarn-matrix bond, characterized by an increment of approximately 17% in the value of τ_{max} . However, with the subsequent enhancement in the strain rate, this gain has decreased to only 4% for both 0.1 s^{-1} and 1 s^{-1} . Despite the improvement in the bond at moderate strain rates, characterized by higher values of τ_{max} , a decrease in the W_{total} was observed within the quasi-static regime. An enhancement in the strain rate to 0.01 s^{-1} and 0.1 s^{-1} led to a drop of approximately 15% and 30%, respectively, in the value of W_{total} . However, with the transition to the dynamic region, there was a recovery of this parameter, and the value of W_{total}

at 1 s^{-1} was in the same order as the one obtained at the lowest quasi-static strain rate.

When comparing the different carbon yarns, it is not possible to state that the bond of one particular type of impregnation/coating with the cementitious matrix was impacted more significantly by the variation in the strain rate than the others. This can be concluded by analyzing the values obtained for the K_s parameters. Additionally, in general, the enhancement of the strain rate positively impacted the bond between the carbon yarns and the cementitious matrix, represented by K_s factors greater than 1.

Regardless of the observed variations caused by the enhancement in the strain rate, the carbon yarns were able to present a good level of bond with the cementitious matrix at all levels. Further studies considering other strain rates, mainly within the dynamic regime, should be carried out to understand the bond behavior with the subsequent increase in loading velocity.

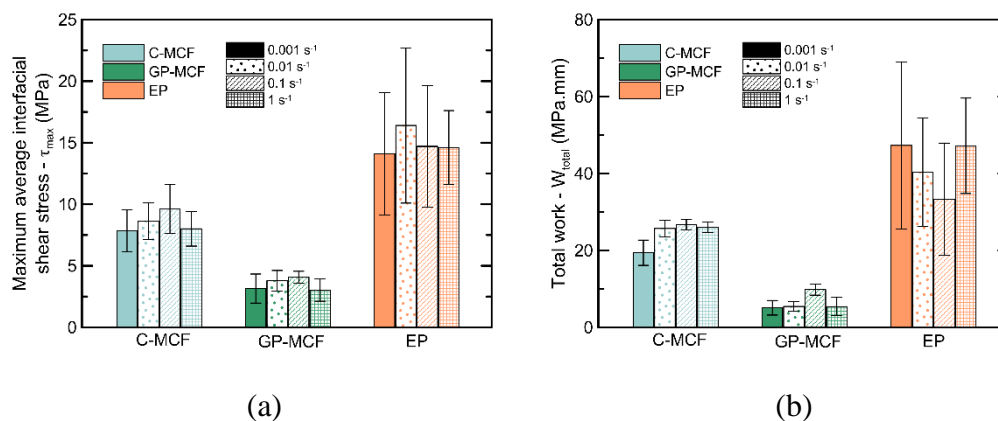


Figure 3.28 – Comparative representation of the (a) Maximum average interfacial shear stress and (b) Total work at different strain rates for the C-MCF, GP-MCF and EP yarns.

3.4. Conclusions

The following conclusions can be drawn from the present investigation on the tensile behavior and bond properties of carbon yarns with mineral and polymeric impregnation.

- The MCF yarns showed high tensile strength and modulus of elasticity, thus demonstrating the effectiveness of the cementitious

and geopolymer suspensions as impregnation materials for carbon yarns.

- Within the quasi-static regime, the MCF yarns did not present a strain-rate dependency. However, a change in the failure mode was observed with increasing strain-rate, occurring earlier for the C-MCF yarns. Further studies contemplating higher strain rates should be performed to understand the mechanical behavior of the MCF yarns within the dynamic regime.
- The C-MCF yarns presented higher bond strength towards the fine-grained concrete matrix in comparison to the GP-MCF yarns due to the better chemical compatibility.
- Geopolymers rich in alkali ions weaken the bond with the cementitious matrix.
- At room temperature, the EP yarns yielded the strongest bond with the fine-grained concrete matrix. In contrast to the MCF, the shape of the pull-out curve indicated a mechanical interaction as the main bond mechanism. Microscopic observations on the pull-out channel corroborated this assumption since no remained fibers could be observed in the channel. Additionally, irregularities along the length of the EP yarn due to its extraction from the textile mesh might have positively influenced the mechanical interlocking.
- Although the bond between the EP yarns and the fine-grained concrete matrix was 80% higher than that of the C-MCF yarns, this difference was considerably smaller at larger pull-out deformations. The specific work to pull-out W_1 obtained for the EP yarns was only 16% higher than that for the C-MCF yarns, and the average interfacial shear stress at 0.5 mm slip $\tau_{0.5}$ of the C-MCF yarns was only 12.5% higher than the one of the EP yarns. These results constitute a positive factor on the use of the C-MCF yarns in practical applications, in which the structural elements must attend the Serviceability Limit State (SLS).
- The bond of the EP yarns with the fine-grained concrete matrix was the one that was most affected by the enhancement of the temperature.

This is attributed to the intrinsic low thermal resistance of the polymeric impregnation matrix.

- The C-MCF and GP-MCF yarns were able to maintain a considerable bond quality with the fine-grained concrete matrix at temperatures up to 200 °C. At 300 °C, a bond with the fine-grained concrete matrix could only be observed for the C-MCF yarns. The GP-MCF yarns were not able to preserve a significant bond at this temperature, probably due to the high extent of shrinkage, and also micro-cracking from a potential ASR at the yarn-matrix interface. To elucidate the latter effect deeper analysis is needed.
- At all strain rates evaluated in this study, the carbon yarns presented a good bond level with the cementitious matrix. Further studies mainly within the dynamic regime should be performed to characterize the bond of carbon yarns with cementitious matrices.

3.5. References

- [1] BRAMESHUBER, W. **Report 36: textile reinforced concrete-state-of-the-art report of RILEM TC 201-TRC**. [s.l.] Rilem publications, 2006.
- [2] AL-SALLOUM, Y. A. et al. Experimental and Numerical Study for the Shear Strengthening of Reinforced Concrete Beams Using Textile-Reinforced Mortar. **Journal of Composites for Construction**, v. 16, n. 1, p. 74–90, 2012.
- [3] AMBRISI, A. D.; FOCACCI, F. Flexural strengthening of RC beams with cement-based composites. **Journal of Composites for Construction**, v. 15, n. 5, p. 707–720, 2011.
- [4] NANNI, A. A New Tool for Concrete and Masonry Repair. **Concrete International**, n. april, p. 43–49, 2012.
- [5] KOUTAS, L. N. et al. Strengthening of Concrete Structures with Textile Reinforced Mortars: State-of-the-Art Review. **Journal of Composites for Construction**, v. 23, n. 1, 2019.
- [6] BABAEIDARABAD, S.; CASO, F. DE; NANNI, A. Out-of-Plane Behavior of URM Walls Strengthened with Fabric-Reinforced Cementitious Matrix Composite. **Journal of Composites for Construction**, v. 18, n. 4, p. 04013057, 2013.
- [7] KOURIS, L. A. S.; TRIANTAFILLOU, T. C. State-of-the-art on strengthening

of masonry structures with textile reinforced mortar (TRM). **Construction and Building Materials**, v. 188, p. 1221–1233, 2018.

[8] BABAEIDARABAD, S.; CASO, F. DE; NANNI, A. URM Walls Strengthened with Fabric-Reinforced Cementitious Matrix Composite Subjected to Diagonal Compression. **Journal of Composites for Construction**, v. 18, n. 2, p. 04013045, 2013.

[9] HEGGER, J. et al. **TRC Pedestrian Bridge - Design, Load-bearing Behavior and Production Processes of a Slender and Light-weight Construction**. International RILEM Conference on Material Science. **Anais...RILEM Publications SARL**, 2010

[10] REMPEL, S. et al. Extremely light and slender precast pedestrian bridge made out of textile reinforced concrete (TRC). **High Tech Concrete: Where Technology and Engineering Meet**, n. November, p. 2530–2537, 2018.

[11] HEGGER, J.; GORALSKI, C.; KULAS, C. **A slender pedestrian bridge made of textile reinforced concrete**. IABSE Symposium: Large Structures and Infrastructures for Environmentally Constrained and Urbanised Areas. **Anais...Venice: 2010**

[12] HEGGER, J. et al. Exterior Cladding Panels as an Application of Textile Reinforced Concrete. **SP-224. Farmington Hills (MI, USA): American Concrete Institute**, p. 55–70, 2004.

[13] JANETZKO, S.; GRIES, T. **Preforming of Textile Reinforcement For Sandwich Building Members**. Seventh Intl. RILEM Symp. on Fibre Reinforced Concrete: Design and Applications. **Anais...2008**

[14] COLOMBO, I. G.; COLOMBO, M.; PRISCO, M. DI. Bending behaviour of Textile Reinforced Concrete sandwich beams. **Construction and Building Materials**, v. 95, p. 675–685, 2015.

[15] SCHOLZEN, A.; CHUDOBA, R.; HEGGER, J. Thin-walled shell structures made of textile-reinforced concrete: Part I: Structural design and construction. **Structural Concrete**, v. 16, n. 1, p. 106–114, 2015.

[16] SHAREI, E. et al. Structural behavior of a lightweight, textile-reinforced concrete barrel vault shell. **Composite Structures**, v. 171, p. 505–514, 2017.

[17] SCHUMANN, A. et al. Parking slabs made of carbon reinforced concrete. **Structural Concrete**, v. 19, n. 3, p. 647–655, 2018.

[18] MAY, S. et al. Lightweight ceiling system made of carbon reinforced concrete.

Structural Concrete, n. October 2017, p. 1–11, 2018.

[19] GOLIATH, K. B.; CARDOSO, D. C. T.; SILVA, F. DE A. Flexural behavior of carbon-textile-reinforced concrete I-section beams. **Composite Structures**, v. 260, p. 113540, 2021.

[20] CHAND, S. Review - carbon fibers for composites. **Journal of Materials Science**, v. 35, n. 6, p. 1303–1313, 2000.

[21] SAUDER, C.; LAMON, J.; PAILLER, R. The tensile behavior of carbon fibers at high temperatures up to 2400 °C. **Carbon**, v. 42, n. 4, p. 715–725, 2004.

[22] ARBOLEDA, D.; BABAEIDARABAD, S.; NANNI, A. **Durability of fabric reinforced cementitious matrix (FRCM) composites**. 7th. International Conference of FRP Composites in Civil Engineering, International Institute for FRP in Construction. **Anais...International Institute for FRP in Construction**, 2014

[23] MEHTA, P. K.; MONTEIRO, P. J. M. **Concrete: Microstructure, properties and materials**. [s.l.] McGraw-Hill, 2006.

[24] BENTUR, A.; MINDESS, S. **Fiber Reinforced Cementitious Composites**. [s.l.] CRC Press, 2006.

[25] RAUPACH, M.; ORLOWSKY, J.; BÜTTNER, T. **Epoxy-impregnated textiles in concrete – Load bearing capacity and durability**. (J. Hegger, W. Brameshuber, N. Will, Eds.) ICTRC'2006 - 1st International RILEM Conference on Textile Reinforced Concrete. **Anais...Aachen: RILEM Publications SARL**, 2006

[26] PELED, A.; ZAGURI, E.; MAROM, G. Bonding characteristics of multifilament polymer yarns and cement matrices. **Composites Part A: Applied Science and Manufacturing**, v. 39, n. 6, p. 930–939, 2008.

[27] PELED, A. et al. **Modifying carbon roving-cement matrix bond by inorganic coating**. High Performance Fiber Reinforced Cement Composites (HPFRCC7). **Anais...Struttgart, Germany: RILEM**, 2015

[28] DVORKIN, D.; PELED, A. Effect of reinforcement with carbon fabrics impregnated with nanoparticles on the tensile behavior of cement-based composites. **Cement and Concrete Research**, v. 85, p. 28–38, 2016.

[29] NADIV, R. et al. Micro- and nanoparticle mineral coating for enhanced properties of carbon multifilament yarn cement-based composites. **Composites Part B: Engineering**, v. 111, p. 179–189, 2017.

[30] KRÜGER, M.; REINHARDT, H.-W.; FICHTLSCHERER, M. Bond behaviour of textile reinforcement in reinforced and prestressed concrete. **Otto-**

Graf-Journal, v. 12, p. 33–50, 2001.

[31] XU, S. et al. Bond Characteristics of Carbon, Alkali Resistant Glass, and Aramid Textiles in Mortar. **Journal of Materials in Civil Engineering**, v. 16, n. 4, p. 356–364, 2004.

[32] DONNINI, J.; CORINALDESI, V.; NANNI, A. Mechanical properties of FRCM using carbon fabrics with different coating treatments. **Composites Part B: Engineering**, v. 88, p. 220–228, 2016.

[33] SILVA, R. M. DE C.; SILVA, F. DE A. Carbon textile reinforced concrete: materials and structural analysis. **Materials and Structures/Materiaux et Constructions**, v. 53, n. 1, 2020.

[34] XU, S.; LI, H. Bond properties and experimental methods of textile reinforced concrete. **Journal Wuhan University of Technology, Materials Science Edition**, v. 22, n. 3, p. 529–532, 2007.

[35] PAPAKONSTANTINO, C. G.; BALAGURU, P.; LYON, R. E. Comparative study of high temperature composites. **Composites Part B:Engineering**, v. 32, n. 8, p. 637–649, 2001.

[36] YOUNES, A. et al. Mechanical behaviour of carbon and glass filament yarns under high temperatures for composite applications. **Journal of the Textile Institute**, v. 104, n. 3, p. 251–259, 2013.

[37] MICHELS, J. et al. Structural Strengthening of Concrete with Fiber Reinforced Cementitious Matrix (FRCM) at Ambient and Elevated Temperature — Recent Investigations in Switzerland. **Advances in Structural Engineering**, v. 17, n. 12, p. 1785–1799, 2014.

[38] MORGAN, P. **Carbon Fibers and their Composites**. [s.l.] CRC Press, 2005.

[39] BRAZILIAN STANDARD. **NBR 6118: Projeto de estruturas de concreto - Procedimento** Associação Brasileira de Normas Técnicas (ABNT), , 2014.

[40] EHLIG, D. et al. **High Temperature Tests on Textile Reinforced Concrete (TRC) Strain Specimens**. (W. Brameshuber, Ed.)International RILEM Conference on Material Science – MATSCI. **Anais...Aachen: Rilem publications**, 2010

[41] SILVA, F. DE A. et al. Effects of elevated temperatures on the interface properties of carbon textile-reinforced concrete. **Cement and Concrete Composites**, v. 48, p. 26–34, 2014.

[42] XU, S.; SHEN, L.; WANG, J. The high-temperature resistance performance

of TRC thin-plates with different cementitious materials: Experimental study. **Construction and Building Materials**, v. 115, p. 506–519, 2016.

[43] DONNINI, J. et al. Fabric-reinforced cementitious matrix behavior at high-temperature: Experimental and numerical results. **Composites Part B: Engineering**, v. 108, p. 108–121, 2017.

[44] SCHNEIDER, K. et al. Verbundverhalten mineralisch gebundener und polymergebundener Bewehrungsstrukturen aus Carbonfasern bei Temperaturen bis 500 °C. **Beton- und Stahlbetonbau**, v. 113, n. 12, p. 886–894, 2018.

[45] SCHNEIDER, K. et al. Mineral-impregnated carbon fibre reinforcement for high temperature resistance of thin-walled concrete structures. **Cement and Concrete Composites**, v. 97, n. December 2018, p. 68–77, 2019.

[46] MECHTCHERINE, V. et al. Extrusion-based additive manufacturing with carbon reinforced concrete: Concept and feasibility study. **Materials**, v. 13, n. 11, 2020.

[47] TRINDADE, A. C. C. et al. On The Mechanical Behavior of Metakaolin Based Geopolymers Under Elevated Temperatures. **Materials Research**, v. 20, n. suppl 2, p. 265–272, 2017.

[48] DUXSON, P.; LUKEY, G. C.; DEVENTER, J. S. J. VAN. Thermal evolution of metakaolin geopolymers: Part 1 - Physical evolution. **Journal of Non-Crystalline Solids**, v. 352, n. 52–54, p. 5541–5555, 2006.

[49] DUXSON, P.; LUKEY, G. C.; DEVENTER, J. S. J. VAN. Physical evolution of Na-geopolymer derived from metakaolin up to 1000 °c. **Journal of Materials Science**, v. 42, n. 9, p. 3044–3054, 2007.

[50] CHINDAPRASIRT, P. et al. High-Strength Geopolymer Using Fine High-Calcium Fly Ash. **Journal of Materials in Civil Engineering**, v. 23, n. 3, p. 264–270, 2011.

[51] GÖRHAN, G.; ASLANER, R.; ŞINIK, O. The effect of curing on the properties of metakaolin and fly ash-based geopolymer paste. **Composites Part B: Engineering**, v. 97, p. 329–335, 2016.

[52] SINGH, N. B.; MIDDENDORF, B. Geopolymers as an alternative to Portland cement: An overview. **Construction and Building Materials**, v. 237, p. 117455, 2020.

[53] TRINDADE, A. C. C. et al. Influence of elevated temperatures on the mechanical behavior of jute-textile-reinforced geopolymers. **Journal of Ceramic**

Science and Technology, v. 8, n. 3, p. 389–398, 2017.

[54] DUXSON, P. et al. Geopolymer technology: The current state of the art. **Journal of Materials Science**, v. 42, n. 9, p. 2917–2933, 2007.

[55] TRINDADE, A. C. C.; BORGES, P. H. R.; SILVA, F. DE A. Evaluation of Fiber–Matrix Bond in the Mechanical Behavior of Geopolymer Composites Reinforced with Natural Fibers. **Advances in Civil Engineering Materials**, v. 8, n. 3, p. 20180136, 2019.

[56] DOAN, T. et al. New Generation of Geopolymer Composite for Fire-Resistance. In: TESINOVA, P. (Ed.). . **Advances in Composite Materials - Analysis of Natural and Man-Made Materials**. [s.l.] InTech, 2011. p. 73–92.

[57] LYON, R. E. et al. Fire-resistant aluminosilicate composites. **Fire and Materials**, v. 21, n. 2, p. 67–73, 1997.

[58] TRAN, D. H. et al. Effect of Curing Temperature on Flexural Properties of Silica-Based Geopolymer-Carbon Reinforced Composite. **Manufacturing Engineering**, v. 37, n. 2, p. 492–497, 2009.

[59] ZHAO, J. et al. Development and testing of fast curing, mineral-impregnated carbon fiber (MCF) reinforcements based on metakaolin-made geopolymers. **Cement and Concrete Composites**, v. 116, n. September 2020, 2021.

[60] ZHU, D.; GENCOGLU, M.; MOBASHER, B. Low velocity flexural impact behavior of AR glass fabric reinforced cement composites. **Cement and Concrete Composites**, v. 31, n. 6, p. 379–387, 2009.

[61] ZHU, D.; PELED, A.; MOBASHER, B. Dynamic tensile testing of fabric-cement composites. **Construction and Building Materials**, v. 25, n. 1, p. 385–395, 2011.

[62] SILVA, F. DE A. et al. Strain rate effect on the tensile behaviour of textile-reinforced concrete under static and dynamic loading. **Materials Science and Engineering A**, v. 528, n. 3, p. 1727–1734, 2011.

[63] YAO, Y. et al. Tension stiffening in textile-reinforced concrete under high speed tensile loads. **Cement and Concrete Composites**, v. 64, p. 49–61, 2015.

[64] YAO, Y. et al. Distributed cracking mechanisms in textile-reinforced concrete under high speed tensile tests. **Materials and Structures/Materiaux et Constructions**, v. 49, n. 7, p. 2781–2798, 2016.

[65] SILVA, F. DE A. et al. High speed tensile behavior of sisal fiber cement composites. **Materials Science and Engineering A**, v. 527, n. 3, p. 544–552, 2010.

- [66] ZHAO, J. et al. Role of sizing agent on the microstructure morphology and mechanical properties of mineral-impregnated carbon-fiber (MCF) reinforcement made with geopolymers. **Applied Surface Science**, v. 567, n. July, p. 150740, 2021.
- [67] TRINDADE, A. C. C. et al. On the mechanical performance of K- and Na-based strain-hardening geopolymer composites (SHGC) reinforced with PVA fibers. **Construction and Building Materials**, v. 248, 2020.
- [68] TRINDADE, A. C. C.; SILVA, F. DE A.; KRIVEN, W. M. Mechanical behavior of K-geopolymers reinforced with silane-coated basalt fibers. **Journal of the American Ceramic Society**, v. 104, n. 1, p. 437–447, 2021.
- [69] NEMATOLLAHI, B.; SANJAYAN, J. Effect of different superplasticizers and activator combinations on workability and strength of fly ash based geopolymer. **Materials and Design**, v. 57, p. 667–672, 2014.
- [70] DIN EN. **197-1: 2011-11 - Zement - Teil 1: Zusammensetzung, Anforderungen und Konformitätskriterien von Normzement**Dtsch. Fass., , 2011.
- [71] EUROPEAN STANDARD EN. **196-1:2005 - Methods of testing cement - Part 1: Determination of strength**European Committee for standardization, , 2005.
- [72] TRINDADE, A. C. C. et al. Tensile behavior of strain-hardening geopolymer composites (SHGC) under impact loading. **Cement and Concrete Composites**, v. 113, n. June, 2020.
- [73] MECHTCHERINE, V. et al. Mineral-impregnated carbon fiber composites as novel reinforcement for concrete construction: Material and automation perspectives. **Automation in Construction**, v. 110, n. September 2019, p. 103002, 2020.
- [74] DUXSON, P. et al. Effect of alkali cations on aluminum incorporation in geopolymeric gels. **Industrial and Engineering Chemistry Research**, v. 44, n. 4, p. 832–839, 2005.
- [75] LY, L. et al. Leaching of Geopolymers in Deionised Water. **Advances in Technology of Materials and Materials Processing Journal**, v. 8, n. January 2006, p. 236–247, 2006.
- [76] BISBY, L. A.; GREEN, M. F.; KODUR, V. K. R. Response to fire of concrete structures that incorporate FRP. **Progress in Structural Engineering and**

Materials, v. 7, n. 3, p. 136–149, 2005.

[77] SUMIDA, A.; MUTSUYOSHI, H. Mechanical properties of newly developed heat-resistant FRP bars. **Journal of Advanced Concrete Technology**, v. 6, n. 1, p. 157–170, 2008.

[78] PIMIENTA, P.; MCNAMEE, R. J.; MINDEGUIA, J.-C. **Physical properties and behaviour of High-Performance Concrete at high temperature**. [s.l.] Springer, 2019.

[79] PAHN, L. T.; CARINO, J. N. **Mechanical Properties of High Strength Concrete At Elevated Temperatures** NISTIR 6726 Washington, D.C. National Institute of Standards and Technology, , 2001.

[80] HAGER, I.; PIMIENTA, P. **The impact of the addition of polypropylene fibres on the mechanical properties of high performance concretes exposed to high temperatures**. (M. Di Prisco, R. Felicetti, G. A. Plizzari, Eds.)6th RILEM Symposium on Fibre-Reinforced Concretes (FRC). **Anais...**Varenna, Italy: RILEM Proceedings PRO, 2004

[81] DWECK, J. et al. Importance of quantitative thermogravimetry on initial cement mass basis to evaluate the hydration of cement pastes and mortars. **Journal of Thermal Analysis and Calorimetry**, v. 113, n. 3, p. 1481–1490, 2013.

[82] DWECK, J. et al. A comparative study of hydration kinetics of different cements by thermogravimetry on calcined mass basis. **Journal of Thermal Analysis and Calorimetry**, v. 128, n. 3, p. 1335–1342, 2017.

[83] DWECK, J. et al. Study by thermogravimetry of the evolution of ettringite phase during type II Portland cement hydration. **Journal of Thermal Analysis and Calorimetry**, v. 69, n. 1, p. 179–186, 2002.

[84] COLLIER, N. C. Transition and decomposition temperatures of cement phases - a collection of thermal analysis data. **Ceramics - Silikaty**, v. 60, n. 4, p. 338–343, 2016.

[85] MALLICK, P. K. **Fiber-reinforced composites: Materials, manufacturing, and design**. 3rd ed. ed. [s.l.] CRC Press Taylor & Francis Group, 2008.

[86] SILVA, F. DE A. et al. Impact behavior of sisal fiber cement composites under flexural load. **ACI Materials Journal**, v. 108, n. 2, p. 168–177, 2011.

[87] ZHANG, Z.; YAO, X.; ZHU, H. Potential application of geopolymers as protection coatings for marine concrete I. Basic properties. **Applied Clay Science**, v. 49, n. 1–2, p. 1–6, 2010.

- [88] VASCONCELOS, E. et al. Concrete retrofitting using metakaolin geopolymer mortars and CFRP. **Construction and Building Materials**, v. 25, n. 8, p. 3213–3221, 2011.
- [89] MENNA, C. et al. Use of geopolymers for composite external reinforcement of RC members. **Composites Part B: Engineering**, v. 45, n. 1, p. 1667–1676, 2013.
- [90] PHOO-NGERNKHAM, T. et al. High calcium fly ash geopolymer mortar containing Portland cement for use as repair material. **Construction and Building Materials**, v. 98, p. 482–488, 2015.
- [91] ALBIDAH, A. et al. Bond strength between concrete substrate and metakaolin geopolymer repair mortars at ambient and elevated temperatures. **Journal of Materials Research and Technology**, v. 9, n. 5, p. 10732–10745, 2020.
- [92] AHMUDHAVALLI, N. K.; MATHEW, J. Effect of silica fume on strength and durability parameters of concrete. **International Journal of Engineering Sciences & Emerging Technologies**, v. 3, n. 1, p. 28–35, 2012.
- [93] BARBHUIYA, S.; QURESHI, M. Effects of Silica Fume on the Strength and Durability Properties of Concrete. **Cesdoc**, p. 117–120, 2016.
- [94] CAMPOS, H. F.; KLEIN, N. S.; MARQUES FILHO, J. Comparison of the Silica Fume Content for High-Strength Concrete Production: Chemical Analysis of the Pozzolanic Reaction and Physical Behavior by Particle Packing. **Materials Research**, v. 23, n. 5, 2020.
- [95] ZHANG, M.-HO.; GJORV, O. E. Effect of silica fume on pore structure and chloride diffusivity of low porosity cement pastes. **Cement and Concrete Composites**, v. 21, p. 1006–1014, 1991.
- [96] GONEN, T.; YAZICIOGLU, S. The influence of mineral admixtures on the short and long-term performance of concrete. **Building and Environment**, v. 42, n. 8, p. 3080–3085, 2007.
- [97] LINDGÅRD, J. et al. Alkali-silica reactions (ASR): Literature review on parameters influencing laboratory performance testing. **Cement and Concrete Research**, v. 42, n. 2, p. 223–243, 2012.
- [98] RAJABIPOUR, F. et al. Alkali-silica reaction: Current understanding of the reaction mechanisms and the knowledge gaps. **Cement and Concrete Research**, v. 76, p. 130–146, 2015.
- [99] SLAMA, A. C.; GALLIAS, J. L.; FIORIO, B. Study of the pull-out test of multifilament yarns embedded in cementitious matrix. **Journal of Composite**

Materials, v. 55, n. 2, p. 169–185, 2021.

[100] SIMÕES, T. et al. Influence of concrete strength and steel fibre geometry on the fibre/matrix interface. **Composites Part B: Engineering**, v. 122, p. 156–164, 2017.

[101] TRINDADE, A. C. C. et al. Influence of elevated temperatures on the residual and quasi in-situ flexural strength of strain-hardening geopolymer composites (SHGC) reinforced with PVA and PE fibers. **Construction and Building Materials**, v. 314, n. November 2021, 2022.

[102] GAUTAM, B. P.; PANESAR, D. K. The effect of elevated conditioning temperature on the ASR expansion, cracking and properties of reactive Spratt aggregate concrete. **Construction and Building Materials**, v. 140, p. 310–320, 2017.

[103] KAWABATA, Y. et al. Impact of temperature on expansive behavior of concrete with a highly reactive andesite due to the alkali–silica reaction. **Cement and Concrete Research**, v. 125, n. August, p. 105888, 2019.

[104] URBANIAK, M. A relationship between the glass transition temperature and the conversion degree in the curing reaction of the EPY® epoxy system. **Polimery/Polymers**, v. 56, n. 3, p. 240–243, 2011.

[105] FIRMO, J. P.; CORREIA, J. R.; BISBY, L. A. Fire behaviour of FRP-strengthened reinforced concrete structural elements: A state-of-the-art review. **Composites Part B: Engineering**, v. 80, p. 198–216, 2015.

4 Mechanical behavior of textile reinforced concrete with newly developed mineral-impregnated carbon fabrics submitted to uniaxial tensile loads and exposed to elevated temperatures

Textile Reinforced Concrete (TRC) is a class of material with potential for construction of thin-walled elements. Additionally, it is an interesting alternative to conventional materials due to the possibility of reducing concrete consumption while maintaining its high performance. Carbon fabrics present excellent mechanical and durability properties. However, they exhibit a low bond towards cementitious matrices, harming the mechanical efficiency of the composite. Polymeric coatings are commonly used to enhance the bond of the TRC. In case of elevated temperatures, due to the low thickness characteristic of the TRC, the textile reinforcements are rapidly degraded. Although carbon fibers present elevated thermal resistance, the polymeric coating does not. Recently, mineral fillers are being used as impregnation of carbon yarns to enhance their bond towards the fine-grained concrete matrix with the additional advantage of presenting elevated thermal resistance. In this work, a Mineral-Impregnated Carbon Fibers (MCF) fabric with a cement-based (C) and geopolymer (GP) suspensions was developed. Direct tensile tests revealed the effectiveness of the textile reinforcement. The tensile mechanical behavior of a TRC with the C- and GP-MCF fabrics was investigated and compared to the response of a TRC with a commercially epoxy-coated (EP) carbon fabric. The residual performance of the composites after exposure to elevated temperatures was also analyzed. A DIC analysis was performed to evaluate the cracking pattern of the TRCs. The results showed that the TRC with MCF fabrics presented a strain-hardening behavior with a multiple-cracking pattern. While the mechanical response of the TRC with GP-MCF and EP carbon fabric was affected by the enhancement of temperature, the heating up to 300 °C did not significantly affect the mechanical performance of the TRC with C-MCF fabric.

The experimental program of this chapter was conducted at the Institute of Construction Materials at the Technische Universität Dresden, Germany.

4.1. Introduction

Materials with a more sustainable approach coming from renewable sources or that are able to reduce the consumption of conventional raw materials have been gaining attention in industry. Textile Reinforced Concrete (TRC) is a cementitious matrix composite reinforced with one or multiple layers of fabrics [1]. This relatively new class of material presents excellent mechanical properties with one major advantage of being suitable for the construction of thin-walled elements, which can considerably reduce Portland cement consumption and, consequently, the CO₂ emissions generated in their production. For these reasons, the TRC is becoming an encouraging alternative to conventional materials for the construction of new structural elements [2–8] and the repair and strengthening of existing structures [9–13].

The mechanical behavior of TRC can be characterized through direct tensile and bending tests. Although bending tests are easier to perform, direct tensile tests provide more details about the composite mechanical performance [14]. When submitted to tensile and flexural loads, the TRC usually presents a strain-hardening behavior with a multiple-cracking pattern. The load capacity and mechanical behavior of TRC under static and quasi-static loading conditions are influenced by the cementitious matrix and the textile reinforcement properties and also by the interaction between these two phases [14]. The fiber material, roving thickness, reinforcement ratio and orientation, and the coating material applied in the textile reinforcement considerably affect the composite response.

Carbon fibers exhibit higher strength and higher ductility when compared to other fibers generally used for textile reinforcing manufacturing, such as AR-glass and basalt [15,16]. Additionally, they present excellent durability properties when embedded into cementitious matrices [17–19]. However, carbon fibers are naturally hydrophobic, and their inadequate wettability and chemical inertness can lower the bond towards water-based materials [20]. Thus, even with the high mechanical properties of carbon, the composites with carbon fabrics exhibit low mechanical performance due to a weak interface [21]. Additionally, the carbon yarns in the

textile structure are composed of thousands of filaments, and due to a incompatibility between the cement particles sizes (ranging from 10 to 75 μm [22]) and the filaments diameter (usually smaller than 10 μm [15]), not all of them are directly anchored to the surrounding cementitious matrix [14]. Hence, the inner filaments are free to slip against the outer ones, and there is a non-uniform distribution of the stresses along the yarn that influences the mechanical response of the TRC, which presents low ultimate loads, but in association with a certain pseudo ductility [14,23].

Nowadays, there are methods to increase the ratio between the inner and outer filaments of a yarn, resulting in an improvement in the mechanical performance of the composite [14,23,24]. One of these methods consists of the impregnation of the yarn with an organic material, usually a thermosetting or thermoplastic polymer [24]. The resin fills the spaces binding all filaments within a yarn, forming a single unit. Hence, the load is efficiently carried by all filaments. Previous studies [21,23,25–27] have demonstrated this effectiveness. Moreover, the polymer material and the impregnation quality significantly affect the bond behavior. Epoxy resins are more efficient in this regard than the styrene-butadiene resin (SBR), probably due to the higher modulus of elasticity and shear modulus of the first, as stated in [28,29]. Nevertheless, large spacing between the cracks and, in some cases, marked delamination between the fabric layers and the matrix could be observed in the TRC with carbon fabrics with epoxy impregnation [23], which can be related to a weak chemical bond between the hydrophobic polymer impregnated fabric and the hydrophilic cementitious matrix [24]. A sand layer addition over the fresh polymer, in addition to further increase the composite mechanical response, reduces the delamination by enhancing the friction and mechanical interlocking mechanisms [21,30,31].

One of the great advantages of the TRC is the possibility of constructing very thin structural elements since the textile reinforcements are usually non-susceptible to corrosion [17,32], thus eliminating the need for a thick concrete cover [33]. However, these elements, due to their thin geometry, are prone to quick heating when exposed to fire having to endure considerably high temperatures. Thus, the fabric temperature resistance is a critical factor when designing a high efficient composite [14]. Carbon fibers present superior temperature resistance compared to glass and aramid fibers [14], mainly due to their manufacturing process, which

involves graphitization and high temperatures for carbonization [16]. Non-coated carbon fibers are able to retain good mechanical properties in temperatures up to 400 °C in an oxygen environment [17,34–36]. However, the polymers used as impregnation present low thermal resistance, and their glass transition (T_g) and decomposition temperatures must be considered. At temperatures close to the T_g , polymers present a sudden decrease in their stiffness, which is relatively high at room temperature. In an oxygen environment, the decomposition of the polymer chains generally occurs in temperatures ranging from 300 °C to 400 °C. Ehlig *et al.* [37] observed significant changes in the TRC strain capacity under tensile loading and escalating temperatures after the decomposition of the polymeric coating. Rambo *et al.* [38] observed an increase in the residual tensile strength of a styrene-acrylic latex coated-basalt-TRC after heating up to 150 °C, which was associated with an enhancement of the matrix-polymer interlock mechanism promoted by the heating followed by the cooling of the thermoplastic polymer. A subsequent increase in the target temperature led to a decrease in the tensile response, due to the coating's thermal decomposition and matrix dehydration, until the complete TRC failure at temperatures ranging from 600 °C to 1000 °C. Donnini *et al.* [39] concluded that when exposed to temperatures between 80 °C - 120 °C, there is a considerable decrease in the composite tensile mechanical response due to a reduction in the bond between the coated fabric and the cementitious matrix. Even with the addition of a sand layer on the polymeric coating, still, a significant drop in the tensile strength could be observed at elevated temperatures. Schneider *et al.* [29], Silva *et al.* [40], and Silva *et al.* [41] also noted an extensive loss in the bond of polymer-coated carbon yarns toward cementitious matrix at temperatures close to the polymer T_g .

Recently, the use of mineral fillers is being evaluated as alternative impregnation materials to the carbon yarns. The mineral particles, with adequate grain sizes, and water content, penetrate the micro spaces between the filaments of the yarn and, similar to the polymer materials, binding all filaments together, making the yarn work as (or more towards as) a unit, which enhances the bond with the cementitious matrix. Peled *et al.* [24], Dvorkin and Peled [23], and Nadiv *et al.* [20] demonstrated that an impregnation based on micro-silica was able to enhance the bond between carbon yarns and a cementitious matrix. The amorphous silica can promote a pozzolanic reaction with the calcium hydroxide present in the cement

matrix, enhancing the interaction between the reinforcement and the matrix. One of the main reasons to use mineral impregnations is their high thermal resistance, which overcomes the main disadvantage of the common commercial polymeric coatings. Schneider *et al.* [29,42] and Silva *et al.* [41] demonstrated that a mineral impregnation based on micro-cements and micro-silica was able to improve the bond of carbon yarns towards cementitious matrices in temperatures up to 500 °C and 300 °C, respectively. Furthermore, the technique applied for the mineral impregnation presents great potential for automation [43], thus showing commercial feasibility to be used as reinforcement into 3D concrete printing layers, and other technologies [44,45]. However, this technology still lacks development towards a viable economic working time window. Cement-based suspensions present considerable change in their viscosity over time due to the advancement of the hydration process. Therefore, advances are needed when considering its market viability.

Geopolymers (GP) are ceramic-like materials produced through the combination of an alkali source, usually sodium- or potassium-based solutions, with an aluminosilicate powder, most commonly fly ash and metakaolin [46,47]. The resulting material presents mechanical properties comparable to cement-based materials [48–53] aligned with elevated chemical and thermal resistances [48,54,55]. Additionally, GP demonstrate faster hardening process, in much shorter windows than common cement, ranging from a few hours up to a maximum of 4 days after curing [46,55,56]. Thus, this growing technology is an interesting alternative to be used as mineral impregnation for carbon yarns. Previous studies [57,58] showed that GP present a good bond with carbon fibers where Zhao *et al.* [59] were able to develop a fast setting and rapid early-strength metakaolin-based Mineral-Impregnated Carbon Fibers (MCF) yarn. Silva *et al.* [41], in a former study, showed that with adequate treatment, the GP-MCF yarns were able to maintain a good bond level towards a fine-grained concrete matrix up to 200 °C.

As previously discussed, different authors already demonstrated the efficiency of mineral impregnations. However, for the practical application of this recently developed technology, it is necessary to understand its behavior in the composite scale. Thus, this work presents a novel evaluation of the mechanical behavior under tensile loading of Textile Reinforced Concrete with Mineral-Impregnated Carbon Fibers (MCF) fabrics. For this, two different mineral

impregnations were used, a cement- (C) and a geopolymer- (GP) based suspensions. The manufacture methodology of the newly developed MCF fabrics is addressed in detail in the paper. To validate the effectiveness of the MCF fabrics, a commercially available epoxy-coated carbon fabric was also used as textile reinforcement. Additionally, the residual mechanical performance of the composites was investigated after exposure to thermal regimes with target temperatures of 150 °C, 200 °C, and 300 °C, aiming at recording their effectiveness under these conditions.

4.2. Experimental Program

4.2.1. Materials

4.2.1.1. Fine grained concrete matrix

A fine-grained concrete with mix proportion of 1: 1 : 0.3 (cementitious material : aggregate : water) was adopted as reference matrix. Portland cement CEM II-A/LL 42.5 N from Dyckerhoff GmbH, Germany, defined by the European Standard [60] was used. Fly ash Steamant H4 from STEAG Power Minerals GmbH, Germany, and silica fume from Elkem, Germany, were incorporated as mineral admixtures. Sand from Ottendorf, Germany, with a maximum particle diameter of 1 mm was used as fine aggregate. To obtain adequate flowability for the casting procedures, the superplasticizer MasterGlenium SKY 593 from BASF Construction Solutions GmbH, Germany, was used. Table 4.1 presents the fine-grained concrete matrix composition and its mechanical properties at room temperature.

Table 4.1 – Fine-grained concrete matrix composition and mechanical properties.

Composition	
Sand (0-1 mm) (kg/m ³)	947
Cement CEM II-A/LL (kg/m ³)	632
Water (kg/m ³)	273.88
Fly ash (kg/m ³)	265
Silica fume (kg/m ³)	50.5
Superplasticizer (kg/m ³)	14.05
Mechanical properties*	
Compressive strength (MPa)	67.8 ± 5.3
Flexural strength (MPa)	6.81 ± 1.07
*Compression and flexural tests based on the European Standard EN 196-1 [61] performed at 28 days.	

Compression tests based on the European Standard EN 196-1 [61] were performed to evaluate the residual mechanical properties of the fine-grained concrete matrix. The specimens were submitted to a thermal regime with target temperatures of 150 °C, 200 °C, and 300 °C in a Universal Furnace UF1060 from Memmet GmbH + Co. KG, Germany, as described in Section 2.2.

4.2.1.2. Carbon fabrics

Carbon fabrics with different impregnations were assessed. Two carbon fabrics with mineral impregnations, namely a cement-based and a geopolymer, were produced (see section 2.1.2.1) using a continuous carbon fiber tow model C T50-4.4/255-E100 from SIGRAFIL®. Additionally, a commercially available carbon fabric coated with an epoxy resin (EP) model GRID Q85/85 – CCE – 21 from Solidian was used. Table 4.2 and

Table 4.3 present the technical data provided by the suppliers for the carbon fiber tow and commercially available carbon fabrics, respectively.

Table 4.2 – Technical data of the continuous carbon fiber tow (according to the supplier).

Number of filaments	50000 (50k)
Fineness (tex)	3420
Single filament diameter (μm)	7
Tensile strength	4400
Modulus of elasticity (GPa)	255

Table 4.3 – Technical data of the commercial carbon fabric (according to the supplier).

Impregnation material	Epoxy resin
Cross-section of the strand (mm^2)	1.81
Tensile strength (MPa)	2500
Modulus of elasticity (GPa)	220

4.2.1.3. Impregnation process and MCF fabric manufacturing

For the manufacture of the carbon fabrics with mineral impregnation, an automated continuous pultrusion process developed at TU Dresden, Germany, was used [43]. Although the system has the potential and the possibility to be automated [43], in this study, the fabrics were assembled manually.

Two mineral suspensions were used to produce the Mineral-impregnated Carbon Fibers (MCF) yarns, a cement-based (C) and a geopolymer (GP) one. The cement-based suspension was based on previous works [29,41], and its composition is presented in Table 4.4. It consists of commercial micro-cements Mikrodur R-X and Mikrodur P-U from Dyckerhoff, Germany. A micro-silica suspension produced by MC-Bauchemie, Germany, with a solid content of 48% to 52%, was used. To obtain proper workability for the impregnation process, the superplasticizer Master Rheobuild 30 from BASF, Germany, was added to the mixture.

Table 4.4 – Cement-based suspension composition

Micro-cement Mikrodur R-X (kg/m ³)	500
Micro-cement Mikrodur P-U (kg/m ³)	500
Micro-silica suspension Centrilit Fume SX (kg/m ³)	500
Water (kg/m ³)	464
Superplasticizer Master Rheobuild 30 (kg/m ³)	45

The geopolymer suspension, as described in Chapter 3 and [59] was produced through the combination of an alkali solution with an aluminosilicate source. Table 4.5 gives its composition. A commercially available potassium-based water glass (WG) Geosil® 14517, from Woellner, Germany, with a solid content of approximately 45% of potassium silicate and a SiO₂/K₂O molar ratio of 1.7, was used as alkali activator. The aluminosilicate source was metakaolin (MK) Metamax® from BASF, Germany, with high reactivity and low average particle diameter of 1.3 μm [62]. The WG-to-MK ratio used is 1.82. To obtain an adequate flowability for the impregnation process, the superplasticizer Sapetin® D27 from Woellner, Germany, with a solid content of approximately 45%, was used in a dosage of 4% by mass of geopolymer.

Table 4.5 – Geopolymer suspension composition

Waterglass Geosil (kg/m ³)	1000
Metakaolin (kg/m ³)	549.33
Superplasticizer Sapetin® D27 (kg/m ³)	61.97
WG/MK ratio	1.82

The mineral suspensions were produced as described in Chapter 3. The cement-based suspension was produced with a stand mixer as follows: (i) the water and the micro-silica were mixed with half of the total amount of superplasticizer; (ii) the micro-cements were gradually added while constantly stirring; (iii) the remaining amount of superplasticizer was added in parts still with stirring. After this process, the cement-based suspension was mixed with a T 50 digital ULTRA-TURRAX® disperser from IKA® at 7000 rpm for 2 minutes to guarantee a full dissolution of the particles and dissolve any possible agglomerates.

To produce the geopolymer suspension, the water glass and the metakaolin were mixed in the T 50 digital ULTRA-TURRAX® disperser from IKA® at 7000 rpm for 3 minutes. Then, the superplasticizer was added, and the suspension was mixed for another 3 minutes. Finally, the geopolymer suspension was vibrated for 2 minutes to eliminate entrapped air voids.

The impregnation process to manufacture the MCF yarns is described in detail in Chapter 3 and also in [43,59]. The yarns are unwound from the spool, pulled via three yarn guiding levels, a kiss-coater, a suspension bath containing five-roller deflections, and are shaped by a plastic nozzle of 4 mm. The yarn guiding levels ensure the yarn alignment during the process, avoiding fiber damages. The five-roller configuration used offers the optical impregnation quality to produce MCF, as discussed in [63]. Nevertheless, unlike the yarns production, described in Chapter 3 and in [59,63,64], for the manufacture of the MCF fabrics, the impregnation process is manually controlled, i.e., the person who assembles the fabric is responsible for pulling the yarn from the spool and, thus, controlling the process.

To join the recently impregnated yarns in a fabric structure, a wooden mold was used, see Figure 4.1. The mold has dimensions of 75 x 55 cm (longitudinal x transversal), and support pins are used to position the yarns during manufacture. Due to the notches along the support pins, it was possible to fabricate up to 5 layers of MCF fabrics in one impregnation batch. These support pins are spaced in an array to form the desired mesh. In this case, a 20 mm opening mesh was used, similar to the commercial fabric with a polymeric coating used as a reference.

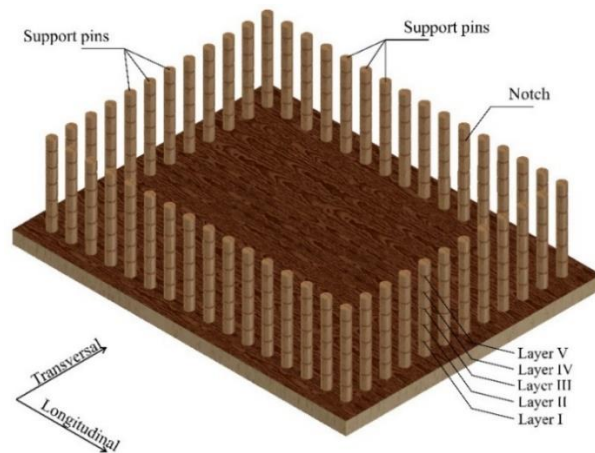


Figure 4.1 – Wooden mold for the fabrication of the MCF fabrics.

The mold was positioned immediately after the impregnation system, and the manufacturing process occurred as follows. First, the carbon yarn is impregnated with the mineral suspension as described previously (Figure 4.2a). The MCF yarn is positioned in the transversal direction (weft yarns) anchored in the support pins as tensioned as possible, see Figure 4.2b. Then, also anchored in the support pins, the MCF yarn is placed in the longitudinal direction (warp yarns) over the transversal yarns, see Figure 4.2c. Figure 4.3 presents the handmade manufactured C-MCF and GP-MCF fabrics in comparison with the commercially available EP carbon fabric.

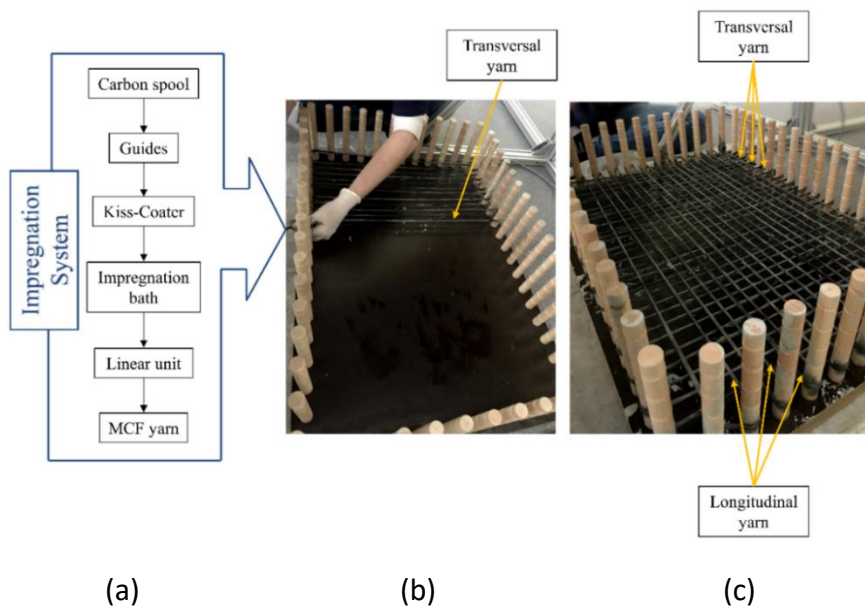


Figure 4.2 – Procedure for the manufacture of the MCF fabrics (a) Impregnation system; (b) Placement of the transversal yarns; (c) Placement of the longitudinal yarns.

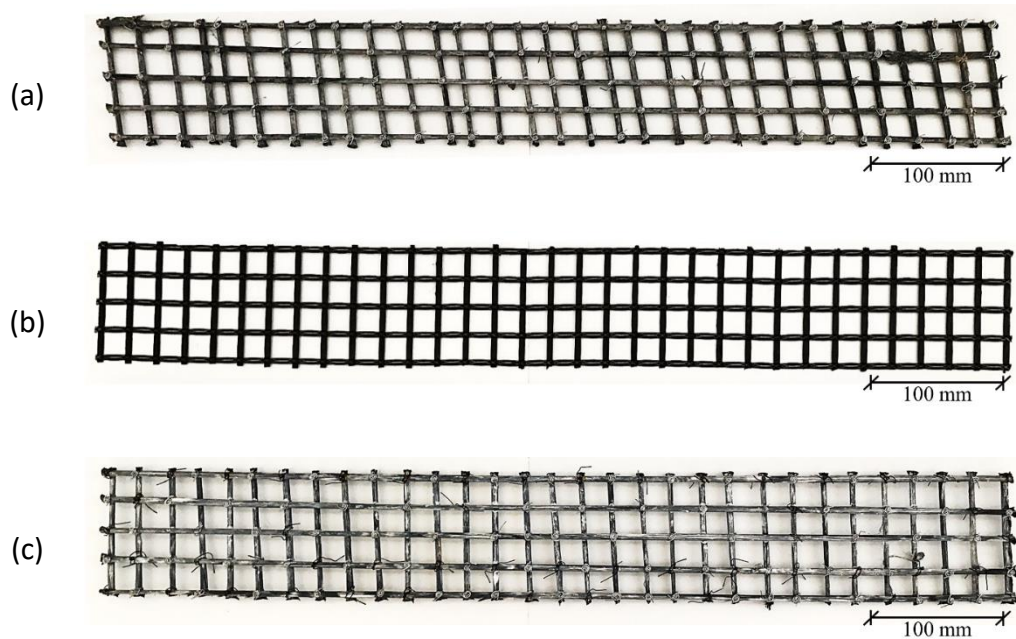


Figure 4.3 – (a) C-MCF (b) EP, and (c) GP-MCF carbon fabrics.

The connection of the longitudinal and transverse yarns was developed only by their overlapping, with the mineral suspension used acting as glue. So, the knots, i.e., the intersections between the longitudinal and transversal yarns, are fragile regions. Therefore, to prevent disassembly of the fabric during the handling, cutting, and transportation, some specific knots were tied with a 0.4 mm diameter conventional wire.

The C-MCF fabrics were removed from the mold after 24h, and the curing process was similar to the one applied for the individual yarns, described in Chapter 3: 7 days over a plane surface to allow initial hydration followed by immersion in water for another 7 days. Then, the C-MCF fabrics were stored in a standard climate (55% RH and 20°C) until composite manufacturing.

The GP-MCF fabrics were submitted to thermal curing. For this, after the fabric manufacturing, the entire mold was covered with a temperature-resistant plastic foil and placed in an oven at 75°C for approximately 20 hours, guaranteeing the suspension geopolymerization. After being removed from the oven, the GP-MCF fabrics were finally removed from the mold and immersed in water for 7 days with water replacement every day so that the alkali concentration on the GP-MCF surface and in the pore solution of the geopolymer matrix could be reduced,

increasing the bond with the fine-grained concrete matrix, as discussed before in Chapter 3.

4.2.2. Composite manufacturing

For the MCF fabrics tensile tests, rectangular specimens with a 100 mm width were produced. To attach the specimens to the machine grips, their edges, with a 225 mm x 100 mm each, were cast with the same fine-grained concrete used as matrix for the TRC. The MCF fabrics presented a total length of 700 mm with a gauge length of 250 mm, as can be seen in Figure 4.4.

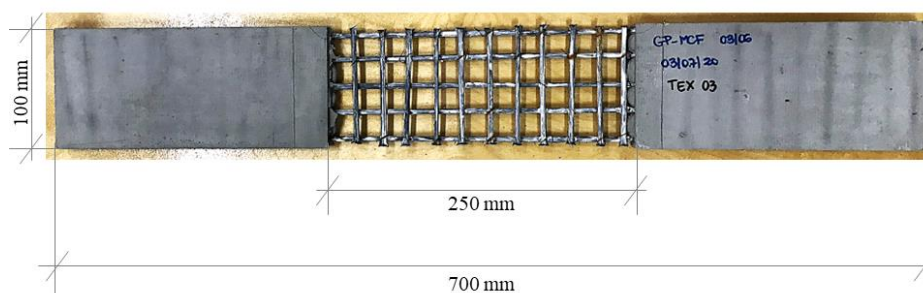


Figure 4.4 – MCF fabric specimen.

The TRC specimens were produced with one textile reinforcement layer throughout the hand lay-up technique, as shown in Figure 4.5. Rectangular plates measuring 700 mm x 100 mm (length x width) with a gauge length of 275 mm were manufactured as follows: (i) first, a thin layer of the fine-grained concrete matrix was placed on the mold (Figure 4.5.a); (ii) then, the fabric was positioned over it (Figure 4.5.b); (iii) and, finally, covered with another matrix layer (Figure 4.5.c and d). At least four specimens were tested for each configuration (type of carbon fabric and temperature). Table 4.6 presents the number of specimens tested at each configuration (#). The specimen's cross-sectional area in the gauge length region was reduced to guarantee that the rupture would occur in this region. For this, two plates with approximately 2.5 mm in thickness were used, one in the bottom, placed before the first matrix layer (Figure 4.5.a), and the other at the top of the mold, placed after the last matrix layer (Figure 4.5.d), reducing the composite thickness, and creating a variable thickness along the length. Table 4.6 presents the average thickness with the standard deviation for each batch of TRC configuration. In the grip regions, all specimens presented a thickness of approximately 15 mm, which

is necessary for the proper gripping in the machine. In the gage length region, the TRC presented approximately 12 mm and 13 mm thickness for the specimens reinforced with the C-MCF and GP-MCF fabrics, respectively. For the TRC specimens with the EP fabrics, this gage length thickness is approximately 8 mm. This difference between the thickness of the specimens with polymer- and mineral-impregnated carbon fabrics is mainly due to the considerably higher thickness of the MCF fabrics compared to the EP one. Due to the manufacturing process, the longitudinal and transversal yarns of the MCF fabrics were just overlaid over each other. Thus, in the knots' areas, the thickness of the fabric is the sum of the diameters of the transversal and longitudinal yarns, as can be seen in Figure 4.6.

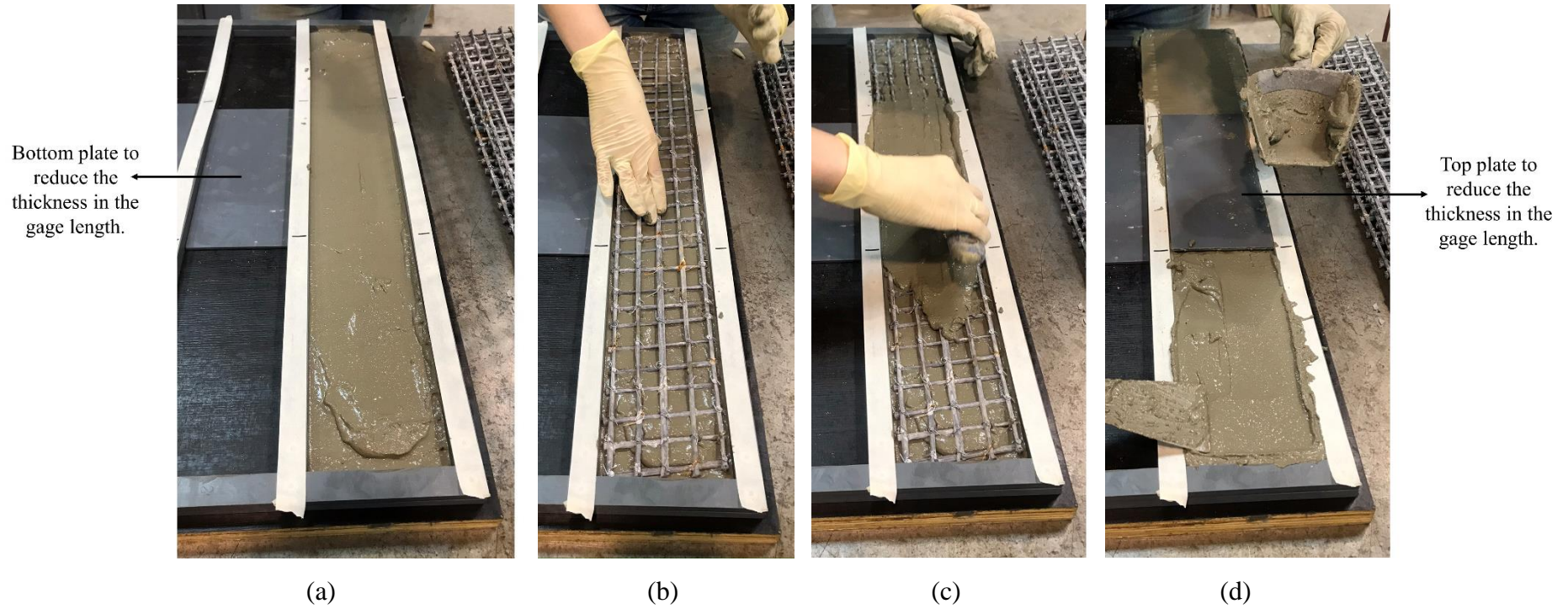


Figure 4.5 – Hand lay-up technique for the TRC manufacturing. (a) placement of a thin layer of the fine-grained concrete matrix over the bottom plate to reduce the thickness in the gage length, (b) positioning of the fabric, (c) and (d) placement of the final matrix layer, the top plate, and finishing procedure.

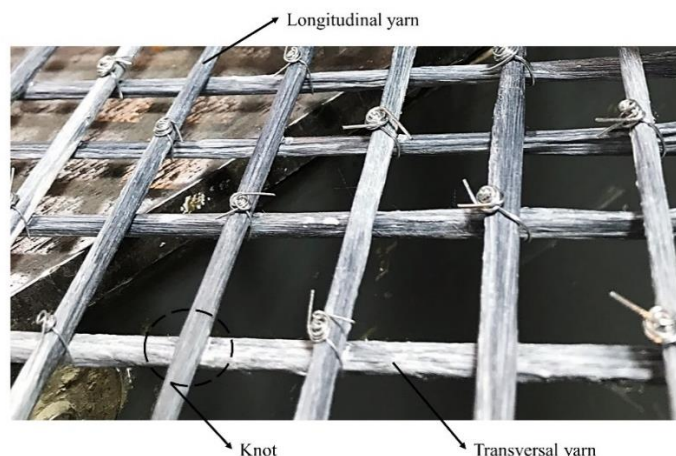


Figure 4.6 – Detail of the MCF fabrics knot regions with the transversal and longitudinal yarns overlaying.

Table 4.6 – TRC specimens for direct tensile tests

Specimen #	Fabric age (days)	Thickness (mm)		
		Gage length	Grip	
<i>Room Temperature</i>				
C-MCF	7	65	12.1 (0.8)	15.5 (0.4)
GP-MCF	5	41	13.4 (1.0)	15.8 (0.4)
EP	4	-	8.0 (1.0)	15.4 (0.4)
<i>150°C</i>				
C-MCF	5	65	11.5 (0.2)	15.2 (0.2)
GP-MCF	5	41	12.9 (0.6)	15.3 (0.3)
EP	5	-	7.6 (0.6)	15.0 (0.6)
<i>200°C</i>				
C-MCF	4	65	11.4 (0.2)	15.5 (0.1)
GP-MCF	5	41	12.8 (0.5)	15.7 (0.3)
EP	5	-	7.7 (0.5)	15.1 (0.3)
<i>300°C</i>				
C-MCF	4	65	11.3 (0.3)	15.4 (0.3)
GP-MCF	5	41	12.9 (0.4)	16.0 (0.2)
EP	5	-	7.6 (0.7)	15.2 (0.2)

4.2.3. Direct tensile tests

Direct tensile tests were performed to evaluate the mechanical behavior of the MCF fabrics and carbon textile reinforced concretes (TRC). A servo-hydraulic testing machine Instron model 8501 with a maximum load capacity of 100 kN was used to perform the uniaxial tension tests at a rate of 1.2 mm/min, see Figure 4.7. The specimens were inserted into steel plates and clamped with a pressure of

approximately 11 MPa (1600 psi) generated by hydraulic jacks. The clamping surface area, 20,000 mm² at each end, were smoothed with a saw to ensure the specimens' proper grip. Two Linear Variable Differential Transducers (LVDTs) were attached at each side of the specimens using a steel frame to obtain the displacement of the specimens in a gage length of 275 mm. Additionally, for the TRC specimens with the MCF fabrics, the deformation and crack formation were evaluated through Digital Image Correlation (DIC) techniques. For this, the specimens were sprayed with a black and white speckle pattern, and high-resolution images were obtained during the tests. A camera Canon E05 700D with a rate of 1 frame every 5 seconds was used. The frames were processed with a software VIC-2D, developed by Correlated Solutions, Inc. This technique was not used for the TRC with EP carbon fabrics due to the risk of matrix spalling, which could damage the camera system.

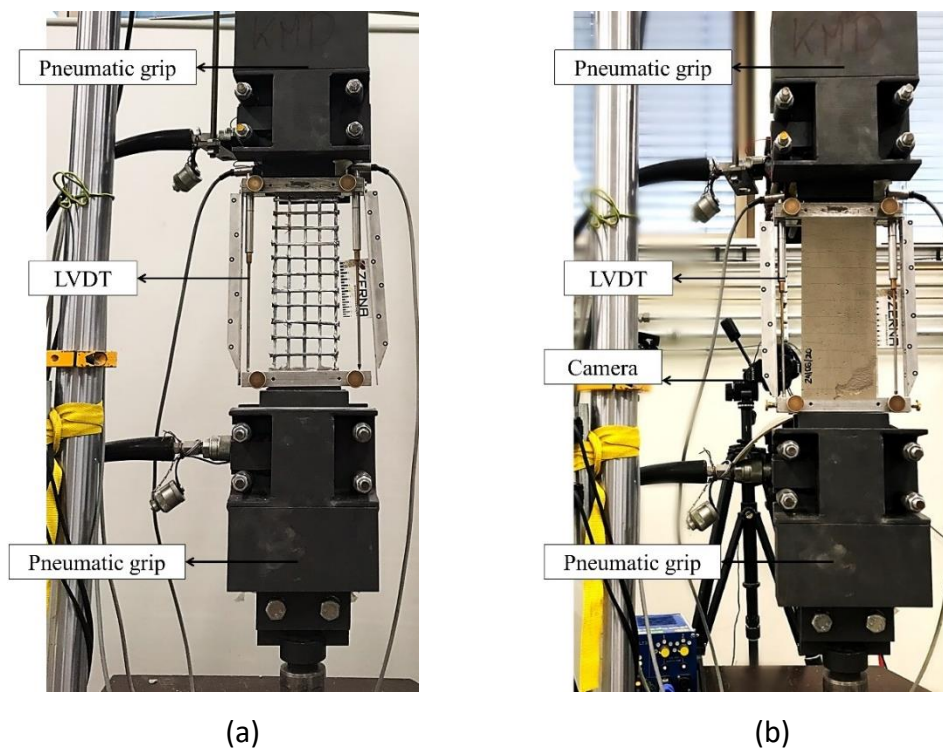


Figure 4.7 – Setup for the direct tensile tests in the (a) MCF fabric specimens, and (b) TRC specimens.

For the evaluation of the residual tensile mechanical behavior, the TRC specimens were submitted to a thermal regime prior to testing, as shown in Figure 4.8. The target temperatures, i.e., 150 °C, 200 °C, and 300 °C, refer to the oven

temperatures and were selected based on the bond behavior of the EP and MCF carbon yarns towards fine-grained concrete matrices, discussed in Chapter 3. A Universal Furnace UF1060 from Memmert GmbH + Co. KG was used to heat the specimens at a rate of approximately 3 °C/min up to the target temperature. Based on previous works [38,65,66] on the residual mechanical performance of TRC, the specimens were maintained at the target temperature for 1 hour aiming to reach the thermal stable state and then submitted to a gradual cooling to room temperature inside the furnace.

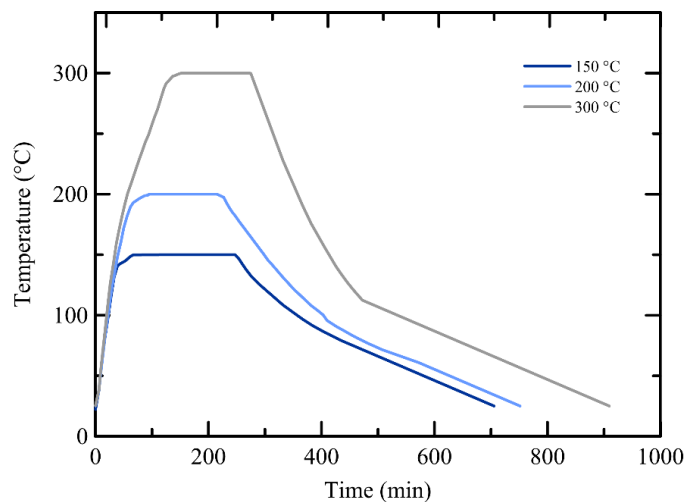


Figure 4.8 – Thermal regime for the TRC specimens.

4.2.4. Morphological characterization

To understand the internal structure, fracture and failure behavior of the TRC without and with thermal damage, a micro-computed topographer (μ CT) scan CT-XPRESS from ProCon X-Ray, Germany, equipped with a high-performance 65 W X-ray tube and a high-resolution flat panel detector was used. The scan conditions were 84 kV and 87 μ A with 1441 projections. Each scan had a duration of around 1 h with a sampling rate of one image per 2 s. Afterward, the scans were iteratively reconstructed with X-AID software (MITOS, Germany). Each slice had 2940 x 2301 pixels.

4.3. Results and discussion

4.3.1. Fine-grained concrete matrix

Figure 4.9 shows the compressive strength of the fine-grained concrete matrix at room temperature ($\sim 20\text{ }^{\circ}\text{C}$) and the residual compressive strength after being submitted to thermal regimes with target temperatures of $150\text{ }^{\circ}\text{C}$, $200\text{ }^{\circ}\text{C}$, and $300\text{ }^{\circ}\text{C}$. Considering the scattering of the results, the thermal regime up to $150\text{ }^{\circ}\text{C}$ did not significantly affect the residual compressive strength of the fine-grained concrete matrix. The subsequent heating up to $200\text{ }^{\circ}\text{C}$ followed by the cooling to room temperature led to a considerable increase in the residual compressive strength of the matrix. As the target temperature was increased to $300\text{ }^{\circ}\text{C}$, a drop in the residual compressive strength can be observed. However, it still remains above the values obtained at room temperature and in the thermal regime up to $150\text{ }^{\circ}\text{C}$. When submitted to elevated temperatures, hardened cement pastes exhibit a gradual loss of the free water at temperatures up to $100\text{ }^{\circ}\text{C}$ [67]. With the increase of the temperature up to $300\text{ }^{\circ}\text{C}$, part of the chemically bonded water and the interlayered C-S-H water is also lost [22]. At approximately $35\text{ }^{\circ}\text{C}$, there is the start of the dehydration of the ettringite [68,69], which is completely decomposed at temperatures in the range of $120\text{ }^{\circ}\text{C} - 130\text{ }^{\circ}\text{C}$ [70,71].

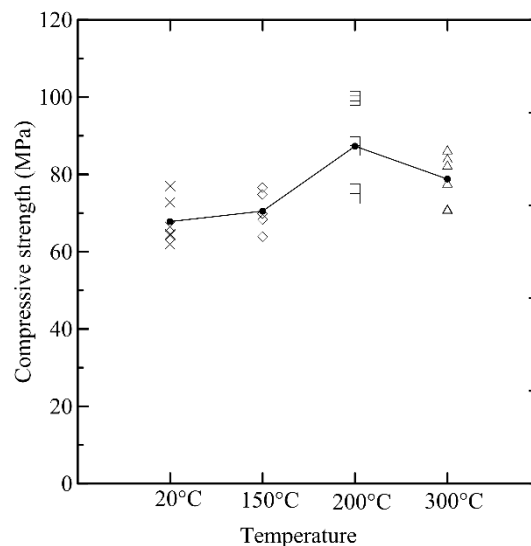


Figure 4.9 – Residual compressive strength of the fine-grained concrete matrix at room temperature ($\sim 20\text{ }^{\circ}\text{C}$) and after being submitted to thermal regimes with target temperatures of $150\text{ }^{\circ}\text{C}$, $200\text{ }^{\circ}\text{C}$, and $300\text{ }^{\circ}\text{C}$.

The fine-grained, high-strength concrete presented a residual performance in terms of compressive strength after exposure to the thermal regime considered superior to the in-situ performance, being further discussed in Chapter 3. This trend was also observed in the results of Pahn and Carino [72] and Hagger and Pimienta, available in [73]. However, in these two studies a decrease in the residual compressive strength was observed with the increase in temperature, which goes against the results obtained in the study at hand. In contrast, the results obtained by Khoury, available in [73], show an increase in the residual compressive strength at temperatures up to 200 °C. At 300 °C, the compressive strength obtained was at the same level as the one at room temperature, similar to what can be observed in Figure 4.9. It should be mentioned that the studies discussed above were carried out with concrete, which presents coarse aggregate besides fine aggregate. Differently, the fine-grained concrete matrix used in TRC usually presents only fine aggregates due to the limitations of the textile reinforcement mesh [14]. It is called concrete due to its high compressive strength, but in terms of constituents, it is classified as a mortar. Menou et al. [74] performed 3-point bending tests on a mortar constituted of cement, silica fume, sand, and water with a w/c ratio of 0.3 and observed little or no variation in the residual tensile strength after heating up to 400 °C. A concrete with no silica fume and a calcareous coarse aggregate was submitted to the same heating regime, and the results obtained showed a decrease in the residual tensile strength. These results could indicate a significative role performed by the coarse aggregates in the residual thermal behavior of concretes, thus explaining the difference in the compressive strength of concretes and mortars. Moreover, microsilica usually increases the mechanical strength of mortar and concretes at elevated temperatures [75–77]. Yüzer et al. [75] also observed an increase in the residual compressive strength of a mortar composed of cement, silica fume, sand, and water with a w/c ratio of 0.5 in temperatures up to 300 °C. Ibrahim et al. [76] evaluated a mortar made of cement, nanosilica, sand, polypropylene fiber, and water with a w/c ratio of 0.4. An increase in the residual compressive strength at temperatures up to 400 °C was observed, and this improvement was attributed to the acceleration of pozzolanic reactions promoted by the nanosilica due to the exposure to elevated temperatures.

4.3.2. Tensile mechanical behavior – MCF fabrics

Figure 4.10 shows the tensile stress vs. strain curves of the C- and GP-MCF fabrics obtained from the direct tensile tests. For comparison purposes, the tensile stress versus strain curves obtained for the MCF yarns (Chapter 3) were also plotted. Table 4.7 presents the average tensile strength σ_t , modulus of elasticity E , and rupture strain ε_{rup} obtained for the MCF fabrics. The tensile stresses f_t were derived from the effective cross-sectional area of single yarns through the equation:

$$f_t = \frac{F}{n \times A_{yarn}} \quad (4.1)$$

where F is the load measured in the test; A_{yarn} is the cross-sectional of one single yarn obtained from the data shown in Table 4.2; and n is the number of longitudinal yarns contained in the tested specimen, i.e. $n = 5$ (see Figure 4.4).

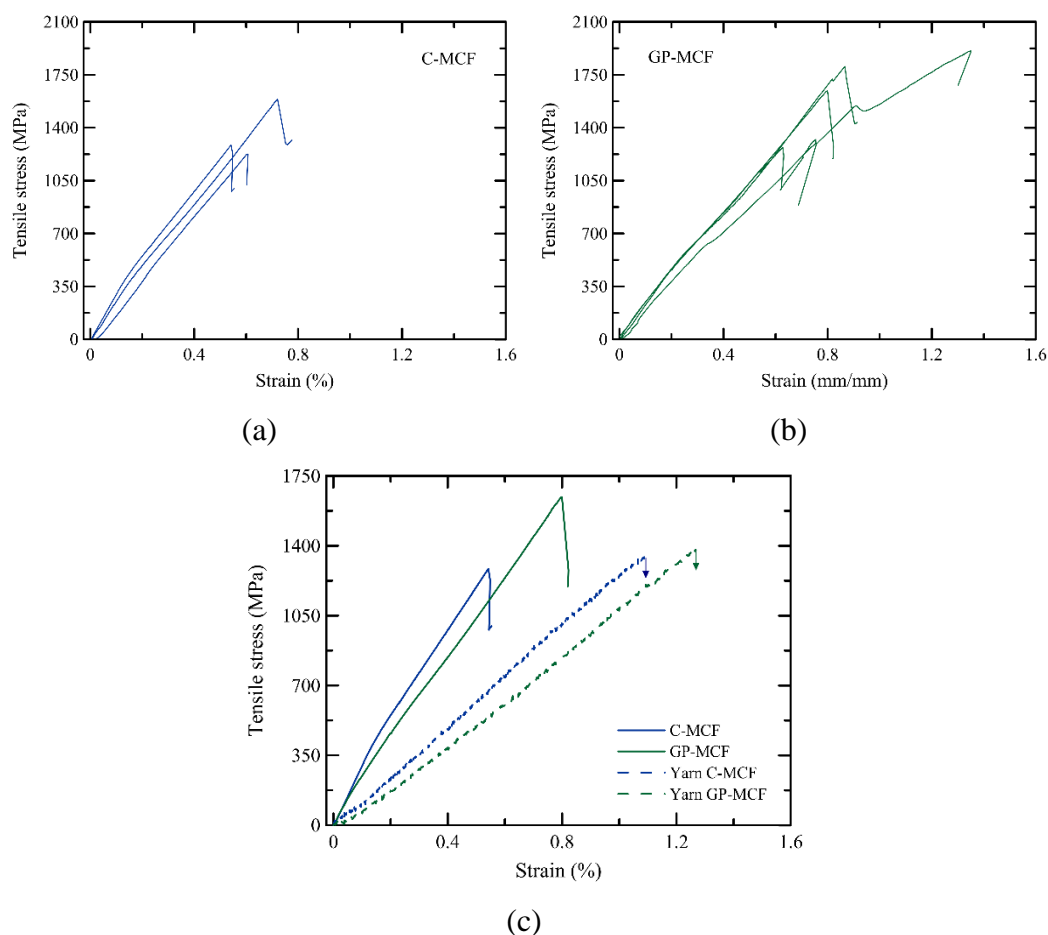


Figure 4.10 – Tensile stress vs. strain curves obtained from the direct tension tests for the (a) C-MCF and (b) GP-MCF fabrics. (c) Representative tensile stress vs. strain curves obtained from the direct tension tests for the C-MCF and GP-MCF fabrics and yarns.

Table 4.7 – Average results and standard deviation of the MCF fabrics obtained from the direct tensile tests

Fabric	σ_t (MPa)	E (GPa)	ϵ_{rup} (%)
C-MCF	1367	220	0.622
	(160)	(9.63)	(0.0742)
GP-MCF	1591	196	0.807
	(201)	(0.650)	(0.0459)

Both MCF fabrics presented an elastic behavior up to their brittle rupture, which is accordance with the mechanical behavior observed for the single MCF yarns, already addressed in Chapter 3. The C-MCF fabric reached a tensile strength of 1367 MPa while the GP-MCF fabric yielded 1591 MPa. Similar to what was observed for the MCF yarns, discussed in Chapter 3, the GP-MCF fabrics reached higher tensile strength than the C-MCF, approximately 16%. This difference can be due to a better efficiency of the geopolymer-based suspension in filling the spaces between the multi-filaments in the yarn. Moreover, the mechanical properties of the suspension material can also influence the strength of the MCF fabric. The MCF itself can be considered a composite in which the mineral suspension is the matrix and the multi-filaments the reinforcement. More studies must be conducted to better understand the role of this mechanism in the mechanical response of the MCF yarns and fabrics.

The C-MCF fabric reached a modulus of elasticity of 220 GPa and the GP-MCF fabric yielded 196 GPa. Both are in accordance with the literature data for carbon fibers [1]. Since both MCF fabrics are made with carbon fibers it was expected that they exhibited the same modulus of elasticity. However, a difference of approximately 10% is observed. This can be related to the mineral suspension materials used. Usually, geopolymers present a lower modulus of elasticity than cementitious materials due to their polymer-like hardening behavior [78,79].

The MCF fabrics presented a higher modulus of elasticity than the MCF yarns, as shown in Figure 4.10.c, which was not expected since the modulus of elasticity is a material property. The C-MCF fabrics presented a modulus of elasticity 86% higher than the C-MCF yarn. For the GP-MCF, the difference in the modulus of elasticity was approximately 72%. Previous studies show that the longer the length, the lower the tensile strength and ultimate strain of fibers [80] and yarns [81]. The authors related this behavior to the greater probability of the specimens

presenting internal or external defects that can affect such mechanical properties. However, this was not observed in the results presented in this study. The tensile strength obtained for the MCF fabrics was at the same level as the results for the MCF yarns, approximately 1370 MPa and 1500 MPa for the C-MCF and GP-MCF, respectively. Thus, the increase in the number of flaws in the specimen could not be the reason for the difference in the modulus of elasticity. Nevertheless, it is important to consider the presence of the transversal yarns that also contribute to the strength of the fabric. Thus, the decrease in the tensile strength due to the presence of flaws in longer yarns could be balanced by the increase promoted by the presence of the transversal yarns. But that would not explain the considerably disparity in the modulus of elasticity. In addition to the difference in the specimens' length, another divergence between the two tests was regarding the measurement of the specimens' displacement. As already mentioned in Chapter 3, the MCF yarn displacement recorded by the video extensometer corresponded to the displacement of the entire system, including the gripping, the specimen holder, and the specimen itself, which was verified by the practically coincident representative tensile stress *vs.* strain curves obtained with the displacement recorded by the video-extensometer and the actuator displacement. In the case of MCF fabrics tests, in which two LVDTs were coupled to the gage length of the specimen, the tensile stress *vs.* strain curves obtained from the external instrumentation (LVDTs) and the actuator displacement present considerably different slopes, as can be seen in Figure 4.11, validating that the displacement measured by the video-extensometer was related to the entire system. Thus, it is possible to say that the modulus of elasticity obtained from the direct tensile tests in the MCF fabrics are closer to the actual properties of the textile. To further confirm this, the curves obtained from the MCF yarn tests should be corrected through the compliance of the machine so that only the displacement of the specimen is considered.

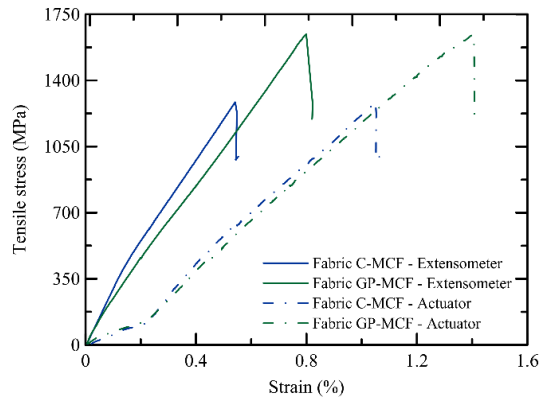


Figure 4.11 – Representative tensile stress vs. strain curves obtained from the direct tension tests comparing the strain obtained with the displacement recorded by LVDTs and the actuator displacement for the C-MCF and GP-MCF fabrics.

It is important to emphasize here that differently from what seems from the curves in Figure 4.10, the MCF fabrics specimen did not present a total rupture at once. Each longitudinal yarn failed at a different displacement, as it can be seen in Figure 4.12 **Erro! Fonte de referência não encontrada.** The letters A-D and A'-C' indicate the points in which occurred the failure of one longitudinal yarn for the C-MCF and GP-MCF fabrics, respectively. The fragile rupture of one yarn significantly disturbed the measurements from the LVDTs, and, for that reason, after the first longitudinal yarn rupture, it was not possible to obtain the correct specimen strain. Thus, the curves in Figure 4.12 were constructed using the actuator displacement. Although the MCF fabrics present a fragile behavior, the textile structure with multiple longitudinal yarns enables a “pseudo-ductile” rupture, in which the specimen is able to maintain a certain load level before its complete failure. This behavior is interesting mostly when considering the safety aspects of structures, in which the current standards available [33] limit the mechanical performance of concrete structures to domains governed by ruptures with notice, i.e., the materials do not fail suddenly.

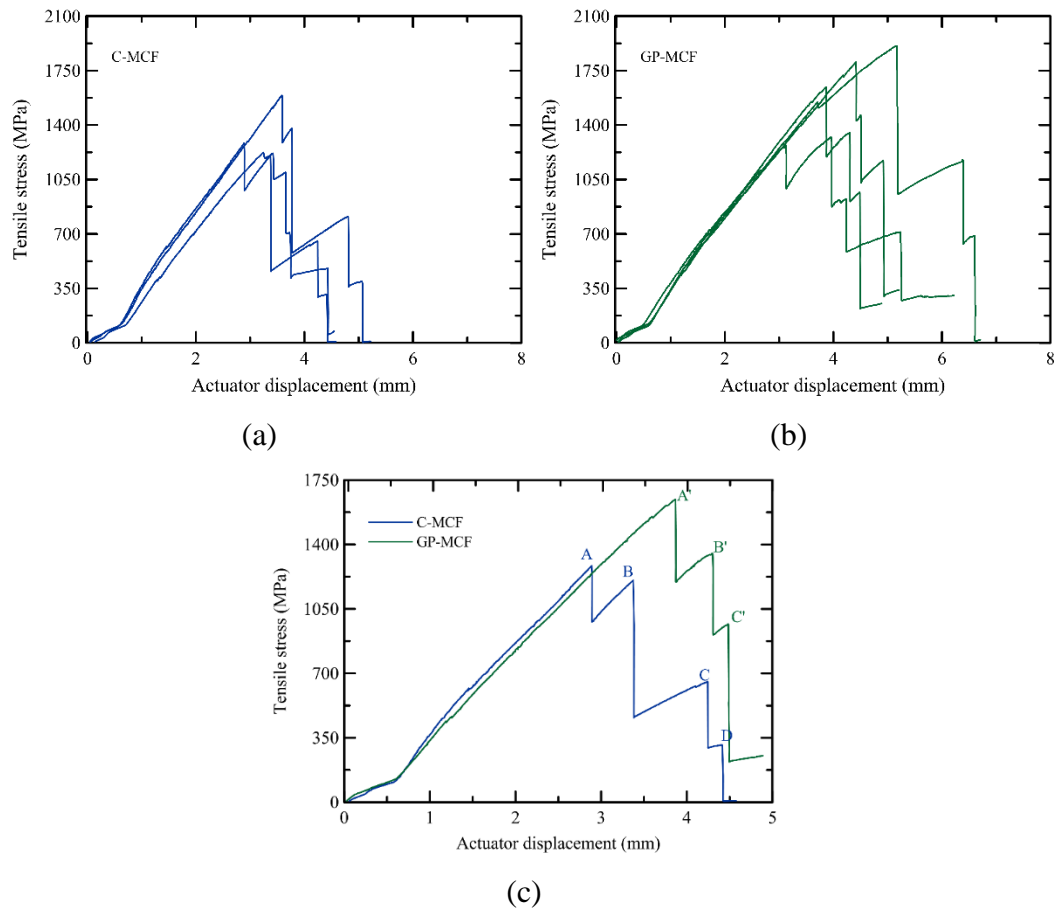


Figure 4.12 – Tensile stress vs. actuator displacement curves obtained from the direct tension tests for the (a) C-MCF and (b) GP-MCF fabrics specimens, and (c) representative curves.

4.3.3. Tensile mechanical behavior – TRC

Figure 4.13 and Figure 4.14 show the tensile stress vs. strain curves of the TRC with C-MCF, GP-MCF, and EP fabrics specimens and representative, respectively, obtained from the direct tensile tests. Table 4.8 presents the average tensile strength σ_t , rupture strain ϵ_{rup} , tensile strength at the first matrix crack σ_{BOP} , strain at the first matrix crack ϵ_{BOP} , and the modulus of elasticity in the Stage I E_I obtained for the TRC composites. The modulus of elasticity in the Stage I was obtained between 30 and 70% of the strength at the first matrix crack. The tensile stresses f_t were derived from the effective cross-sectional area of the composite through the equation:

$$f_t = \frac{F}{A_{composite}} \quad (4.2)$$

where F is the load measured in the test; $A_{composite}$ is the cross-sectional of the composite, i.e. $A_{composite} = w \times t$, in which w is the width of the rectangular specimen (100 mm) and t is the gage length thickness of the specimen, as shown in Table 4.6.

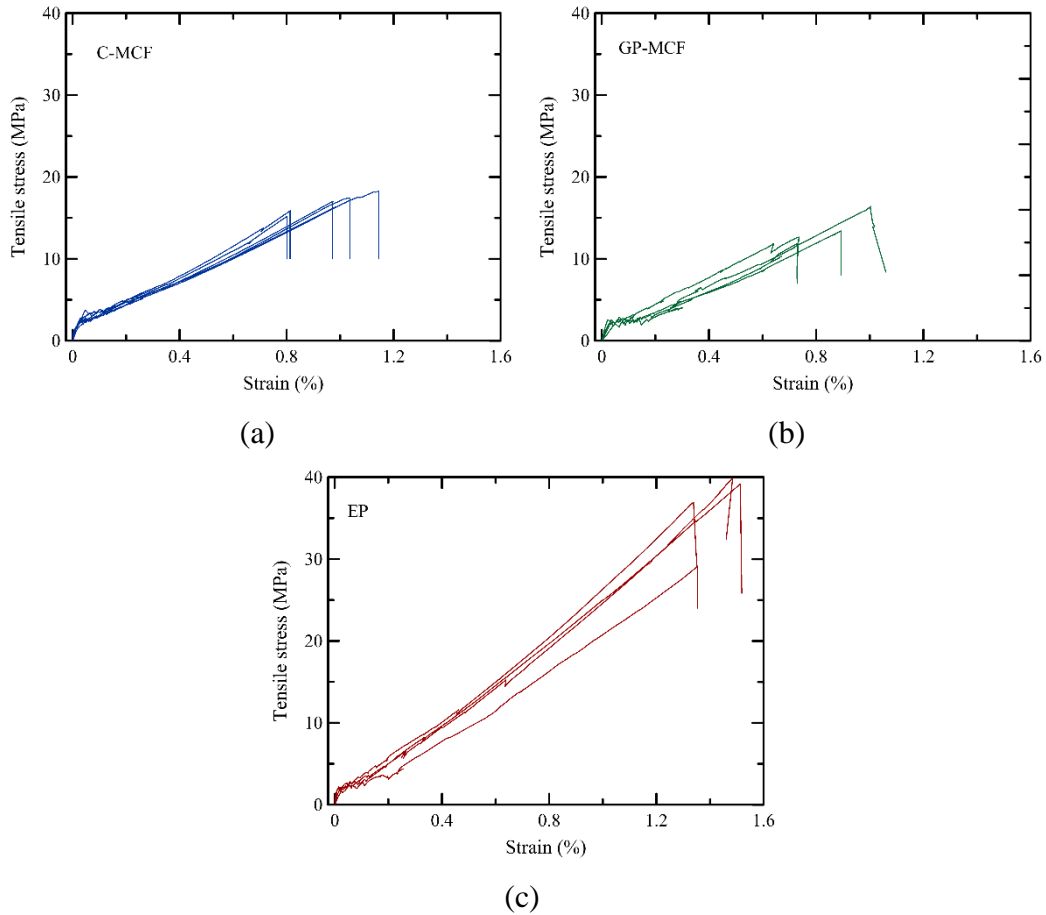


Figure 4.13 – Tensile stress vs. strain curves obtained from the direct tension tests for the TRC with the (a) C-MCF, (b) GP-MCF, and (c) EP fabrics.

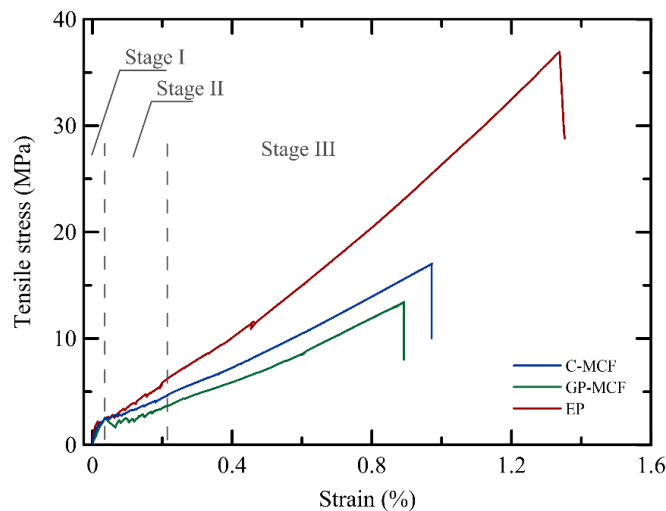


Figure 4.14 – Representative tensile stress vs. strain curves obtained from the direct tension tests for the TRC with the C-MCF, GP-MCF, and EP fabrics.

Table 4.8 – Average results and standard deviation from the direct tensile tests on TRC

TRC	σ_t (MPa)	ε_{rup} (%)	σ_{BOP} (MPa)	ε_{BOP} (%)	E_I (GPa)
C-MCF	16.8 (1.01)	0.967 (0.123)	2.69 (0.472)	0.0362 (0.0129)	8.58 (1.98)
GP-MCF	13.6 (1.72)	0.841 (0.115)	2.54 (0.248)	0.0398 (0.0161)	7.75 (2.91)
EP	36.3 (4.27)	1.42 (0.0772)	2.10 (0.150)	0.0221 (0.0105)	13.1 (4.65)

Usually, the tensile stress vs. strain curves of textile reinforced concretes can be divided into three different stages [14], as shown in Figure 4.14. In Stage I, both matrix and textile reinforcement present a linear elastic behavior. However, due to the low volume fraction of reinforcement, the stiffness of the composite is mainly influenced by the modulus of elasticity of the matrix. With the increase of the load, there is the formation and opening of the matrix's first crack. This point, also known as Bend Over Point (BOP), delimits the end of Stage I. After the first crack, more cracks appear in the composite, characterizing a multiple-cracking behavior, defined as Stage II. This stage ends when no more cracks are formed. In Stage III, there is the widening of the existing cracks, majorly due to the stretching of the textile reinforcement, until the composite rupture.

All composites presented a strain-hardening behavior with a multiple-cracking pattern, as expected to textile reinforced concretes. For a composite to

achieve this behavior, it must contain a certain level of reinforcement volume fraction, otherwise, it will present a strain-softening behavior when submitted to loading, as observed in most Fiber Reinforced Concrete (FRC) composites [82–84]. In the case of the TRC, it is not so difficult to achieve the reinforcement volume fraction necessary to characterize the strain-hardening behavior due to the presence of multiple longitudinal yarns containing several multifilaments. Additionally, the transversal yarns, although usually not considered in the calculation to obtain the volume fraction, also positively influence the performance of the composite, contributing to the strain-hardening behavior.

In the TRC, the most critical point to achieve the strain-hardening behavior is the bond of the textile towards the cementitious matrix. A poor bond presents a considerable effect on the stresses transfer from the matrix to the textile reinforcement, negatively influencing the mechanical performance of the composite. Carbon fabrics are known to present a weak bond towards cementitious matrix. Thus, the yarns are impregnated with different types of coatings, normally polymeric ones, to improve this bond. However, not all types of coating can significantly improve the bond and, consequently, the mechanical performance of the composite, as is the case for more flexible resins, such as SBR [31,85]. Both TRC with the MCF fabrics presented a strain-hardening behavior, which seems to corroborate that the bond of the MCF yarns towards the cementitious matrix achieved an adequate level, even though lower than the bond of the EP yarn, as demonstrated in Chapter 3.

The TRC with the GP-MCF fabric presented a slightly lower performance than the TRC with the C-MCF fabric, showing a difference of approximately 20% in the tensile strength and 13% in the ultimate strain. This difference can be traced back to the difference in the chemical bond between the GP-MCF and the C-MCF yarns toward the fine-grained concrete matrix, discussed in Chapter 3. What is interesting to observe is that even with a weaker bond, the composites with the GP-MCF fabrics were still able to present strain-hardening behavior. However, due to the poorer interface between the GP-MCF fabric and the fine-grained concrete matrix, the cracks that are formed in the composite are wider and less spaced between them, which is corroborated by the DIC analysis (see discussion below), characterized by sharper drops in the tensile stress *vs.* strain curves in Stage II. As mentioned before, the bond significantly influences the stress transfer mechanisms,

which is related to the crack bridging effect efficiency of the textile reinforcement [85].

The TRC with the EP carbon fabric presented the highest mechanical performance, reaching a tensile strength of 36.3 MPa, which is approximately 216% and 267% higher than the ones yielded by the TRC with C-MCF and GP-MCF fabrics, respectively. This enhanced behavior can be attributed to the elevated bond between the EP carbon fabric and the fine-grained concrete matrix, as demonstrated in Chapter 3. Additionally, the superior mechanical properties, i.e., the tensile strength and modulus of elasticity, of the EP carbon fabric can also contribute to the enhanced mechanical performance of the composite, mainly in the Stage III. As discussed in section 3.1, the C-MCF and GP-MCF fabrics presented a tensile strength of 1367 MPa and 1591 MPa, respectively, while the EP carbon fabric presents a tensile strength of 2500 MPa, according to the supplier. The TRC is a composite material, and its mechanical properties are guided by the rule of mixtures, which states that the properties of both matrix and reinforcement proportionally to their volume fractions are responsible for the overall composite properties. However, this rule is only valid for the pre-cracked zone (Stage I) of the TRC, in which both components present an elastic-linear behavior. It is important to emphasize that the rule of mixtures considers a perfect bond between matrix and reinforcement and, therefore, should be considered as an upper limit of the mechanical properties of the composite since, in practice, this is not valid. In the post-cracked zone, i.e., Stage III of the tensile stress vs. strain curves, the contribution of the matrix can be neglected. Thus, the mechanical properties of the TRC are only dependent on the mechanical parameters of the textile reinforcement [15].

Although the excellent mechanical behavior observed for the TRC with the EP carbon fabric, the composites presented a significant concrete spalling, as can be seen in Figure 4.15. The EP carbon yarns present a higher bond towards fine-grained concrete matrices than the MCF yarns, as demonstrated in Chapter 3. However, different from the MCF yarns, the main bond mechanism is a mechanical interlock one. According to Dvorkin and Peled [23], the lack of or a low chemical bond can lead to delamination between the fabric and matrix layers. This delamination associated with an elevated strength yielded by the specimen may have resulted in the observed spalling [22,86,87]. Longitudinal cracks can also be

observed in the specimen prior to the rupture, as seen in Figure 4.15. According to Jerabek et al. [88], those cracks contribute to the spalling occurrence. Preinstorfer and Kollegger [89] stated that such cracks are more common to occur in TRC with fabrics impregnated with a high-modulus material, such as stiff epoxy resins. Additionally, the spalling phenomenon can be related to the thickness of the concrete cover; higher thickness leads to higher spalling resistance [90,91]. The thickness of the concrete cover is also related to presence of longitudinal cracks [89]. The specimens with the EP carbon fabric present lower thickness than the specimens with the C- and GP-MCF fabrics, as can be seen in Table 4.6. As previously mentioned, since this spalling was at some level expected, DIC analysis were not carried out on these specimens, as there was the risk of damaging the equipment with the concrete fragments.



Figure 4.15 – TRC with the EP fabric after the direct tensile test.

A DIC analysis was performed to evaluate the crack pattern of the TRC during the direct tensile tests. Figure 4.16 presents the crack pattern of the TRC with the C-MCF, GP-MCF and EP carbon fabrics just before failure, i.e., at the ultimate load. Table 4.9 presents the number of cracks (# cracks), the mean crack opening $w_{m,max}$, and the mean crack spacing $s_{m,max}$ obtained from the cracking analysis of the TRC specimens at the maximum load in the direct tensile tests. The results of the TRC with C-MCF and GP-MCF fabrics were obtained through the DIC analysis. As mentioned before, the DIC analysis was not performed on the TRC with the EP carbon fabric due to the expected concrete spalling of these specimens. Thus, pictures were taken during the test at a safe distance, and visual analysis was performed to obtain the number of cracks at the ultimate load. To measure the mean

crack spacing the ImageJ software was used. It was not possible to obtain the mean crack opening for the TRC with EP carbon fabrics specimens due to the low quality of the pictures taken at a safe distance. Figure 4.17 presents the crack pattern of the TRC with the C-MCF and GP-MCF fabrics at the end of the Stage II (strain of 0.2%), at approximately the middle of the strain capacity (strain of 0.5%), and in an advanced stage of the Stage III (strain of 0.7%).

Table 4.9 – Average results and standard deviation obtained from the cracking analysis of the TRC specimens at the ultimate load in the direct tensile tests.

TRC	# cracks	$w_{m,max}$ (μm)	$s_{m,max}$ (mm)
C-MCF	13.6 ^a (2.24)	30.9 ^a (6.88)	16.7 ^a (2.98)
GP-MCF	8.8 ^a (0.829)	81.5 ^a (37.4)	26.3 ^a (2.18)
EP	11.8 ^b (0.433)	- ^c	21,0 ^d (1,46)

^a Data obtained from the DIC analysis.

^b Data obtained from visual analysis.

^c Data not possible to be measured due to the low quality of images.

^d Data obtained from analysis through ImageJ.

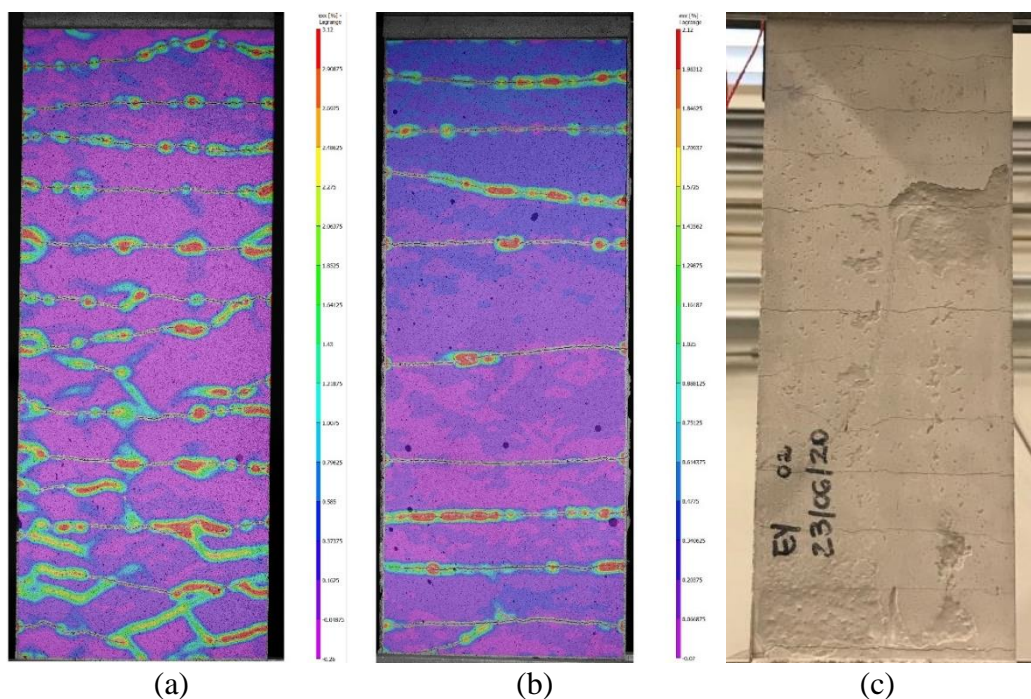


Figure 4.16 – Crack pattern just before failure for the TRC with (a) C-MCF, (b) GP-MCF, and (c) EP fabrics.

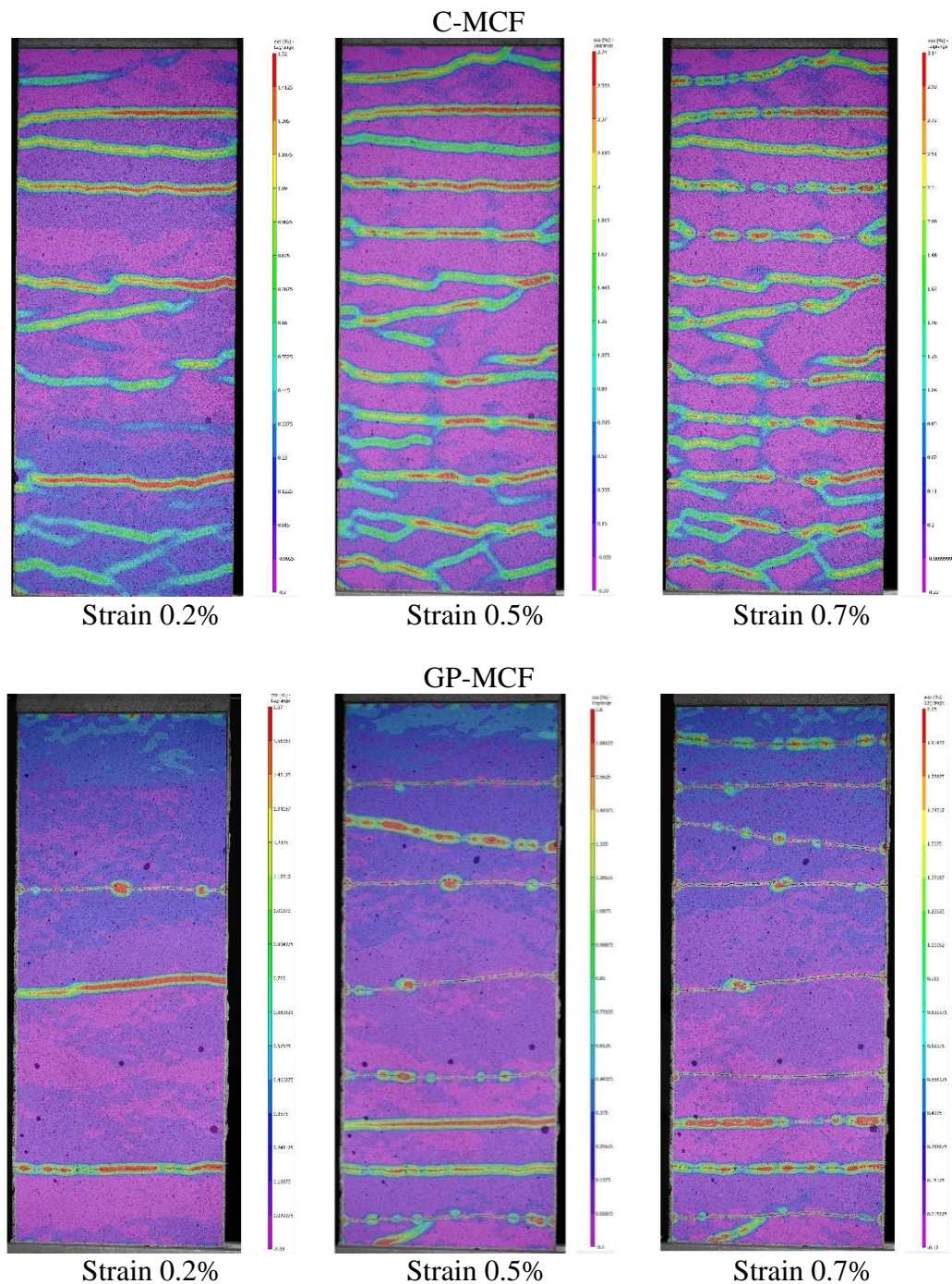


Figure 4.17 – Crack pattern of the TRC with the C-MCF and GP-MCF fabric at the strain of 0.2% and 0.7%.

All composites presented a multiple-cracking pattern. Although the TRC with the EP carbon fabric showed the best mechanical tensile performance, it was the TRC with the C-MCF fabric that presented the highest number of cracks and the smallest spacing between them (see Table 4.9), which corroborates the assumption previously mentioned regarding the mechanism involved in the bond between the

EP carbon fabric and the fine-grained concrete matrix. The TRC with the GP-MCF fabric was the composite with the lower number of cracks and the highest crack width and spacing. Once more, this is related to the bond between the textile reinforcement and the cementitious matrix. As discussed in Chapter 3, there is a chemical incompatibility between the geopolymer of the mineral suspension and the cementitious matrix, which impairs the bond between the textile reinforcement and the matrix. As discussed, the bond is a crucial factor in the stress transfer mechanism and the crack control of the TRC.

4.3.3.1. Effect of temperature on the residual capacity

To obtain the residual mechanical behavior of the TRC with C-MCF, GP-MCF, and EP carbon fabrics, the specimens were submitted to direct tensile tests after being exposed to different temperature levels and cooled down to room temperature, as described in Section 2.2.

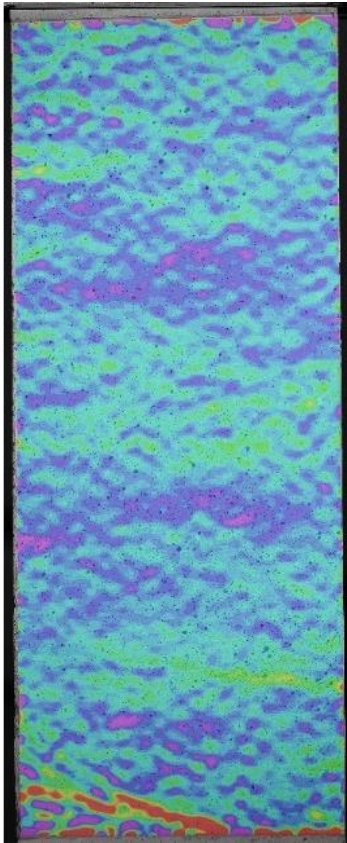
After the specimens were removed from the furnace, some cracks were observed in the composites with the MCF fabrics at all evaluated temperatures. Figure 4.18 and Figure 4.19 presents the thermal crack pattern observed in the TRC specimens with the C-MCF and GP-MCF fabrics, respectively, post-heating regime. Table 4.10 presents the average results for the number and the mean crack opening $w_{m,max}$ of the thermal cracking.

Table 4.10 – Average results and standard deviation obtained from the cracking analysis of the TRC specimens post-heating regime and post-testing at the ultimate load in the direct tensile tests.

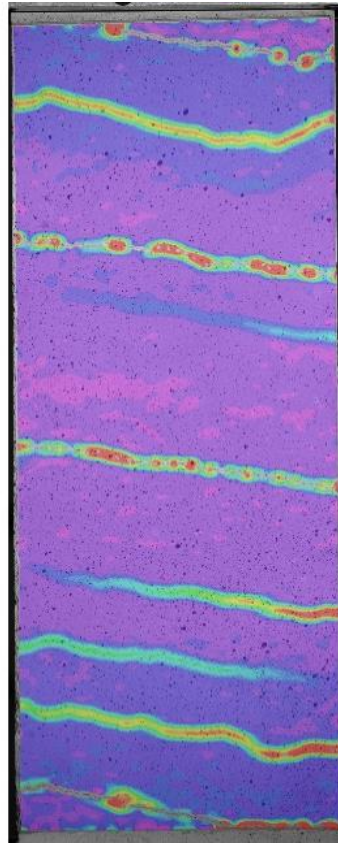
TRC	Post-heating		Post-testing		
	# cracks	$w_{m,max}$ (μm)	# cracks	$w_{m,max}$ (μm)	$s_{m,max}$ (mm)
150 °C					
C-MCF	1.80 ^a (0.748)	0.184 ^a (0.0797)	12.6 ^a (1.36)	48.3 ^a (6.97)	19.1 ^a (1.98)
GP-MCF	1.00 ^a (0.632)	3.04 ^a (1.01)	2.25 ^a (0.433)	599 ^a (167)	116 ^a (15.9)
EP	-	-	11.8 ^b (0.829)	- ^c	21.1 ^d (0.712)
200 °C					
C-MCF	0.750 ^a (0.829)	0.192 ^a (0.0700)	13.0 ^a (0.707)	44.4 ^a (14.0)	18.1 ^a (2.05)
GP-MCF	1.40 ^a (0.490)	3.53 ^a (0.860)	2.67 ^a (1.25)	250 ^a (31)	90 ^a (25.1)
EP	-	-	10.8 ^b (1.17)	- ^c	22.8 ^d (3.31)
300 °C					
C-MCF	7.50 ^a (1.12)	0.577 ^a (0.0690)	11.8 ^a (0.829)	82.8 ^a (11.2)	19.5 ^a (1.51)
GP-MCF	2.80 ^a (0.980)	3.40 ^a (1.75)	3.00 ^a (1.10)	278 ^a (117)	76.4 ^a (13.6)
EP	-	-	- ^e	- ^c	- ^e

^a Data obtained from the DIC analysis
^b Data obtained from visual analysis
^c Data not possible to be measured due to the low quality of images
^d Data obtained from analysis through ImageJ
^e Not enough data for the analysis

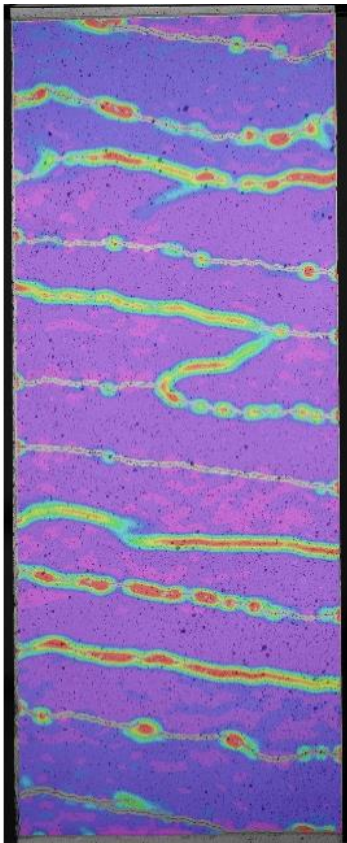
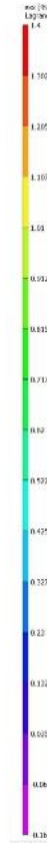
C-MCF
150 °C



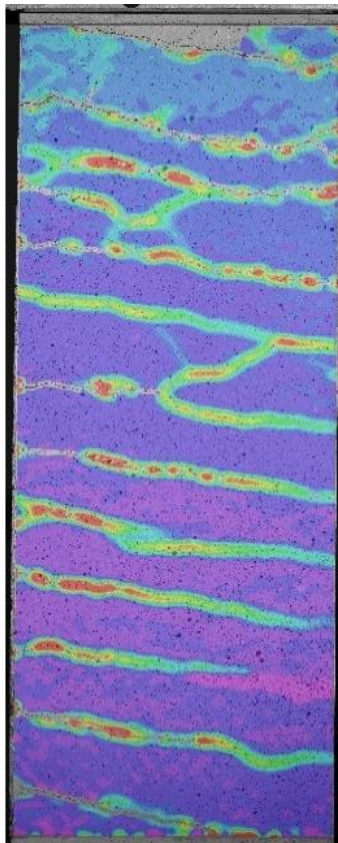
Post-heating



Strain 0.2%



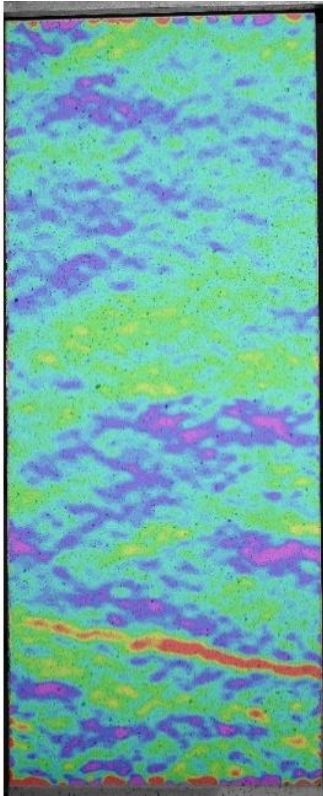
Strain 0.5%



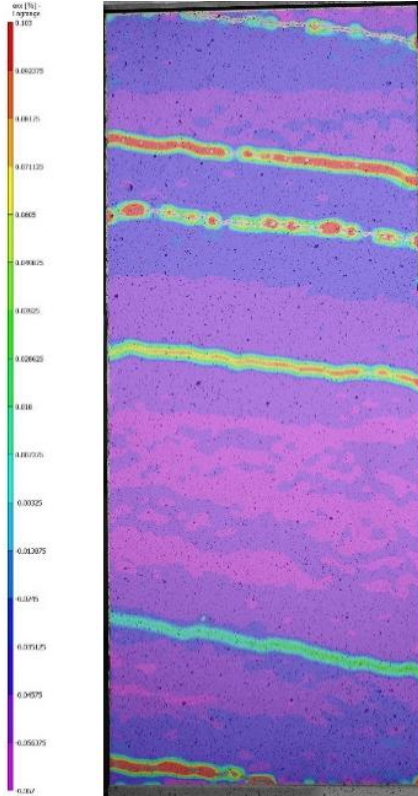
ϵ_{rup}



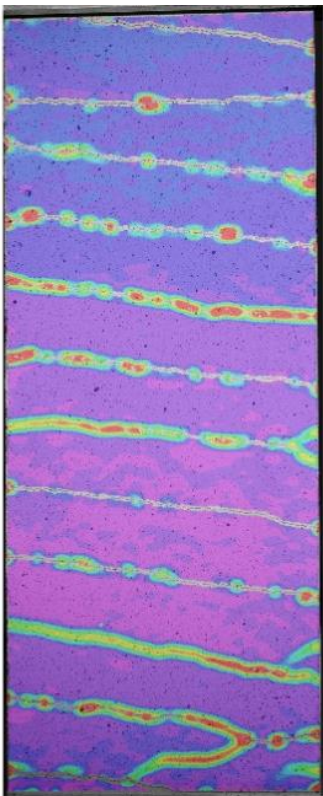
200 °C



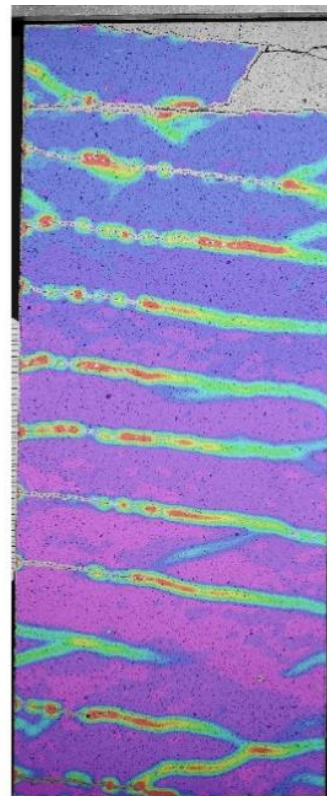
Post-heating



Strain 0.2%



Strain 0.5%



ϵ_{rup}

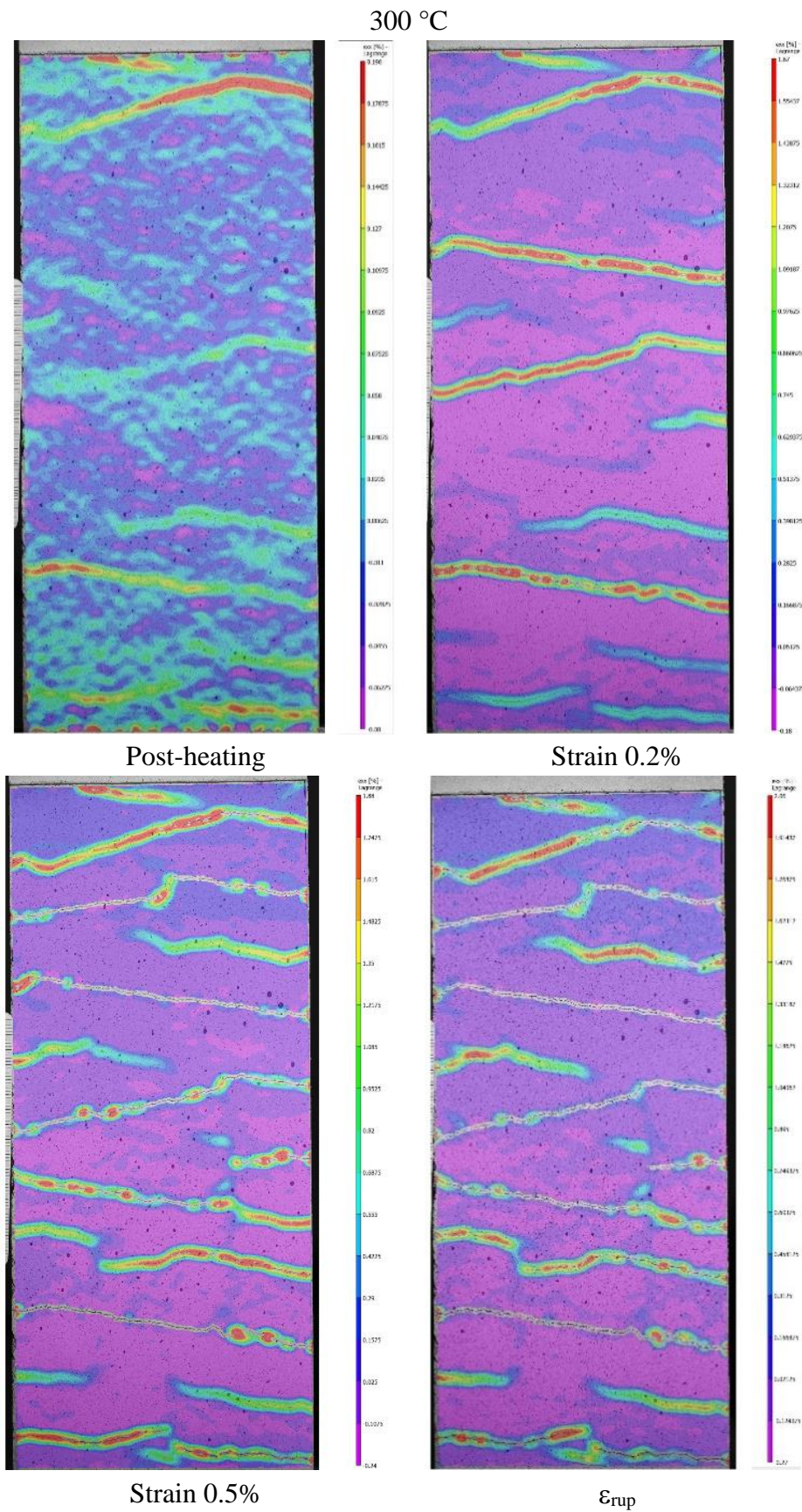
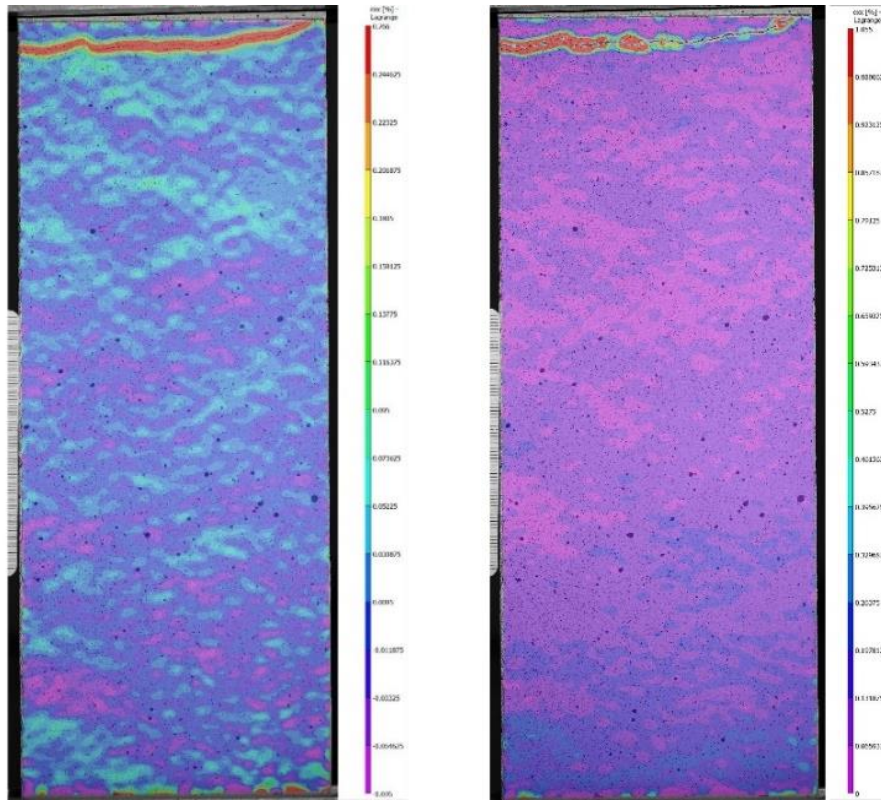


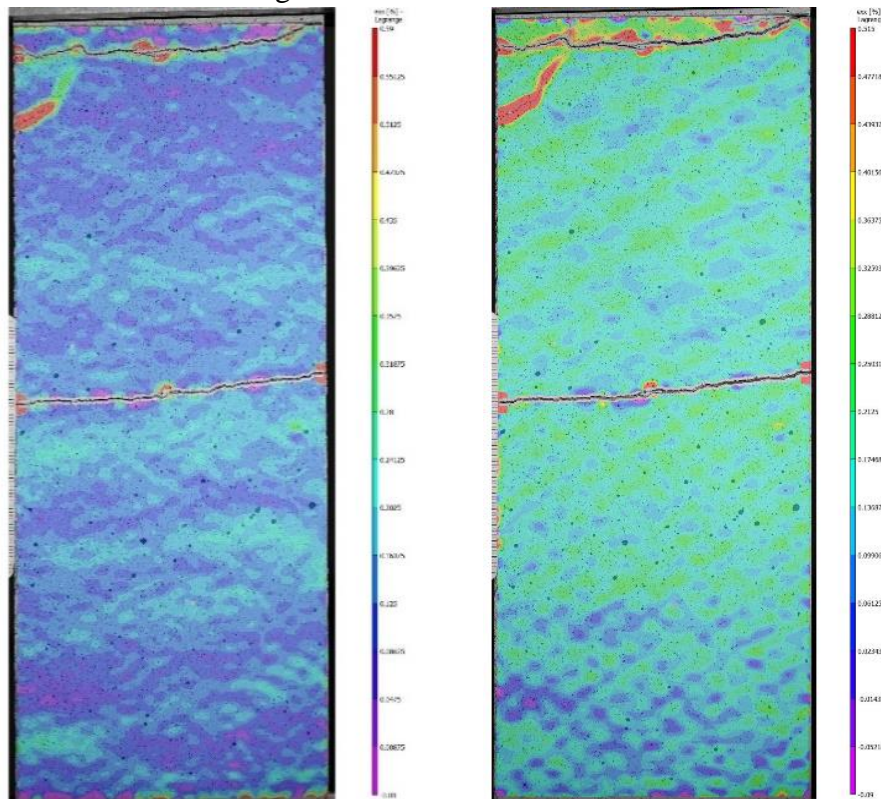
Figure 4.18 – Crack pattern observed in the TRC specimens with the C-MCF fabrics immediately post-heating regime and at various strain levels.

GP-MCF
150 °C



Post-heating

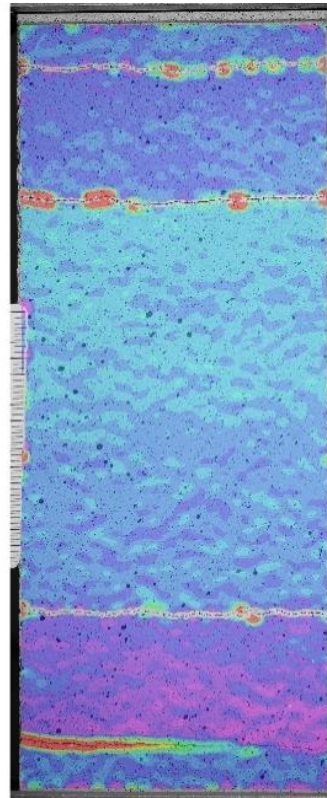
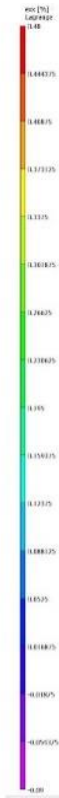
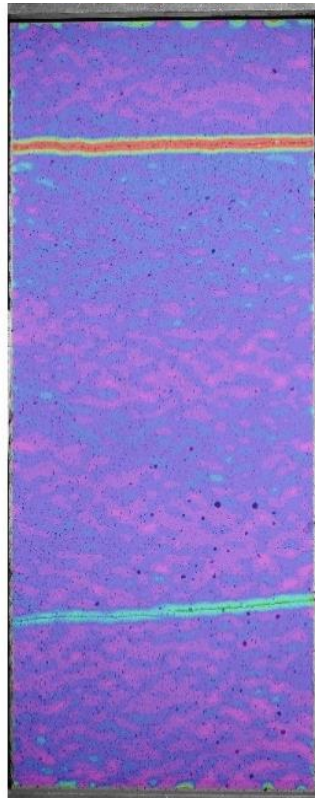
Strain 0.2%



Strain 0.5%

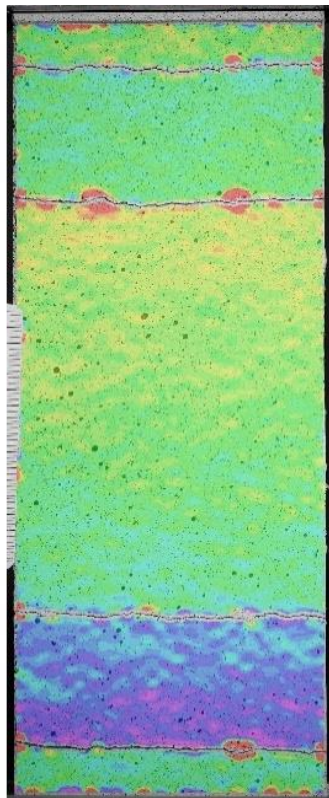
ϵ_{rup}

200 °C

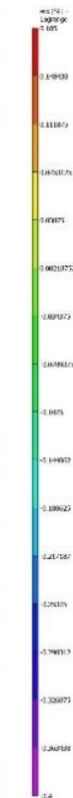
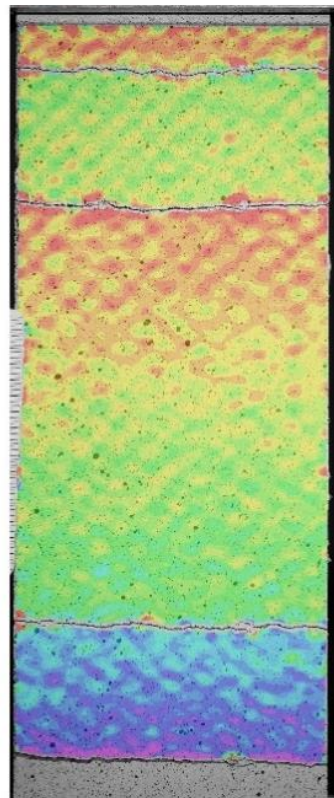


Post-heating

Strain 0.2%



Strain 0.5%



ϵ_{rup}

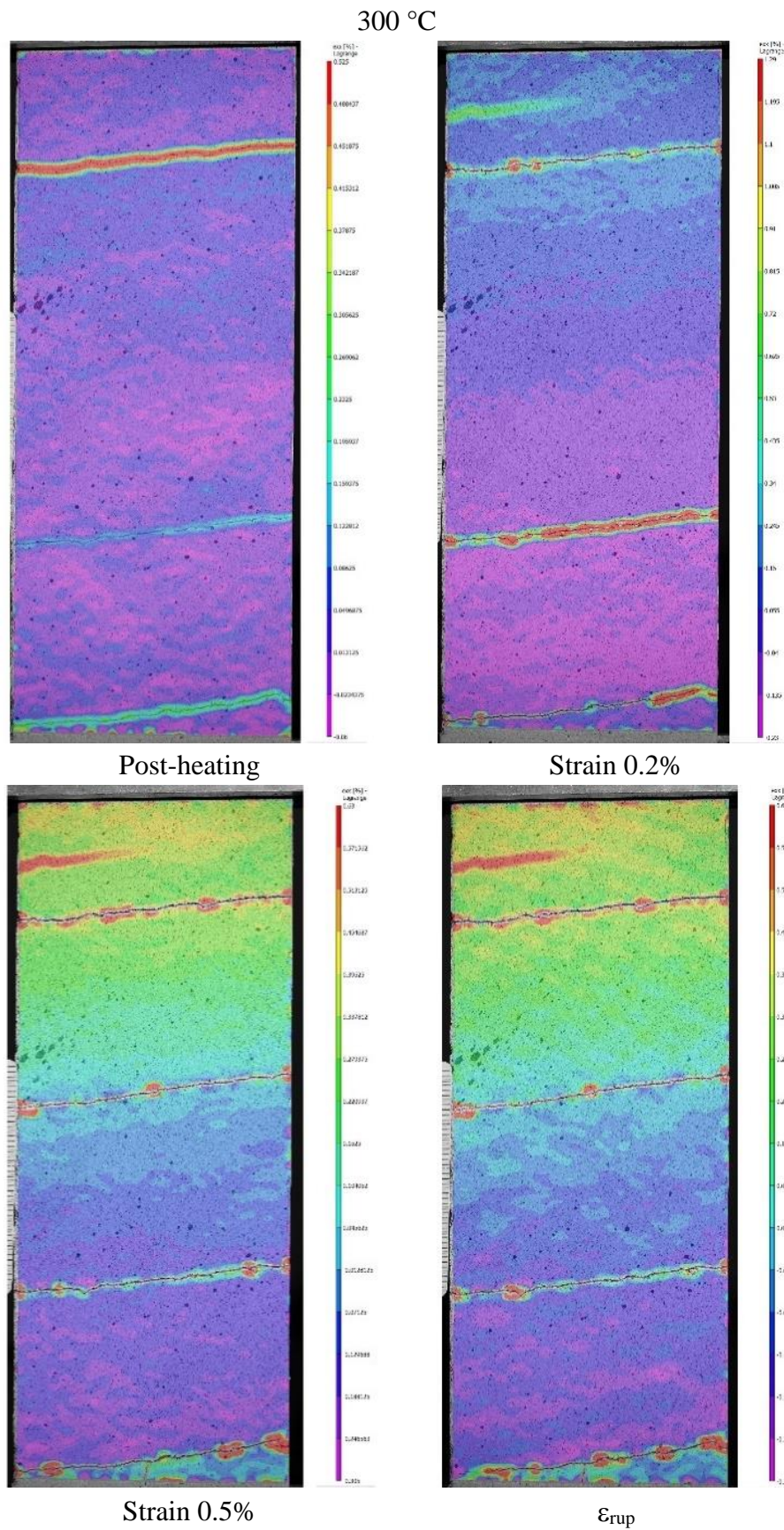


Figure 4.19 – Crack pattern observed in the TRC specimens with the C-MCF fabrics immediately post-heating regime and at various strain levels.

Figure 4.20, Figure 4.21, and Figure 4.22 show the residual tensile stress vs. strain curves of the TRC with C-MCF, GP-MCF, and EP fabrics, respectively, obtained from the direct tensile tests after exposure to elevated temperatures for all specimens and the representative ones. Table 4.11 presents the average tensile strength σ_t , rupture strain ε_{rup} , tensile strength at the first matrix crack σ_{BOP} , strain at the first matrix crack ε_{BOP} , and the modulus of elasticity in the Stage I E_I obtained for the TRC composites. The tensile stresses f_t were derived from the effective cross-sectional area of the composite through Equation 4.2. A Temperature Modification Factor k_d was also obtained to easily compare the average values of σ_t , σ_{BOP} , and E_I at elevated temperatures with the respective average values obtained at room temperature. Figure 4.18 presents the crack pattern of the TRC with the C-MCF and GP-MCF fabrics at the end of the Stage II (strain of 0.2%), at approximately the middle of the strain capacity at room temperature (strain of 0.5%), and at the ultimate load. Table 4.10 presents the number of cracks, the mean crack opening $w_{m,max}$, and the mean crack spacing $s_{m,max}$ obtained from the cracking analysis of the TRC specimens at the maximum load in the direct tensile tests after exposure to thermal regimes.

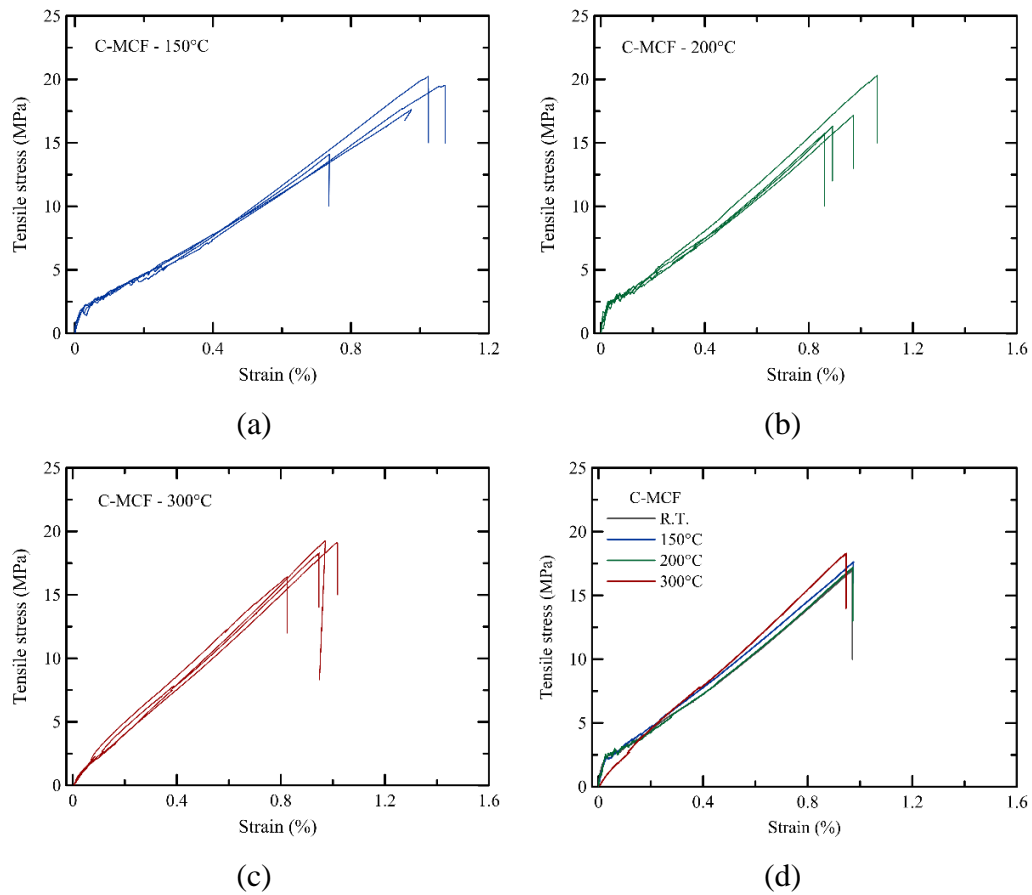


Figure 4.20 – Residual tensile stress vs. strain curves obtained from the direct tension tests after the thermal regime up to (a) 150 °C, (b) 200 °C, and 300 °C for the TRC with the C-MCF fabric specimens. (d) Representative residual tensile stress vs. strain curves.

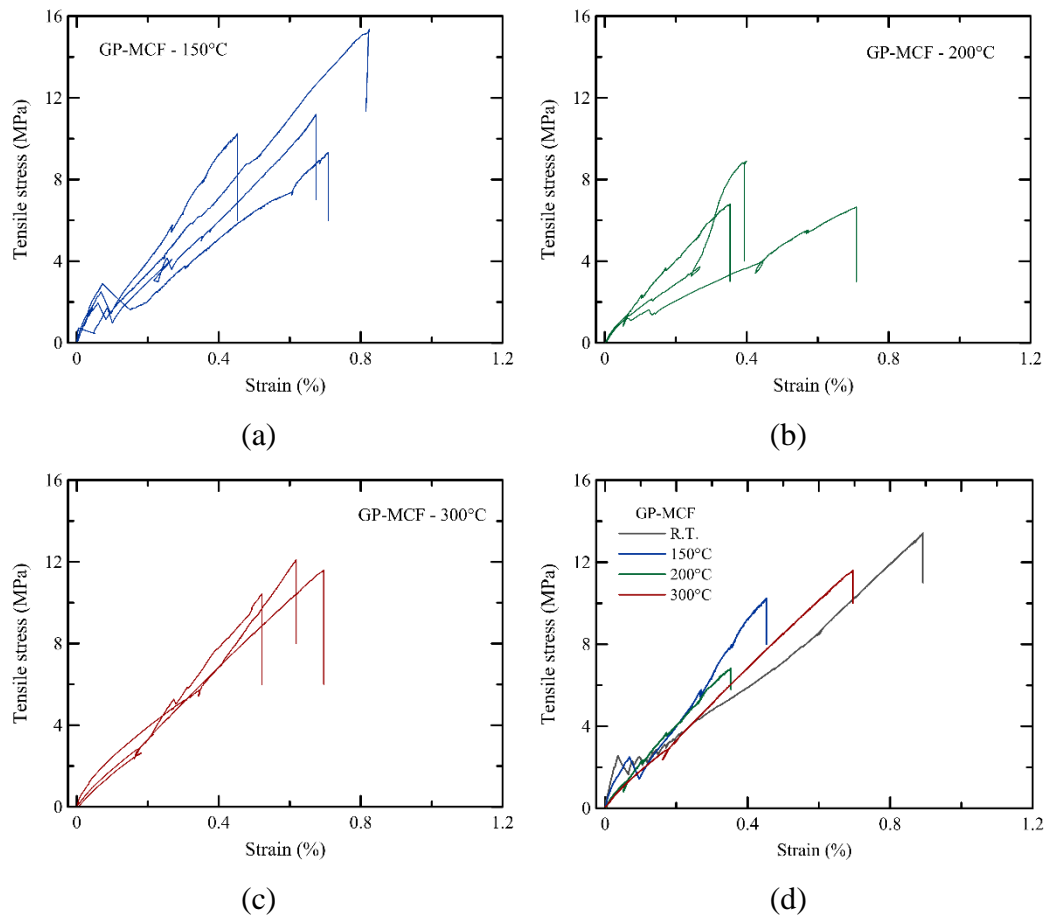


Figure 4.21 – Residual tensile stress vs. strain curves obtained from the direct tension tests after the thermal regime up to (a) 150 °C, (b) 200 °C, and 300 °C for the TRC with the GP-MCF fabric specimens. (d) Representative residual tensile stress vs. strain curves.

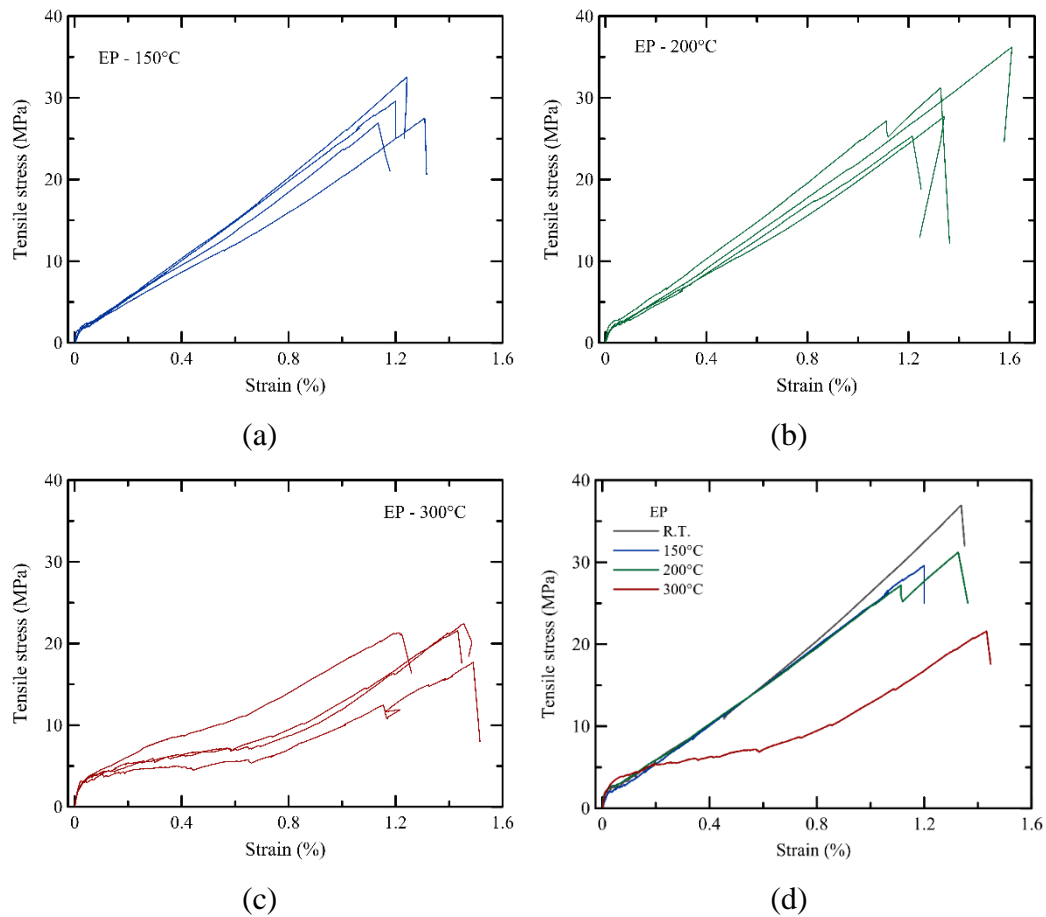


Figure 4.22 – Residual tensile stress vs. strain curves obtained from the direct tension tests after the thermal regime up to (a) 150 °C, (b) 200 °C, and 300 °C for the TRC with the EP carbon fabric specimens. (d) Representative residual tensile stress vs. strain curves.

Table 4.11 – Average results and standard deviation from the direct tensile tests on TRC after exposure to elevated temperatures

TRC	σ_t (MPa)	$k_d \sigma_t$	ε_{rup} (%)	σ_{BOP} (MPa)	$k_d \sigma_{BOP}$	ε_{BOP} (%)	E_t (GPa)	$k_d E_t$
150 °C								
C-MCF	17.9 (2.37)	1.06 -	0.952 (0.129)	1.93 (0.165)	0.716 -	0.0240 (0.00615)	8.24 (0.83)	0.961 -
GP-MCF	11.5 (2.31)	0.849 -	0.665 (0.135)	2.00 (0.80)	0.789 -	0.0506 (0.0271)	3.28 (1.35)	0.424 -
EP	29.1 (2.20)	0.803 -	1.22 (0.0626)	1.62 (0.318)	0.771 -	0.0210 (0.00904)	11.0 (3.59)	0.840 -
200 °C								
C-MCF	17.4 (1.75)	1.03 -	0.947 (0.0782)	1.95 (0.461)	0.725 -	0.0183 (0.00894)	13.5 (5.12)	1.57 -
GP-MCF	7.05 (1.03)	0.549 -	0.487 (0.158)	- -	- -	- -	- -	- -
EP	30.1 (4.09)	0.830 -	1.37 (0.145)	2.04 (0.299)	0.972 -	0.0314 (0.00870)	9.46 (2.61)	0.722 -
300 °C								
C-MCF	18.3 (1.13)	1.09 -	0.939 (0.0708)	- -	- -	- -	- -	- -
GP-MCF	11.4 (0.694)	0.838 -	0.612 (0.0713)	- -	- -	- -	- -	- -
EP	20.7 (1.81)	0.520 -	1.40 (0.110)	2.47 (0.568)	1.18 -	0.0195 (0.00587)	16.8 (0.841)	1.28 -

- C-MCF

The exposure to temperatures of 150 °C, 200 °C, and 300 °C did not significantly affect the mechanical performance of the TRC with the C-MCF fabric, as can be seen in Figure 4.20. These composites were able to maintain approximately the same level of tensile strength at all temperature levels evaluated. However, it is interesting to observe that the residual tensile stress *vs.* strain curve of the specimens heated up to 300 °C does not show the typical three stages of the strain-hardening behavior. This can be attributed to the extensive cracking that occurred during the heating regime. The TRC with the C-MCF presented an average of approximately 7.5 cracks with a thickness of 0.577 μm (see Table 4.10). Thus, when the composite was subjected to the tensile loading, not many new cracks were formed. After the tests, the TRC with the C-MCF fabric presented an average of 11.8 cracks with a thickness of 82.8 μm . In the residual tensile stress *vs.* strain curve, it is not possible to identify either Stage I or Stage II, with Stage III, in which there

is the stretching of the textile reinforcement, being the most predominant. Although difficult to be identified on the curve, Stage II somehow occurred, as the number of cracks increased from 7.5 to 11.8, on average, which means that during the loading, 4.3 new cracks opened. Nevertheless, it is valid to emphasize that, as mentioned before, the ultimate capacity of the composite was not decreased due to this thermal cracking. Additionally, even after being submitted to the tested thermal regimes the TRC with C-MCF fabric presented a dense crack pattern, with no major variation in the number of cracks formed. Figure 4.23 shows the multiple-cracking pattern of the composites after the direct tension tests after exposure to different temperatures.

The cement-based suspension used as an impregnation material is basically a cement paste with a silica addition. Previous studies [92,93] show that cement pastes expand when submitted to temperatures up to approximately 150 - 200 °C. The subsequent heating leads to the shrinkage of the cement paste. Conversely, mortar and concretes only expand when exposed to elevated temperatures, as their thermal stability is governed by the expansion of the mineral aggregates [92]. This difference in the thermal behavior of the impregnation material and the fine-grained concrete matrix of the TRC could explain the significative thermal cracking of the TRC with C-MCF exposed to the thermal regime up to 300 °C. While the matrix tends to expand, simultaneously, the mineral impregnation of the textile reinforcement suffers a retraction, which could lead to the appearance of internal tensile stress that eventually can lead to microcracking formation [94]. However, as stated in Chapter 3, after being heated up to 300 °C, the C-MCF yarns presented an increase in their diameter, which does not agree with the theory previously assumed. Then, one could think that if both materials expand with increasing temperature, the coefficients of thermal expansion of the textile reinforcement and the fine-grained concrete can be considerably different. This incompatibility can also lead to development of internal tensile stress and possible microcracking [94,95]. More studies should be performed in order to fully understand the thermal behavior of the TRC with C-MCF fabric.

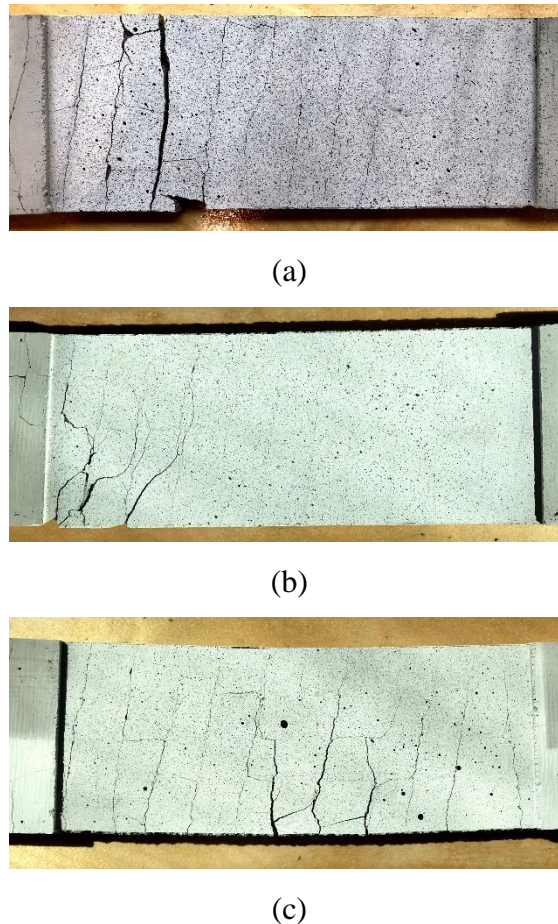


Figure 4.23 – TRC with C-MCF fabrics after the direct tensile tests after temperature exposure of a) 150 °C, b) 200 °C, and c) 300 °C.

- GP-MCF

As can be seen in Figure 4.21, the heating regime considerably affected the residual mechanical behavior of the TRC with the GP-MCF fabric. For temperatures up to 200 °C, the increase in the temperature exposure led to a decrease in the residual tensile strength. This decrease was approximately 16% and 48% to 150 °C and 200 °C, respectively. However, for the composites submitted to 300°C, the decrease in the residual tensile strength was about 16%, i.e., the same level observed for the composite exposed to 150 °C. The enhancement of the target temperature also affected the strain capacity of the composites with the GP-MCF fabric. A reduction of approximately 20%, 42%, and 27% were observed for the heating regimes up to 150 °C, 200 °C, and 300 °C, respectively. The thermal regime also considerably reduced the number of cracks formed during the tests. At room

temperature, the TRC with GP-MCF fabric presented an average of 8.8 cracks, and at 150 °C, 200 °C, and 300 °C this number was reduced to approximately 3 cracks.

Similar to what was observed in the composites with C-MCF, the heating regime also changed the shape of the tensile stress *vs.* strain curve of the TRC with the GP-MCF fabrics, which no longer presented the three typical stages of the strain-hardening behavior. This difference could be observed in lower temperature levels for the GP-MCF composites. Already after the exposure to 200 °C, it is not possible to distinguish the three stages, and the same occurs at 300 °C. Once more, the thermal cracking observed immediately after the heating regime was quite expressive. However, unlike the C-MCF composites, the number of cracks in the TRC with the GP-MCF fabric was smaller but with a significantly larger width, 3.53 μm and 3.40 μm at 200 °C and 300 °C, respectively (see Table 4.10). Probably this significant crack opening during the heating regime affected the multiple-cracking characteristic of the TRC, and only a few cracks formed during Stage II. When these specimens were tested in tension, Stage III was the most predominant, and the tensile loading led directly to the stretching of the textile reinforcement. Although not many new cracks were formed, approximately only one crack opened during the test for both thermal regimes, the existing cracks were considerably widened, with their width increasing from around 3.5 μm to 250 μm and 278 μm after exposure to 200 °C and 300 °C, respectively. Figure 4.24 shows the cracking pattern of the composites after the direct tension tests after exposure to different temperatures.

The expressive thermal cracking, mainly regarding the cracks' width, presented by the TRC with the GP-MCF fabric could be related to a thermal incompatibility between the two materials. The fine-grained concrete matrix and the mineral impregnation geopolymer present considerably different coefficients of thermal expansion. Trindade et al. [96] performed dilatometer tests on a potassium (K)-based geopolymer and observed a significative dimensional instability in the temperature range between 150 °C and 300 °C, with the specimens presenting a shrinkage behavior. For this temperature level, the coefficient of thermal expansion can be estimated at approximately $-4.5 \times 10^{-4} / ^\circ\text{C}$, where the negative sign indicates a shrinkage of the material with the temperature increase. As discussed in Chapter 3, a shrinkage behavior of GP-MCF yarns after being submitted to heating at 150 °C, 200 °C, and 300 °C was observed. On the other hand, when submitted to

temperatures of up to 500 °C, mortars made of Portland cement and quartz sand expand [92] with a coefficient of thermal expansion of approximately $0,1 \times 10^{-4} / ^\circ\text{C}$ [92,97,98]. Thus, for all temperature targets evaluated in this work, while the fine-grained concrete matrix exhibits expansion, the impregnation material in the textile reinforcement undergoes a shrinkage process. Additionally, considering the values of the coefficients of thermal expansion of both materials, the contraction experienced by the geopolymer is considerably higher than the expansion of the concrete. This could lead to considerable internal tensile stress and consequent cracking of the composite. More studies must be performed to better understand the thermal behavior of the specific geopolymer and fine-grained concrete used.

Another point that is worth mentioning is the reduction in the slope of the linear-elastic section (Stage I) of the TRC with the GP-MCF fabric heated to 150 °C compared to the results obtained at room temperature. The modulus of elasticity at the Stage I presented a decrease of approximately 58% after the heating regime up to 150 °C. As mentioned before, at the Stage I, the stiffness of the composite is mainly governed by the modulus of elasticity of the matrix. It is possible that the thermal cracking may have reduced the stiffness of the matrix, leading, consequently, to a decrease in the residual stiffness of the composite. For this range of temperature, this reduction in the Stage I modulus of elasticity was not observed for the composites with C-MCF fabric. Since after exposure to 150 °C, the number of thermal cracks for the composites with C-MCF fabric was higher than for the TRC with GP-MCF fabric, the decrease in the matrix stiffness is probably related to the width of the thermal cracks. The composites with GP-MCF fabric presented a mean width of 3.04 μm , while this value was 0.838 μm for the composites with C-MCF fabric, see Table 4.10.

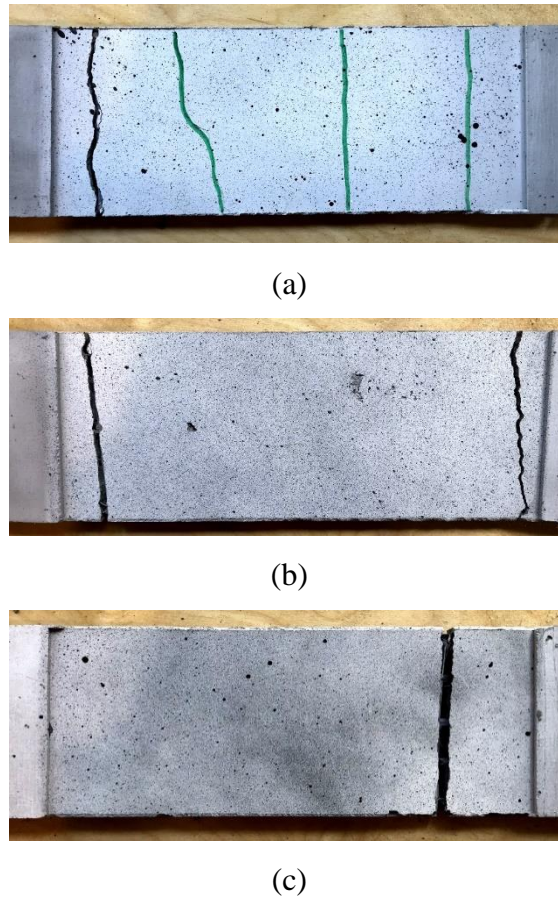


Figure 4.24 – TRC with GP-MCF fabrics after the direct tensile tests after temperature exposure of a) 150 °C, b) 200 °C, and c) 300 °C.

- EP carbon fabric

The exposure to temperatures up to 200 °C did not cause significant changes in the residual mechanical behavior of the TRC with EP carbon fabric. Compared to room temperature, a reduction of approximately 20% in the tensile strength can be observed. However, it is interesting to mention that, for this temperature level, the in-situ bond performance of EP carbon yarns towards a fine-grained concrete matrix was already drastically compromised, as demonstrated in Chapter 3. The difference in the in-situ and residual behavior, even considering that one analysis is at the bond level while the other is at the composite level, can be related to the epoxy resin re-hardening after the cooling since temperatures up to this range are not enough to cause its complete degradation [39,40]. Additionally, in the in-situ bond evaluation, part of the EP carbon yarn was completely exposed to the heating, without any concrete cover, due to the test setup configuration (see Chapter 3)[41].

This could have accelerated the coating material degradation and, consequently, the performance of the composite.

The subsequent heating to 300 °C led to significant degradation of the residual mechanical behavior of the TRC with the EP carbon fabric, as can be seen in Figure 4.22. At this temperature level, the tensile strength presented a decrease of about 43%. Furthermore, it is possible to observe a significant reduction in the composite stiffness, characterized by the slope of the tensile stress *vs.* strain curve, in the Stage III. This could be related to the complete degradation of the polymeric coating, which in turn could have led to a decrease in the textile reinforcement performance and also in the bond of the textile towards the fine-grained concrete matrix. Figure 4.25.c shows the specimen of the TRC with EP carbon fabric submitted to 300 °C after the direct tensile test, and it is possible to observe that there is no longer any evidence of the polymeric coating on the fabric yarns. In fact, not even the transversal yarns can be seen anymore, which may have further contributed to the degradation of the residual mechanical performance of these specimens. However, it is interesting to observe that, for all temperature levels evaluated, the TRC with the EP carbon fabric presented spalling (see Figure 4.25), even after the thermal regime up to 300 °C that considerably affected the mechanical response of the composite.

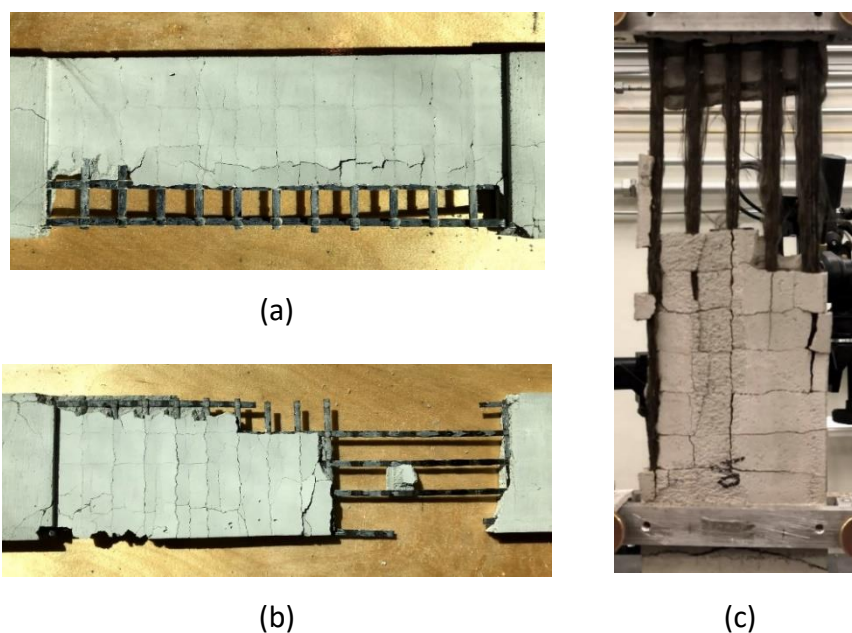


Figure 4.25 – TRC with EP carbon fabrics after the direct tensile tests after temperature exposure of a) 150 °C, b) 200 °C, and c) 300 °C.

4.3.4. Morphological characterization of the TRC

Figure 4.26 presents the failure process of the TRC composites and interfacial characteristics between the reinforcement and concrete by μ CT images. According to the density of each component, different grey variations are detected. The light grey corresponds to a dense concrete microstructure or impregnation matrix, while black areas represent air by, e.g., cracks or voids. Dark grey represents plain filaments due to their low densities. Very bright irregular areas represent the metal wires used for the assemblage between the longitudinal and transversal yarns (see Figure 4.26.b and c). Note, due to strong delamination during specimen preparation, the results of the EP-yarn at 20 °C were unreliable and cannot be shown here.

At room temperature, the C-MCF and GP-MCF yarns were well attached to the matrix without apparent cracks (Figure 4.26. b and c, 20 °C), confirming good embedment within the surrounding concrete. The well-embedded yarns are favorable to form a physical interlocking due to the transverse pressure of the matrix and the chemical bond towards cementitious matrices. Considering the loading areas, i.e., the gage length region, the matrix crack was created in the weak region of the concrete matrix and propagated orthogonally to the longitudinal yarn or along the boundary area of the transversal yarn; see Figure 4.26. b and d. Therefore, the feature of the textile structure, e.g., the distance between the transversal yarns and their geometry, plays an important role in the localization of the stress and, consequently, the crack formation, influencing the Stage II of the stress-strain curve development. However, the textile structure is not enough to describe the multiple-cracking behavior of the TRC composite, since all carbon fabrics used in this work have the same geometry and mesh size, and even so, the composites presented different cracking patterns. As already discussed, the bond between the textile reinforcement and the cementitious matrix also influences the mechanical and cracking behavior.

After the exposure to 300 °C and cooling, the EP and C-MCF yarns could still be well attached to the concrete matrix before testing, despite minor cracks in the boundary area of the transversal yarn and the concrete matrix; see Figure 4.26.a and b. However, some disappearance of the grey zone between the longitudinal GP-MCF yarns and the concrete matrix can be seen, which indicates that partially distributed cracks were formed in the interfacial area (Figure 4.26.c). This fact can

be traced back to the lower compatibility of the geopolymer with cementitious materials, which could eventually induce premature failure by yarn slippage.

Compared to the room temperature, the exposure to elevated temperatures led to the formation of more connected pores through the cracks within the concrete matrix. After loading, a noticeable interfacial cracking was also seen at various locations for the EP specimens heated up to 300 °C (Figure 4.26.a). This was attributed to the thermal degradation of the epoxy resin and the delamination failure arising from the poor chemical compatibility with the cementitious materials. These microscale observations can be well related to the different thermal shrinkage in the polymer- and mineral-impregnations and the fine-grained concrete matrix, explaining the reduced load-bearing capacity and failure behavior of TRC composites at elevated temperatures.

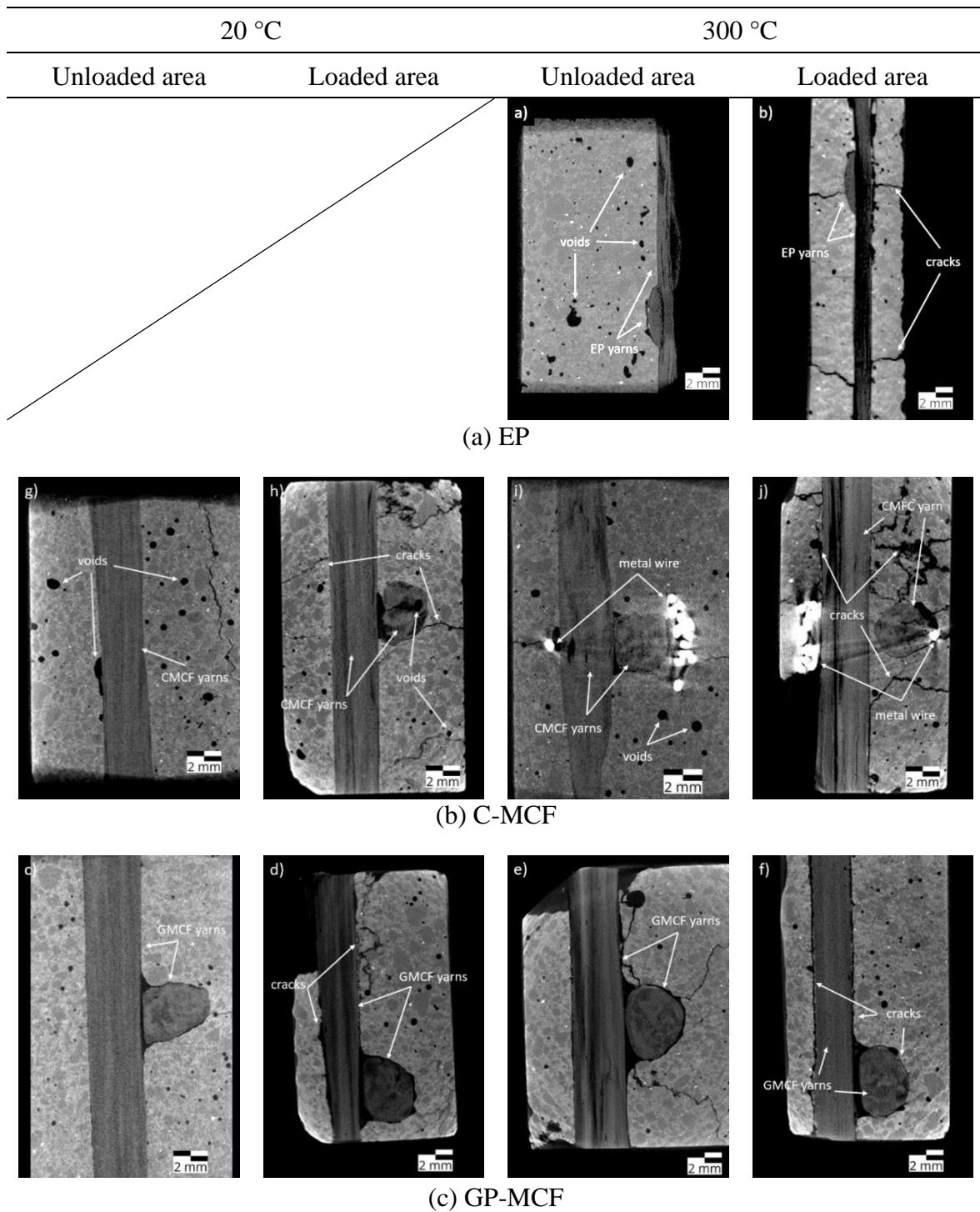


Figure 4.26 – μ CT images showing the TRC specimens with (a) EP carbon, (b) C-MCF, and (c) GP-MCF fabrics after temperature exposure of 20 °C and 300 °C.

4.4. Conclusions

The mechanical behavior under tensile loading of Textile Reinforced Concrete (TRC) with polymeric- and mineral-impregnated carbon fabrics was

evaluated after exposure to different thermal regimes with target temperatures of 150 °C, 200 °C, and 300 °C and the following conclusions can be drawn:

- The MCF fabrics developed presented tensile strength and modulus of elasticity comparable to commercially available polymeric-coated carbon fabrics, which validates the effectiveness of this new technology as textile reinforcement.
- The MCF fabrics are fragile materials with linear-elastic behavior up to the rupture. However, because the fabrics are formed by multiple longitudinal yarns, the textile reinforcement did not present a sudden collapse. Instead, the failure was characterized by the successive rupture of the yarns. From a structural safety point of view, this is an interesting behavior.
- The TRC with MCF fabrics presented a strain-hardening behavior with a multiple cracking pattern under tensile loadings. The composites with the C-MCF fabric exhibited superior mechanical performance than the ones reinforced with the GP-MCF fabric, probably due to the better bond towards the fine-grained concrete matrix of the C-MCF fabric.
- The TRC with the EP carbon fabric presented the best mechanical performance compared to the others. However, the rupture of these composites was characterized by significant spalling, probably due to the main bond mechanism involved between the EP carbon yarns and the fine-grained concrete, which is a mechanical one, associated with the high tensile stresses reached.
- The DIC analysis of the TRC with different carbon fabrics showed that the composites with the C-MCF fabric presented more cracks with smaller widths than the composites with the GP-MCF fabric, corroborating the assumption of the better bond of the C-MCF towards the fine-grained concrete matrix.
- The TRC with MCF fabrics presented cracks after being submitted to the thermal regimes, being more pronounced in the composites with GP-MCF. This thermal cracking can be related to the incompatibility

between the thermal coefficients of the mineral suspensions and the fine-grained concrete matrix.

- The residual mechanical behavior under tensile loading of the TRC with C-MCF was not significantly affected by the thermal regime, and the composites were able to present a strain-hardening behavior with a multiple-cracking pattern at all temperature levels evaluated.
- The TRC with GP-MCF was considerably affected by the thermal regimes. The exposure to elevated temperatures led to a decrease in the residual tensile strength and strain capacity of the composites. Additionally, the crack pattern, i.e., the number of cracks, spacing, and width, was considerably modified.
- The TRC with EP carbon fabric did not present a significant reduction in the residual mechanical behavior in temperatures up to 200 °C. However, with the subsequent heating to 300 °C, a considerable decrease in the mechanical behavior was observed, mostly due to the complete degradation of the epoxy resin coating. At all temperature levels, including at room temperature, a substantial spalling was noted in the composites with the EP carbon fabric.

4.5. References

- [1] PELED, A.; BENTUR, A.; MOBASHER, B. **Textile Reinforced Concrete**. [s.l.] CRC Press Taylor & Francis Group, 2017.
- [2] HEGGER, J. et al. Exterior Cladding Panels as an Application of Textile Reinforced Concrete. **SP-224. Farmington Hills (MI, USA): American Concrete Institute**, p. 55–70, 2004.
- [3] REINHARDT, H. W.; KRUEGER, M. **Prestressed concrete plates with high strength fabric**. 6th RILEM Symposium on Fibre-Reinforced Concretes (FRC) - BEFIB. **Anais...** Varenna, Italy: 2004
- [4] COLOMBO, I. G.; COLOMBO, M.; PRISCO, M. DI. Bending behaviour of Textile Reinforced Concrete sandwich beams. **Construction and Building Materials**, v. 95, p. 675–685, 2015.
- [5] SCHOLZEN, A.; CHUDOBA, R.; HEGGER, J. Thin-walled shell structures made of textile-reinforced concrete: Part II: Experimental characterization, ultimate

limit state assessment and numerical simulation. **Structural Concrete**, v. 16, n. 1, p. 115–124, 2015.

[6] HEGGER, J. et al. Innovative design concepts: Application of textile reinforced concrete to shell structures. **Structural Concrete**, v. 19, n. 3, p. 637–646, 2018.

[7] MAY, S. et al. Precast Slab Structures Made of Carbon Reinforced Concrete. **Structures**, p. #pagerange#, 2018.

[8] GOLIATH, K. B.; CARDOSO, D. C. T.; SILVA, F. DE A. Flexural behavior of carbon-textile-reinforced concrete I-section beams. **Composite Structures**, v. 260, p. 113540, 2021.

[9] BRÜCKNER, A.; ORTLEPP, R.; CURBACH, M. Textile reinforced concrete for strengthening in bending and shear. **Materials and Structures**, v. 39, n. 8, p. 741–748, 2006.

[10] TRIANTAFILLOU, T. C.; PAPANICOLAOU, C. G. Shear strengthening of reinforced concrete members with textile reinforced mortar (TRM) jackets. **Materials and Structures/Materiaux et Constructions**, v. 39, n. 285, p. 93–103, 2006.

[11] NANNI, A. A New Tool for Concrete and Masonry Repair. **Concrete International**, n. april, p. 43–49, 2012.

[12] AMBRISI, A. D.; FOCACCI, F. Flexural strengthening of RC beams with cement-based composites. **Journal of Composites for Construction**, v. 15, n. 5, p. 707–720, 2011.

[13] D'ANTINO, T. et al. Relationship between the effective strain of PBO FRCM-strengthened RC beams and the debonding strain of direct shear tests. **Engineering Structures**, v. 216, n. August 2019, p. 110631, 2020.

[14] BRAMESHUBER, W. **Report 36: textile reinforced concrete-state-of-the-art report of RILEM TC 201-TRC**. [s.l.] Rilem publications, 2006.

[15] BENTUR, A.; MINDESS, S. **Fiber Reinforced Cementitious Composites**. [s.l.] CRC Press, 2006.

[16] MOBASHER, B. **Mechanics of Fiber and Textile Reinforced Cement Composites**. [s.l.] CRC Press, 2012.

[17] CHAND, S. Review - carbon fibers for composites. **Journal of Materials Science**, v. 35, n. 6, p. 1303–1313, 2000.

[18] SAUDER, C.; LAMON, J.; PAILLER, R. The tensile behavior of carbon fibers at high temperatures up to 2400 °C. **Carbon**, v. 42, n. 4, p. 715–725, 2004.

- [19] ARBOLEDA, D.; BABAEIDARABAD, S.; NANNI, A. **Durability of fabric reinforced cementitious matrix (FRCM) composites**. 7th. International Conference of FRP Composites in Civil Engineering, International Institute for FRP in Construction. **Anais...**International Institute for FRP in Construction, 2014
- [20] NADIV, R. et al. Micro- and nanoparticle mineral coating for enhanced properties of carbon multifilament yarn cement-based composites. **Composites Part B: Engineering**, v. 111, p. 179–189, 2017.
- [21] DONNINI, J.; CORINALDESI, V.; NANNI, A. Mechanical properties of FRCM using carbon fabrics with different coating treatments. **Composites Part B: Engineering**, v. 88, p. 220–228, 2016.
- [22] MEHTA, P. K.; MONTEIRO, P. J. M. **Concrete: Microstructure, properties and materials**. [s.l.] McGraw-Hill, 2006.
- [23] DVORKIN, D.; PELED, A. Effect of reinforcement with carbon fabrics impregnated with nanoparticles on the tensile behavior of cement-based composites. **Cement and Concrete Research**, v. 85, p. 28–38, 2016.
- [24] PELED, A. et al. **Modifying carbon roving-cement matrix bond by inorganic coating**. High Performance Fiber Reinforced Cement Composites (HPFRCC7). **Anais...**Struttgart, Germany: RILEM, 2015
- [25] KRÜGER, M.; REINHARDT, H.-W.; FICHTLSCHERER, M. Bond behaviour of textile reinforcement in reinforced and prestressed concrete. **Otto-Graf-Journal**, v. 12, p. 33–50, 2001.
- [26] XU, S. et al. Bond Characteristics of Carbon, Alkali Resistant Glass, and Aramid Textiles in Mortar. **Journal of Materials in Civil Engineering**, v. 16, n. 4, p. 356–364, 2004.
- [27] RAUPACH, M.; ORLOWSKY, J.; BÜTTNER, T. **Epoxy-impregnated textiles in concrete – Load bearing capacity and durability**. (J. Hegger, W. Bramehuber, N. Will, Eds.)ICTRC'2006 - 1st International RILEM Conference on Textile Reinforced Concrete. **Anais...**Aachen: RILEM Publications SARL, 2006
- [28] SILVA, R. M. DE C.; SILVA, F. DE A. **Mechanical and Bond Behavior of Carbon Textile Reinforced Concretes Under Tensile Loading**. 4th Brazilian Conference on Composite Materials. **Anais...**Rio de Janeiro: 2018
- [29] SCHNEIDER, K. et al. Mineral-impregnated carbon fibre reinforcement for high temperature resistance of thin-walled concrete structures. **Cement and Concrete Composites**, v. 97, n. December 2018, p. 68–77, 2019.

- [30] XU, S.; LI, H. Bond properties and experimental methods of textile reinforced concrete. **Journal Wuhan University of Technology, Materials Science Edition**, v. 22, n. 3, p. 529–532, 2007.
- [31] SILVA, R. M. DE C.; SILVA, F. DE A. Carbon textile reinforced concrete: materials and structural analysis. **Materials and Structures/Materiaux et Constructions**, v. 53, n. 1, 2020.
- [32] MORGAN, P. **Carbon Fibers and their Composites**. [s.l.] CRC Press, 2005.
- [33] BRAZILIAN STANDARD. **NBR 6118: Projeto de estruturas de concreto - Procedimento** Associação Brasileira de Normas Técnicas (ABNT), , 2014.
- [34] PAPAKONSTANTINO, C. G.; BALAGURU, P.; LYON, R. E. Comparative study of high temperature composites. **Composites Part B:Engineering**, v. 32, n. 8, p. 637–649, 2001.
- [35] YOUNES, A. et al. Mechanical behaviour of carbon and glass filament yarns under high temperatures for composite applications. **Journal of the Textile Institute**, v. 104, n. 3, p. 251–259, 2013.
- [36] MICHELS, J. et al. Structural Strengthening of Concrete with Fiber Reinforced Cementitious Matrix (FRCM) at Ambient and Elevated Temperature — Recent Investigations in Switzerland. **Advances in Structural Engineering**, v. 17, n. 12, p. 1785–1799, 2014.
- [37] EHLIG, D. et al. **High Temperature Tests on Textile Reinforced Concrete (TRC) Strain Specimens**. (W. Brameshuber, Ed.)International RILEM Conference on Material Science – MATSCI. **Anais...Aachen: Rilem publications**, 2010
- [38] RAMBO, D. A. S.; SILVA, F. DE A.; TOLEDO FILHO, R. D. Effect of elevated temperatures on the mechanical behavior of basalt textile reinforced refractory concrete. **Materials and Design**, v. 65, p. 24–33, 2015.
- [39] DONNINI, J. et al. Fabric-reinforced cementitious matrix behavior at high-temperature: Experimental and numerical results. **Composites Part B: Engineering**, v. 108, p. 108–121, 2017.
- [40] SILVA, F. DE A. et al. Effects of elevated temperatures on the interface properties of carbon textile-reinforced concrete. **Cement and Concrete Composites**, v. 48, p. 26–34, 2014.
- [41] SILVA, R. M. DE C. et al. Bond behavior of polymer- and mineral-impregnated carbon fiber yarns towards concrete matrices at elevated temperature

levels. **Cement concrete composite**, v. 133, p. 104685, 2022.

[42] SCHNEIDER, K. et al. Verbundverhalten mineralisch gebundener und polymergebundener Bewehrungsstrukturen aus Carbonfasern bei Temperaturen bis 500 °C. **Beton- und Stahlbetonbau**, v. 113, n. 12, p. 886–894, 2018.

[43] MECHTCHERINE, V. et al. Mineral-impregnated carbon fiber composites as novel reinforcement for concrete construction: Material and automation perspectives. **Automation in Construction**, v. 110, n. September 2019, p. 103002, 2020.

[44] MECHTCHERINE, V. et al. Extrusion-based additive manufacturing with carbon reinforced concrete: Concept and feasibility study. **Materials**, v. 13, n. 11, 2020.

[45] NEEF, T.; MÜLLER, S.; MECHTCHERINE, V. **Integration of Mineral Impregnated Carbon Fibre (MCF) into Fine 3D-Printed Concrete Filaments**. (R. Buswell et al., Eds.) Third RILEM International Conference on Concrete and Digital Fabrication. **Anais...**Loughborough: Springer Cham, 2022. Disponível em: <http://dx.doi.org/10.1007/978-3-031-06116-5_59>

[46] DUXSON, P. et al. Geopolymer technology: The current state of the art. **Journal of Materials Science**, v. 42, n. 9, p. 2917–2933, 2007.

[47] TRINDADE, A. C. C.; BORGES, P. H. R.; SILVA, F. DE A. Evaluation of Fiber–Matrix Bond in the Mechanical Behavior of Geopolymer Composites Reinforced with Natural Fibers. **Advances in Civil Engineering Materials**, v. 8, n. 3, p. 20180136, 2019.

[48] KRIVEN, W. M.; BELL, J. L.; GORDON, M. Microstructure and microchemistry of fully- reacted geopolymers and geopolymer matrix composites. **Ceramic Transactions**, v. 153, p. 227–250, 2003.

[49] TRINDADE, A. C. C. et al. Influence of elevated temperatures on the mechanical behavior of jute-textile-reinforced geopolymers. **Journal of Ceramic Science and Technology**, v. 8, n. 3, p. 389–398, 2017.

[50] TRINDADE, A. C. C. et al. On The Mechanical Behavior of Metakaolin Based Geopolymers Under Elevated Temperatures. **Materials Research**, v. 20, n. suppl 2, p. 265–272, 2017.

[51] CHINDAPRASIRT, P. et al. High-Strength Geopolymer Using Fine High-Calcium Fly Ash. **Journal of Materials in Civil Engineering**, v. 23, n. 3, p. 264–270, 2011.

- [52] GÖRHAN, G.; ASLANER, R.; ŞINIK, O. The effect of curing on the properties of metakaolin and fly ash-based geopolymer paste. **Composites Part B: Engineering**, v. 97, p. 329–335, 2016.
- [53] SINGH, N. B.; MIDDENDORF, B. Geopolymers as an alternative to Portland cement: An overview. **Construction and Building Materials**, v. 237, p. 117455, 2020.
- [54] DAVIDOVITS, J. Geopolymers: inorganic polymeric new materials. **Journal of Thermal Analysis and Calorimetry**, v. 37, n. 8, p. 1633–1656, 1991.
- [55] KRIVEN, W. M.; GORDON, M.; BELL, J. L. Geopolymers: Nanoparticulate, nanoporous ceramics made under ambient conditions. **Microscopy and Microanalysis**, v. 10, n. SUPPL. 2, p. 404–405, 2004.
- [56] DOAN, T. et al. New Generation of Geopolymer Composite for Fire-Resistance. In: TESINOVA, P. (Ed.). . **Advances in Composite Materials - Analysis of Natural and Man-Made Materials**. [s.l.] InTech, 2011. p. 73–92.
- [57] LYON, R. E. et al. Fire-resistant aluminosilicate composites. **Fire and Materials**, v. 21, n. 2, p. 67–73, 1997.
- [58] TRAN, D. H. et al. Effect of Curing Temperature on Flexural Properties of Silica-Based Geopolymer-Carbon Reinforced Composite. **Manufacturing Engineering**, v. 37, n. 2, p. 492–497, 2009.
- [59] ZHAO, J. et al. Development and testing of fast curing, mineral-impregnated carbon fiber (MCF) reinforcements based on metakaolin-made geopolymers. **Cement and Concrete Composites**, v. 116, n. September 2020, 2021.
- [60] DIN EN. **197-1: 2011-11 - Zement - Teil 1: Zusammensetzung, Anforderungen und Konformitätskriterien von Normzement**Dtsch. Fass., , 2011.
- [61] EUROPEAN STANDARD EN. **196-1:2005 - Methods of testing cement - Part 1: Determination of strength**European Committee for standardization, , 2005.
- [62] TRINDADE, A. C. C. et al. On the mechanical performance of K- and Na-based strain-hardening geopolymer composites (SHGC) reinforced with PVA fibers. **Construction and Building Materials**, v. 248, 2020.
- [63] LIEBSCHER, M. et al. Influence of roller configuration on the fiber-matrix distribution and mechanical properties of continuously produced mineral-impregnated carbon-fibers (MCF). **Fibers**, v. 10, n. 5, p. 42, 2022.

- [64] ZHAO, J. et al. Role of sizing agent on the microstructure morphology and mechanical properties of mineral-impregnated carbon-fiber (MCF) reinforcement made with geopolymers. **Applied Surface Science**, v. 567, n. July, p. 150740, 2021.
- [65] XU, S.; SHEN, L.; WANG, J. The high-temperature resistance performance of TRC thin-plates with different cementitious materials: Experimental study. **Construction and Building Materials**, v. 115, p. 506–519, 2016.
- [66] RAMBO, D. A. S. et al. Experimental investigation and modelling of the temperature effects on the tensile behavior of textile reinforced refractory concretes. **Cement and Concrete Composites**, v. 75, p. 51–61, 2017.
- [67] DIEDERICHS, U.; JUMPPANEN, U.-M.; PENTTALA, V. **Behavior of high strength concrete at high temperatures**Helsinki University of Technology, Department of Structural Engineering, Report 92. [s.l.: s.n.].
- [68] DWECK, J. et al. Importance of quantitative thermogravimetry on initial cement mass basis to evaluate the hydration of cement pastes and mortars. **Journal of Thermal Analysis and Calorimetry**, v. 113, n. 3, p. 1481–1490, 2013.
- [69] DWECK, J. et al. A comparative study of hydration kinetics of different cements by thermogravimetry on calcined mass basis. **Journal of Thermal Analysis and Calorimetry**, v. 128, n. 3, p. 1335–1342, 2017.
- [70] DWECK, J. et al. Study by thermogravimetry of the evolution of ettringite phase during type II Portland cement hydration. **Journal of Thermal Analysis and Calorimetry**, v. 69, n. 1, p. 179–186, 2002.
- [71] COLLIER, N. C. Transition and decomposition temperatures of cement phases - a collection of thermal analysis data. **Ceramics - Silikaty**, v. 60, n. 4, p. 338–343, 2016.
- [72] PAHN, L. T.; CARINO, J. N. **Mechanical Properties of High Strength Concrete At Elevated Temperatures**NISTIR 6726Washington, D.C.National Institute of Standards and Technology, , 2001.
- [73] PIMIENTA, P.; MCNAMEE, R. J.; MINDEGUIA, J.-C. **Physical properties and behaviour of High-Performance Concrete at high temperature**. [s.l.] Springer, 2019.
- [74] MENOU, A. et al. Residual fracture energy of cement paste, mortar and concrete subject to high temperature. **Theoretical and Applied Fracture Mechanics**, v. 45, n. 1, p. 64–71, 2006.

- [75] YÜZER, N.; AKÖZ, F.; ÖZTÜRK, L. D. Compressive strength-color change relation in mortars at high temperature. **Cement and Concrete Research**, v. 34, n. 10, p. 1803–1807, 2004.
- [76] IBRAHIM, R. K.; HAMID, R.; TAHA, M. R. Strength and microstructure of mortar containing nanosilica at high temperature. **ACI Materials Journal**, v. 111, n. 2, p. 163–170, 2014.
- [77] HEIKAL, M. et al. Behavior of composite cement pastes containing microsilica and fly ash at elevated temperature. **Construction and Building Materials**, v. 38, p. 1180–1190, 2013.
- [78] TRINDADE, A. C. C. et al. Tensile behavior of strain-hardening geopolymer composites (SHGC) under impact loading. **Cement and Concrete Composites**, v. 113, n. June, 2020.
- [79] TRINDADE, A. C. C. **A study on the mixture design and mechanical performance of strain-hardening geopolymer composites (SHGC) under extreme conditions**. 2021. Pontifícia Universidade Católica do Rio de Janeiro (PUC-Rio). 2021.
- [80] LANGSTON, T. The tensile behavior of high-strength carbon fibers. **Microscopy and Microanalysis**, v. 22, n. 4, p. 841–844, 2016.
- [81] ZHU, D. et al. Strain rate and gage length effects on tensile behavior of Kevlar 49 single yarn. **Composites Part A: Applied Science and Manufacturing**, v. 43, n. 11, p. 2021–2029, 2012.
- [82] ALENCAR MONTEIRO, V. M. DE; LIMA, L. R.; ANDRADE SILVA, F. DE. On the mechanical behavior of polypropylene, steel and hybrid fiber reinforced self-consolidating concrete. **Construction and Building Materials**, v. 188, p. 280–291, 2018.
- [83] CASTOLDI, R. DE S.; SOUZA, L. M. S. DE; ANDRADE SILVA, F. DE. Comparative study on the mechanical behavior and durability of polypropylene and sisal fiber reinforced concretes. **Construction and Building Materials**, v. 211, p. 617–628, 2019.
- [84] SOUZA, F. R. et al. **Experimental Study of Polyvinyl Alcohol (PVA) Fiber Reinforced Concrete under Cyclic Loading**. Proceedings of the XLII Ibero-Latin-American Congress on Computational Methods in Engineering and III Pan-American Congress on Computational Mechanics. **Anais...Rio de Janeiro**: 2021
- [85] GONG, T. et al. Tensile behavior of hybrid fiber reinforced composites made

of strain-hardening cement-based composites (SHCC) and carbon textile. **Construction and Building Materials**, v. 262, p. 120913, 2020.

[86] FOSTER, S. J.; LIU, J.; SHEIKH, S. A. Cover Spalling in HSC Columns Loaded in Concentric Compression. **Journal of Structural Engineering**, v. 124, n. 12, p. 1431–1437, 1998.

[87] BAE, S.; BAYRAK, O. Early Cover Spalling in High-Strength Concrete Columns. **Journal of Structural Engineering**, v. 129, n. 3, p. 314–323, 2003.

[88] JERABEK, J. et al. Experimental and Numerical Analysis of Spalling Effect in TRC Specimens. **4th Colloquium on Textile Reinforced Structures (CTRS4)**, p. 289–300, 2009.

[89] PREINSTORFER, P.; KOLLEGGER, J. New insights into the splitting failure of textile-reinforced concrete. **Composite Structures**, v. 243, n. March, p. 112203, 2020.

[90] MECHTCHERINE, V. Towards a durability framework for structural elements and structures made of or strengthened with high-performance fibre-reinforced composites. **Construction and Building Materials**, v. 31, p. 94–104, 2012.

[91] REISGEN, U. et al. Theoretical and Experimental Investigations on Textile-Reinforced Concrete Spalling Behavior. **International RILEM Conference on Material Science-MATSCI**, v. I, p. 153–162, 2010.

[92] CRUZ, C. R.; GILLEN, M. Thermal expansion of Portland cement paste, mortar and concrete at high temperatures. **Fire and Materials**, v. 4, n. 2, p. 66–70, 1980.

[93] GUERRIERI, M.; SANJAYAN, J.; COLLINS, F. Residual compressive behavior of alkali-activated concrete exposed to elevated temperatures. **Fire and Materials**, v. 33, n. 1, p. 51–62, 2009.

[94] GRATTAN-BELLEW, P. E.; BEAUDOIN, J. J.; VALLÉE, V.-G. Effect of aggregate particle size and composition on expansion of mortar bars due to delayed ettringite formation. **Cement and Concrete Research**, v. 28, n. 8, p. 1147–1156, 1998.

[95] NEVILLE, A. M. **Properties of concrete**. London: Pitman Publishing Limited, 1995.

[96] TRINDADE, A. C. C. et al. Influence of elevated temperatures on the residual and quasi in-situ flexural strength of strain-hardening geopolymer composites

(SHGC) reinforced with PVA and PE fibers. **Construction and Building Materials**, v. 314, n. November 2021, 2022.

[97] MEYERS, S. L. Thermal Coefficient of Expansion of Portland Cement: Long-time tests. **Industrial and Engineering Chemistry**, v. 32, n. 8, p. 1107–1112, 1940.

[98] ZENG, Q. et al. Effect of porosity on thermal expansion coefficient of cement pastes and mortars. **Construction and Building Materials**, v. 28, n. 1, p. 468–475, 2012.

5 Strengthening of RC beams using textile reinforced concrete (TRC) with polymer- and mineral-impregnated carbon fabrics

Steel reinforced concrete (RC) structures may need strengthening during their useful life. Textile Reinforced Concrete (TRC) is an interesting alternative to be used as a strengthening material due to its elevated mechanical properties, low self-weight, and good compatibility with concrete substrates. The mechanical behavior of the TRC is extremely dependent on the bond between the textile reinforcement and the cementitious matrix. Polymeric and mineral impregnations have already been demonstrated to be successful in enhancing the bond between carbon fabrics and the fine-grained concrete matrix. However, to be effective as a strengthening in concrete structures, it is necessary to ensure a good bond between the TRC layer and the structural element substrate. Thus, this work aims to evaluate the efficiency of TRCs with polymer- and mineral-impregnated carbon fabrics as strengthening material of RC beams through four-point bending tests. For this, different strengthening protocols were assessed to obtain the optimized substrate preparation method, ensuring the joint work between the TRC-strengthening and the RC beam: roughening of the surface and aggregate exposure technique. For the epoxy-coated (EP) carbon fabric, total roughening of the surface was the most effective substrate preparation protocol, while for the mineral-impregnated carbon (MCF) fabrics, the best strengthening protocol was based on an aggregate exposure technique. All TRC-strengthened beams exhibited higher maximum loads, with an enhancement of 67.8%, 59.6%, and 53.8% for the TRC with the EP carbon, C-MCF, and GP-MCF fabrics, respectively. The TRC strengthening also altered the cracking pattern of the RC beams, with the strengthened beams presenting a greater number of thinner cracks. Finally, an analytical model based on moment vs. curvature curves was proposed.

The experimental program of this chapter was conducted at the Structures and Materials Laboratory of PUC-Rio (LEM-Dec), Brazil. The MCF fabrics were

manufactured at the Institute of Construction Materials at the Technische Universität Dresden, Germany.

5.1. Introduction

Steel-reinforced concrete (RC) structures are prone to suffer damages throughout their life cycle due to degradation issues or loadings originally not considered in the design. In addition, they can have their design purposes altered, resulting in additional loading conditions. From a sustainability point of view, demolishing and rebuilding such structures is not interesting, thus creating the need for their rehabilitation. Nowadays, there are several repair and strengthening methods, from traditional techniques, such as cross-section enlargement [1–4], and external prestressing with tendons [5–8], to more recent fiber-based composite systems [9–15].

Fiber Reinforced Polymers (FRPs) are a combination of fibers, such as aramid, carbon, and glass, embedded in a polymeric matrix, usually epoxy resin [16]. The use of FRP for strengthening RC structures has been reported in the literature since the early 1990s [12], and its use has become widely spread mainly due to the materials' high tensile strength, low weight, corrosion resistance, and ease of application compared to conventional methods [16]. The ACI 440.2R [16] provides recommendations for the design of externally bonded FRP systems for strengthening RC structures. However, despite the various advantages, FRP has significant disadvantages, such as low thermal resistance, which implies additional costs with special fire protection, and incompatibility with the concrete substrate, which can lead to long-term durability issues [16,17]. The use of inorganic matrices instead of the organic (polymeric) one is an attractive alternative to overcome the aforementioned drawbacks.

Textile reinforced concrete (TRC) (also referred as *Fabric Reinforced Cementitious Matrix*, FRCM) consists of a cementitious (inorganic) matrix reinforced with one or multiple layers of fabrics made of different material types, such as aramid, basalt, carbon, glass, or natural fibers [18]. This material presents elevated mechanical and durability properties. The textile reinforcements are non-corrosive [19]; thus, low thin concrete covers are necessary, reducing the weight of the elements. Additionally, the lower concrete amount required results in lower

cement consumption, leading to a reduction of the CO₂ emissions involved in the cement production. The TRC characteristic, i.e., low weight and high mechanical and durability properties, make it an outstanding material to be used for the strengthening and repair of RC structures. Furthermore, cementitious materials are known to present elevated temperature resistance [20]. This characteristic and the compatibility between the TRC matrix and the concrete substrate are interesting advantages for the use of this class of material over other strengthening systems.

Previous studies show the successful use of TRC as flexural strengthening of RC beams [21–29]. Brückner et al. [21], Larbi et al. [26], and Verbruggen et al. [25] demonstrated the enhancement of the load-bearing capacity of RC beams strengthened with a glass TRC. Furthermore, the TRC-strengthening was able to better control the cracking behavior, increasing the serviceability of the RC element. Ambrisi and Focacci [22] showed that carbon- and PBO-TRCs were able to increase the maximum load of RC concrete beams. The rupture of the strengthened beams was associated with the loss of strengthening action of the TRC layer due to the fibers debonding. Ombres [23] and Babaeidarabad et al. [24] also demonstrated the ability of a PBO-TRC to increase the bending load performance of RC beams. The failure mode was directly related to the amount of textile reinforcement; higher PBO layers led to beam premature failure due to debonding of the TRC-strengthening system. Gopinath et al. [27] demonstrated that a basalt-TRC strengthening was able to increase the energy absorption and ductility of RC beams under monotonic and low-cycle fatigue loading. Teixeira and Silva [28] observed an increase in the maximum load of RC beams strengthened with a curauá-TRC-like composite submitted to bending tests. Hadad et al. [29] showed an increase in the ultimate capacity of RC beams strengthened with a carbon-TRC.

In the literature, there are also reports on the use of TRC as strengthening of existing RC structures all over the world [17,30–32]. In Italy, the flexural and shear capacity of the RC beams of the Stadium San Siro were increased with a carbon-TRC [30]. Also in Italy, the vaults of a concrete bridge were strengthened with a PBO-TRC aiming to change the failure mechanism of the structure and increase its safety [17]. Butler et al. [31] reported the strengthening of a roof shell that presented large deformations with a carbon-TRC in Germany. In Russia, an RC bridge pier was strengthened with a PBO-TRC after a repair with epoxy resin failed [17]. A PBO-TRC was chosen to increase the circumferential flexural strength of a tunnel

lining in Greece [17]. A carbon-TRC was used for strengthening a concrete roof that presented insufficient load-carrying capacity and, due to monument conservation, could not withstand a new structure system [31]. A carbon-TRC was used to strengthen a motorway bridge, in Germany, aiming to increase its lifespan [32]. Another bridge in Germany, considered a historic monument, was also strengthened with a carbon-TRC due to corrosion damages in the structure [32].

The mechanical behavior of TRCs depends on the properties of the concrete matrix, the textile reinforcement, and also on the bond between the textile reinforcement and the concrete matrix [18]. Carbon fabrics present elevated mechanical and durability properties, making them a suitable option to be used as textile reinforcement in the TRC. However, due to the hydrophobic character of the carbon, this material presents a low bond towards the cementitious matrix [33]. Additionally, the multifilament nature of the yarns that form the textile contributes to jeopardizing the bond and, consequently, the mechanical behavior of the carbon TRC composites [34]. Polymeric impregnations are usually used to fill the spaces between the multifilaments, anchoring all of them in the surrounding matrix and contributing to increasing bond performance [35–38]. The main disadvantage of polymeric-coated carbon fabrics is their use at elevated temperatures due to the intrinsic low thermal behavior of most common polymer materials [39–42]. Once again, inorganic materials seem to be an appealing alternative due to their elevated thermal resistance. Dvorkin and Peled [38], Peled et al. [43], and Nativ et al. [33] demonstrated that micro silica fillers used as impregnation material of carbon yarns enhance the bond of the yarns and cementitious matrices. Schneider et al. [44,45] and Silva et al. [46] observed that Mineral-Impregnated Carbon Fibers (MCF) yarns with cement-based (C) and geopolymer (GP) suspensions were able to maintain a good level of bond towards fine-grained concrete matrix in temperatures up to 500 °C. Silva et al. [47] evaluated the mechanical behavior of such MCF fabrics as reinforcements in TRCs, and the results showed that the composites presented the expected strain-hardening behavior with a multiple-cracking pattern. Additionally, the TRC with the C-MCF fabrics did not present any significant change in the residual mechanical performance after submission to temperatures up to 300 °C.

One concern regarding the use of TRCs as strengthening is related to the adhesion between the TRC and the concrete substrate of the RC element. The bond models developed for FRP and steel plate strengthening systems, basically based

on adhesive bond laws with the assumption of slip in the adhesive joint, are not valid for the TRC strengthening [48]. According to Ortlepp et al. [49], there are three characteristic failure modes in a TRC-strengthened RC element: i) failure of the TRC layer characterized by the delamination in the textile layer; ii) failure in the substrate/TRC-strengthening interface; iii) failure in the RC element. The first and third modes depend mainly on the individual mechanical capacity of the TRC and RC elements. The second mode is related to the bond between the old and new concretes and can be avoided with an adequate pre-treatment of the RC surface. The sandblasting of the concrete substrate, followed by the casting of the TRC directly to the RC element, improves the bond by creating a strong interlocking between the old concrete and the TRC-strengthening layer [48]. Additionally, the multiple-cracking behavior of the TRC leads to discontinuities of the strain behavior in the bond area with the RC substrate [48]. Usually, single- and double-lap shear tests are performed to analyze the bond behavior between the TRC-strengthening layer and the concrete substrate. Most studies are carried out taking into account a pre-treatment of the concrete substrate, either with sandblasting [50–53] or water jetting [54]. Results obtained without any substrate pre-treatment can also be found, although in lesser frequency [52,55]. Several factors can influence the bond capacity of TRC-strengthening systems towards concrete substrates, such as the TRC properties, which are directly related to the bond between the textile reinforcement and the fine-grained concrete matrix [54,55]. The effect of the number of textile reinforcement layers in the bond behavior depends on the failure mode of the strengthened beams [54]. For elements presenting a failure in the textile-matrix interface, the increase in the number of textile layers leads to an increase in the bond behavior due to a lower shear stress per unit area of the textile for a particular load [54]. On the other hand, when the failure occurs in the interface of the strengthening and the concrete substrate, the addition of textile layers leads to an enhancement in the strengthening thickness and, thus, to a lower bond capacity [54,56]. According to D'Antino et al. [52], the substrate preparation has a limited role in the bond between the TRC strengthening and the concrete element. However, pre-existing cracks in the TRC matrix, due to shrinkage, for example, can negatively affect the bond behavior and lead to premature failure of the strengthened element due to detachment of the TRC layer. The bond length also impacts the bond behavior, with higher bond lengths leading to higher bond

capacity [50,54,55]. For bond lengths higher than an effective bond length, this enhancement can be attributed to an increase in the interlocking mechanism [53–55]. Differently from what is observed in FRP systems, the width of the TRC strengthening does not considerably affect the bond behavior between the strengthening layer and the concrete substrate, which is attributed to the independent behavior of the longitudinal yarns of the textile reinforcement [50,51].

Over the years, different analytical models have been proposed for the prediction of the flexural mechanical capacity of TRC-strengthened concrete elements. The ACI 549.4R [57] addresses the use of TRC as a strengthening material for RC structures with recommendations for its design and application based on the experimental research available. The following hypotheses are considered: (i) plane sections remain plane; (ii) the bond between the TRC layer and the concrete substrate remains effective; (iii) the maximum concrete strain is 0.003. For the TRC, the ACI 549.4R [57] assumes a bi-linear behavior with a maximum strain of 0.012. The ACI disregards the initial section (Stage I) of the TRC stress vs. strain curve in its design model for TRC-strengthened beams. To obtain the ultimate moment of the cross-section, a strength reduction factor dependent on the tensile strain level in the steel bars is considered. Haddad et al. [29] found a good correlation in the load capacity of TRC-strengthened beams obtained experimentally and calculated by the ACI design model. However, a difference was observed in the experimental and analytical values of the first crack, which was attributed to the contribution of the TRC matrix, which is neglected by the analytical model. Usually, the TRC matrices present high strength and, consequently, high stiffness before cracking. Bencardino et al. [58] performed a literature review on the flexural behavior of RC beams strengthened with TRCs and proposed an analytical model for their design based on the effective strain of the TRC, which is associated with the failure mode of the structural element. Most of the experimental results available in the literature report a rupture associated with debonding in one of the interfaces (concrete/TRC or textile/matrix). Thus, it is assumed that the ultimate strain of the TRC is equivalent to the debonding strain, which can be obtained experimentally for each strengthening system or estimated through the surface properties of the weakest interface, usually the textile/matrix one. Scheerer et al. [59] also proposed a design model based the Bernoulli's hypothesis considering the equilibrium of internal and external forces through an

iterative process. The maximum resistance of the cross-section is reached when at least one of the materials, i.e., the concrete, the steel reinforcement, and the TRC, reaches its ultimate capacity. The constitutive law of the TRC is based on the linear stress *vs.* strain curve of the textile reinforcement. Other types of failure, such as debonding or anchorage failure, are not considered in the model proposed and must be evaluate separately.

Thus, this study aims to investigate the potential use of carbon TRCs as an external strengthening material in RC beams. Three different carbon fabrics were assessed: a commercially epoxy-coated (EP) carbon fabric and two lab-developed Mineral-Impregnated Carbon Fiber (MCF) fabrics, one with a cement-based (C) and the other with a geopolymer suspension. First, the best strengthening protocol was evaluated, and for that, different substrate preparation methods were performed: surface roughening and aggregate exposure. Secondly, the efficiency of the TRC strengthening in enhancing the mechanical behavior of RC beams was analyzed through bending tests. A DIC analysis was conducted to evaluate the crack pattern of the reference and TRC-strengthened beams. Finally, an analytical model based on the moment *vs.* curvature curve was proposed.

5.2. Experimental Program

5.2.1. Materials

5.2.1.1. Carbon fabrics

Three types of carbon fabrics with different impregnation materials were evaluated in this work: two lab-developed Mineral-Impregnated Carbon Fibers (MCF) fabrics and a commercially available carbon fabric.

A cement-based (C) and a geopolymer (GP) MCF fabric were used. The carbon fiber (CF) town used for the MCF fabrics was a SIGRAFIL[®] C T50-4.4/255 – E100 from SGL Group, Germany. Table 5.1 provides the technical data according to the supplier. The cement-based suspension used consists of commercial micro-cements Mikrodur R-X and Mikrodur P-U, from Dyckerhoff, and a micro-silica suspension produced by MC-Bauchemie. Its composition is presented in

Table 5.2, and further information can be found in [45–47]. The geopolymer suspension was produced through the combination of commercially available

potassium (K)-based water glass (WG) Geosil® 14517, from Woellner, with a metakaolin (MK) Metamax®, from BASF.

Table 5.2 presents the geopolymer suspension composition, and further information can be found in [46,47,60]. The impregnation process and the manufacturing of the MCF fabrics can be found in detail in [46,47]. Table 5.3 presents the mechanical properties of the C- and GP-MCF fabrics according to [47]. Additionally, a carbon fabric impregnated with an epoxy resin, namely GRID Q85/85 – CCE – 21, from Solidian was selected. Table 5.4 presents the technical data provided by the supplier.

Table 5.1 – Technical data of the continuous carbon fiber tow according to the supplier.

Number of filaments	50000 (50k)
Fineness (tex)	3420
Single filament diameter (μm)	7
Tensile strength	4400
Modulus of elasticity (GPa)	255

Table 5.2 – Mineral suspensions compositions

Cement-based suspension	
Micro-cement Mikrodur R-X (kg/m^3)	500
Micro-cement Mikrodur P-U (kg/m^3)	500
Micro-silica suspension Centrilite Fume SX (kg/m^3)	500
Water (kg/m^3)	464
Superplasticizer Master Rheobuild 30 (kg/m^3)	45
Geopolymer suspension	
Waterglass Geosil (kg/m^3)	1000
Metakaolin (kg/m^3)	549.33
Superplasticizer Sapetin® D27 (kg/m^3)	61.97
WG/MK ratio	1.82

Table 5.3 – Mechanical properties of the MCF fabrics according to [47].

C-MCF fabric	
Tensile strength (MPa)	1367 ± 160
Modulus of elasticity (GPa)	220 ± 9.63
GP-MCF fabric	
Tensile strength (MPa)	1591 ± 201
Modulus of elasticity (GPa)	196 ± 0.650

Table 5.4 – Technical data of the commercial carbon fabric according to the supplier.

Impregnation material	Epoxy resin
Cross-section of the strand (mm ²)	1.81
Tensile strength (MPa)	2500
Modulus of elasticity (GPa)	220

5.2.1.2. Fine-grained concrete matrix

A fine-grained concrete with a mix proportion of 1:1:0.3 (sand: cementitious material: water by weight) was used as the TRC matrix. Table 5.5 presents its composition. Portland cement CP II-F 32 from LafargeHolcim defined by the Brazilian Standard ABNT NBR 16697 [61], and river sand with a maximum particle diameter of 1.18 were used. Fly ash from Pozofly[®] and silica fume from Tecnosil were incorporated as mineral admixtures. A superplasticizer, Glenium[®] 51, from BASF, with a solid content of approximately 30% was added to obtain proper workability for casting. The average compressive strength and modulus of elasticity at 28 days are 70 MPa and 35 GPa, respectively.

Table 5.5 – Fine-grained concrete matrix composition

Composition	
Sand (0-1.18 mm) (kg/m ³)	947
Cement CP II-F 32 (kg/m ³)	632
Water (kg/m ³)	280.8
Fly ash (kg/m ³)	265
Silica fume (kg/m ³)	50.5
Superplasticizer (kg/m ³)	4.74

5.2.1.3. Steel reinforced concrete

To evaluate the efficiency of the carbon TRC as external flexural strengthening, steel-reinforced concrete (RC) beams were produced. All RC beams present dimensions of 1.2 m x 0.12 m x 0.15 m (length x width x high) with a longitudinal reinforcement ratio of 0.56%, a shear reinforcement ratio of 0.35% (only in the region with shear stresses), and a concrete cover of 25 mm (see Figure 5.1).

An ordinary concrete based on previous works [28,62,63] was used as a matrix for the structural element. Table 5.6 presents its composition. Portland

cement CP II-F 32, from LafargeHolcim, defined by the Brazilian Standard ABNT NBR 16697 [61], and locally available aggregates were used. Natural river sand was used as fine aggregate, and gravel with two different volume fractions (maximum diameter of 9 and 19 mm) was used as coarse aggregates. Superplasticizer Glenium® 51, from BASF, with a solid content of approximately 30% was added to the mix to ensure proper workability for casting. The compressive mechanical properties at 28 days and 60 days are presented in Table 5.6.

The RC beams were designed to present a flexural failure. Steel ribbed rebars CA-50 (characteristic tensile yielding strength of 500 MPa), defined according to ABNT NBR 7480 [64], with diameters of 6.3 mm and 8 mm were used as stirrups and longitudinal reinforcement, respectively. Figure 5.1 presents details of the beams.

Table 5.6 – Concrete composition and mechanical properties

Composition	
Natural Sand (kg/m ³)	642
Cement CP II-F 32 (kg/m ³)	336
Gravel (9 mm) (kg/m ³)	441
Gravel (19 mm) (kg/m ³)	782
Water (kg/m ³)	168
Superplasticizer (kg/m ³)	1.11
Mechanical properties	
28 days	
Compressive strength (MPa)	24 ± 3.82
Modulus of elasticity (GPa)	24 ± 5.64
60 days	
Compressive strength (MPa)	27 ± 3.08
Modulus of elasticity (GPa)	26 ± 2.91

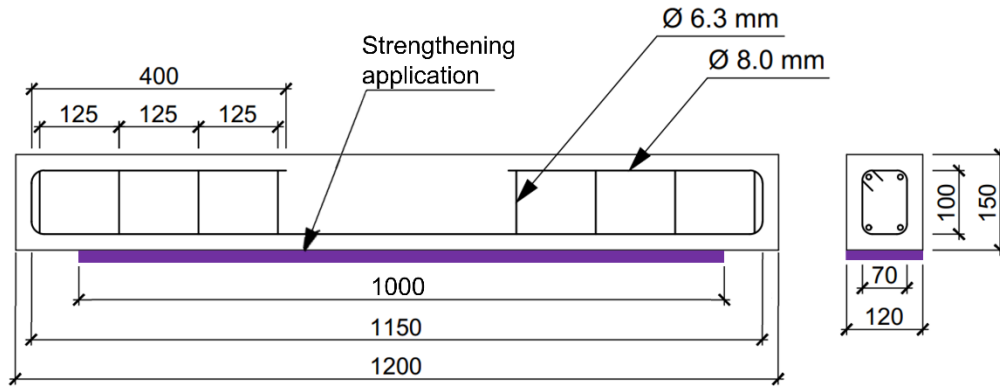


Figure 5.1 – Schematic beam details and dimensions (dimensions in mm).

5.2.2. Strengthening protocol

To evaluate the carbon TRC as external strengthening, laminates with 1.0 m x 0.15 m x 0.02 m (length x width x thickness) were cast directly in the beam inferior side, i.e., the side submitted to tensile stresses. Aiming for the joint mechanical work between the RC beam and the TRC layer, different strengthening protocols with varied substrate preparation mode were adopted. Figure 5.2 and Table 5.7 present the summary of the strengthening protocols evaluated, as well as the execution order in which they were performed. In all the cases, only the region in which the strengthening layer was going to be applied was prepared with the adopted protocol, see Figure 5.3, representing a practical situation in which the supports regions cannot be assessed. One beam was kept without strengthening for comparison purposes (REF).

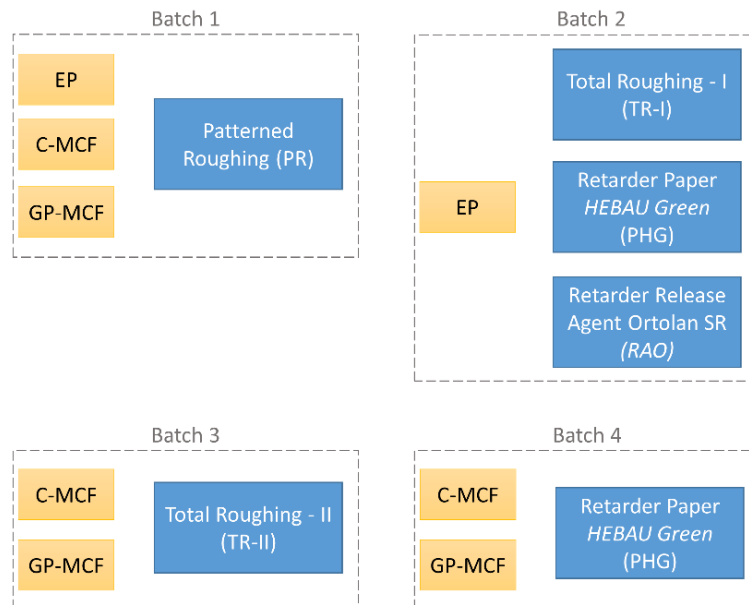


Figure 5.2 – Summary of the adopted strengthening protocols.

Table 5.7 – Summary of the adopted strengthening protocols

Specimen	Batch	Strengthening protocol	Carbon fabric	Beam's damage level
REF	-	-	-	Pre-loaded
PR-EP	1	Patterned Roughing	EP	Pre-loaded
PR-C	1	Patterned Roughing	C-MCF	Pre-loaded
PR-G	1	Patterned Roughing	GP-MCF	Pre-loaded
TR-I-EP	2	Total Roughing - I	EP	Pre-loaded
PHG-EP	2	Retarder Paper HEBAU "Green"	EP	Pre-loaded
RAO-EP	2	Retarder Release Agent Ortolan SR	EP	Pre-loaded
TR-II-C	3	Total Roughing - II	C-MCF	Pre-loaded
TR-II-G	3	Total Roughing - II	GP-MCF	Pre-loaded
PHG-C	4	Retarder Paper HEBAU "Green"	C-MCF	Pre-loaded
PHG-G	4	Retarder Paper HEBAU "Green"	GP-MCF	Pre-loaded

The strengthening protocols based on the manual roughening of the surface were applied after the pre-cracking process, while the ones based on the aggregate exposure processes, namely the Retarder Paper and the Retarder Release Agent, were applied in the casting phase. The Pattern Roughing (PR) was based on a previous work by Tinoco et al. [65]. The surface of the PR beams where the

strengthening was going to be applied was roughened with a hammer drill coupled with a bit of $\phi 13$ mm. Grooves of 20 mm width spaced between each other of 60 mm were produced, see Figure 5.3.a. The Total Roughing (TR) followed the same procedure as the Pattern Roughing with the difference that the entire region in which the strengthening was going to be applied was roughened. As this process was done manually, the TR protocol could be divided into two groups according to the thickness and occupation area of the resulting grooves. Figure 5.3.b shows the TR-I, in which the grooves present an average thickness of 2.5 ± 0.596 mm and are uniformly distributed on the whole strengthening surface area. The TR-II presents grooves with an average thickness of 3.22 ± 1.07 mm, and they are more concentrated in some regions and not uniformly distributed in the whole strengthening surface area, as shown in Figure 5.3.c. The other two methods used for the substrate preparation consisted of exposing the aggregates, a method successfully used by Figueiredo et al. [66]. For this, two commercially materials that delay the superficial setting time of the cement paste were used: a retarder paper WB-Paper Type “green” with an exposure depth of approximately 3-5 mm, from HEBAU, Germany and a retarder release agent Ortolan-SR, from MC-Bauchemie, Brazil. In both cases, the retarder agent was applied in the mold before casting, as indicated by the suppliers. After demolding, the beams were washed with pressure water to remove the layer of cement that did not set. Figure 5.3.d,e present the beam surface with the exposed aggregates.

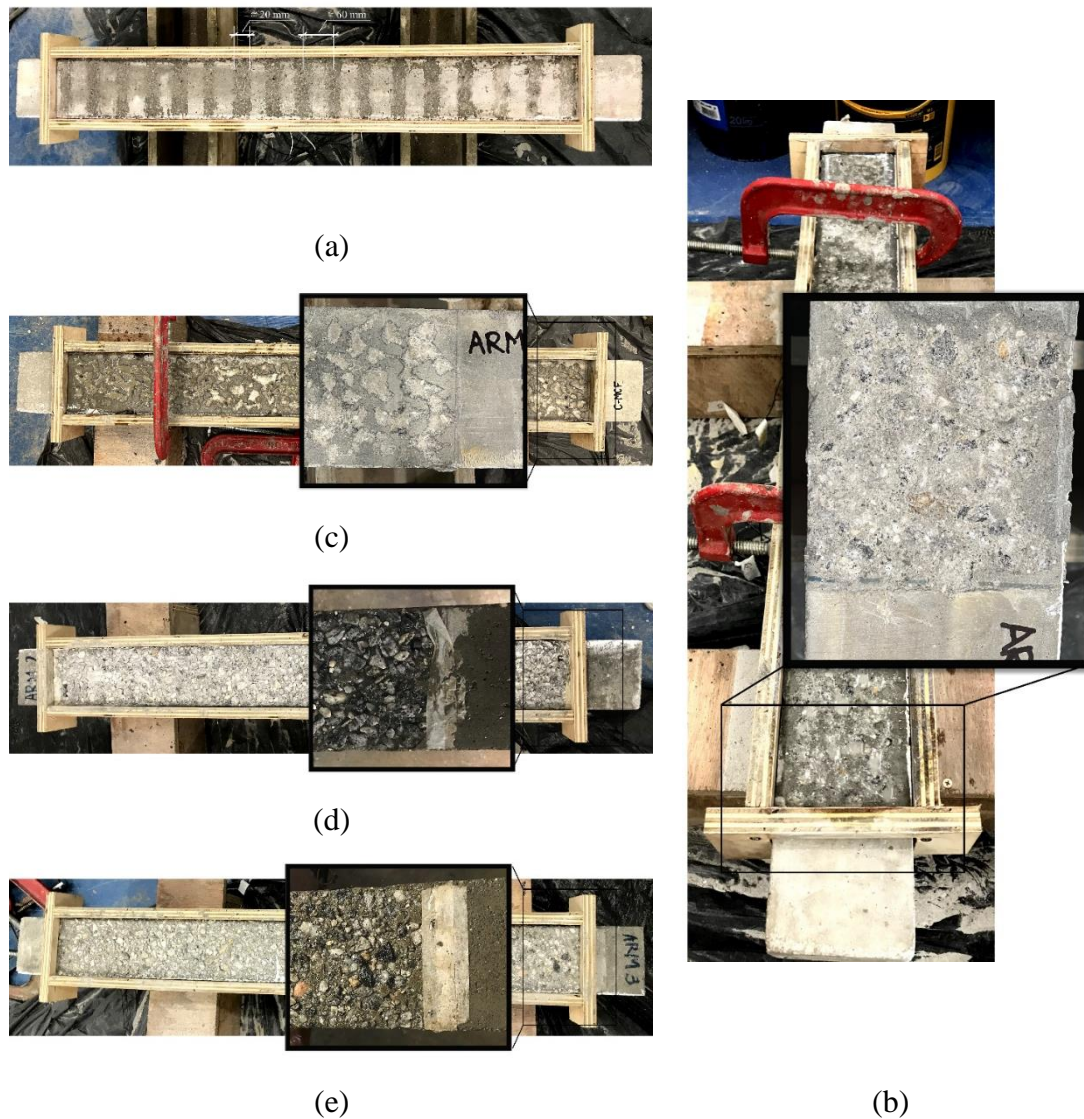


Figure 5.3 – Strengthening protocols: (a) Pattern Roughing (PR); (b) Total Roughening - I (TR-I); (c) Total Roughening - II (TR-II); (d) Retarder Paper HEBAU “Green” (PHG); (e) Retarder Release Agent Ortolan SR (RAO).

The RC beams were produced in a conventional way, with the concrete being mixed in a 50 L capacity concrete mixer, cast in the molds that already contained the steel reinforcement assembly, and consolidated with an external vibrator. In the beams that the strengthening protocol was based on the aggregate exposure, the molds were prepared with the retarder paper or the retarder release agent, only in the region of the posterior strengthening, before the casting. After 24h, the beams were demolded and cured for 28 days in a humid chamber. As mentioned before, the PHG and RAO beams, after being released from the molds, passed through a washing process so that the cement paste that did not set could be removed, exposing the aggregates.

Before being strengthened, all RC beams were pre-loaded to apply a certain level of damage, simulating practical conditions. The reference beam was also pre-loaded for comparison purposes. Usually, the design of RC beams is limited by the Deflection Serviceability Limit State (SLS-DEF), which limits the maximum displacement allowed in order to guarantee sensory acceptability to users and the correct functioning of all structural and non-structural elements [67–69]. Thus, the beams from batches 1 to 4 were pre-loaded to a maximum deflection of approximately 4.4 mm, which represents the maximum displacement allowed in the Deflection Serviceability Limit State (SLS-DEF). For this, four-point bending tests were performed as described in Section 5.2.3.

For all strengthening evaluated, the TRCs were reinforced with one carbon fabric layer. To achieve the desired length of the reinforcement textile (1.0 m), overlaps of 140 mm were adopted as demonstrated in Figure 5.4. The commercial EP carbon fabric is available in panels with 5 m x 1.2 m (transversal x longitudinal yarns), which does not configure as a problem to obtain the desired reinforcement length. However, the lab-developed MCF fabrics presented a maximum length of approximately 750 mm due to their manufacturing process. The TRC thickness (20 mm) was also governed by the thickness of the MCF fabrics that, due to their manufacturing process, present overlapping of the longitudinal and transversal yarns at the intersections. Further information regarding the manufacturing of the lab-developed MCF fabrics can be found in [47].

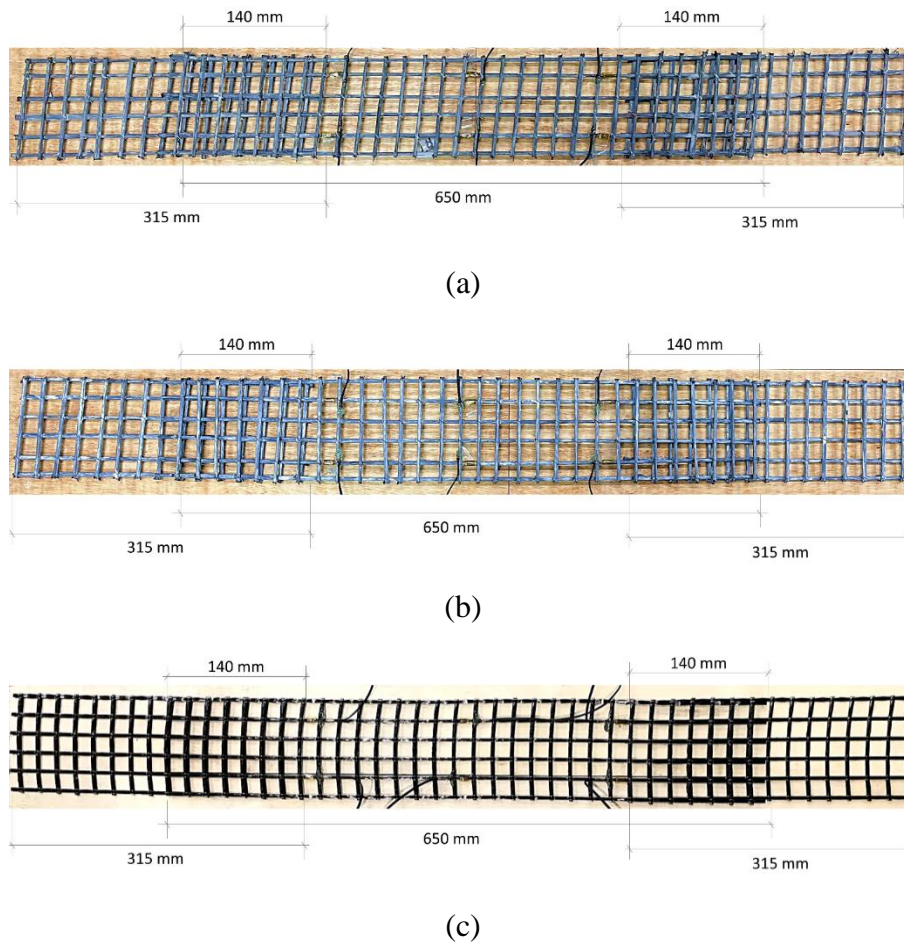


Figure 5.4 – Textile reinforcements with the overlap for the external TRC strengthening.
 (a) C-MCF; (b) GP-MCF; (c) EP carbon fabric.

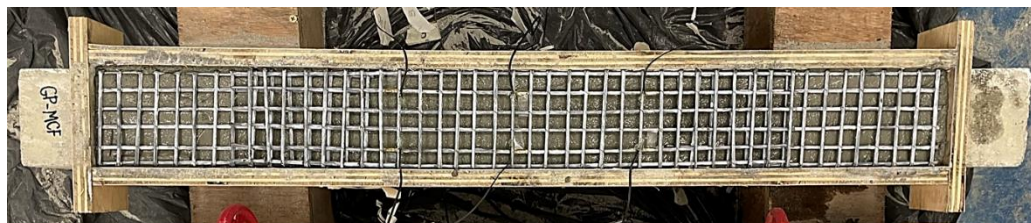
For the application of the TRC strengthening layer, the beams were placed upside down, i.e., with their tensile stress zone faced up, and the preparation of the substrate for the PR and TR beams took place. For all beams, the substrate was cleaned and slightly moistened, and a wood mold with the strengthening thickness (20 mm) was assembled. The composite application consisted of a hand lay-up technique, in which a first layer of the fine-grained concrete matrix was placed, followed by the positioning of the textile reinforcement, and then a second and final layer of the fine-grained concrete matrix was poured over. Figure 5.5 presents the strengthening procedure of the TR-II-G beam, as an example. After 24h, the mold was disassembled, and the TRC-strengthened beams were cured in the humid chamber for another 28 days so that the fine-grained concrete matrix could achieve its design strength.



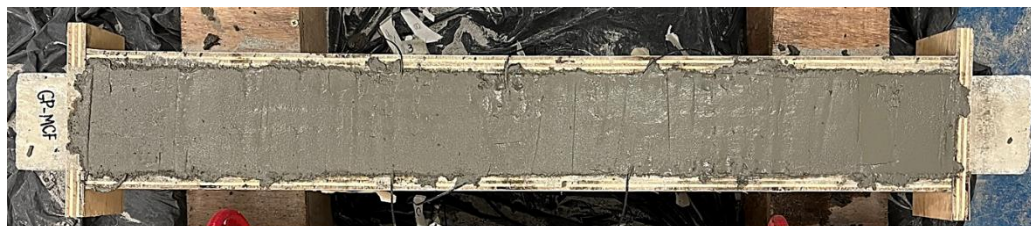
(a)



(b)



(c)



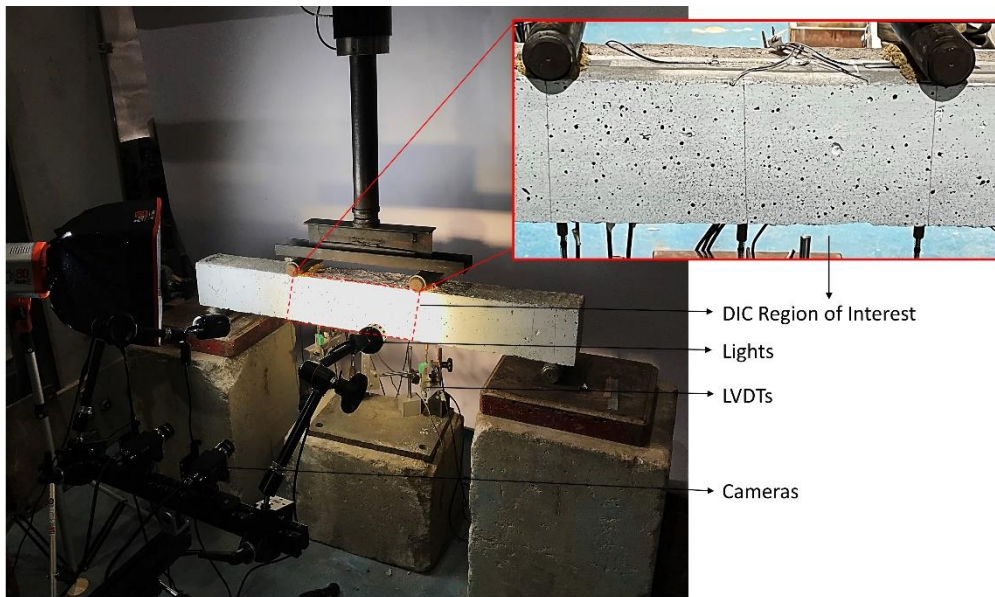
(d)

Figure 5.5 – Strengthening procedure with TRC composites. (a) Substrate moistening with the adopted strengthening protocol already executed and assembly of the strengthening mold; (b) Placement of the first fine-grained concrete matrix layer; (c) Positioned of the carbon textile reinforcement; (d) Placement of the second and last fine-grained concrete matrix layer and finishing operations.

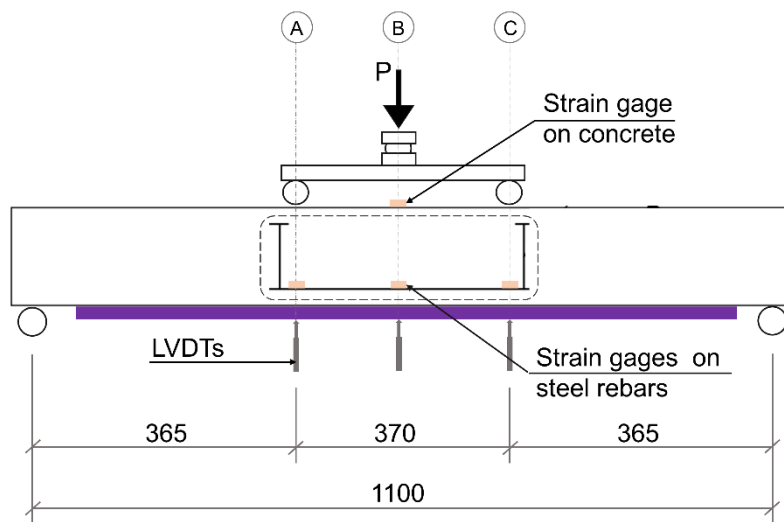
5.2.3. Bending tests

To evaluate the efficiency of the carbon TRC as external flexural strengthening of RC beams, four-point bending tests were performed in an MTS servo-hydraulic system with 500 kN load capacity. All beams were submitted to bending two times, with one pre-load before the strengthening (first loading) and then up to a complete failure after the strengthening (second loading). All tests were controlled by displacement at a rate of 1 mm/min, and the same rate was adopted

for the loading and unloading phases of the pre-load tests. Figure 5.6 presents the overview and scheme setup of the bending tests. The beams were tested with an 1100 mm span, and the load was applied by two rollers 370 mm distant from each other. Both support and load application rollers had free horizontal displacement. Three LVDTs were positioned on the bottom of the tested beam aligned with the load application points and at the midspan to obtain the deflection values. Additionally, 13 strain gages were used to obtain strain measurements. They were placed as follows: (i) six on the steel rebars, three in each bar in the direction of the ordinates A, B, and C indicated in Figure 5.6.b; (ii) one on the concrete top surface in the direction of the ordinate B indicated in Figure 5.6.b; and (iii) six on the textile reinforcement aligned with the ones of the steel rebars. The strain gages in the textile reinforcement were glued in the longitudinal yarns as shown in detail in Figure 5.7. A DIC analysis was also conducted to evaluate the cracking propagation in the maximum bending moment region (length of 370 mm). For this, a black-and-white speckle pattern was painted on one of the lateral surfaces of the beam, and a two-camera system, from Correlated Solutions, was used to take pictures with an interval of 1 second and 3 seconds for the first and second loading, respectively.



(a)



(b)

Figure 5.6 – (a) Overview and (b) scheme of the experimental setup of the beams four-point bending tests.

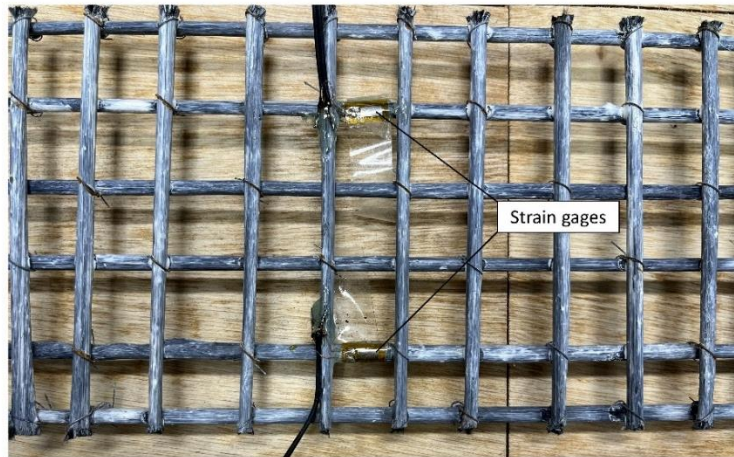


Figure 5.7 – Detail of the strain gage placed on the textile reinforcements.

5.3. Results and discussion

5.3.1. Strengthening protocols

To evaluate the efficiency of the carbon TRC composites as external strengthening of RC beams, first it was necessary to assess if the strengthening protocol adopted was adequate to guarantee the joint behavior of the existing structural element and the new strengthening layer applied. Thus, a qualitative evaluation of the obtained results for the different strengthening protocols investigated in this work was performed.

Figure 5.8 presents the load *vs.* actuator displacement curves obtained from the tests, separated by batches. The Reference beam results was plotted for comparison to all batches. The measurements obtained with the LVDTs were not used in this initial stage because some failure modes altered their reading in more advanced loading stages, as will be discussed. Figure 5.9 presents the failure modes of the reference and TRC-strengthened beams, and Table 5.8 shows the main results obtained. The *Increase of maximum load* is a ration between the maximum load of the TRC-strengthened beam and the maximum load of the Reference beam. Figure 5.10 presents the crack pattern at the actuator displacement (δ_{MTS}) of 2 mm, 3 mm, and 5 mm obtained from the DIC analysis. Here, it is important to emphasize that the actuator displacement was used as a reference to compare the different crack patterns. Therefore, there is a slightly variation in the real deflection level and deformation field of the beams, which can be attributed to the residual deflection of

the beams after the pre-loading phase and also to the small gaps in the test setup that are inherent to the load application methodology. At this stage of discussion this difference is not critical since the main objective here is to determine the best strengthening protocol that leads to the joint mechanical behavior of the RC concrete beam and the TRC-strengthening layer.

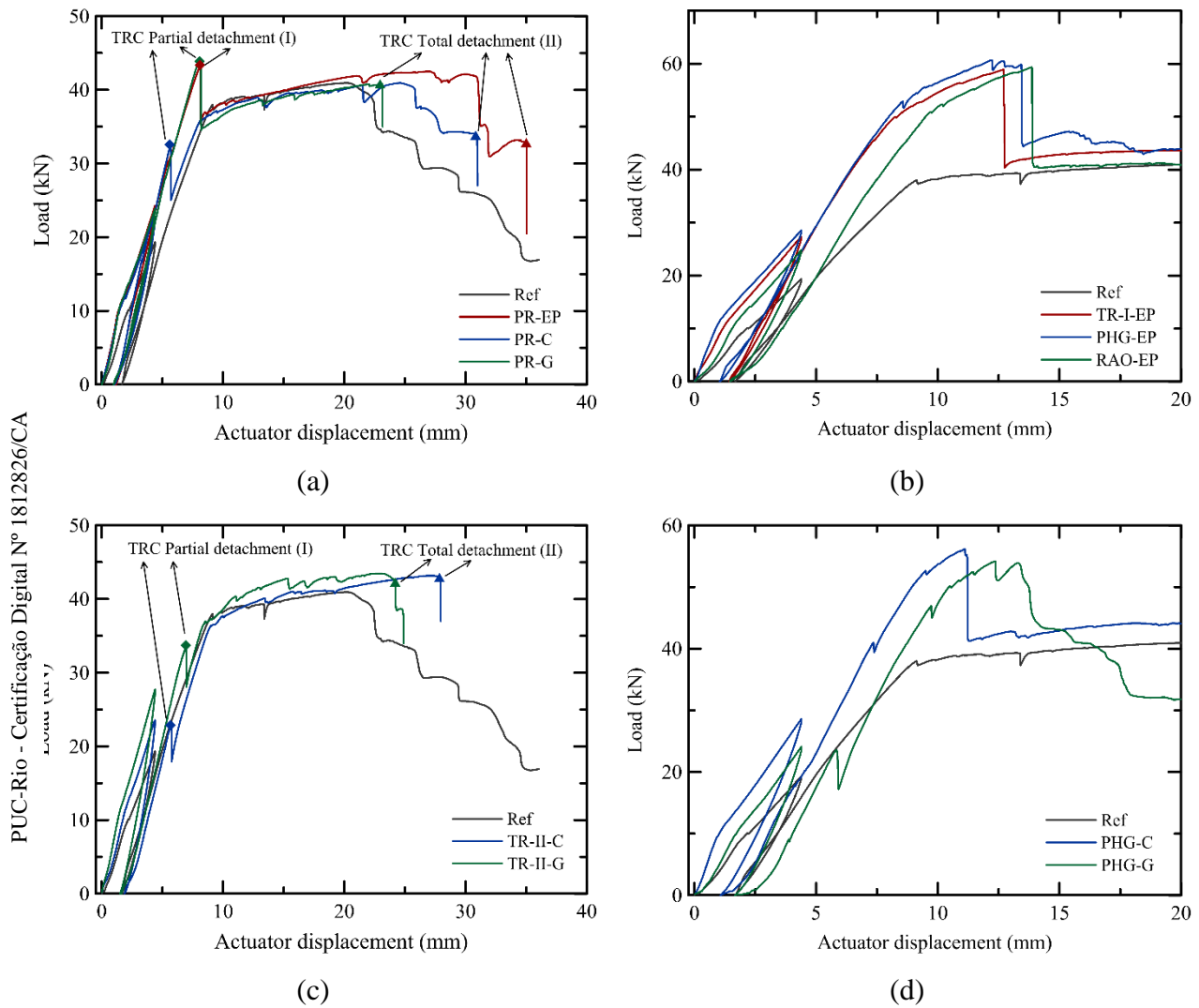
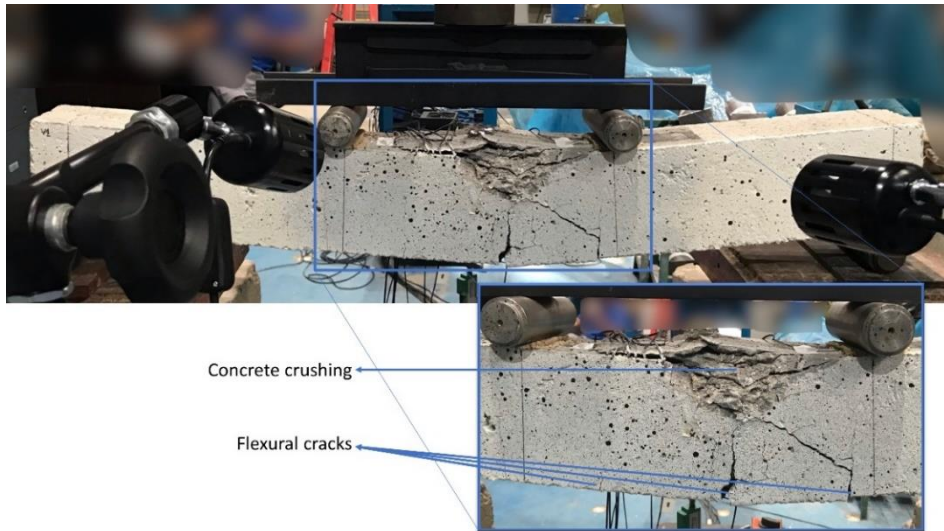
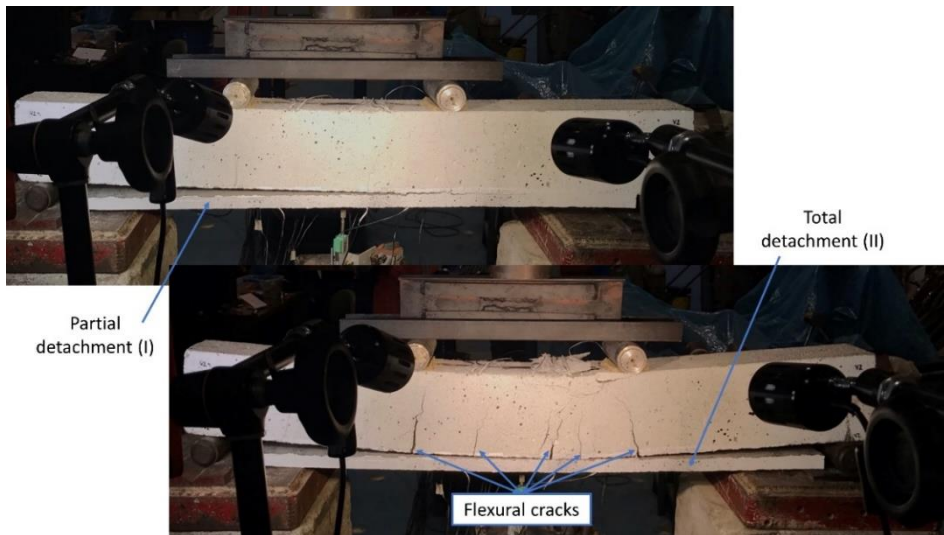


Figure 5.8 – Load vs. actuator displacement of the beams from (a) Batch 1 – PR-EP, PR-C, and PR-G; (b) Batch 2 – TR-I-EP, PHG-EP, and RAO-EP; (c) Batch 3 – TR-II-C and TR-II-G; and (d) Batch 4 – PHG-C and PHG-G.



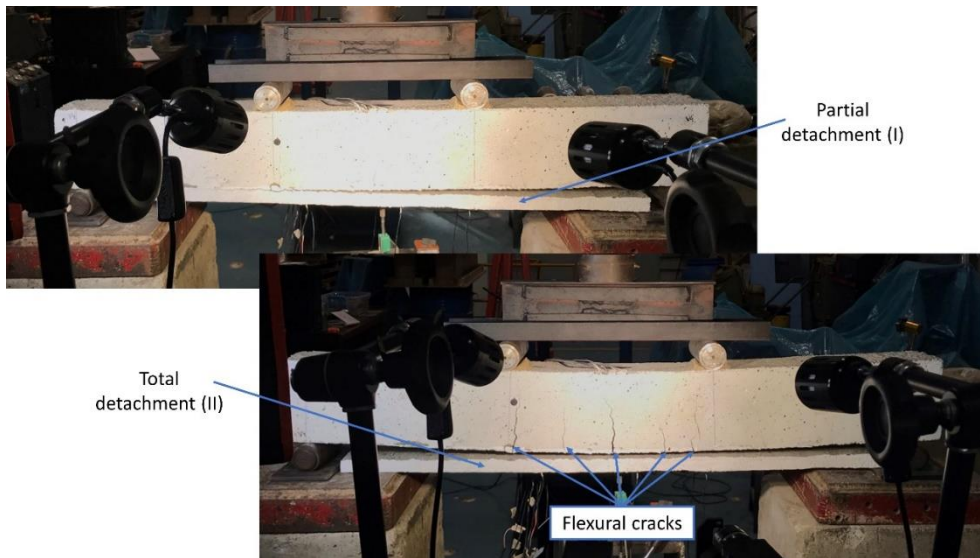
(a) REF



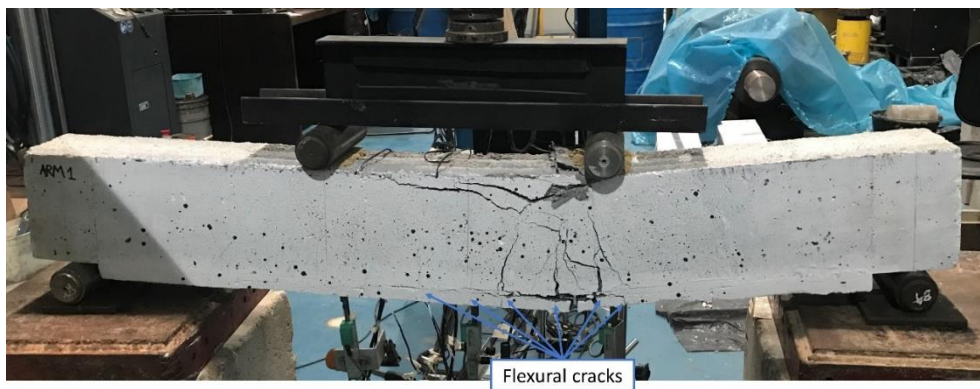
(b) PR-EP



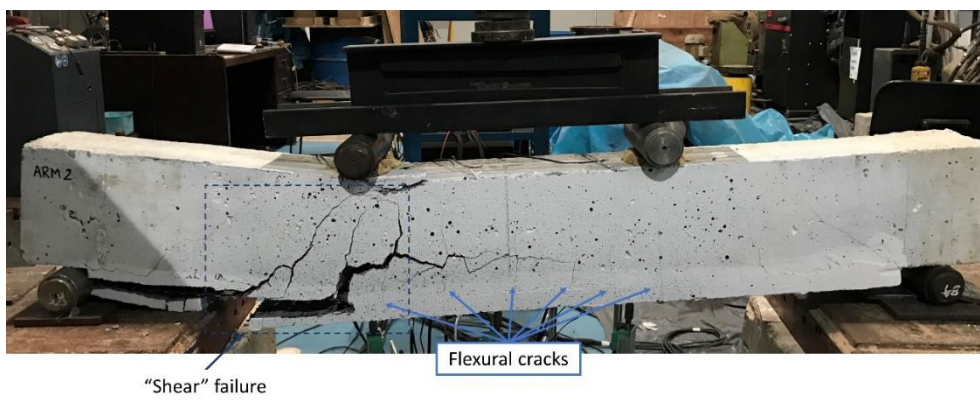
(c) PR-C



(d) PR-G



(e) TR-I-EP



(f) PHG-EP



"Shear" failure

(g) RAO-EP



Partial detachment (I)

Total detachment (II)

Flexural cracks

(h) TR-II-C



Partial detachment (I)

Total detachment (II)

Flexural cracks

(i) TR-II-G



(j) PHG-C



Shear failure

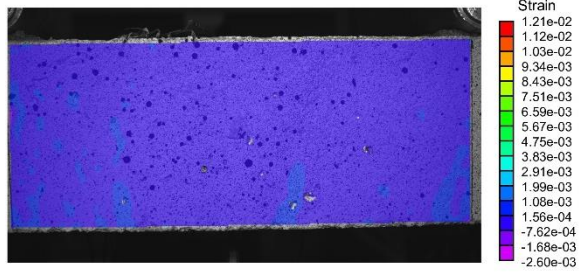
(k) PHG-G

Figure 5.9 – Failure modes of the (a) REF; (b) PR-EP; (c) PR-C; (d) PR-G; (e) TR-I-EP; (f) PHG-EP; (g) RAO-EP; (h) TR-II-C; (i) TR-II-G; (j) PHG-C; (k) PHG-G beams.

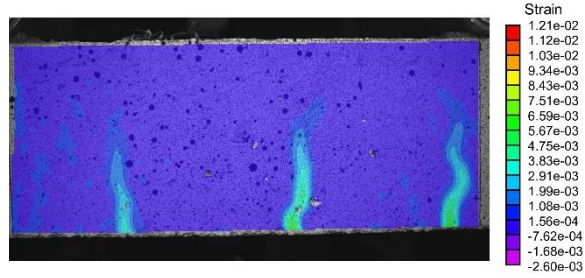
Table 5.8 – Main results obtained for the reference and strengthened RC beams.

Beam	Max load (kN)	Increase of max load (%)
Ref	41.0	-
PR-EP	43.6	6.34
PR-C	41.1	0.244
PR-G	44.2	7.80
TR-I-EP	59.2	44.4
PHG-EP	60.7	48.0
RAO-EP	59.4	44.9
TR-II-C	43.2	5.37
TR-II-G	43.5	6.10
PHG-C	56.2	37.1
PHG-G	54.3	32.4

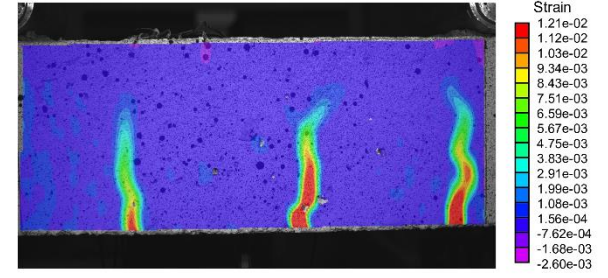
$\delta_{MTS} = 2 \text{ mm}$



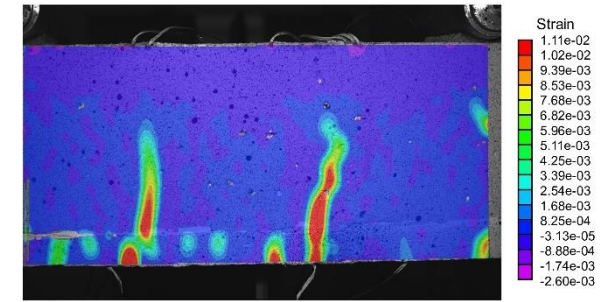
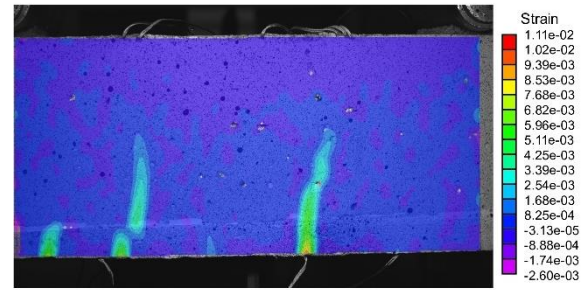
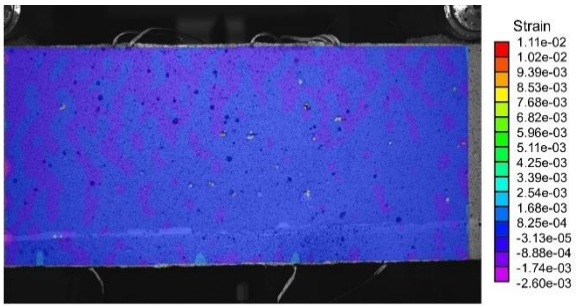
$\delta_{MTS} = 3 \text{ mm}$



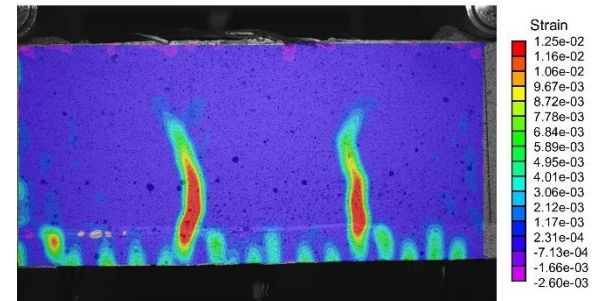
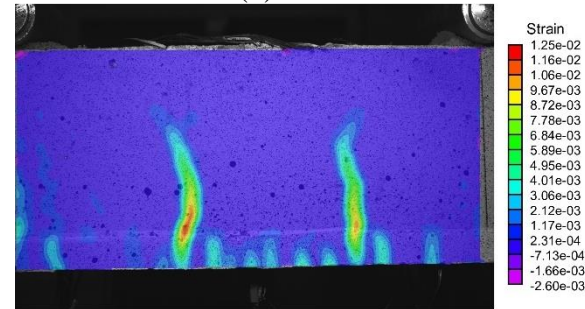
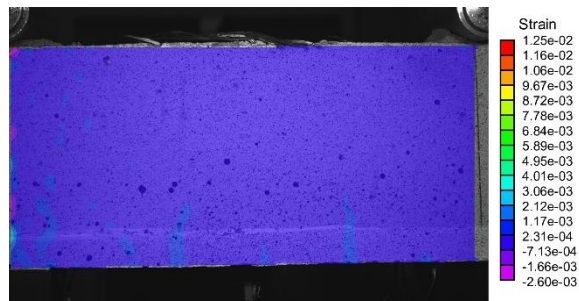
$\delta_{MTS} = 5 \text{ mm}$



(a) REF

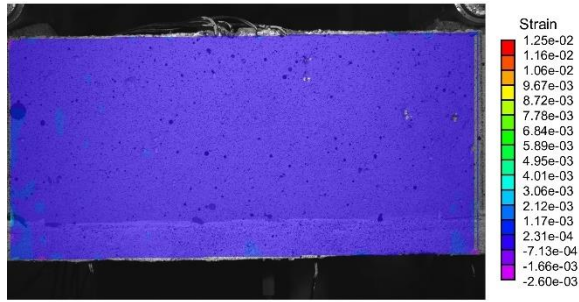


(b) PR-EP

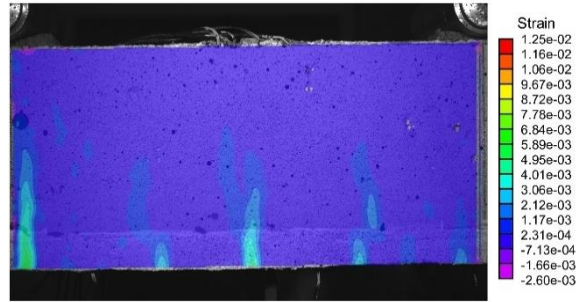


(c) PR-C

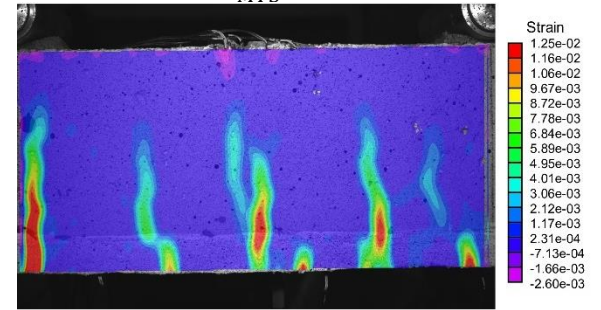
$\delta_{MTS} = 2 \text{ mm}$



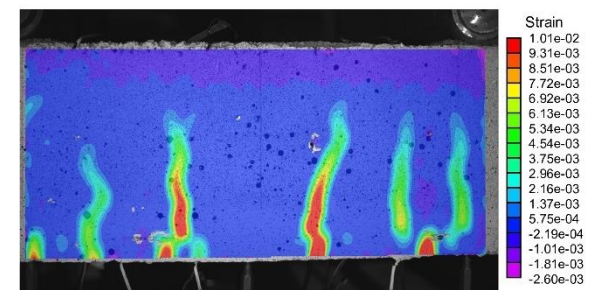
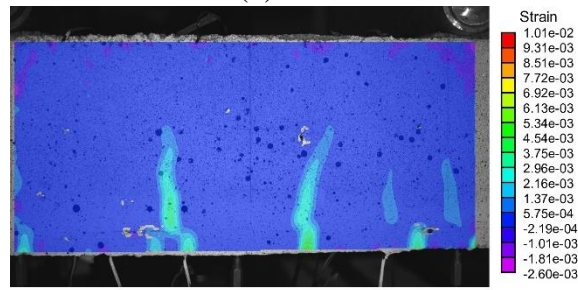
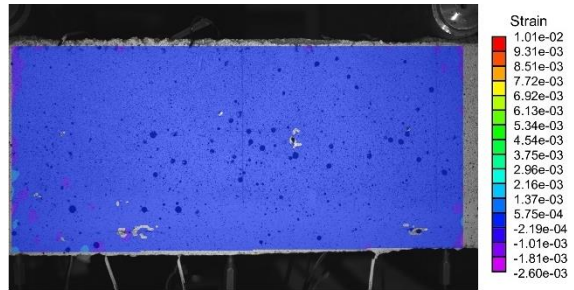
$\delta_{MTS} = 3 \text{ mm}$



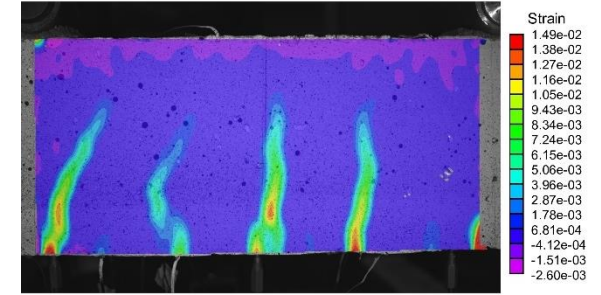
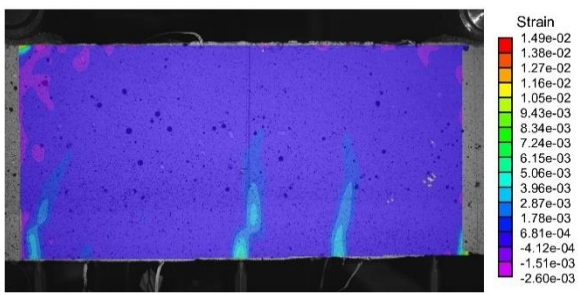
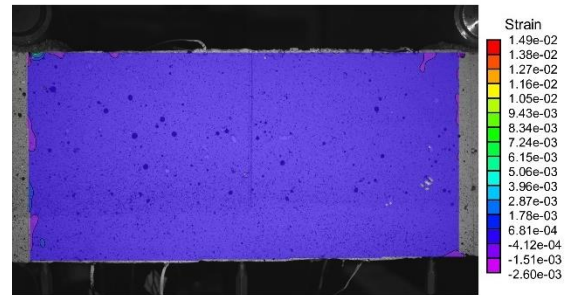
$\delta_{MTS} = 5 \text{ mm}$



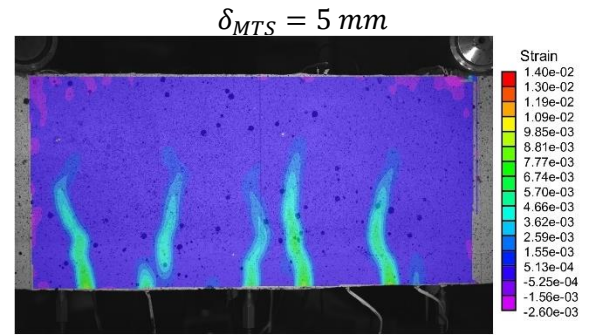
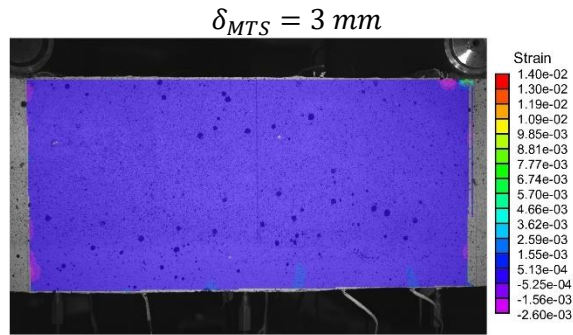
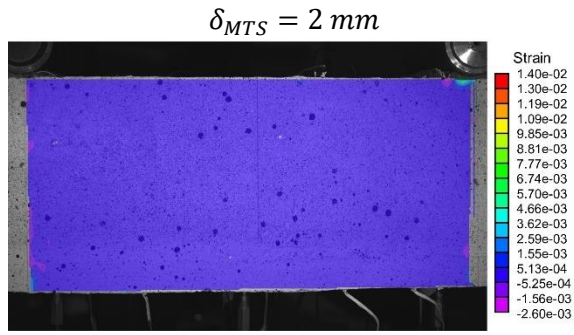
(d) PR-G



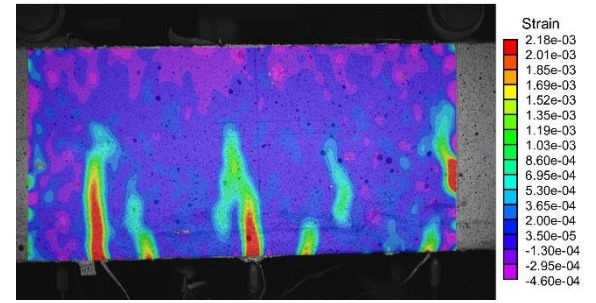
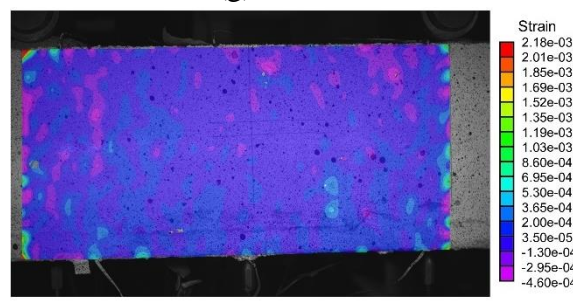
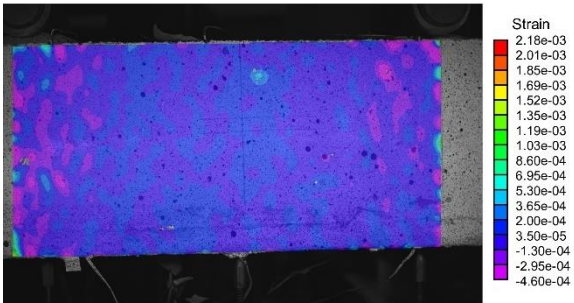
(e) TR-I-EP



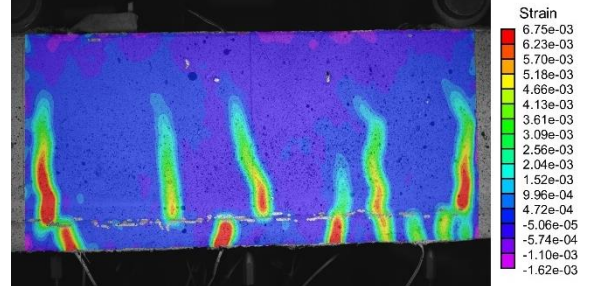
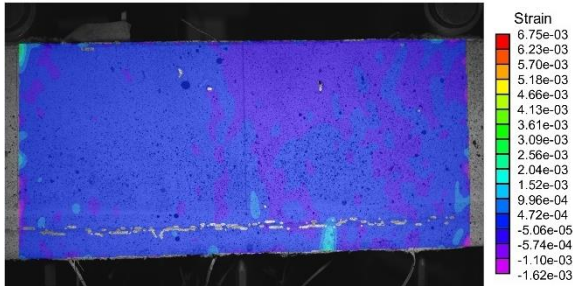
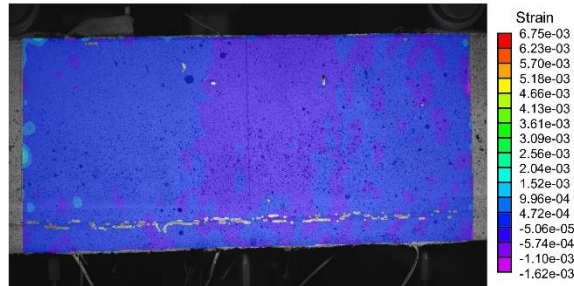
(f) PHG-EP



(g) RAO-EP



(h) TR-II-C



(i) TR-II-G

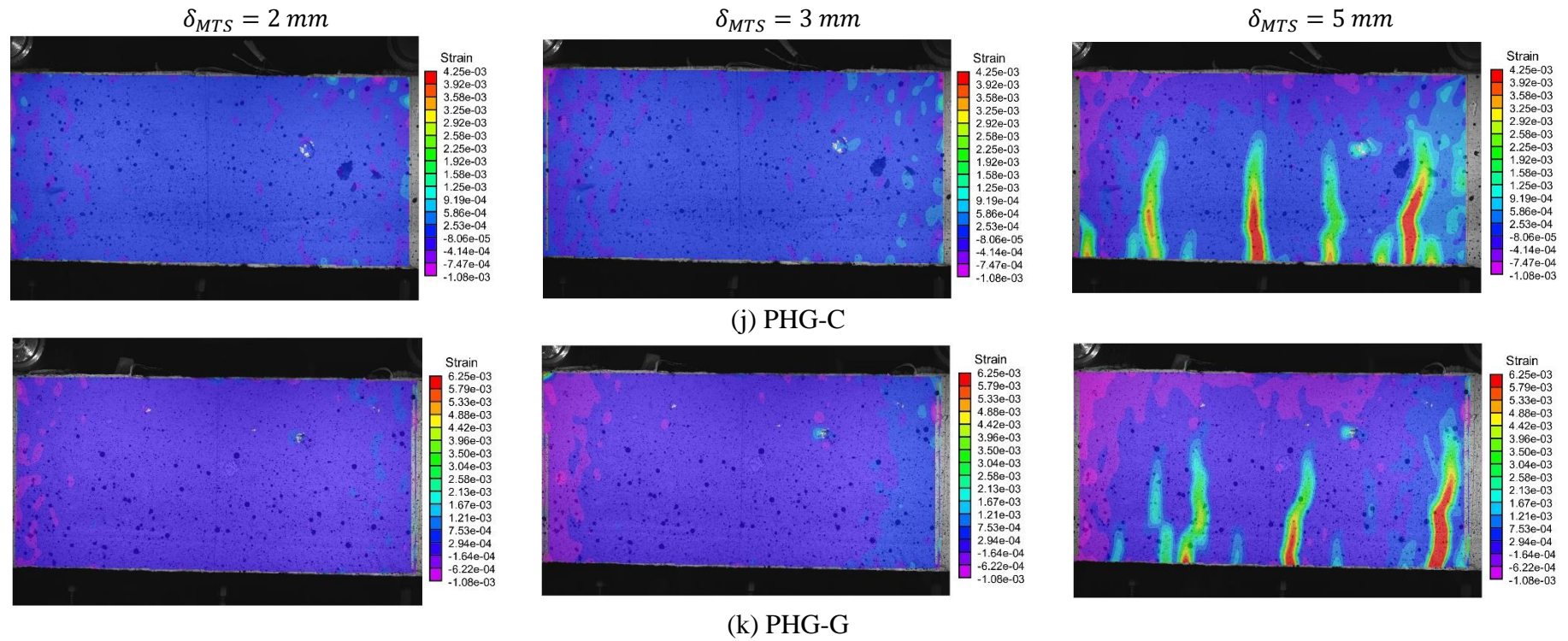


Figure 5.10 – Crack pattern at the actuator displacement (δ_{MTS}) of 2 mm, 3 mm, and 5 mm obtained from the DIC analysis for the (a) REF; (b) PR-EP; (c) PR-C; (d) PR-G; (e) TR-I-EP; (f) PHG-EP; (g) RAO-EP; (h) TR-II-C; (i) TR-II-G; (j) PHG-C; (k) PHG-G beams.

The first strengthening protocol adopted was the Patterned Roughing (PR), as described in Section 5.2.2. As can be seen in Figure 5.9.b, c, and d, there was a total detachment of the TRC-strengthening layer, regardless of the textile reinforcement type used in the composite. However, the strengthening layer did not completely detach all at once; first, it detached only on one side (Partial detachment), and, with the subsequent increase in load, there was the total detachment. The disassembly points can be identified as sudden drops in the load vs. actuator displacement curves (see Figure 5.8. a and c). Thus, the PR substrate preparation method was not adequate to guarantee a collaborative behavior of the TRC-strengthening layer and the RC beam. On the contrary, this same strengthening protocol but with a different material (SHCC) was used by Tinoco et al. [65], and good results regarding the adherence of the strengthening layer to the RC beam were obtained. The external strengthening evaluated consisted of an SHCC whose matrix had a small proportion of fine aggregate to cementitious material, and, in addition, the cement used was a Portland Cement CP V, defined by the Brazilian Standard ABNT NBR 16697 [61], which presents thinner grains than the CP II-F 32 used in this work. In this way, it seems that the strengthening matrix constituted with finer particles is able to better penetrate the grooves created by the roughing process, improving the bond of the strengthening layer towards the RC substrate. Teixeira and Silva [28] also obtained successful results by externally strengthening a RC beam with a natural curauá reinforced cement-based composite made with Portland cement CP V, further corroborating this assumption. Awani et al. [70] prepared the concrete substrate with a manual roughening using an electrical saw performing a pattern coincident to the fabric mesh used as reinforcement in the TRC-strengthening, and obtained good adhesion on double shear tests, with no specimens presenting failure at the concrete/strengthening interface. Nevertheless, even with the total detachment of the strengthening layer, it was possible to observe some evidence that the carbon-TRC presents potential to enhance the load-bearing capacity of RC beams, as long as the strengthening protocol adopted is adequate to guarantee sufficient adhesion for the joint work of the two materials. The PR-EP and PR-G beams were able to achieve 6.34% and 7.80% higher maximum loads, respectively. Additionally, the images obtained from the DIC analysis showed that, before the detachment of the TRC strengthening layer, the flexural cracks were passing through both concrete elements, thus indicating that the RC beam and the TRC were working together (see

Figure 5.10.b, c, and d). It was also possible to observe the starting of the multiple-cracking pattern in the TRC strengthening layer, mainly in the PR-C beam.

Thus, a new batch of beams was prepared with different strengthening protocols, i.e., the Total Roughing (TR) and the aggregate exposure with Retarder paper (PHG) and Retarder Release Agent (RAO). This step was performed only using the EP carbon fabric for comparison reasons. The objective was to find the most suitable strengthening protocol to replicate in the RC beams strengthened with the TRC composed by the MCF fabrics. All methods evaluated in Batch 2 proved to be effective in guarantee proper adhesion and, consequently, the joint work between the RC beam and the strengthening TRC layer. No detachment could be observed in the TR-I-EP, PHG-EP, and RAO-EP beams, as shown in Figure 5.9.e, f, and g. Furthermore, it was possible to see that the flexural cracks formed during the loading passed through the TRC strengthening layer to the RC beam (see Figure 5.10.e, f, and g), corroborating that both concrete elements were working together. The TR-I-EP beam presented a flexural failure, and the PHG-EP and RAO-EP beams exhibited a more aggressive failure mode, with a combination of flexural and shear failure. It was possible to observe a mechanism similar to the dowel effect in the level of the textile reinforcement in the TRC strengthening layer. Probably, the exposure of the aggregates was so intense that the shear resistance mechanisms of the RC beam were affected. The shear strength of a RC element is governed by the transfer of the forces through the non-cracked zone, the transversal reinforcement capacity, the aggregate interlock, and the dowel action [71]. Regardless of the failure mode, all strengthening protocols from Batch 2 were able to enhance the maximum load of the RC beam in the range of 45 – 50%. Therefore, to evaluate the efficiency of the TRC with MCF fabrics as external strengthening of RC beams, the Total Roughing (TR) method was selected, based on the failure mode of the Batch 2 beams, to proceed with the investigation.

Batch 3 was then manufactured for this evaluation. However, as previously mentioned, the roughing was performed manually, and in this case (Total Roughing, TR – II), it was obtained a different result from the first Total Roughing (TR-I), with deeper grooves, but not uniformly distributed in the whole surface (see Figure 5.3.b and d). This difference in the grooves' distribution turned out to be crucial in the bond between the strengthening TRC layer and the RC substrate, and a detachment similar to what occurred in beams PR was observed (see Figure 5.9.h

and i). Additionally, another point that could contribute to the poor bond between the two different aged concretes is the thickness of the textile reinforcement and the amount of matrix in the TRC strengthening layer. The MCF fabrics present higher thickness than the EP carbon fabrics due to the overlapping of the longitudinal and transversal yarns in the knots' regions. Since the thickness of the TRC strengthening layer was kept constant, this means that in the TRC with the MCF fabrics, there is a smaller volume of the fine-grained concrete, which could also influence the adherence between the strengthening layer and the RC substrate. Nevertheless, it is possible to observe in Figure 5.10.h and i that, before the detachment, the formed flexural cracks were passing from the TRC-strengthening layer to the RC beam.

The methods based on the aggregate exposition create a substrate with more edges and hollows that could be advantageous for the strengthening based on the MCF fabrics due to the lower volume of the TRC matrix. Therefore, aiming to establish the best strengthening protocol and to evaluate the effectiveness of the MCF-TRC as a strengthening layer of RC beams, Batch 4 was produced using the Retarder Paper (PHG) strengthening protocol. The Retarder Paper was selected based on the superior enhancement in the maximum load achieved with this strengthening protocol compared to the Retarder Release Agent for the beams in Batch 2. The results obtained show that this strengthening protocol is adequate to guarantee a proper bond and, consequently, the joint mechanical work of the RC beam and the TRC with MCF fabrics strengthening layer. Figure 5.9.j and k show that no detachment took place, and the flexural cracks passed through from the strengthening layer to the RC beam (see Figure 5.10.j and k). The C- and the GP-TRC were able to increase in approximately 30% the ultimate load of the RC beam. The failure mode and the mechanical behavior of the MCF-TRC-strengthened beams will be discussed in the following section.

5.3.2. Strengthening efficiency

The first part of this chapter was focused on establishing the best strengthening protocol for RC beams with carbon TRC based on the joint mechanical work of the strengthening layer and the RC substrate. The results obtained indicated that while for the TRC with EP carbon fabric, the TR-I was the most suitable method, for the TRC with MCF fabrics, the PHG method exhibited

the desired results. Thus, in this second part of the chapter, the mechanical behavior of the TR-I-EP, PHG-C, and PHG-G beams, as well as the effectiveness of the respective TRCs in the strengthening, will be addressed. The reference beam will be also analyzed for comparison purposes.

Figure 5.11 presents the load vs. deflection at mid-span of the reference and the RC beams strengthened with the TRC with the C-MCF, GP-MCF, and EP carbon fabrics. For better visualization and discussion of the results, the curves referring to the 1st loading (pre-loading before the strengthening) and to the 2nd loading (up to failure after the strengthening) were plotted separately. Table 5.9 presents the main results obtained from the bending tests.

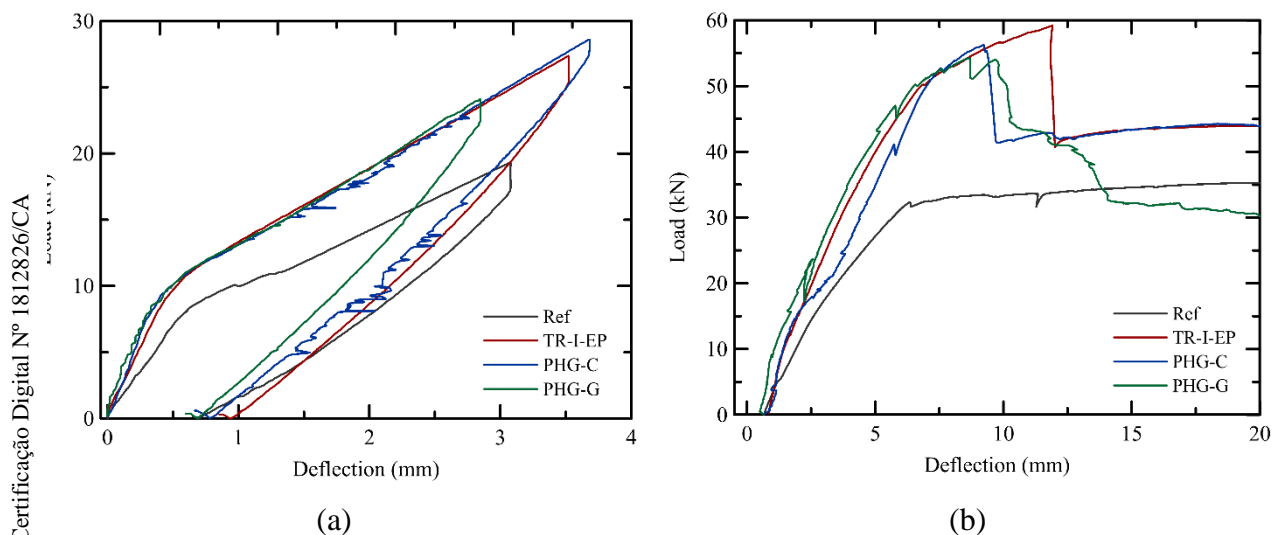


Figure 5.11 – Load vs. deflection at midspan of the reference beam and the RC beams strengthened with the TRC with the C-MCF, GP-MCF, and EP carbon fabric at the a) 1st loading stage (pre-loading); and (b) 2nd loading stage.

Table 5.9 – Main results obtained from the four-point bending tests for the reference and TRC-strengthened beams.

	Ref	TR-I-EP	PHG-C	PHG-G
$f_{c,28d}$ (MPa)	26.7	32.7	23.3	24.9
$E_{c,28d}$ (GPa)	20.0	28.1	26.3	22.7
F_{PL} (kN)	19.3	27.4	28.6	24.1
δ_{PL} (mm)	3.08	3.52	3.68	2.85
δ_r (mm)	0.653	0.856	0.667	0.600
$M_{cr,PL}$ (kNm)	1.09	1.65	1.67	1.50
ρ_{cr} (1/m)	0.000938	0.00165	0.00200	0.00187
$EI_{I,PL}$ (kNm ²)	1166	1291	1094	907
$EI_{II,PL}$ (kNm ²)	192	188	162	171
F_{max} (kN)	35.3	59.2	56.3	54.3
$\delta_{F,max}$ (mm)	19.7	11.9	9.23	8.67
$F_{\delta=15mm}$ (kN)	34.5	43.4	43.3	32.2
$M_{cr,rup}$ (kNm)	-	1.91	1.62	1.67
$M_{y,rup}$ (kNm)	6.94	10.3	9.97	9.33
$EI_{I,rup}$ (kNm ²)	-	1231	1332	1244
$EI_{II,rup}$ (kNm ²)	204	218	242	255

$f_{c,28d}$, $E_{c,28d}$ – concrete compressive strength and modulus of elasticity at 28 days, respectively.

F_{PL} , δ_{PL} – maximum load and deflection at midspan in the pre-loading, respectively.

δ_r – residual deflection at midspan after the pre-loading.

$M_{cr,PL}$, $M_{cr,rup}$ – bending moment equivalent to the limit between State I and II in the moment vs. curvature curve in the pre-loading and second loading, respectively.

ρ_{cr} – curvature equivalent to the limit between State I and II in the moment vs. curvature curve.

$M_{y,rup}$ – Steel Yielding Bending Moment in the moment vs. curvature curve in the second loading..

$EI_{I,PL}$, $EI_{II,PL}$ – bending stiffness in State I and State II in the pre-loading, respectively.

F_{max} , $\delta_{F,max}$ - maximum load and deflection at midspan in the second loading, respectively.

$F_{\delta=15mm}$ – load at the deflection of 15 mm in the second loading.

$EI_{I,rup}$, $EI_{II,rup}$ – bending stiffness in State I and State II in the second loading, respectively.

At the pre-loading stage, all beams are supposed to present the same mechanical behavior since all of them are RC beams with the same dimensions and reinforcement configuration. However, it is possible to observe slight differences in the loading and unloading curves (see Figure 5.11.a), mostly regarding the maximum load and deflection. These variations can be related to the beams' manufacturing process once each beam was cast individually. Additionally, there is a point that is intrinsic to the testing procedure. As previously mentioned, the pre-loading was performed up to a displacement of 4.4 mm, referring to the deflection SLS. The tests were controlled by the actuator displacement until it reached 4.4

mm. However, any existing gap in the setup system can lead to a difference in the beam deflection in the mid-span measured by the LDVT. Nonetheless, all beams presented a residual deflection between 0.600 mm and 0.856 mm.

As can be seen in Figure 5.11.b, all TRC-strengthenings were able to increase the ultimate load of the RC beam. This enhancement was 67.8%, 59.6%, and 53.8% for the TRC with the EP carbon, C-MCF, and GP-MCF fabrics, respectively. After the yielding of the steel rebars, the RC beams strengthened with the TRC-EP e TRC-C were able to maintain higher load levels than the reference beam. The beam strengthened with the G-TRC presented a shear failure (see Figure 5.9.k).

The increase in the load-bearing capacity of the strengthened RC beams followed the same performance pattern of the TRC submitted to tensile loadings, with the TRC with EP carbon fabric presenting the highest tensile strength, followed by the composites with the C-MCF and GP-MCF [47]. However, there is a variation between the difference in the performance of the three types of TRC when submitted to uniaxial tension tests and when applied as external strengthening. In the direct tensile tests, the EP-TRC reached a tensile strength of 116% and 163% higher than the C-MCF- and GP-MCF-TRC, respectively. Applied as external strengthening, the load-bearing capacity increase promoted by the EP-TRC was 5% and 9% higher than the increases promoted by the C-MCF, and GP-MCF-TRC, respectively. The disparity between the difference performance of the TRC submitted to direct tensile loads and flexural reinforcement may be related to a bond issue between the TRC strengthening layer and the concrete substrate. The EP-TRC strengthening layer did not present a complete rupture, which corroborates the assumption that the failure of the strengthened beam could have occurred before the ultimate capacity of the EP-TRC had been reached. This could be associated with a failure in the bond between the TRC-strengthening layer and the RC substrate at higher load levels, even though no detachment was observed. The considerably smaller variation in the performance of the TRC with MCF fabrics as external strengthening allows their application, making them a more suitable alternative, especially in situations that may require a material with elevated thermal resistance.

Figure 5.12 presents the moment vs. curvature curves obtained for the reference and TRC-strengthened beams. The curvatures were obtained through the data recorded by the strain gages placed in the steel rebars. For better visualization

and discussion of the results, the curves referring to the 1st loading (pre-loading before the strengthening) and to the 2nd loading (up to failure after the strengthening) were plotted separately.

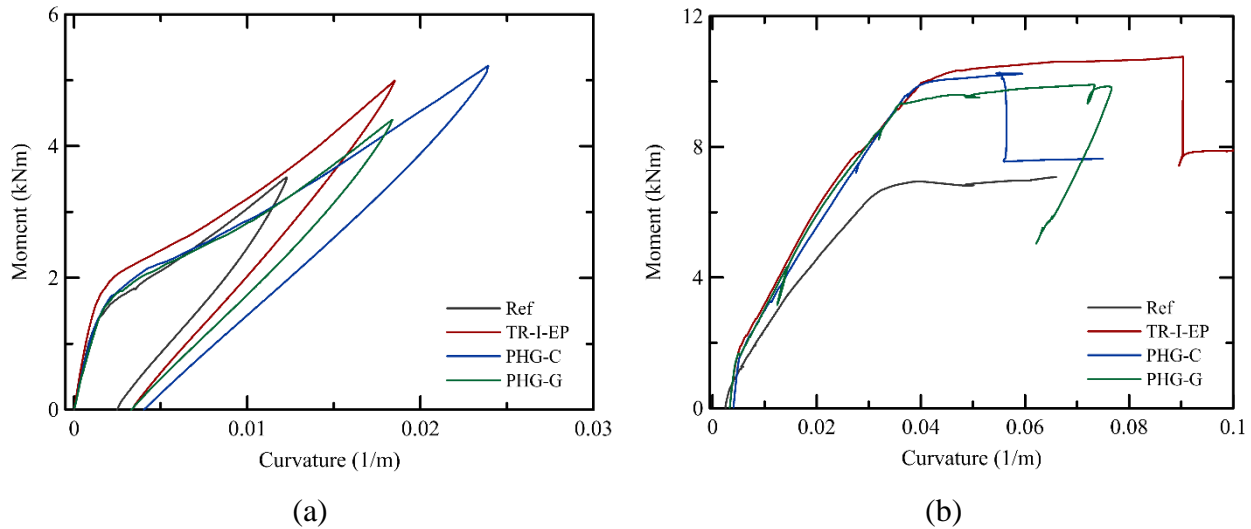


Figure 5.12 – Moment vs. curvature of the reference beam and the RC beams strengthened with the TRC with the C-MCF, GP-MCF, and EP carbon at the a) 1st loading stage (pre-loading); and (b) 2nd loading stage.

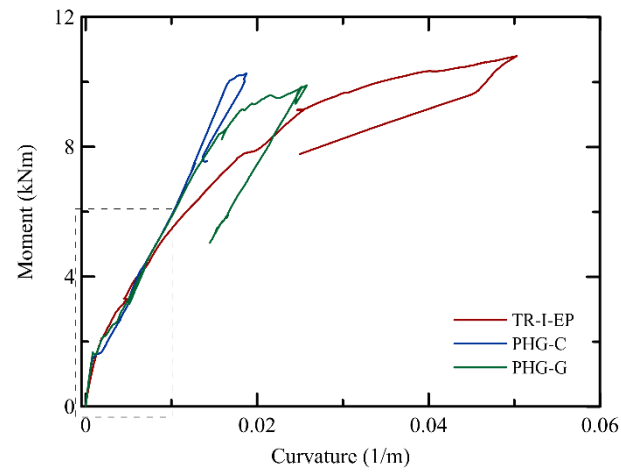
The moment vs. curvature curve of RC beams can be divided into three stages: (i) in State I, the element is uncracked and presents an elastic behavior; (ii) in State II, the element is cracked but also presents an approximately elastic behavior, but with a smaller slope of the curve due to the cracking; (iii) in State III there is the yielding of the steel reinforcement or the crushing of the concrete [71]. All beams presented the typical moment vs. curvature expected for RC beams. However, due to the two-step loading process, the transition between the states occurred in different loading stages. During the pre-loading (1st loading stage), all RC beams achieved State II. The bending moment equivalent to the threshold from State I to State II is the Cracking Bending Moment ($M_{cr,PL}$). Table 5.9 presents the $M_{cr,PL}$ value for each RC beam. After unloading in the 1st loading stage, the RC beams showed a residual curvature due to their cracked configuration. In the 2nd loading stage, the reference beam and the TRC strengthened beams presented a different behavior. The reference beam was already in State II, and with the subsequent increase in the load, the Steel Yielding Bending Moment ($M_{y,rup}$) was reached, and the beam passed to State III. On the other hand, due to the addition of the uncracked TRC strengthening layer, the TRC-strengthened beam presented a new State I when

they were loaded for the second time. The new Cracking Bending Moment ($M_{cr,rup}$) is presented in Table 5.9. After the $M_{cr,rup}$ was reached, the beams entered State II, and similar to the reference beam, with the achievement of the Steel Yielding Bending Moment ($M_{y,rup}$), the TRC-strengthened beams entered State III. The TRC strengthening layer was able to considerably increase the beams' Steel Yielding Bending Moment ($M_{y,PL}$). An enhancement of approximately 48%, 44%, and 34% was observed for the EP-TRC, C-TRC, and GP-TRC beams.

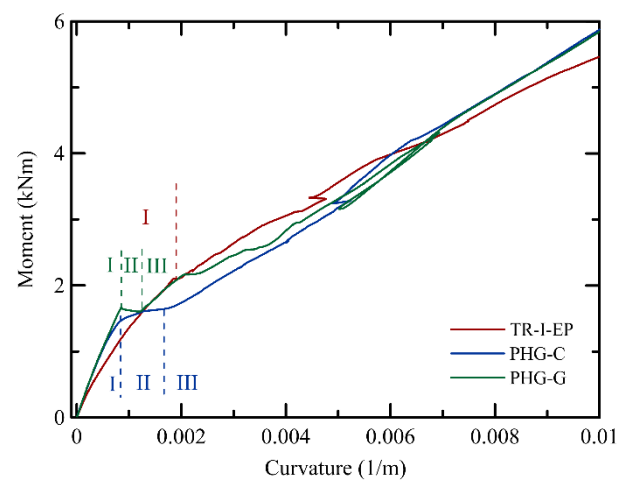
The bending stiffness (EI), i.e., the slope in the moment *vs.* curvature curve, was obtained for State I and II for both loading stages, and its results are shown in Table 5.9. As expected, there is a significant decrease in the stiffness of the RC beams when passing from State I to State II due to concrete cracking. When comparing the State I of the TRC-strengthened beams during both loading stages, an increase of 22% and 37% in the stiffness in the 2nd loading stage can be observed for the C-TRC and GP-TRC beams, respectively. This enhancement can be attributed to the addition of the uncracked TRC layer. However, this was not observed in the beam with the EP-TRC, instead, there was a decrease of 4.7% in the State I stiffness. In addition to the type of carbon fabric, the main difference between the EP-TRC, C-TRC, and GP-TRC strengthened beams was the protocol adopted to prepare the RC substrate to receive the strengthening. The EP-TRC strengthened beam was manually roughened with a hammer drill, which could have contributed to increasing the damage generated in the beam due to the 1st loading. Furthermore, the TRC-strengthened beams presented a higher stiffness in State II than the reference beam, see Figure 5.12.b. This enhancement was 6.9%, 19%, and 25% for the EP-TRC, C-TRC, and GP-TRC strengthened beams, respectively.

The curvature relative to the TRC strengthening layer was also obtained, and Figure 5.13 presents the moment *vs.* textile curvature curves for the TR-I-EP, PHG-C, and PHG-G beams. After reaching the maximum moment, there is an abrupt drop in the curve, characteristic of materials with fragile behavior. In the PHG-C and PHG-G curves, it is possible to identify the three stages characteristic of TRCs, i.e., the linear elastic region, the multiple cracking, and the widening of the cracks (Figure 5.13.b). However, in the TR-I-EP beam curve, Stages II and III are not so distinct, and the specimen presents a less fragile behavior with a higher ultimate curvature than the other two. The moment *vs.* textile curvature of the PHG-EP and RAO-EP specimens shown in Figure 5.14 corroborate that this behavior is a

characteristic of the EP-TRC and not a characteristic of the test since only one specimen was manufactured for each variable.



(a)



(b)

Figure 5.13 – (a) Moment vs. textile curvature curve of the RC beams strengthened with the TRC with the C-MCF, GP-MCF, and EP carbon; and (b) zoom in the early stages.

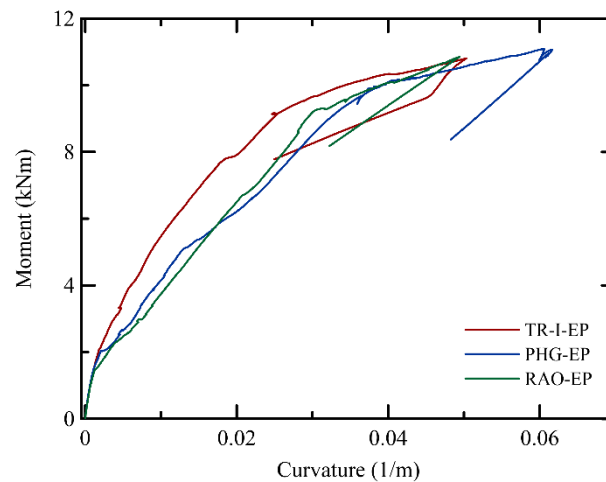


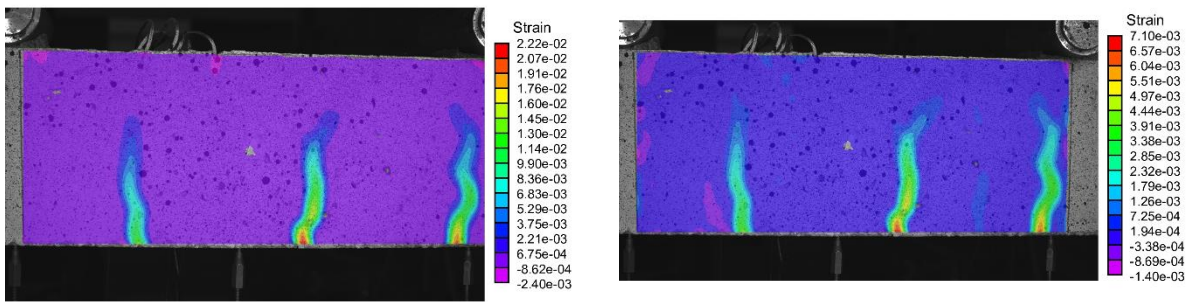
Figure 5.14 – Moment vs. textile curvature curve of the TR-I-EP, PHG-EP, and RAO-EP beams.

- DIC analysis

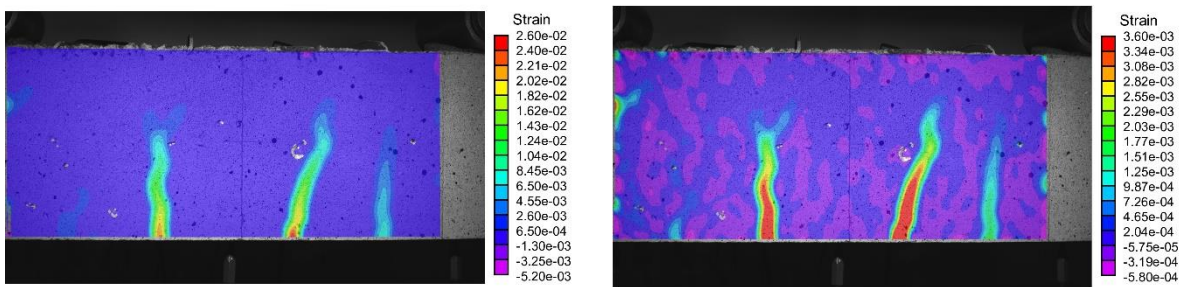
When submitted to tensile stresses, TRC presents a strain-hardening behavior associated with a multiple-cracking pattern [18]. Therefore, in addition to increasing the load-bearing capacity of RC beams, the TRC as a strengthening material could also modify the cracking pattern of the structural elements, inducing the formation of more cracks with smaller widths. Once the cracks are the entrance for deleterious agents that could deteriorate the RC elements [20], it is interesting, in terms of durability, to have a structure with a thinner cracking pattern. To evaluate this assumption, a DIC analysis was performed. Figure 5.15 presents the cracking pattern of the RC beams at the maximum load and after unloading in the pre-loading stage. Figure 5.16 presents the cracking pattern at different deflection levels for the reference and TRC-strengthened beams in the second loading. Table 5.10 exhibits the number of cracks (#), mean spacing between cracks (s_m), and mean crack width (w_m) at the maximum load (equivalent to the SLS-DEF) and immediately after the unloading in the first loading stage, and at the displacement equivalent to the SLS-DEF and maximum load in the second loading stage.

Maximum load

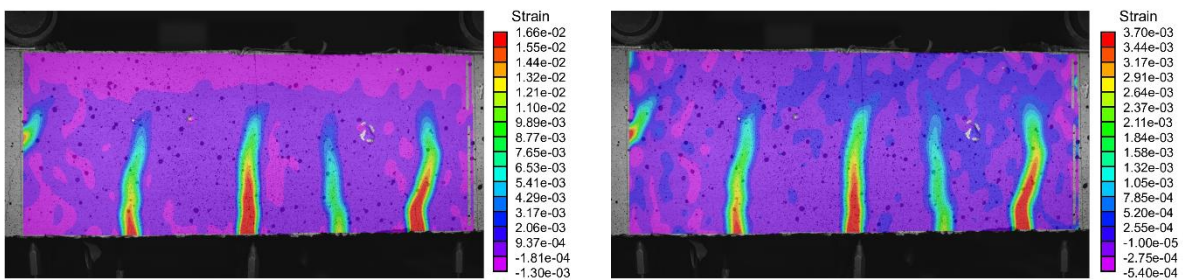
After unloading



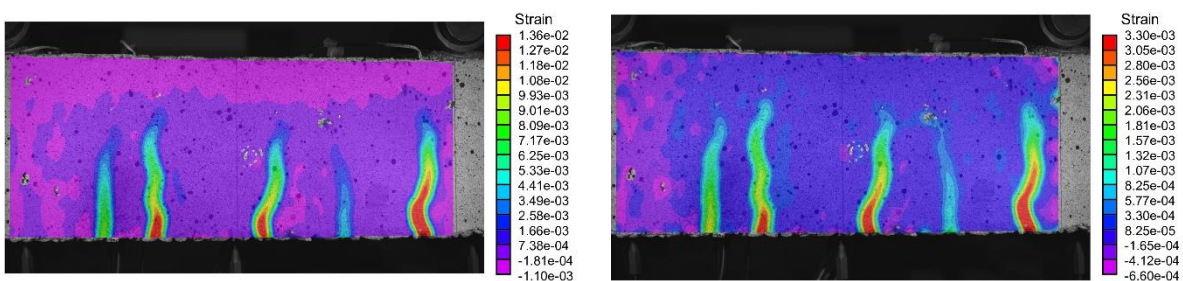
(a)



(b)



(c)



(d)

Figure 5.15 – Cracking pattern of the (a) REF; (b) TR-I-EP; (c) PHG-C; and (d) PHG-G beams at the maximum load (equivalent to the SLS-DEF) and after unloading in the pre-loading stage.

In general RC elements submitted to direct or indirect tension stresses present cracks. The first loading stage was performed to simulate this condition of a RC beam in service condition. The unstrengthen RC beams exhibited 3 to 5 cracks with a mean crack width ranging from 11.6 μm to 20.3 μm at the maximum load point. The mean crack width is inversely proportional to the number of cracks, i.e., the smaller the number of cracks, the greater their width, due to the redistribution of the tensile stresses. As mentioned before, at this point of the experimental program, all beams are equivalent, i.e., they are all RC beams designed with the same concrete properties and steel rebar configuration. These minor variations in the cracking pattern of the RC beams may be related to the small differences observed in their mechanical behavior. With the subsequent removal of the load, the closure of the cracks can be observed, and after the complete unloading, the RC beams exhibited cracks with a mean width varying from 3.3 μm to 7.4 μm .

The TRC-strengthening considerably increased the number of cracks formed during the bending loading, as can be seen in Figure 5.16. At the maximum load, the reference beam exhibited only three cracks, and the TRC-strengthened beams presented from 8 to 15 cracks, depending on the textile reinforcement, representing an increase of approximately 167% to 400%. This enhancement in the crack amount suggests that the TRC achieved the multiple-cracking behavior expected and also indicates that the bond between the RC beam and the TRC strengthening layer was adequate. The PHG-C beam was the one with the greatest number of cracks, followed by the TR-I-EP and PHG-G beams. These results are in accordance with the characterization of the TRC composites submitted to direct tensile loadings [47]. Silva et al. [46] demonstrated that, between the C-MCF and GP-MCF fabrics, the former presents a higher bond towards the fine-grained concrete matrix than the latter, which is related to a chemical incompatibility of the geopolymer impregnation and the cementitious matrix. For this reason, it was expected that the PHG-G beam exhibited a less dense cracking pattern than the PHG-C beam. The TR-I-EP beam presented a slightly less dense cracking pattern than the PHG-C beam, which is also in agreement with the results of the TRC composite characterization [47].

The Reference beam presented the highest crack width at the maximum load, with a mean value of 2.64 mm. The TRC-strengthening was able to significantly reduce this crack parameter, mostly due to its multiple-cracking capacity. The PHG-

C beam exhibited the finest cracking pattern, with a mean crack width of 4.72 μm , followed by the PHG-G (33.3 μm) and the TR-I-EP (64.2 μm) beams. It is interesting to mention that, focusing on the durability of reinforced concrete elements, the Brazilian Standard NBR 6118 [68] recommends a maximum crack width in the range of 0.2 to 0.4, depending on the structure exposure environment class. Considering this parameter, all the TRC strengthened beams meet the recommendation of the standard, even at the maximum load level, which is considerably distant from the maximum recommended deflection in service. Although the TR-I-EP beam presented a greater number of cracks, these cracks, at the maximum load level, are more opened than the cracks of the PHG-G beam. This can be traced back to the different bond mechanisms between the textile reinforcement and the cementitious matrix involved in each case. As discussed by Silva et al. [46], the main bond mechanism between the EP carbon yarn and the fine-grained concrete matrix is a mechanical interlocking, while for the GP-MCF yarn, the chemical bond is the predominant mechanism involved. It is important to emphasize that the standard deviation for the mean cracking width is considerably high for the TR-I-EP and PHG-G beams. This occurs because these two beams present cracks with very different opening levels.

The TRC strengthening also considerably reduced the mean crack width at the SLS-DEF, from 28.7 μm (REF) to 13.3 μm , 3.6 μm , and 15.9 μm for the TR-I-EP, PHG-C, and PHG-G beams. This decrease is related to the increase in the crack number promoted by the TRC multiple-cracking characteristic, from 3 (REF) to 6, 9, and 7, respectively. Usually, the service load of a structure usually does not lead to its collapse. However, it is capable to promote crack formation and growth, which increases the concrete permeability. More permeable concretes facilitate the entrance of water and gases with deleterious agents that promote the degradation of the steel rebars and concrete, negatively impacting the RC durability. Several factors influence concrete permeability, and the crack width is one of them [20]. A specimen with multiple fine cracks is less permeable than one with only one large crack [72]. The higher number of cracks but with smaller widths leads to a lower permeability of water and gas in TRC composites than ordinary concretes [73–75], indicating that the entrance of corrosive substances that can lead to deterioration of the concrete and steel rebars may be considerably reduced. The mechanical properties of the textile affect the TRC permeability, and the use of

coated/impregnated textiles results in more impermeable composites [76]. The use of the TRC as external strengthening is able not only to increase the load-bearing capacity but also to act as a protective layer ensuring good durability of RC structures [77].

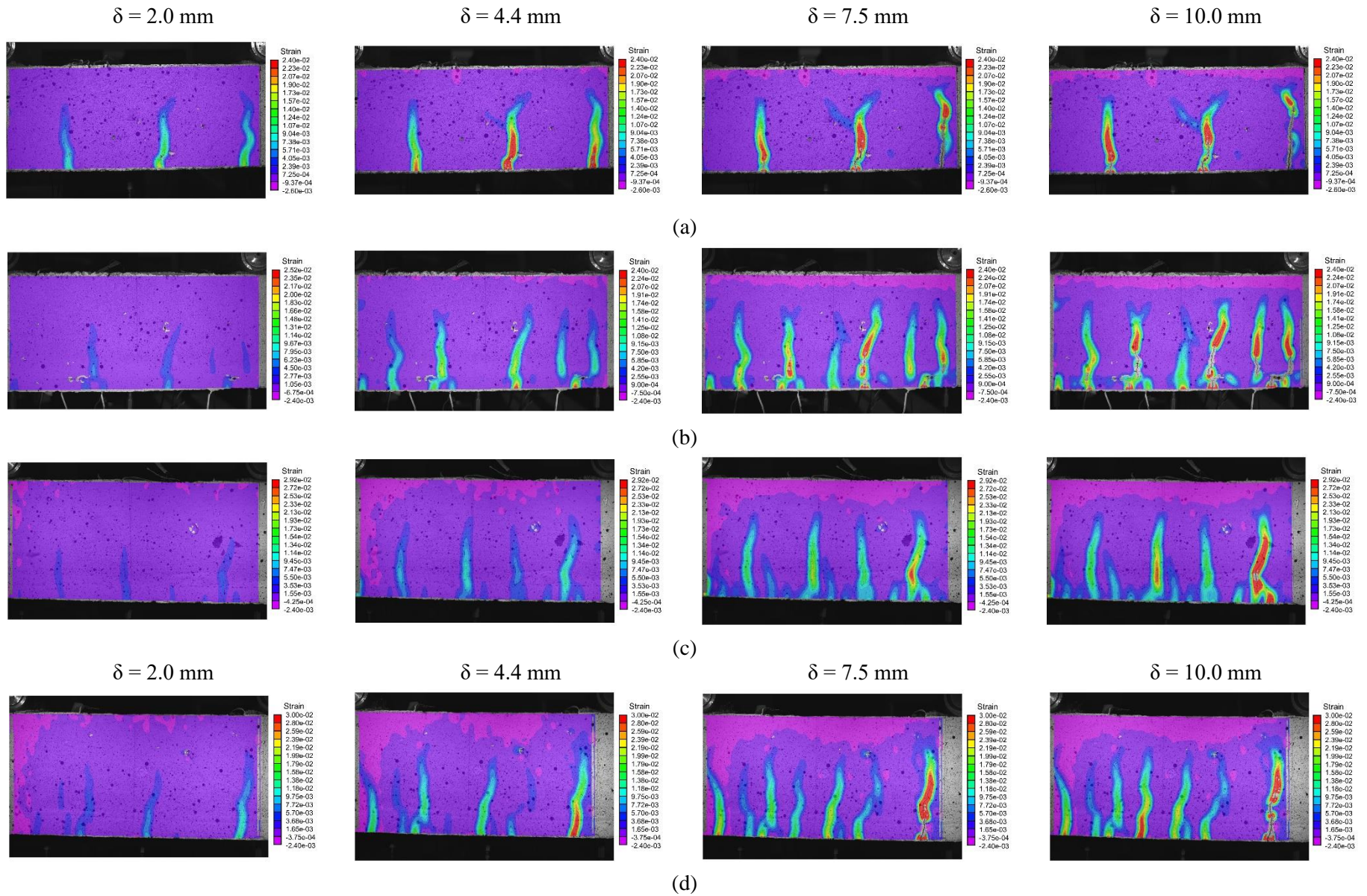


Figure 5.16 – Cracking pattern at different deflection levels in the second loading for the (a) REF; (b) TR-I-EP; (c) PHG-C; and (d) PHG-G beams.

Table 5.10 – Number of cracks, mean spacing between cracks, and mean crack width at different deflection levels in both loading stages.

Beam	#	1 st loading				2 nd loading						
		P _{max} (≈ SLS-DEF)		P _{unloading}		δ = 4.4 mm (SLS-DEF)		P _{max}				
		s _m (mm)	w _m (μm)	#	s _m (mm)	w _m (μm)	#	s _m (mm)	w _m (μm)	#	s _m (mm)	w _m (μm)
REF	3	126 (2.56)	20.3 (2.61)	3	126 (2.52)	7.4 (3.17)	3	128 (2.05)	28.7 (10.5)	3	106 (19.2)	2.64 x 10 ³ (1.24 x 10 ³)
TR-I-EP	3	89.5 (16.5)	15.7 (4.39)	3	89.3 (16.5)	4.5 (1.20)	6	75 (18.6)	13.3 (5.14)	12	27.7 (7.38)	64.2 (101)
PHG-C	4	78.7 (10.8)	14.0 (3.85)	4	78.5 (10.8)	2.8 (0.79)	9	35 (14.9)	3.6 (0.65)	15	17.9 (7.17)	4.72 (2.98)
PHG-G	5	65.3 (15.8)	11.6 (0.579)	5	65.2 (15.8)	3.3 (1.72)	7	48 (20.3)	15.9 (7.05)	8	40.7 (22.3)	33.3 (40.3)

5.3.3. Analytical model

An analytical model of the bending capacity of the TRC-strengthened beams was proposed to validate the experimental results. The following assumptions, based on the design method for RC beams, were considered: i) plane sections remain plane after bending (Bernoulli's principle); ii) perfect bond between the concrete and the steel reinforcement and between the concrete and the TRC strengthening layer; and iii) collaboration of the concrete between cracks (*tension stiffening*).

The analytical model proposed is based on the moment-curvature relationship of the beam. Figure 5.17 presents a typical scheme based on the internal strain and stress distribution for RC beams. For a given curvature, there is a pair “neutral axis, resistant moment (MR)” that can be obtained through the balancing of forces and moments by Equations (5.1) to (5.3).

$$\sum F = 0 \rightarrow -F_{cc} + F_{ct} + F_s + F_{TRC} = 0 \quad (5.1)$$

$$-(0.8x \times b \times \sigma_{cc}) + \left(\frac{(h-x) \times b}{2} \times \sigma_{ct} \right) + [A_s \times \sigma_s] + [A_{TRC} \times \sigma_{TRC}] = 0 \quad (5.2)$$

$$M_R = -(F_{cc} \times x) + \left[F_{ct} \times \frac{2}{3}(h-x) \right] + [F_s(d-x)] + \left[F_{TRC} \left(h + \frac{h_{TRC}}{2} - x \right) \right] = 0 \quad (5.3)$$

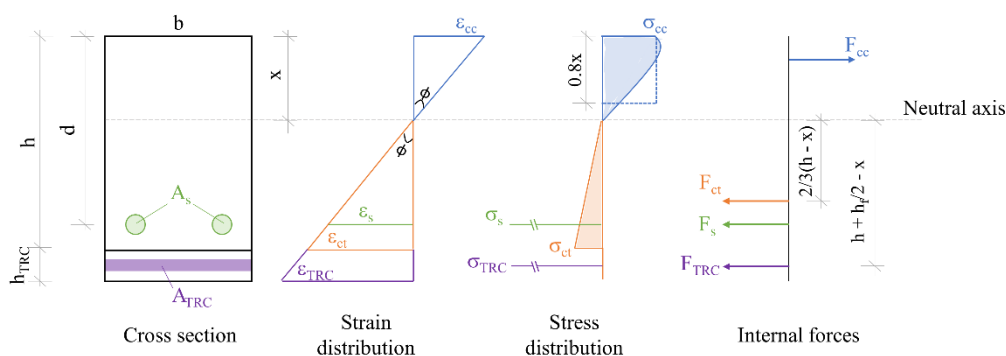


Figure 5.17 – Internal strain and stress distribution for the RC beams.

Figure 5.18 presents the constitutive laws adopted for the concrete in compression and tension, the steel reinforcement, and the TRC-strengthening necessary to implement the analytical model.

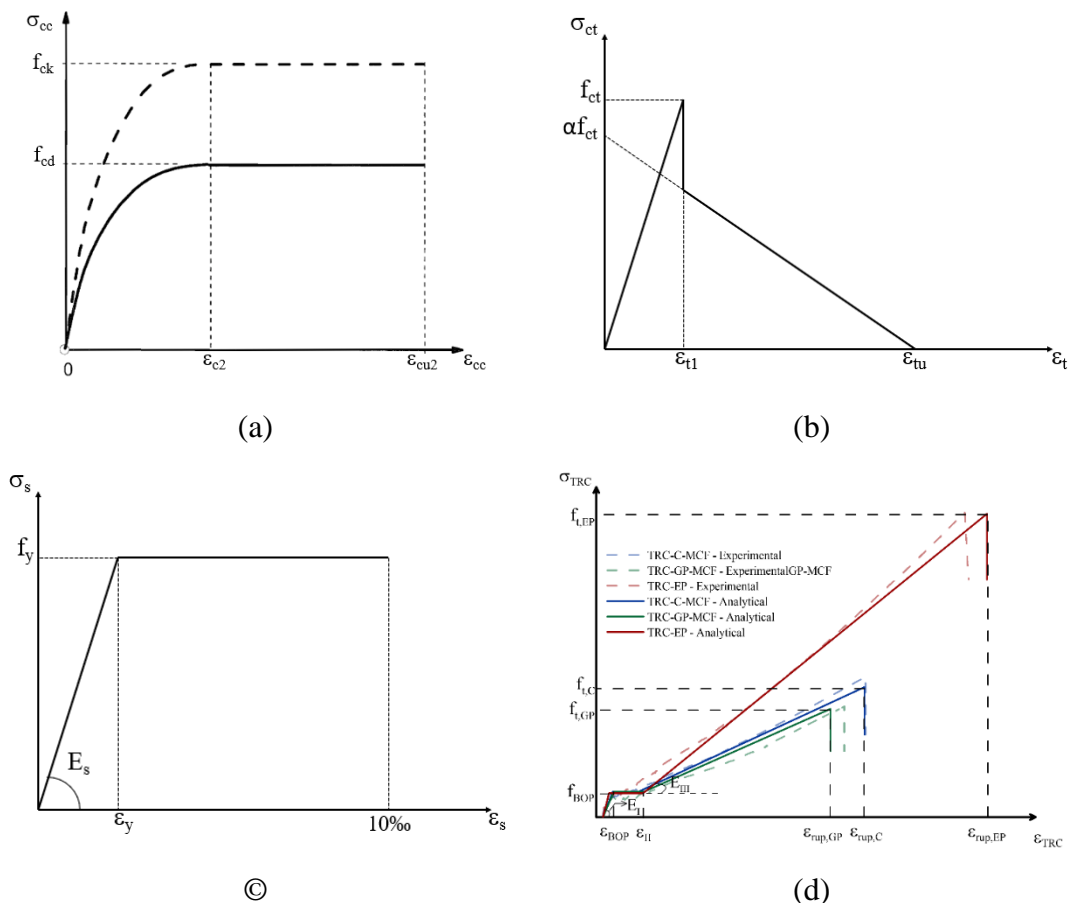


Figure 5.18 – Constitutive laws assumed in the model for the (a) concrete in compression (adapted from [69]); (b) concrete in tension (adapted from Hinton and Owen apud [78]); (c) steel reinforcement in tension (adapted from [68]); (d) TRC strengthening layer.

For the concrete in compression, it was assumed a parabola-rectangle diagram described by Equations (5.4) and (5.5), according to Eurocode 2 [69].

$$\sigma_{cc} = f_{cd} \left[1 - \left(1 - \frac{\epsilon_c}{\epsilon_{c2}} \right)^n \right] \quad \text{for } 0 \leq \epsilon_c \leq \epsilon_{c2} \quad (5.4)$$

$$\sigma_{cc} = f_{cd} \quad \text{for } \epsilon_{c2} \leq \epsilon_c \leq \epsilon_{cu2} \quad (5.5)$$

where f_{cd} is the compressive strength; n is 2; ϵ_{c2} is the strain at reaching the maximum strength (= 2.0 ‰); ϵ_{cu2} is the ultimate strain (= 3.5 ‰). The compressive strength value obtained in the experimental tests was adopted (see Table 5.9).

For the concrete in tension, the tension stiffening behavior was considered by a model suggested by Hinton and Owen (apud [78]) described by Equations (5.6) and (5.7).

$$\sigma_{ct} = \varepsilon_t \times E_c \quad \text{for } 0 \leq \varepsilon_t \leq \varepsilon_{t1} \quad (5.6)$$

$$\sigma_{ct} = \alpha f_{ctm} \left(1 - \frac{\varepsilon_t}{\varepsilon_{tu}}\right) \quad \text{for } \varepsilon_{t1} \leq \varepsilon_t \leq \varepsilon_{tu} \quad \text{and } 0.5 \leq \alpha \leq 0.7 \quad (5.7)$$

where f_{ctm} is the concrete tensile strength. According to the Brazilian Standard NBR 6118 [68], it was adopted as $f_{ctm} = 0.3f_{ck}^{2/3}$ with f_{ck} being the concrete compressive strength obtained in the experimental tests (see Table 5.9). The modulus of elasticity obtained from the compression experimental tests (see Table 5.9) was adopted. In the present work, $\alpha = 0.6$ and $\varepsilon_{tu} = 0.002$ were adopted, as suggested by Hinton and Owen (apud [78]).

An elastic-linear behavior up to the yielding point described by Equations (5.8) and (5.9) was assumed for the steel reinforcement, according to traditional standards for the design of RC elements [68,69].

$$\sigma_s = \varepsilon_s \times E_s \quad \text{for } 0 \leq \varepsilon_s \leq \varepsilon_y \quad (5.8)$$

$$\sigma_s = f_y \quad \text{for } \varepsilon_y \leq \varepsilon_s \leq 10\% \quad (5.9)$$

where E_s and f_y were adopted as 210 GPa and 500 MPa, respectively, according to the Brazilian Standard NBR 6118 [68].

A tri-linear diagram based on the experimental results reported in [47] was used as the constitutive law for the TRCs, see Figure 5.18.d. The first stage represents Stage I, in which the composite is intact (uncracked). The multiple-cracking stage (Stage II) was represented by a plateau with the first crack stress. Finally, the last stage was represented by an elastic-linear behavior governed by the modulus of elasticity of Stage III. All parameters limiting the stages for each TRC were obtained from the direct tensile test results performed in the composites and are shown in Table 5.11. The first crack stress (f_{BOP}) and the maximum tensile stress (f_t) were obtained as a function of the modulus of elasticity in Stage I and Stage III and the respective strains.

Table 5.11 – Limit parameters for the tri-linear tensile vs. strain analytical curve for the TRC.

TRC	ε_{BOP} (%)	E_I (GPa)	f_{BOP} (MPa)	ε_{II} (%)	E_{III} (GPa)	ε_{rup} (%)	f_t (MPa)
EP	0.0221	13.1	2.90	0.148	2.59	1.42	36.8
C-MCF	0.0362	8.58	3.11	0.133	1.63	0.967	15.8
GP-MCF	0.0398	7.75	3.08	0.152	1.56	0.841	13.1

An interactive method was applied following the sequence of steps presented in Figure 5.19, and the moment-curvature vectors were determined for each position of the neutral axis.

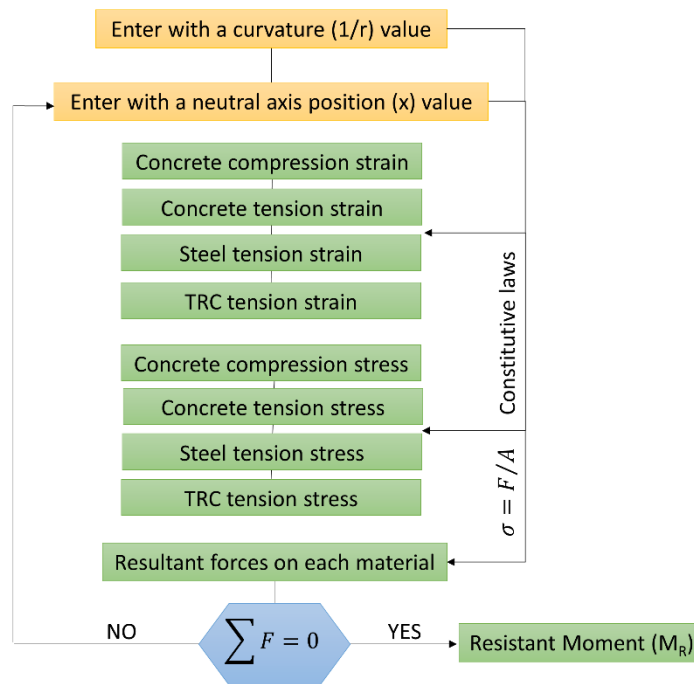


Figure 5.19 – Flow of steps to obtain the moment-curvature vectors of the reference beam.

Figure 5.20 presents the analytical and experimental moment vs. curvature curves for the reference and TRC-strengthened beams. Additionally, an experimental curve of an RC beam with the same geometry and steel reinforcement configuration and only one loading stage performed by Teixeira and Silva [28] was also plotted as a comparison.

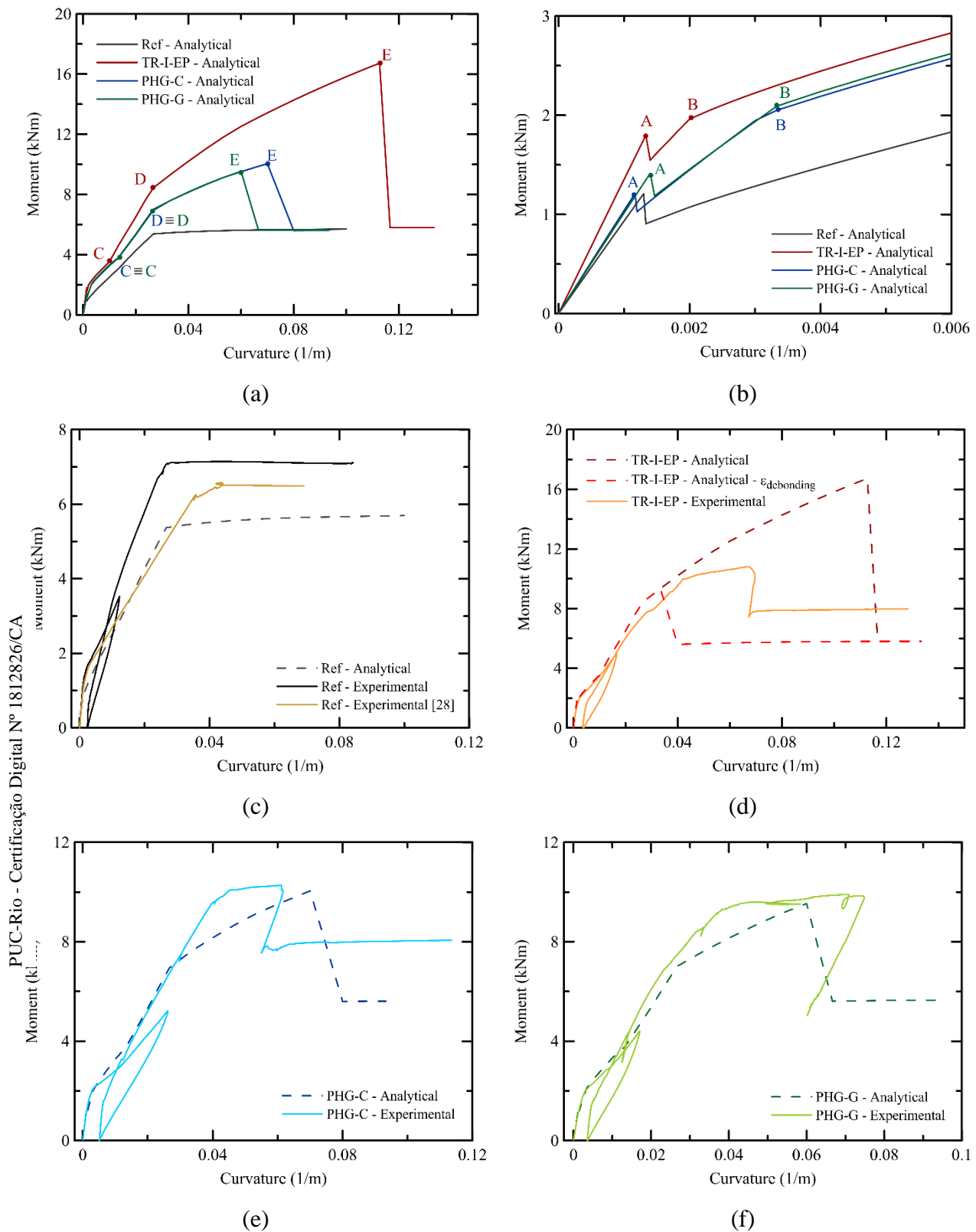


Figure 5.20 – Moment vs. curvature curves. (a) Analytical for the reference and TRC strengthened beams; (b) zoom of the initial section of the curves in a; (c) Experimental and analytical curves for the reference beam; (d) Experimental and analytical curves for the TR-I-EP beam; (e) Experimental and analytical curves for the PHG-C beam; (f) Experimental and analytical curves for the PHG-G beam.

All analytical curves of the strengthened beams demonstrated the better performance of these beams compared to the reference beam. The analytical curve for the reference beam presents the expected three different stages, i.e., uncracked state, cracked state, and yielding of the steel reinforcement. However, different from the experimental results, there is a sudden drop in the moment value in the transition between States I and II. This is probably because, in the analytical model, an abrupt transition from one stage to another is considered, whereas in practice, this transition occurs gradually. The analytical curves of the TRC-strengthened beams showed more than the 3 stages, mainly due to the constitutive model adopted for the TRC strengthening layer, and can be divided into 5 parts, as can be seen in Figure 5.20.d, e, and f. The first part, up to point A, corresponds to State I. Similar to the reference beam, at this point, there is a drop in the curve due to the abrupt transition between states considered in the analytical model. At point B, there is a change in the slope of the curve due to the transition from Stage I to Stage II of the TRC layer. Stage II of the TRC ends at point C. At point D, there is the yielding of the steel reinforcement. The curve does not present a plateau after this point due to the contribution of the TRC-strengthening layer to the moment resistance of the section. The maximum capacity of the TRC is reached at point E. After this point, the analytical curves of the TRC-strengthened beams presented the same load level as the reference beam. This may be related to the brittle rupture of the TRC layer considered in the constitutive model.

In the early stages, the analytical curves of the TRC-strengthened beams presented behavior very similar to the experimental curves. Furthermore, the analytical curves of the PHG-C and PHG-G beams reached a bending moment capacity at the same level as those obtained experimentally. This indicates that the proposed analytical model can be used to estimate the maximum bending capacity of RC beams strengthened with C- and GP-MCF carbon fabrics. On the other hand, for the TR-I-EP beam, the maximum bending moment obtained by the analytical model was considerably higher than the experimental one. As the proposed analytical model considers the maximum capacity of the TRC used as strengthening, this difference indicates that in practice, the TRC-EP did not reach its maximum capacity. This could be related to a not-perfect bond between the concrete substrate and the TRC layer, which led to the premature failure of the beam, even though no detachment could be detected during the test.

Up to this point, the analytical model was considering the ultimate capacity of the TRC-strengthening obtained from direct tension tests. However, due to debonding mechanisms that can govern the failure mode of TRC-strengthened elements, the limit of the TRC-strengthening capacity can be related to a debonding strain. To evaluate the influence of this parameter in the overall behavior of the TR-I-EP, an estimation for the debonding strain of the TR-I-EP was obtained through Equation (5.10), proposed by Bencardino et al. [58].

$$\varepsilon_{debonding} = \frac{\Delta M}{0.9hA_{TRC}E_{TRC}} \quad (5.10)$$

$$\Delta M = \frac{\Delta F}{2}L_1 \quad (5.11)$$

where ΔM is the TRC contribution to the flexural strength, ΔF is the load difference of the TRC-strengthened beam and the reference beam at the point of the maximum load of the TRC-strengthened beam ($\Delta F = 59.2 - 35 [kN]$), L_1 is the distance of the support to the load application point ($L_1 = 365 \text{ mm}$), h is the height of the cross-section, A_{TRC} is the composite cross-section area, and E_{TRC} is the modulus of elasticity of the TRC in Stage III of the stress vs. strain curve obtained from direct tensile tests.

Figure 5.20.d presents the analytical moment vs. curvature of the TR-I-EP beam considering the debonding strain ($\varepsilon_{debonding}$) as the capacity limit of EP-TRC instead of the rupture strain (ε_{rup}). A better correlation with the experimental results was obtained. However, the analytical maximum moment was smaller than the experimental one, which may be related to the fact that the debonding is considered to occur all at once. After the debonding strain is reached, the TRC no longer contributes to the resistant moment.

5.4. Conclusions

The present work investigated the efficiency of different carbon-TRCs in the strengthening of RC beams. For this, the most suitable strengthening protocol was defined depending on the type of carbon fabric used as textile reinforcement. Bending tests were conducted, and an analytical model was proposed to estimate the flexural capacity of the TRC-strengthened beams. The following conclusions can be taken:

- For the strengthening with the EP-TRC, the total roughening of the surface proved to be the most effective substrate preparation protocol, as there was a joint work between the TRC-strengthening layer and the RC beam without changing the failure mode. For the strengthening with the MCF-TRCs, the best strengthening protocol was based on the aggregate exposure with the retarder paper. The difference between substrate preparation methods depending on the type of textile reinforcement was associated with the amount of matrix in each TRC since the thickness of the TRC was kept constant, and the MCF fabrics present a thickness considerably higher than the EP carbon fabric due to their manufacturing method.
- With the proper strengthening protocol, all TRC-strengthened beams exhibited higher maximum loads. This enhancement was 67.8%, 59.6%, and 53.8% for the TRC with the EP carbon, C-MCF, and GP-MCF fabrics, respectively. The small difference in the load capacity gain makes the strengthening with MCF-TRCs a viable option to replace EP-TRCs, especially in high-temperature situations. After the yielding of the steel rebars, the RC beams strengthened with the TRC-EP e TRC-C were able to maintain higher load levels than the reference beam.
- The TRC strengthening was also able to increase the flexural stiffness of the RC beams in State II. This enhancement was 6.9%, 19%, and 25% for the EP-TRC, C-TRC, and GP-TRC strengthened beams, respectively.
- The TRC strengthening altered the cracking pattern of the RC beams. The TRC-strengthened beams presented a greater number of finer cracks. This is particularly interesting from a durability aspect. Cracks with smaller widths limit the entry of deleterious agents that can lead to damage to the concrete and steel reinforcement.
- An analytical model based on moment *vs.* curvature curves was proposed. The results show that the proposed model can be used to estimate the maximum bending capacity of RC beams strengthened with C- and GP-TRCs. However, the model overestimated the

ultimate moment of the EP-TRC strengthened beams. This may be related to the fact that the EP-TRC did not reach its maximum capacity, which could be related to a failure in the bond between the TRC-strengthening layer and the RC substrate, which may have led to a premature failure of the beam, even without any detachment having been detected. When implementing a debonding strain in the model, a better correlation between the analytical and experimental moment vs. curvature curves was obtained for the TR-I-EP beam.

5.5. References

- [1] DIAB, Y. G. Strengthening of RC beams by using sprayed concrete: Experimental approach. **Engineering Structures**, v. 20, n. 7, p. 631–643, 1998.
- [2] TSONOS, A. D. G. Performance enhancement of R/C building columns and beam-column joints through shotcrete jacketing. **Engineering Structures**, v. 32, n. 3, p. 726–740, 2010.
- [3] DEMIR, A.; TEKIN, M. Strengthening of reinforced concrete (RC) beams with prefabricated reinforced concrete (RC) plates. **Scientific Research and Essays**, v. 6, n. 21, p. 4577–4586, 2011.
- [4] GANESH, P.; MURTHY, A. R. Repair, retrofitting and rehabilitation techniques for strengthening of reinforced concrete beams - A review. **Advances in Concrete Construction**, v. 8, n. 2, p. 101–117, 2019.
- [5] HARAJLI, M. H. Strengthening of Concrete Beams by External Prestressing. **PCI Journal**, v. 38, n. 6, p. 76–88, 1993.
- [6] TAN, K. H.; TJANDRA, R. A. Strengthening of RC Continuous Beams by External Prestressing. **Journal of Structural Engineering**, v. 133, n. 2, p. 195–204, 2007.
- [7] ZOU, J. et al. Experimental study on flexural behavior of concrete T-beams strengthened with externally prestressed tendons. **Mathematical Biosciences and Engineering**, v. 16, n. 6, p. 6962–6974, 2019.
- [8] SEREÇA, S.; FAUSTMANN, D. H. Flexural strengthening of reinforced concrete beams using external tendons. **Engineering Structures**, v. 252, n. November 2021, 2022.
- [9] TRIANTAFILLOU, T. C.; PLEVRIS, N. Strengthening of RC beams with

epoxy-bonded fibre-composite materials. **Materials and Structures**, v. 25, n. 4, p. 201–211, 1992.

[10] CHAJES, M. J. et al. Flexural strengthening of concrete beams using externally bonded composite materials. **Construction and Building Materials**, v. 8, n. 3, p. 191–201, 1994.

[11] ARDUINI, M.; NANNI, A. Behavior of precracked RC beams strengthened with carbon FRP sheets. **Journal of Composites for Construction**, v. 1, n. 2, p. 63–70, 1997.

[12] NANNI, A. Carbon FRP Strengthening: New Technology Becomes Mainstream. **Concrete International**, v. 19, n. 6, p. 1–23, 1997.

[13] KHALIFA, A.; NANNI, A. Rehabilitation of rectangular simply supported RC beams with shear deficiencies using CFRP composites. **Construction and Building Materials**, v. 16, n. 3, p. 135–146, 2002.

[14] ESHWAR, N.; IBELL, T. J.; NANNI, A. Effectiveness of CFRP strengthening on curved soffit RC beams. **Advances in Structural Engineering**, v. 8, n. 1, p. 55–68, 2005.

[15] BAGGIO, D.; SOUDKI, K.; NOËL, M. Strengthening of shear critical RC beams with various FRP systems. **Construction and Building Materials**, v. 66, p. 634–644, 2014.

[16] AMERICAN CONCRETE INSTITUTE (ACI). **ACI 440.2R-17: Guide for the Design and Construction of Externally Bonded FRP Systems for Strengthening Concrete Structures**, 2017.

[17] NANNI, A. A New Tool for Concrete and Masonry Repair. **Concrete International**, n. april, p. 43–49, 2012.

[18] BRAMESHUBER, W. **Report 36: textile reinforced concrete-state-of-the-art report of RILEM TC 201-TRC**. [s.l.] Rilem publications, 2006.

[19] PELED, A.; BENTUR, A.; MOBASHER, B. **Textile Reinforced Concrete**. [s.l.] CRC Press Taylor & Francis Group, 2017.

[20] MEHTA, P. K.; MONTEIRO, P. J. M. **Concrete: Microstructure, properties and materials**. [s.l.] McGraw-Hill, 2006.

[21] BRÜCKNER, A.; ORTLEPP, R.; CURBACH, M. Textile reinforced concrete for strengthening in bending and shear. **Materials and Structures**, v. 39, n. 8, p. 741–748, 2006.

[22] AMBRISI, A. D.; FOCACCI, F. Flexural strengthening of RC beams with

cement-based composites. **Journal of Composites for Construction**, v. 15, n. 5, p. 707–720, 2011.

[23] OMBRES, L. Flexural analysis of reinforced concrete beams strengthened with a cement based high strength composite material. **Composite Structures**, v. 94, n. 1, p. 143–155, 2011.

[24] BABAEIDARABAD, S.; LORETO, G.; NANNI, A. Flexural strengthening of RC beams with an externally bonded fabric-reinforced cementitious matrix. **Journal of Composites for Construction**, v. 18, n. 5, p. 04014009-1- 04014009–12, 2014.

[25] VERBRUGGEN, S. et al. Bending of beams externally reinforced with TRC and CFRP monitored by DIC and AE. **Composite Structures**, v. 112, n. 1, p. 113–121, 2014.

[26] SI LARBI, A.; CONTAMINE, R.; HAMELIN, P. TRC and hybrid solutions for repairing and/or strengthening reinforced concrete beams. **Engineering Structures**, v. 45, p. 12–20, 2012.

[27] GOPINATH, S. et al. Behaviour of reinforced concrete beams strengthened with basalt textile reinforced concrete. **Journal of Industrial Textiles**, v. 44, n. 6, p. 924–933, 2015.

[28] TEIXEIRA, F. P.; ANDRADE SILVA, F. DE. On the use of natural curauá reinforced cement based composites for structural applications. **Cement and Concrete Composites**, v. 114, n. July, 2020.

[29] AKBARI HADAD, H.; ERICKSON, B.; NANNI, A. Flexural analysis and design of FRCM-strengthened RC beams. **Construction and Building Materials**, v. 244, p. 118371, 2020.

[30] TRIANTAFILLOU, T. C. **Textile Fibre Composites in Civil Engineering**. [s.l.] Woodhead Publishing, 2016.

[31] BUTLER, M.; LIEBOLDT, M.; MECHTCHERINE, V. Application of Textile-Reinforced Concrete (TRC) for structural strengthening and in prefabrication. **Advances in Cement-Based Materials**, p. 127–136, 2010.

[32] WAGNER, J. et al. Strengthening of Reinforced Concrete Structures with Carbon Reinforced Concrete—Possibilities and Challenges. **CivilEng**, v. 3, n. 2, p. 400–426, 2022.

[33] NADIV, R. et al. Micro- and nanoparticle mineral coating for enhanced properties of carbon multifilament yarn cement-based composites. **Composites**

Part B: Engineering, v. 111, p. 179–189, 2017.

[34] PELED, A.; ZAGURI, E.; MAROM, G. Bonding characteristics of multifilament polymer yarns and cement matrices. **Composites Part A: Applied Science and Manufacturing**, v. 39, n. 6, p. 930–939, 2008.

[35] XU, S. et al. Bond Characteristics of Carbon, Alkali Resistant Glass, and Aramid Textiles in Mortar. **Journal of Materials in Civil Engineering**, v. 16, n. 4, p. 356–364, 2004.

[36] RAUPACH, M.; ORLOWSKY, J.; BÜTTNER, T. **Epoxy-impregnated textiles in concrete – Load bearing capacity and durability**. (J. Hegger, W. Brameshuber, N. Will, Eds.)ICTRC'2006 - 1st International RILEM Conference on Textile Reinforced Concrete. **Anais...Aachen: RILEM Publications SARL**, 2006

[37] DONNINI, J.; CORINALDESI, V.; NANNI, A. Mechanical properties of FRCM using carbon fabrics with different coating treatments. **Composites Part B: Engineering**, v. 88, p. 220–228, 2016.

[38] DVORKIN, D.; PELED, A. Effect of reinforcement with carbon fabrics impregnated with nanoparticles on the tensile behavior of cement-based composites. **Cement and Concrete Research**, v. 85, p. 28–38, 2016.

[39] EHLIG, D. et al. **High Temperature Tests on Textile Reinforced Concrete (TRC) Strain Specimens**. (W. Brameshuber, Ed.)International RILEM Conference on Material Science – MATSCI. **Anais...Aachen: Rilem publications**, 2010

[40] SILVA, F. DE A. et al. Effects of elevated temperatures on the interface properties of carbon textile-reinforced concrete. **Cement and Concrete Composites**, v. 48, p. 26–34, 2014.

[41] XU, S.; SHEN, L.; WANG, J. The high-temperature resistance performance of TRC thin-plates with different cementitious materials: Experimental study. **Construction and Building Materials**, v. 115, p. 506–519, 2016.

[42] DONNINI, J. et al. Fabric-reinforced cementitious matrix behavior at high-temperature: Experimental and numerical results. **Composites Part B: Engineering**, v. 108, p. 108–121, 2017.

[43] PELED, A. et al. **Modifying carbon roving-cement matrix bond by inorganic coating**. High Performance Fiber Reinforced Cement Composites (HPFRCC7). **Anais...Struttgart, Germany: RILEM**, 2015

[44] SCHNEIDER, K. et al. Mineral-impregnated carbon fibre reinforcement for

high temperature resistance of thin-walled concrete structures. **Cement and Concrete Composites**, v. 97, n. December 2018, p. 68–77, 2019.

[45] SCHNEIDER, K. et al. Verbundverhalten mineralisch gebundener und polymergebundener Bewehrungsstrukturen aus Carbonfasern bei Temperaturen bis 500 °C. **Beton- und Stahlbetonbau**, v. 113, n. 12, p. 886–894, 2018.

[46] SILVA, R. M. DE C. et al. Bond behavior of polymer- and mineral-impregnated carbon fiber yarns towards concrete matrices at elevated temperature levels. **Cement concrete composite**, v. 133, p. 104685, 2022.

[47] SILVA, R. M. DE C. et al. Mechanical behavior of textile reinforced concrete with newly developed mineral-impregnated carbon fabrics submitted to uniaxial tensile loads and exposed to elevated temperatures. 2023.

[48] ORTLEPP, R.; ORTLEPP, S.; CURBACH, M. Stress transfer in the bond joint of subsequently applied textile reinforced concrete strengthening. **6th International RILEM Symposium on Fibre Reinforced Concretes**, n. September, p. 1483–1494, 2004.

[49] ORTLEPP, R.; HAMPEL, U.; CURBACH, M. A new approach for evaluating bond capacity of TRC strengthening. **Cement and Concrete Composites**, v. 28, n. 7, p. 589–597, 2006.

[50] SNEED, L. H. et al. A comparison of the bond behavior of PBO-FRCM composites determined by double-lap and single-lap shear tests. **Cement and Concrete Composites**, v. 64, p. 37–48, 2015.

[51] D'ANTINO, T. et al. Matrix-fiber bond behavior in PBO FRCM composites: A fracture mechanics approach. **Engineering Fracture Mechanics**, v. 117, p. 94–111, 2014.

[52] D'ANTINO, T. et al. Influence of the substrate characteristics on the bond behavior of PBO FRCM-concrete joints. **Construction and Building Materials**, v. 101, p. 838–850, 2015.

[53] SNEED, L. H.; D'ANTINO, T.; CARLONI, C. Investigation of bond behavior of polyparaphenylene benzobisoxazole fiber-reinforced cementitious matrix composite-concrete interface. **ACI Materials Journal**, v. 111, n. 5, p. 569–580, 2014.

[54] YOUNIS, A.; EBEAD, U. Bond characteristics of different FRCM systems. **Construction and Building Materials**, v. 175, p. 610–620, 2018.

[55] D'ANTINO, T. et al. Experimental analysis of the bond behavior of glass,

carbon, and steel FRCM composites. **Key Engineering Materials**, v. 624, n. January, p. 371–378, 2015.

[56] OMBRES, L. Analysis of the bond between Fabric Reinforced Cementitious Mortar (FRCM) strengthening systems and concrete. **Composites Part B: Engineering**, v. 69, p. 418–426, 2015.

[57] AMERICAN CONCRETE INSTITUTE (ACI). **ACI 549.4R-20: Guide to Design and Construction of Externally Bonded Fabric-Reinforced Cementitious Matrix and Steel-Reinforced Grout Systems for Repair and Strengthening Concrete Structures** ACI, , 2020.

[58] BENCARDINO, F. et al. Flexural behaviour of RC members strengthened with FRCM: State-of-the-art and predictive formulas. **Composites Part B: Engineering**, v. 148, n. April, p. 132–148, 2018.

[59] SCHEERER, S. et al. Flexural strengthening of rc structures with TRC- experimental observations, design approach and application. **Applied Sciences (Switzerland)**, v. 9, n. 7, 2019.

[60] ZHAO, J. et al. Development and testing of fast curing, mineral-impregnated carbon fiber (MCF) reinforcements based on metakaolin-made geopolymers. **Cement and Concrete Composites**, v. 116, n. September 2020, 2021.

[61] BRAZILIAN STANDARD. **NBR 16697: Cimento Portland - Requisitos** Associação Brasileira de Normas Técnicas (ABNT), , 2018.

[62] LIMA, V. N.; CARDOSO, D. C. T.; SILVA, F. DE A. **Flexural creep behavior of steel and polypropylene fiber reinforced concrete**. (G. Pijaudier-Cabot, P. Grassl, C. La Borderie, Eds.) 10th International Conference on Fracture Mechanics of Concrete and Concrete Structures (FraMcoS-X). **Anais...** 2019

[63] TEIXEIRA, F. P.; CARDOSO, D. C. T.; ANDRADE SILVA, F. DE. On the shear behavior of natural curauá fabric reinforced cement-based composite systems. **Engineering Structures**, v. 246, n. August, 2021.

[64] BRAZILIAN STANDARD. **NBR 7480: Aço destinado às armaduras para estruturas de concreto armado - Requisitos** Associação Brasileira de Normas Técnicas (ABNT), , 2022.

[65] PIMENTEL TINOCO, M.; ANDRADE SILVA, F. DE. Repair of pre-damaged RC beams using hybrid fiber reinforced strain hardening cementitious composites. **Engineering Structures**, v. 235, n. October 2020, 2021.

[66] FIGUEIREDO, T. C. S. P. **On the mechanical behavior of strain- hardening**

- cementitious composites (SHCC) under combined and impact loading.** 2021. Universidade Católica do Rio de Janeiro (PUC-Rio). 2021.
- [67] INTERNATIONAL FEDERATION FOR STRUCTURAL CONCRETE. **fib Model Code - Bulletin 66**, 2012.
- [68] BRAZILIAN STANDARD. **NBR 6118: Projeto de estruturas de concreto - Procedimento** Associação Brasileira de Normas Técnicas (ABNT), , 2014.
- [69] EUROPEAN STANDARD EN. **EN 1992 - Eurocode 2: Design of concrete structures - Part 1-1: General rules and rules for buildings**, 2004.
- [70] AWANI, O.; REFAI, A. EL; EL-MAADDAWY, T. Bond characteristics of carbon fabric-reinforced cementitious matrix in double shear tests. **Construction and Building Materials**, v. 101, p. 39–49, 2015.
- [71] WIGHT, J. K.; MACGREGOR, J. G. **Reinforced Concrete - Mechanics & Design**. 6th editio ed. [s.l.] Pearson, 2012.
- [72] HOSEINI, M.; BINDIGANAVILE, V.; BANTHIA, N. The effect of mechanical stress on permeability of concrete: A review. **Cement and Concrete Composites**, v. 31, n. 4, p. 213–220, 2009.
- [73] MECHTCHERINE, V.; LIEBOLDT, M. Permeation of water and gases through cracked textile reinforced concrete. **Cement and Concrete Composites**, v. 33, n. 7, p. 725–734, 2011.
- [74] LIEBOLDT, M.; MECHTCHERINE, V. Capillary transport of water through textile-reinforced concrete applied in repairing and/or strengthening cracked RC structures. **Cement and Concrete Research**, v. 52, p. 53–62, 2013.
- [75] MECHTCHERINE, V. Towards a durability framework for structural elements and structures made of or strengthened with high-performance fibre-reinforced composites. **Construction and Building Materials**, v. 31, p. 94–104, 2012.
- [76] POURASEE, A.; PELED, A.; WEISS, J. Fluid Transport in Cracked Fabric-Reinforced-Cement-Based Composites. **Journal of Materials in Civil Engineering**, v. 23, n. 8, p. 1227–1238, 2011.
- [77] MECHTCHERINE, V. Novel cement-based composites for the strengthening and repair of concrete structures. **Construction and Building Materials**, v. 41, p. 365–373, 2013.
- [78] PRATES JUNIOR, N. P. **Um modelo elasto-viscoplástico para análise de peças de concreto estrutural, submetidas a estados planos de tensão, através**

do método dos elementos finitos. 1992. Universidade Federal do Rio Grande do Sul (UFRGS). 1992.

6 Conclusions and suggestions for future works

6.1. Conclusions

In this study, the mechanical characterization of textile reinforced concrete (TRC) with polymer- and mineral-impregnated carbon fabrics was evaluated. A literature review was performed to understand the current state and limitations of the use of carbon-TRC, and based on that, an experimental program was structured to meet the thesis objectives. To overcome the low thermal resistance of polymer-coated carbon fabrics, Mineral-Impregnated Carbon Fiber (MCF) fabrics with a cement-based (C) and a geopolymer (GP) suspension were developed. The bond behavior of the MCF yarns towards cementitious matrices was characterized through pull-out tests at different temperature levels. The mechanical behavior of the MCF-TRC was addressed through direct tensile tests performed at room temperature and after the specimens were submitted to different thermal regimes. The results obtained were compared to the results from a commercially available epoxy-coated (EP) carbon fabric. Finally, the feasibility of the TRC with polymer- and mineral-impregnated carbon fabrics as strengthening of RC beams was evaluated.

The MCF yarns showed high tensile strength and modulus of elasticity, thus demonstrating the effectiveness of the cementitious matrix and the geopolymer suspensions as impregnation materials for the carbon yarns. It is important to emphasize the considerable difference in the curing time required for both materials. While the C-MCF yarns need at least 28 days to achieve their mechanical strength, the GP-MCF yarns are ready to be used in just 7 days. The C-MCF yarns exhibited higher bond strength towards the fine-grained concrete than the GP-MCF yarn, which was attributed to the better chemical compatibility of the cement-based suspension with the matrix. Geopolymers are rich in alkali ions, which jeopardize the bond of the GP-MCF yarn with the cementitious matrix. At room temperature, the EP yarns yielded the strongest bond with the fine-grained concrete matrix. However, the shape of the pull-out curve indicated that a mechanical interaction

was the main bond mechanism, which was corroborated by microscopic observations. The bond of the EP yarns with the fine-grained concrete matrix was the most affected by temperature increase, mainly due to the intrinsic low thermal resistance of the epoxy resin. The C- and GP-MCF yarns were able to maintain a considerable bond quality with the cementitious matrix at temperatures up to 200 °C. At 300 °C, only the C-MCF yarn presented a suitable bond level towards the matrix. The GP-MCF yarn was not able to preserve its bond, probably due to the high extent of shrinkage and micro-cracking at the yarn-matrix interface.

The MCF fabrics developed presented tensile strength and modulus of elasticity comparable with the commercially available epoxy-coated carbon fabric, which validates the effectiveness of this new material as textile reinforcement. The TRC with MCF fabrics exhibited a strain-hardening behavior with a multiple-cracking pattern under tensile loadings. The composites with the C-MCF fabric showed superior mechanical performance than the ones with the GP-MCF fabric, probably due to the better bond towards the fine-grained concrete matrix of the C-MCF fabric. This assumption was corroborated by the DIC analysis, which showed that the composites with the C-MCF fabric presented more cracks with smaller widths than the composites with the GP-MCF fabric. The TRC with the EP carbon fabric presented the best mechanical performance. However, its failure was characterized by a significant spalling. The exposure to different thermal regimes leads to the formation of cracks in the TRC with MCF cracks, with these cracks being more pronounced in the composites with the GP-MCF fabric. This thermal cracking can be related to an incompatibility between the thermal coefficients of the mineral suspensions and the fine-grained concrete. The residual tensile mechanical behavior of the TRC with C-MCF fabric was not significantly affected by the thermal regimes, and the composites presented a strain-hardening behavior at all temperature levels evaluated. On the other hand, the thermal regimes considerably affected the residual mechanical behavior of the TRC with GP-MCF fabric. A decrease in the residual tensile strength and strain capacity was observed for these composites. Temperatures up to 200 °C did not significantly affect the residual mechanical behavior of the TRC with EP carbon. However, subsequent heating to 300 °C, led to a considerable decrease in the mechanical behavior, mostly due to the complete degradation of the epoxy resin coating. At all temperature

levels, including at room temperature, a substantial spalling was noted in the composites with the EP carbon fabric.

Different strengthening protocols were evaluated, and the best substrate preparation method is dependent on the textile reinforcement used in the TRC-strengthening layer. For the strengthening with the EP-TRC, the total roughening of the surface proved to be the most effective substrate preparation protocol, as there was a solidary work between the TRC-strengthening layer and the RC beam without changing the failure mode. For the strengthening with the MCF-TRCs, the best strengthening protocol was based on the aggregate exposure with the retarder paper. With the proper strengthening protocol, all TRC-strengthened beams exhibited higher maximum loads. This enhancement was 67.8%, 59.6%, and 53.8% for the TRC with the EP carbon, C-MCF, and GP-MCF fabrics, respectively. The small difference in the load capacity gain makes the strengthening with MCF-TRCs a viable option to replace EP-TRCs, especially in high-temperature situations. After the yielding of the steel rebars, the RC beams strengthened with the TRC-EP e TRC-C were able to maintain higher load levels than the reference beam. The cracking pattern of the RC beams was modified by the TRC strengthening. The TRC-strengthened beams presented a greater number of finer cracks, which is particularly interesting from a durability aspect since cracks with smaller widths limit the entry of deleterious agents that can lead to damage to the concrete and steel reinforcement. Finally, an analytical model base on moment *vs.* curvature curves was proposed. The results show that the proposed model can be used to estimate the maximum bending capacity of RC beams strengthened with C- and GP-TRCs. However, the model overestimated the ultimate moment of the EP-TRC strengthened beams. This may be related to the fact that the EP-TRC did not reach its maximum capacity, which could be related to a failure in the bond between the TRC-strengthening layer and the RC substrate and may have led to a premature failure of the beam, even without any detachment having been detected. When implementing a debonding strain in the model, a better correlation between the analytical and experimental moment *vs.* curvature curves was obtained for the TR-I-EP beam.

In general, the outcome of this study demonstrated that MCF fabrics can be used as an alternative reinforcement in textile reinforced concretes, mainly in situations in which elevated temperatures are expected. With adequate substrate

preparation, the MCF-TRC system can also be successfully implemented as a strengthening material for RC beams.

6.2. Suggestions for future works

Although this study has presented novel results regarding the use of MCF fabrics as reinforcement in textile reinforced concretes, it is evident that, in parallel, it demonstrates new demands for specific investigations that may be explored in future works, such as:

- Regarding the influence of the mineral-suspension on the mechanical properties of the MCF yarns, more studies could be performed to better understand the contribution of the hardened suspension properties and the bond between the inner filaments.
- It would be interesting to perform yarn tension tests and pull-out tests at dynamic conditions to assess the strain rate dependency of the material in order to allow its use in impact scenarios.
- The chemical incompatibility between the GP-MCF yarn and the cementitious matrix should be further evaluated, focusing on finding alternatives that could overcome this. Focusing on commercial application, the use of geopolymer suspension seems to be more interesting than the cement-based one due to the faster curing.
- Regarding the thermal behavior of the TRC with the MCF fabrics, it is important to obtain the coefficient of thermal expansion of the materials used, namely the mineral suspensions, the MCF yarns, and the fine-grained concrete, to evaluate the compatibility between them. Additionally, it would be interesting to investigate the interface between the textile reinforcement and the fine-grained concrete just after the heating and after the cooling process since it is not possible to know at this point if the thermal cracking occurred due to heating, cooling, or both processes.
- The manufacturing method of the MCF fabric could be improved, aiming to reduce the thickness of the fabric in the knots' regions. The MCF fabric production also has the potential to be automated, which would be very interesting in terms of commercial application in the future.

- Finally, it would be interesting to evaluate the bond behavior between the TRC-strengthening layer and the concrete substrate. This characterization would provide more data to improve analytical design modes, aiming to create guides and standards on RC strengthening with TRCs.